Inaugural Dissertation

for obtaining the doctoral degree of the
Combined Faculty of Mathematics, Engineering and
Natural Sciences of the Ruprecht-Karls-University Heidelberg

Presented by

M.Sc. Alessia Cais

born in Frankfurt am Main, Germany

Oral Examination: June 8th, 2026

Preclinical Investigation of Radiotherapy Combination Strategies and Targeted Therapy Resistance in Pediatric-type Diffuse High-Grade Glioma

Referees:

Prof. Dr. Peter Angel

Prof. Dr. med. Stefan M. Pfister

Declaration

The results of the following thesis were obtained during my doctoral research conducted between August 2021 and February 2026 under the supervision of Dr. Marc Zuckermann at the division of ‘Pediatric Neurooncology’ in the ‘Preclinical Modeling’ group at the German Cancer Research Center (DKFZ) and the Hopp Children’s Cancer Center (KiTZ), Heidelberg, Germany.

I hereby declare that I wrote and submitted this dissertation independently, using only the sources acknowledged herein. I have clearly stated the contributions by others involved in the work included within my thesis. Prior to submission, this thesis was subjected to plagiarism detection using the iThenticate service. I further declare that I have not applied to be examined at any other institution, nor have I used the dissertation in this or any other form at any other institution as an examination paper, nor submitted it to any other faculty as a dissertation.

Parts of this thesis have been previously published as conference abstracts and were presented at the ‘International Symposium of Pediatric Neuro-Oncology’ (ISPNO) in 2024 (Philadelphia, USA) and the ‘Brain Tumors’ conference in 2025 (Warsaw, Poland).

Alessia Cais

Abstract

Pediatric-type diffuse high-grade gliomas (pHGGs) are among the most aggressive and lethal childhood brain tumors, and current treatment strategies provide only limited clinical benefit. Radiotherapy (RT) remains a central component of standard care, particularly for diffuse midline glioma, yet its effects are largely palliative. In parallel, targeted therapies have shown promise in selected molecular subgroups, such as receptor tyrosine kinase-driven infant-type hemispheric glioma (IHG), but are frequently limited by the development of acquired resistance.

In the first project, I sought to improve RT-based treatment strategies for pHGGs by systematically identifying and comparing targeted compounds with radiosensitizing potential. I performed a high-throughput combination screening using a curated library of FDA-approved drugs in combination with RT across a diverse panel of patient-derived pHGG models, alongside non-malignant control cells. I validated candidate radiosensitizers *in vitro* using multiple orthogonal assays, including measurements of cell viability, apoptosis induction, long-term growth suppression and DNA damage responses. I subsequently evaluated promising drug+RT combinations in orthotopic xenograft models to assess antitumor efficacy under physiologically relevant conditions. In addition, I conducted pharmacokinetic analyses to determine whether limited bioavailability or brain penetration constrained *in vivo* efficacy despite robust *in vitro* activity.

In the second project, I focused on elucidating mechanisms of acquired resistance to targeted therapy in anaplastic lymphoma kinase (ALK)-fusion-driven IHG. Although treatment with the third-generation ALK inhibitor Lorlatinib induces marked initial responses in patients, disease progression frequently occurs. To investigate this phenomenon, I established stable *in vitro* and *in vivo* models of acquired Lorlatinib resistance through prolonged drug exposure. I functionally characterized resistant models with respect to proliferation and apoptosis under continued ALK inhibition and assessed cross-resistance to an alternative ALK inhibitor. Using bulk RNA sequencing, I identified resistance-associated transcriptional programs and signaling pathways that support tumor survival. Based on these findings, I explored candidate vulnerabilities of the resistant state using targeted drug combinations and prioritized them for further preclinical evaluation.

Collectively, this work provides a systematic preclinical framework for the rational development of RT-based combination therapies in pHGGs and offers mechanistic insights into ALK inhibitor resistance in IHG. My findings contribute to a deeper understanding of treatment resistance and therapeutic synergy in pHGGs and may inform the design of future translational and clinical studies.

Zusammenfassung

Pädiatrische diffuse hochgradige Gliome (pHGG) zählen zu den aggressivsten und tödlichsten Hirntumoren im Kindesalter, während die derzeitigen Behandlungsstrategien nur einen begrenzten klinischen Nutzen bieten. Die Radiotherapie (RT) stellt einen zentralen Bestandteil der Standardtherapie dar, insbesondere beim diffusen Mittelliniengliom, ihre Wirkung ist jedoch überwiegend palliativ. Parallel dazu zeigen zielgerichtete Therapien in ausgewählten molekularen Subgruppen vielversprechende therapeutische Wirksamkeit, etwa bei durch Rezeptor-Tyrosinkinasen getriebenen infantilen hemisphärischen Gliomen (IHG), ihr Nutzen wird jedoch häufig durch das Auftreten erworbener Resistenzen limitiert.

Im ersten Projekt verfolgte ich das Ziel, RT-basierte Therapiestrategien für pHGG durch die systematische Identifizierung zielgerichteter Substanzen mit radiosensibilisierendem Potenzial zu verbessern. Hierzu führte ich ein Hochdurchsatz-Kombinationsscreening mit einer Kollektion FDA-zugelassener Medikamente in Kombination mit RT an einem diversen Panel patientenabstammenden pHGG-Modelle sowie an nicht-malignen Kontrollzellen durch. Potenzielle Radiosensitizer validierte ich *in vitro* mithilfe mehrerer orthogonaler Assays, darunter Analysen zur Zellviabilität, zur Induktion von Apoptose, zur langfristigen Wachstumshemmung und zur DNA-Schäden-Persistenz. Vielversprechende Medikament+RT-Kombinationen evaluierte ich anschließend in orthotopen Xenograft-Modellen, um ihre anti-tumorale Wirksamkeit unter physiologisch relevanten Bedingungen zu untersuchen. Ergänzend führte ich pharmakokinetische Analysen durch, um zu prüfen, ob eine eingeschränkte Bioverfügbarkeit oder Hirnpenetration die *in vivo*-Wirksamkeit trotz ausgeprägter *in vitro*-Aktivität limitierte.

Im zweiten Projekt untersuchte ich die Mechanismen erworbener Resistenz gegenüber zielgerichteten Therapien in durch Fusionen der anaplastischen Lymphomkinase (ALK) getriebenen IHG. Obwohl die Behandlung mit dem ALK-Inhibitor der dritten Generation Lorlatinib initial ausgeprägte Therapieansprechen in Patienten induziert, treten häufig Resistenzen auf. Zur Untersuchung dieses Phänomens etablierte ich durch prolongierte Wirkstoffexposition stabile *in vitro*- und *in vivo*-Modelle einer erworbenen Lorlatinib-Resistenz. Die resistenten Modelle charakterisierte ich funktionell hinsichtlich Proliferation und Apoptose unter fortgesetzter ALK-Inhibition und untersuchte Kreuzresistenzen gegenüber einem alternativen ALK-Inhibitor. Mithilfe von Bulk-RNA-Sequenzierung identifizierte ich resistenzassoziierte transkriptionelle Programme und Signalwege, die das Tumorüberleben unterstützen. Auf Basis dieser Ergebnisse explorierte ich potenzielle therapeutische Vulnerabilitäten des resistenten Zustands mittels gezielter Wirkstoffkombinationen und priorisierte diese für weiterführende präklinische Untersuchungen.

Zusammenfassend liefert diese Arbeit ein systematisches präklinisches Rahmenkonzept für die rationale Entwicklung RT-basierter Kombinationstherapien bei pHGG und bietet mechanistische Einblicke in die Resistenz gegenüber ALK-Inhibitoren beim IHG. Meine Ergebnisse tragen zu einem vertieften Verständnis von Therapieresistenz und therapeutischer Synergie bei pHGG bei und können zur Konzeption zukünftiger translationaler und klinischer Studien beitragen.

Table of contents

Declaration 1
Abstract 2
Zusammenfassung 3
Table of contents 5
List of tables 9
List of figures 10
List of abbreviations 13
1. Introduction 19
1.1. Pediatric CNS tumors 19
1.2. Pediatric-type diffuse high-grade gliomas 19
1.2.1. Diffuse midline glioma, H3 K27-altered 20
1.2.2. Diffuse hemispheric glioma, H3 G34-mutant 21
1.2.3. Diffuse pediatric-type high-grade glioma, H3- and IDH-wildtype 22
1.2.4. Infant-type hemispheric glioma 22
1.3. Treatments for pHGG 23
1.3.1. Standard treatments for pHGGs 23
1.3.2. Radiotherapy 24
1.3.3. Targeted agents for pHGGs 26
1.3.4. Therapeutic strategies to overcome the blood-brain barrier 28
1.3.5. Immunotherapeutic approaches 29
1.3.6. Combination treatments for pHGGs 30
2. Aims and objectives 34
2.1. Comparing the radiosensitization potential of various compound classes in pediatric-type diffuse high-grade glioma 34
2.2. Overcoming ALK inhibitor resistance in ALK-fusion infant-type hemispheric glioma 34
3. Materials and Methods 36
3.1. Materials 36
3.1.1. Cells 36

3.1.2. Cell culture reagents 37
3.1.3. Mice 38
3.1.4. Reagents, kits and dyes 38
3.1.5. Consumables 38
3.1.6. Drugs 40
3.1.7. Solvents 40
3.1.8. Devices and machines 41
3.1.9. Softwares 41
3.2. Methods 43
3.2.1. Cell culture 43
3.2.2. Inhibitor treatment 44
3.2.3. Irradiation (*in vitro*) 44
3.2.4. Drug screening 45
3.2.5. Cell viability assays 45
3.2.6. Apoptosis assays 46
3.2.7. Long-term growth inhibition assays 46
3.2.8. yH2AX staining 46
3.2.9. RNA isolation 46
3.2.10. Bulk RNA sequencing 47
3.2.11. EdU assay 47
3.2.12. Mice and ethical compliance 47
3.2.13. Intracranial transplantation 47
3.2.14. Bioluminescence imaging (IVIS) 49
3.2.15. Irradiation (*in vivo*) 49
3.2.16. Drug treatment 50
3.2.17. Processing of endpoint samples 51
3.2.18. Pharmacokinetic analysis 52
3.2.19. Immunohistochemistry and Hematoxylin-Eosin staining 52
3.2.20. Graphs and statistical analysis 54

3.2.21. Illustrations and figure design 54

3.2.22. Use of artificial intelligence 54

4. Results 55

4.1. Comparing the radiosensitization potential of various compound classes in pediatric-type diffuse high-grade glioma 55

4.1.1. Heterogeneous intrinsic radiosensitivity across PDX-derived pHGG cell models 55

4.1.2. Comprehensive drug+RT screening identifies potential radiosensitizers for pHGG cells 55

4.1.3. Selected compounds exhibit nanomolar potency in pHGG cells 59

4.1.4. Selected compounds induce radiosensitization in pHGG cells as determined by cell viability assays 61

4.1.5. Drug+RT combination treatment enhances apoptosis in pHGG cells 66

4.1.6. Drug+RT combination treatment leads to long-term growth inhibition in pHGG cells 69

4.1.7. Candidate compounds differentially influence radiotherapy-induced DNA double-strand breaks 72

4.1.8. NXG mice are unable to tolerate fractionated whole-brain irradiation 74

4.1.9. Orthotopic pHGG xenografts exhibit model-dependent engraftment and growth behavior 75

4.1.10. Fractionated radiotherapy delays tumor progression in the DIPG-007 xenograft model 78

4.1.11. Preclinical evaluation of the radiosensitizing potential of identified compounds in the DIPG-007 model 79

4.2. Overcoming ALK inhibitor resistance in ALK-fusion infant-type hemispheric glioma 87

4.2.1. Chronic Lorlatinib treatment induces stable Lorlatinib-resistance in PPP1CB::ALK-driven pHGG cells 87

4.2.2. ALK-inhibition enhances proliferation and inhibits apoptosis in Lorlatinib-resistant cells 90

4.2.3. Continuous Lorlatinib treatment suppresses tumor growth but does not induce stable resistance *in vivo* 92

4.2.4. Re-transplantation of Lorlatinib-pretreated tumors induces stable disease in Lorlatinib-treated mice 95

4.2.5. Tumor-derived cells retain partial Lorlatinib sensitivity despite prior *in vivo* exposure 97

4.2.6. Bulk RNA sequencing reveals targetable vulnerabilities of Lorlatinib-resistant tumor cells 98

4.2.7. Lorlatinib-resistant cells show selective vulnerability to BCL-2/-XL inhibition .. 99

5. Discussion 101

5.1. Comparing the radiosensitization potential of various compound classes in pediatric-type diffuse high-grade glioma 101

5.1.1. Outlook and future directions 107

5.1.2. Conclusion 109

5.2. Overcoming ALK inhibitor resistance in ALK-fusion infant-type hemispheric glioma 109

5.2.1. Outlook and future directions 113

5.2.2. Conclusion 114

6. References 115

7. Supplementary data 142

8. Acknowledgments 161

List of tables

Table 1: Composition of the TSM media 43
Table 2: Composition of the NSC media 44
Table 3: Injection coordinates for the intracranial transplantation of pHGG cells. 48
Table 4: Formulation and application of the drugs used in the *in vivo* experiments. 50
Table 5: Ranking of the drug candidates according to the Best CDI Sum in pHGG cells. 58
Table 6: Ranking of the drug candidates according to the Best CDI Sum in non-malignant control cells. 58

List of figures

Figure 1: Overview of pediatric-type diffuse high-grade gliomas according to the latest WHO classification in 2021. 20
Figure 2: Composition of the drug library used for the drug+RT screening (provided by the Translational Drug Screening Unit 2022). 45
Figure 3: Injection coordinates for the intracranial transplantation of pHGG cells. 48
Figure 4: Positioning of the two irradiation beams for the whole-brain irradiation with the SmART+ machine. 50
Figure 5: Radiosensitivity of PDX-derived pHGG cell cultures. 55
Figure 6: Heatmap of the Best CDI of all tested cells in the drug+RT screens. 57
Figure 7: Drug response curves of selected drug candidates in DIPG-19 (H3K27M). 60
Figure 8: Cell viability assays after HDACi and RT combination treatment in DIPG-007 cells. 62
Figure 9: Cell viability assays after MEKi and RT combination treatment in DIPG-007 cells. 63
Figure 10: Cell viability assays after BCLi and RT combination treatment in DIPG-007 cells. 64
Figure 11: Cell viability assays after Proteasomei and RT combination treatment in DIPG-007 cells. 65
Figure 12: Heatmap comparing the Best CDIs of the tested drug+RT combinations of the cell viability assays in different pHGG cell cultures (X-axis). 65
Figure 13: Apoptosis induction after drug+RT combination treatment in DIPG-007 cells. 67
Figure 14: Heatmap comparing the Best CDI of the tested drug+RT combinations of the apoptosis assays of different pHGG cell cultures (X-axis). 68
Figure 15: Representative pictures of the long-term growth inhibition assay in DIPG-007 spheres at day 14. 70
Figure 16: Quantification of the sphere size of the long-term growth inhibition assays in DIPG-007 cells. 71
Figure 17: Effects of drug+RT treatment on RT-induced DNA double-strand breaks (DSB). 73
Figure 18: Fractionated whole-brain RT causes severe toxicities in immunodeficient NXG mice. 75
Figure 19: pHGG xenograft model establishment in CD1 nude and NRG mice. 77
Figure 20: Representative pictures of pHGG tumors in the brainstem of CD1 nude mice. ... 78
Figure 21: Radiosensitivity of the DIPG-007 mouse model in CD1 nude mice. 79
Figure 22: Preclinical evaluation of Marizomib (Mari, Proteasemei), Cobimetinib (Cobi, MEKi), and Romidepsin (Romi, HDACi) in combination with 12 Gy RT in the DIPG-007 mouse model. 81

Figure 23: Preclinical evaluation of Marizomib (Mari, Proteasemei), Cobimetinib (Cobi, MEKi), and Valproic acid (VPA, HDACi) in combination with 12 Gy RT in the DIPG-007 mouse model. 83
Figure 24: Pharmacokinetic (PK) analysis of Romidepsin and Cobimetinib in CD1 nude mice. 84
Figure 25: Preclinical evaluation of AZD4320 (AZD, BCLi), Trametinib (MEKi), and Panobinostat (Pano, HDACi) in combination with 12 Gy RT in the DIPG-007 mouse model.86
Figure 26: Generation of Lorlatinib-resistant cells *in vitro*. 88
Figure 27: Lorlatinib resistance is stable even after Lorlatinib withdrawal. 89
Figure 28: Lorlatinib treatment enhances proliferation and inhibits apoptosis in Lorlatinib-resistant cells. 91
Figure 29: Effects of Crizotinib treatment on DMSO cells and Lorlatinib-resistant cells (Res.cells 2). 92
Figure 30: PPP1CB::ALK-driven pHGG cell-derived tumors are responsive to Lorlatinib treatment *in vivo*. 94
Figure 31: Lorlatinib-treatment induces stable disease in mice harboring tumors deriving from Lorlatinib pre-treated tumor cells. 96
Figure 32: Lorlatinib pre-treated tumors respond less to Lorlatinib treatment *in vitro* compared to Lorlatinib-naïve cells. 97
Figure 33: Bulk RNA sequencing analysis from Lorlatinib resistant cells and *in vivo* tumors.98
Figure 34: Combination treatment identified vulnerabilities of Lorlatinib-resistant cells (Res.cells 2). 100

Supplementary figure 1: Drug response curves of selected drug candidates in DIPG-007 (H3K27M). 142
Supplementary figure 2: Cell viability assays after HDACi and RT combination treatment in DIPG-19 cells. 143
Supplementary figure 3: Cell viability assays after MEKi and RT combination treatment in DIPG-19 cells. 144
Supplementary figure 4: Cell viability assays after BCLi and RT combination treatment in DIPG-19 cells. 145
Supplementary figure 5: Cell viability assays after Proteasomei and RT combination treatment in DIPG-19 cells. 146
Supplementary figure 6: Cell viability assays after HDACi and RT combination treatment in DIPG-21 cells. 147

Supplementary figure 7: Cell viability assays after MEKi and RT combination treatment in DIPG-21 cells. 148
Supplementary figure 8: Cell viability assays after A-B) Proteasomei and C) BCLi and RT combination treatment in DIPG-21 cells....149
Supplementary figure 9: Representative pictures of the long-term growth inhibition assay in DIPG-19 spheres at day 14. 150
Supplementary figure 10: Quantification of the sphere size of the long-term growth inhibition assays in DIPG-19 cells. 151
Supplementary figure 11: Representative pictures of the long-term growth inhibition assay in DIPG-17 spheres at day 14. 152
Supplementary figure 12: Quantification of the sphere size of the long-term growth inhibition assays in DIPG-17 cells. 153
Supplementary figure 13: Body weight of the animals from the first preclinical trial (Figure 22). 154
Supplementary figure 14: Body weight of the animals from the second preclinical trial (Figure 23). 155
Supplementary figure 15: Body weight of the animals from the third preclinical trial (Figure 25). 156
Supplementary figure 16: Generation of Lorlatinib-resistant cell replicates *in vitro*....157
Supplementary figure 17: Lorlatinib resistance is stable even after Lorlatinib withdrawal for 3 weeks. 158
Supplementary figure 18: Lorlatinib resistance is stable even after Lorlatinib withdrawal for 8 weeks. 159
Supplementary figure 19: A) IVIS signal and B) body weight of the animals treated with vehicle and Lorlatinib during the first transplantation experiment (Figure 30). 160
Supplementary figure 20: A) IVIS signal and B) body weight of the animals treated with Lorlatinib during the second transplantation experiment (Figure 31). 160

List of abbreviations

AAV ..... Adeno associated virus
ABCB1 ..... ATP binding cassette subfamily B member 1
ACVR1 ..... Activin A receptor type 1
AKT ..... Protein kinase B
AKTi ..... AKT inhibitor
ALCL ..... Anaplastic large-cell lymphoma
ALK ..... Anaplastic lymphoma kinase
ALKi ..... ALK inhibitor
ANOVA ..... Analysis of variance
ATM ..... Ataxia telangiectasia mutated
ATP ..... Adenosine triphosphate
ATRX ..... ATRX chromatin remodeler
AZD AZD-4320
B7-H3 ..... CD276 immune checkpoint molecule
BBB ..... Blood brain barrier
BCL-2/-XL ..... B-cell lymphoma 2 and BCL extra large
BCLi ..... BCL-2 family inhibitor
BER ..... Base excision repair
Best CDI ..... lowest CDI across all tested drug concentrations
Best CDI Sum ..... summed Best CDI values across all tested cells
BIM ..... BCL-2-like protein 11
CAR ..... Chimeric antigen receptor
Cas9 ..... CRISPR associated protein 9
CCDC88A ..... Coiled-coil domain containing 88A
CCNU ..... Lomustine
CD1 ..... Crl:CD1
CD1 nude Crl:CD1-Foxn1nu
CDI ..... Coefficient of Drug Interaction
CDK4/6 ..... Cyclin dependent kinases 4 and 6
CED ..... Convection enhanced delivery
CLIP2A ..... CAP-Gly domain containing linker protein 2

ClpP ..... Caseinolytic mitochondrial matrix peptidase proteolytic subunit
CO2..... Carbon dioxide
Cobi..... Cobimetinib
CoIP ..... Co-immunoprecipitation
CRISPR..... Clustered regularly interspaced short palindromic repeats
CSF ..... Cerebrospinal fluid
CTG ..... CellTiter-Glo
CTLA-4..... Cytotoxic T lymphocyte associated protein 4
CXCL9 ..... C-X-C motif chemokine ligand 9
DHG ..... Diffuse hemispheric glioma
DIPG ..... Diffuse intrinsic pontine glioma
DKFZ..... German Cancer Research Center
DMG..... Diffuse midline glioma
DMSO ..... Dimethyl sulfoxide
DNA ..... Deoxyribonucleic acid
DNA-PK..... DNA dependent protein kinase
DSB..... Double strand break
EdU ..... 5-ethynyl-2′-deoxyuridine
EGFR ..... Epidermal growth factor receptor
EML4..... Echinoderm microtubule associated protein like 4
EMT ..... Epithelial mesenchymal transition
ERK..... Extracellular signal-regulated kinase
FAM150..... Family with sequence similarity 150
FBS ..... Fetal bovine serum
FDA..... U.S. Food and Drug Administration
FFPE..... Formalin fixed paraffin embedded
FGFRi ..... Fibroblast growth factor receptor inhibitor
FUS..... Focused ultrasound
Fx..... Fraction
GBM..... Glioblastoma
GD2..... Disialoganglioside GD2
GFP..... Green fluorescent protein

GTR ..... Gross total resection
H&E..... Hematoxylin and eosin
H2O..... Water
H3 ..... Histone 3
HDAC..... Histone deacetylase
HDACi ..... Histone deacetylase inhibitor
HEK..... Human embryonic kidney cells
HER2/3 ..... Human epidermal growth factor receptor 2 and 3
HGG..... High-grade glioma
HIP1L ..... Huntingtin interacting protein 1 like
HIT ..... Heidelberg Ion Beam Therapy Center
HR..... Homologous recombination
i.p. ..... Intraperitoneal
i.v. ..... Intravenous
IC50 ..... Half maximal inhibitory concentration
ICI ..... Immune checkpoint inhibitor
IDH..... Isocitrate dehydrogenase
IFN-β ..... Interferon beta
IGF1R ..... Insulin-like growth factor 1 receptor
IHG..... Infant-type hemispheric glioma
iPSC..... Induced pluripotent stem cell
IVC..... Individually ventilated cage
IVIS ..... Bioluminescence imaging
JAK ..... Janus kinase
Ki67..... Ki-67 proliferation marker
KIT ..... KIT proto-oncogene receptor tyrosine kinase
KO..... Knockout
LET ..... Linear energy transfer
LGG ..... Low-grade glioma
LNP ..... Lipid nanoparticle
Lorl. ..... Lorlatinib
MAD1L1 ..... Mitotic arrest deficient 1 like 1

MAP2 ..... Microtubule associated protein 2
MAPK ..... Mitogen-activated protein kinase
Mari ..... Marizomib
MDR ..... Multidrug resistance
MEKi ..... MEK inhibitor
MET ..... MET proto-oncogene receptor tyrosine kinase
METi ..... MET inhibitor
MHC ..... Major histocompatibility complex
mRNA ..... Messenger RNA
MSI2 ..... Musashi RNA binding protein 2
mTOR ..... Mechanistic target of rapamycin
MYCN ..... MYCN proto-oncogene
NF1 ..... Neurofibromin 1
NHEJ ..... Non-homologous end joining
NKG2D ..... Natural killer group 2D receptor
NRG ..... NOD-Rag2tm1-Il2rg^{tm1}/Rj
NSCLC ..... Non-small cell lung cancer
NSG ..... NOD.Cg-Prkdc^{scid} Il2rg^{tm1}Wjl*/SzJ*
NTRK ..... Neurotrophic tyrosine receptor kinase
NTRKi ..... NTRK inhibitor
NXG ..... NOD-Prkdcscid-IL2rg^{Tm1}/Rj
OER ..... Oxygen enhancement ratio
ONC201 ..... Imipridone ONC201
Pano ..... Panobinostat
PARP ..... Poly ADP ribose polymerase
PARPi ..... PARP inhibitor
PBS ..... Phosphate buffered saline
PBT ..... Proton beam therapy
PCV ..... Procarbazine, lomustine, vincristine
PD-1 ..... Programmed cell death protein 1
PDGFRA ..... Platelet-derived growth factor receptor alpha
PDGFRi ..... Platelet-derived growth factor receptor inhibitor

PDX ..... Patient-derived xenograft
PEG ..... Polyethylene glycol
Pelci ..... Pelcitoclax (APG-1252-M1)
PFA ..... Paraformaldehyde
P-gp ..... P-glycoprotein
pHGG ..... Pediatric-type diffuse high-grade glioma
PI ..... Propidium iodide
PI3K ..... Phosphoinositide 3 kinase
pLGG ..... Pediatric low-grade glioma
PPM1D ..... Protein phosphatase Mg2+/Mn2+ dependent 1D
PPP1CB ..... Protein phosphatase 1 catalytic subunit beta
PRC2 ..... Polycomb repressive complex 2
PRKAR2A ..... Protein kinase cAMP dependent type II regulatory subunit alpha
Proteasomei ..... Proteasome inhibitor
RBE ..... Relative biological effectiveness
Res. cells ..... Resistant cells
Romi ..... Romidepsin
ROS ..... Reactive oxygen species
ROS1 ..... ROS proto-oncogene 1 receptor tyrosine kinase
RT ..... Radiotherapy
RTK ..... Receptor tyrosine kinase
RTKi ..... Receptor tyrosine kinase inhibitor
SD ..... Standard deviation
siRNA ..... Small interfering RNA
SPECC1L ..... Sperm antigen with calponin homology and coiled-coil domains 1 like
SPTBN1 ..... Spectrin beta non erythrocytic 1
SSB ..... Single strand break
SSBR ..... Single strand break repair
STAT ..... Signal transducer and activator of transcription
Stauro ..... Staurosporine
SYNDIG1L ..... Synapse differentiation induced gene 1 like
TGFβ ..... Transforming growth factor beta

TGFβR ..... Transforming growth factor beta receptor
TGFβRi ..... Transforming growth factor beta receptor inhibitor
TMZ..... Temozolomide
TP53 ..... Tumor protein p53
TSM ..... Tumor sphere medium
ULA..... Ultra low attachment
US ..... United States of America
VPA..... Valproic acid
Wee1..... WEE1 G2 checkpoint kinase
WGS ..... Whole genome sequencing
WHO ..... World Health Organization
Wnt..... Wingless Integrated signaling pathway
WT ..... Wild type
YAP1 ..... Yes-associated protein 1
ZC3H7A ..... Zinc finger CCCH-type containing 7A
γH2AX..... Phosphorylated histone H2AX

1. Introduction

1.1. Pediatric CNS tumors

Tumors of the central nervous system (CNS) are the leading cause of cancer-related mortality in children in high-income countries (Lupo & Spector, 2020; Price et al., 2025). Although hematological malignancies, particularly leukemias, occur more frequently in the pediatric population (Lam et al., 2019), survival improvements achieved in these diseases have not been matched in CNS tumors.

Gliomas represent the largest category of pediatric CNS neoplasms and exhibit extensive biological diversity. Clinically, they are broadly divided into low-grade gliomas (LGGs) and high-grade gliomas (HGGs), which differ substantially in their molecular characteristics and disease course. Pediatric LGGs frequently harbor alterations activating the mitogen-activated protein kinase (MAPK) signaling pathway and are generally associated with favorable prognoses, with 5-year survival rates approaching 95 % (Cohen, 2022). In contrast, pediatric HGGs are driven by distinct oncogenic mechanisms, often involving epigenetic dysregulation and chromatin remodeling defects, and remain associated with poor outcomes, with a 5-year overall survival below 20 % (Szychot et al., 2025). Although pediatric HGGs are rare, accounting for fewer than 500 cases annually in the United States (Price et al., 2025), their aggressive clinical course and limited responsiveness to existing therapies make them one of the most challenging malignancies in childhood oncology.

The recognition of this biological heterogeneity has fundamentally reshaped approaches to tumor classification. Traditional diagnostic systems relied primarily on histopathological features; however, this paradigm proved insufficient to capture the molecular complexity underlying clinical behavior. The incorporation of molecular criteria into the 2016 revision of the World Health Organization (WHO) CNS tumor classification system marked a decisive shift toward biology-based diagnosis (Louis et al., 2016). Subsequent advances in genome-wide DNA methylation profiling (Capper et al., 2018; Hovestadt et al., 2014) and next-generation sequencing technologies (Sturm et al., 2023) have enabled the identification of molecularly defined tumor subgroups with distinct prognostic and therapeutic implications. Together, these developments have established molecular profiling as a central component of modern CNS tumor diagnostics and a critical foundation for precision oncology approaches.

1.2. Pediatric-type diffuse high-grade gliomas

In the most recent WHO classification update published in 2021, pediatric-type diffuse high-grade gliomas (pHGGs) are defined primarily by their histone H3 status and are subdivided into four distinct entities: (1) diffuse midline glioma, H3 K27-altered; (2) diffuse hemispheric

glioma, H3 G34-mutant; (3) diffuse pediatric-type high-grade glioma, H3-wildtype and IDH-wildtype; and (4) infant-type hemispheric glioma (Louis et al., 2021; Pfister et al., 2022) (Figure 1).

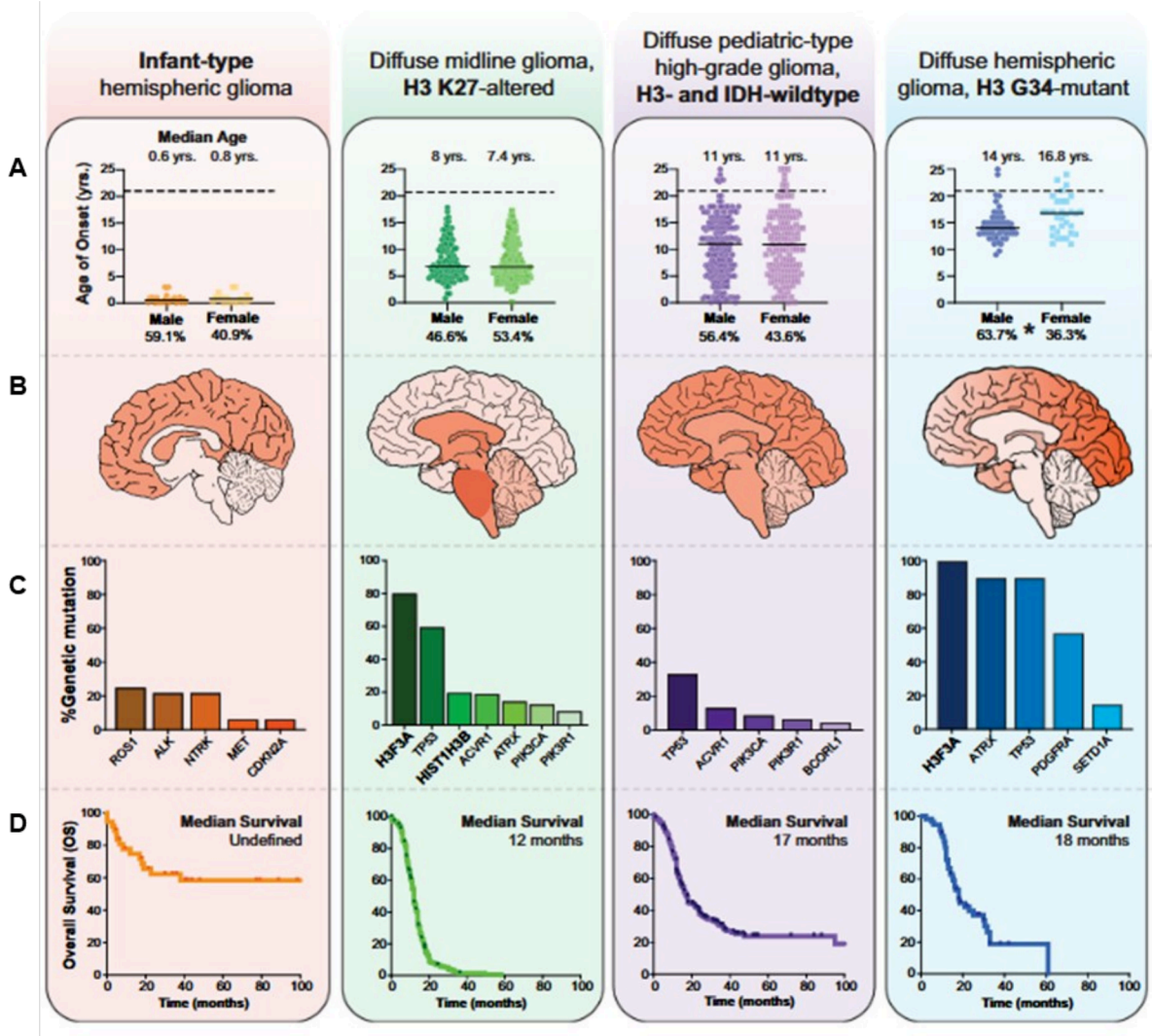


Figure 1: Overview of pediatric-type diffuse high-grade gliomas according to the latest WHO classification in 2021. A) Graphs depicting the age of onset in years across the pHGG subgroups stratified by gender. The median ages are denoted above the graph. The dashed line at 21 years represents the threshold for pediatric classification. B) Common tumor locations across the pHGG subtypes. Darker shades of red represent higher incidences. C) Bar plots showing the mutation frequencies of indicated genes associated with each pHGG subgroup. D) Kaplan-Meier curves depicting overall survival rates with the median survival indicated in the upper right corner. Figure adapted and modified from (Ocasio et al., 2023).

1.2.1. Diffuse midline glioma, H3 K27-altered

Missense mutations affecting genes encoding histone 3 (H3) represent a hallmark of pediatric diffuse midline gliomas (DMGs). Approximately 75 % of these alterations occur in *H3F3A*, which encodes the histone variant H3.3, while the remaining ~25 % arise in *HIST1H3B* or *HIST1H3C*, encoding H3.1 or H3.2, respectively. These mutations result in the substitution of lysine (K) by methionine (M) at position 27 (H3K27M) (Ocasio et al., 2023). The H3K27M

alteration inhibits the activity of the Polycomb Repressive Complex 2 (PRC2), leading to a global reduction of trimethylation at H3K27 (H3K27me3). As H3K27me3 is a repressive chromatin mark involved in silencing genes that regulate developmental processes, stemness, cell cycle progression, and cell survival, its loss has profound epigenetic consequences. The resulting genome-wide hypomethylation at H3K27, together with a concomitant increase in H3K27 acetylation (H3K27ac), promotes a more transcriptionally permissive chromatin state and drives widespread dysregulation of gene expression that favors oncogenic transformation (Andrade et al., 2023; Ocasio et al., 2023).

H3.3K27M mutations frequently co-occur with alterations in TP53 or PPM1D, whereas H3.1K27M mutations are almost invariably associated with activating mutations in ACVR1. Owing to their dominant and oncogenic effects on chromatin regulation, these histone variants are commonly referred to as “oncohistones” (Andrade et al., 2023).

The H3K27M mutation is detected in approximately 80 % of DMGs, which are defined by their infiltrative growth pattern within midline CNS structures, including the brainstem (midbrain, pons, and medulla oblongata), thalamus, and spinal cord (Figure 1). Tumors arising specifically within the pons were historically classified as diffuse intrinsic pontine gliomas (DIPGs). DMGs predominantly affect children between 5 and 10 years of age and are characterized by an aggressive clinical course, with a median overall survival of approximately 12 months, representing the poorest prognosis among pediatric high-grade gliomas (Ocasio et al., 2023; Sharie et al., 2023).

1.2.2. Diffuse hemispheric glioma, H3 G34-mutant

Diffuse hemispheric gliomas (DHGs) occur exclusively within the cerebral cortex and predominantly affect adolescents and young adults between 12 and 35 years of age. At the molecular level, these tumors are characterized by mutations confined to the *H3F3A* gene, which leads to the substitution of glycine (G) at position 34 by either arginine (R) or valine (V), resulting in the so called H3G34R/V variants (Andrade et al., 2023; Ocasio et al., 2023).

In contrast to H3K27M mutations, G34R/V alterations do not induce global chromatin remodeling but instead lead to localized, nucleosome-specific epigenetic perturbations at sites containing the mutant histone. Specifically, the G34R substitution interferes with trimethylation of the adjacent lysine residue at position 36 (H3K36me3), thereby disrupting normal chromatin regulation. This alteration promotes aberrant recruitment of PRC2 and results in inappropriate gene silencing, including repression of tumor suppressor-associated transcriptional programs.

H3G34R/V mutations frequently co-occur with loss of ATRX, mutations in TP53, or amplification of PDGFRA (Ocasio et al., 2023) (Figure 1).

1.2.3. Diffuse pediatric-type high-grade glioma, H3- and IDH-wildtype

pHGGs that do not harbor histone H3 and isocitrate dehydrogenase (IDH) mutations represent a heterogeneous group of brain tumors that lack the characteristic 'oncohistone' mutations observed in diffuse midline and diffuse hemispheric gliomas. Instead, these tumors are commonly defined by recurrent genetic alterations, including amplifications or mutations affecting *PDGFRA*, *TP53*, *NF1*, *EGFR*, and *MYCN*. H3- and IDH-wildtype pHGGs have been reported to arise in both supratentorial and midline CNS compartments and occur across a broad age spectrum encompassing children, adolescents, and young adults (Ocasio et al., 2023) (Figure 1).

1.2.4. Infant-type hemispheric glioma

Infant-type hemispheric gliomas arise within the cerebral hemispheres and predominantly affect very young children, with a reported median age at diagnosis of approximately 2.8 months. The majority of these tumors (around 80 %) are driven by oncogenic gene fusions involving receptor tyrosine kinases (RTKs), including c-ros oncogene 1 receptor tyrosine kinase (*ROS1*), anaplastic lymphoma kinase (*ALK*), neurotrophic tyrosine kinase receptor (*NTRK*), and mesenchymal-epithelial transition factor (*MET)* (Clarke et al., 2020; Ocasio et al., 2023) (Figure 1). In the resulting fusion proteins, the native regulatory domains of the RTKs are replaced by fusion partners, resulting in constitutive kinase activation and sustained proliferative signaling, that bypasses normal growth control mechanisms. Owing to their strong oncogenic potential, these RTK fusions typically occur as isolated driver events and are not accompanied by additional recurrent genetic mutations or alterations (Bagchi et al., 2025; Clarke et al., 2020)

1.2.4.1. Anaplastic lymphoma kinase-driven IHGs

Anaplastic lymphoma kinase (ALK), encoded by the *ALK* gene in humans, functions as a RTK involved in the regulation of multiple oncogenic signaling cascades, including the Wnt/β-catenin, MAPK/AKT/mTOR, and JAK/STAT pathways (Ahmed et al., 2024). Under physiological conditions, activation of ALK is initiated through binding of FAM150 family ligands to its extracellular domain, which induces receptor dimerization and subsequent activation of the intracellular kinase domain, leading to downstream signal transduction (Hallberg & Palmer, 2016; Poei et al., 2024).

In IHGs, ALK represents one of the most frequently altered RTKs. Approximately 47 % of RTK fusion-positive IHGs harbor ALK rearrangements (Chavaz et al., 2025), and patients with ALK-altered tumors have been reported to exhibit a 5-year overall survival rate of 53.8 % (Guerreiro Stucklin et al., 2019). A broad range of ALK fusion partners has been described in IHGs, including PPP1CB, CCDC88A, EML4, HIP1L, PRKAR2A, SPTBN1, MAD1L1, MAP2, MSI2, SPECC1L1, SYNDIG1L, ZC3H7A, and CLIP2A (Clarke et al., 2020). ALK fusions are not restricted to IHGs and have also been identified in other malignancies, such as anaplastic large-cell lymphoma (ALCL) and non-small-cell lung cancer (NSCLC) (Hallberg & Palmer, 2016).

1.3. Treatments for pHGG

1.3.1. Standard treatments for pHGGs

The WHO classification has highlighted that pediatric gliomas are molecularly and biologically distinct from adult gliomas, exhibiting marked differences in clinical behavior and therapeutic response that require age- and entity-specific treatment strategies. Nevertheless, current therapeutic regimens for pHGGs remain largely adapted from adult treatment paradigms and demonstrate limited efficacy in children (Chatwin et al., 2021).

Standard treatment for pHGGs typically involves a multimodal approach consisting of maximal safe surgical resection followed by radiotherapy (RT), administered with concurrent or adjuvant chemotherapy (Vanan & Eisenstat, 2014), although therapeutic strategies vary depending on tumor subtype. Gross total resection (GTR) is considered the preferred initial intervention, as it has been shown to significantly prolong patient survival (Yang et al., 2013). Accordingly, the surgical objective is maximal safe resection, aiming to achieve complete tumor removal whenever possible while preserving neurological function. However, this goal is often difficult or unattainable in diffusely infiltrative or midline tumors, such as DMGs, due to the involvement of critical brain regions that regulate vital functions including respiration and cardiac control (Noon & Galban, 2023).

Consequently, RT constitutes the standard of care for most children following surgery or in cases where surgical resection is not feasible. Owing to the high risk of neurodevelopmental toxicity, RT is generally avoided in children younger than three years of age. When applied, RT is typically delivered as focal irradiation with total doses ranging from 54 to 60 Gy, fractionated at 1.8 Gy per day over five days per week for approximately six weeks (Fernando et al., 2024). In certain tumor entities, most notably DMGs, RT provides only transient

symptomatic improvement and a modest delay in tumor progression and is therefore regarded as largely palliative (Bartels et al., 2011; Jansen et al., 2012; Metselaar et al., 2021).
Chemotherapy aims to target proliferating tumor cells and can be administered before, during, or after RT. In this context, chemotherapy plays a particularly important role in patients for whom irradiation is contraindicated or must be delayed. Temozolomide (TMZ), an alkylating agent, is the most frequently used chemotherapeutic drug in pHGGs. However, when administered as monotherapy, TMZ has failed to demonstrate a survival benefit in pediatric patients (Blionas et al., 2018; Kline, Felton, et al., 2018) and is therefore commonly combined with surgery, radiotherapy, or other chemotherapeutic agents (Mallick et al., 2015; Perwein et al., 2023). Additional agents such as CCNU (chloroethyl-cyclohexyl nitrosourea) and Vincristine have been extensively evaluated in pediatric glioma trials (Jakacki et al., 2016), yet combination regimens including PCV (Procarbazine, CCNU, and Vincristine) have not shown superior survival outcomes compared with TMZ-based approaches (Brada et al., 2010; Parasramka et al., 2017). Although the incorporation of TMZ has improved certain treatment protocols, its use is associated with increased hematological, gastrointestinal, and hepatic toxicities in clinical trials (Shi et al., 2021; Wang et al., 2015).
Overall, despite the application of intensive multimodal treatment strategies, meaningful improvements in survival outcomes for children with pHGGs have remained limited.

1.3.2. Radiotherapy

Radiation therapy (RT) represents one of the most established and widely used treatment modalities in oncology. In clinical practice, RT is typically delivered focally to the tumor using ionizing radiation beams. Ionizing radiation induces DNA damage in target cells either directly, through the generation of single-strand breaks (SSBs) and double-strand breaks (DSBs), or indirectly via the formation of reactive oxygen species (ROS), which subsequently damage DNA (Gong et al., 2021). When such lesions cannot be adequately repaired, they result in irreversible growth arrest, and ultimately cell death.

At present, photon-based radiotherapy (X-rays) remains the most commonly applied form of ionizing radiation worldwide (Pompos et al., 2022). In recent years, however, particle-based irradiation modalities, including proton and carbon ion therapy, have gained increasing attention. Proton beam therapy (PBT) provides a dosimetric advantage over photon radiotherapy owing to the ‘Bragg peak’ phenomenon, whereby protons deposit relatively low energy along their entry path, followed by a sharp peak of energy deposition at a defined tissue depth, with minimal dose beyond this point. As a result, PBT reduces radiation exposure to surrounding healthy brain tissue and is associated with a lower risk of long-term toxicities,

including neurocognitive impairment, endocrine dysfunction, vascular injury, and secondary malignancies (Chambrelant et al., 2021; Lassaletta et al., 2023; Zając-Grabiec et al., 2025). Despite these advantages, clinical evidence supporting proton therapy specifically in pHGGs remains limited, and no convincing survival benefit over modern photon radiotherapy techniques has been demonstrated to date (Chambrelant et al., 2021; Muroi et al., 2020).

Carbon ion radiotherapy is characterized by a higher linear energy transfer (LET), defined as the amount of energy deposited per unit track length (keV/µm), and a higher relative biological effectiveness (RBE), which reflects the biological potency of a radiation type compared with reference radiation, typically photons. Owing to these properties, carbon ions induce more direct, complex, and less repairable DNA damage than photons or protons. Whereas photon and proton irradiation predominantly cause indirect and relatively simple DNA lesions, such as base damage, SSBs, and spatially separated DSBs, carbon ion beams mainly generate direct, densely clustered DNA damage consisting of multiple DSBs within nanometer-scale regions, which are repaired inefficiently or incompletely (Melia & Parsons, 2023). In addition, the biological effectiveness of carbon ions is less dependent on oxygen availability, resulting in a lower oxygen enhancement ratio (OER). This property underlies the proposed advantage of carbon ion therapy in hypoxic and radioresistant tumors (Sokol & Durante, 2023). However, clinical data on carbon ion therapy in pHGGs are extremely sparse, and no large pediatric cohorts or randomized clinical trials have evaluated its efficacy in this setting.

Both photon- and particle-based radiotherapy activate the same fundamental DNA repair pathways, including non-homologous end joining (NHEJ), homologous recombination (HR), base excision repair (BER), and single-strand break repair (SSBR). The nature and complexity of radiation-induced DNA lesions largely determine which repair mechanisms are preferentially engaged. Highly complex DNA damage, as induced by high-LET radiation such as carbon ions, is associated with increased reliance on HR, whereas the repair of photon- and proton-induced DNA damage is more frequently dominated by BER, SSBR, and classical NHEJ (Roobol et al., 2020).

In the context of pHGGs, proton therapy is increasingly implemented with the primary goal of reducing radiation-associated toxicity, although a survival advantage over state-of-the-art photon radiotherapy has not been demonstrated. In contrast, carbon ion therapy remains investigational and is currently supported mainly by radiobiological rationale and limited adult clinical data rather than robust pediatric evidence.

1.3.3. Targeted agents for pHGGs

The clinical use of targeted therapies for pHGGs has increased in cases where validated and druggable oncogenic drivers are present. However, for the majority of pHGGs, particularly histone mutant tumors, targeted treatment options remain scarce, investigational and associated with only modest clinical benefit.

A major recent milestone was achieved in 2025, when Dordaviprone (ONC201; Modeyso) received approval from the U.S. Food and Drug Administration (FDA) for the treatment of adults and children aged at least one year with H3K27M mutant DMGs. This approval represents the first FDA-approved systemic therapy for this entity (Zafar et al., 2025). ONC201 is a first in class imipridone that exerts antitumor effects through dual mechanisms, including antagonism of dopamine receptor D2/3 and hyperactivation of the mitochondrial caseinolytic protease P (ClpP). These actions suppress pro-survival signaling, disrupt mitochondrial oxidative phosphorylation, and activate the integrated stress response, ultimately promoting proapoptotic signaling pathways (Prabhu et al., 2020; Venneti et al., 2023). In addition to monotherapy, ONC201 has been evaluated in combination with phosphoinositide 3 kinase (PI3K) pathway inhibitors (Jackson et al., 2023), RT and/or TMZ (Zhou et al., 2025), and histone deacetylase inhibitors (HDACi) (Bentayebi et al., 2024; Borsuk et al., 2021).

Given that many pHGGs are driven by profound epigenetic dysregulation and lack readily druggable genetic alterations, particularly H3-altered tumors, HDACi have attracted increasing interest as therapeutic candidates. By inhibiting histone deacetylases, these agents increase histone acetylation and are thought to restore expression of silenced tumor suppressor genes, induce differentiation, and promote apoptosis in tumor cells (Xiang et al., 2025). Despite strong preclinical rationale, HDACi have shown limited efficacy as monotherapy in pHGGs and have not achieved broad regulatory approval. Consequently, their potential clinical utility is currently viewed primarily within combination regimens, especially as radiosensitizers or components of multimodal treatment strategies (Hennika et al., 2017; Metselaar et al., 2021).

For pHGGs harboring RTK alterations, such as IHGs, receptor tyrosine kinase inhibitors (RTKi) are increasingly incorporated into clinical management.
To date, five ALK inhibitors (ALKi) have been approved by the FDA, including Crizotinib as a first-generation agent, Alectinib, Ceritinib, and Brigatinib as second-generation agents, and Lorlatinib as a third-generation agent (Ahmed et al., 2024; Poei et al., 2024). Lorlatinib is characterized by high blood-brain barrier (BBB) penetrance and has demonstrated objective radiographic and clinical responses in patients with IHG (Shahab et al., 2023; Tsai et al., 2024;

Wilson et al., 2025). However, as observed in both clinical and preclinical settings, acquired resistance frequently develops, limiting the durability of therapeutic responses (Clarke et al., 2020; Gene-Olaciregui et al., 2023; Liang et al., 2021).

NTRK inhibitors (NTRKi) approved for solid tumors harboring NTRK gene fusions, including IHGs, include Larotrectinib, Entrectinib, and Repotrectinib, all of which demonstrate intracranial activity (Drilon et al., 2018; Lassen, 2019; Mayr et al., 2020). Clinical outcomes have been encouraging, with higher response rates and progression free survival reported in pediatric patients compared with adults (Drilon, 2019; Rizzaro et al., 2025).

Avapritinib is currently the only FDA-approved PDGFRA inhibitor (PDGFRAi) with reported clinical activity in PDGFRA-altered pHGGs, based on early compassionate use data from a small cohort (Mayr et al., 2025). In contrast, a phase I pediatric trial evaluating Imatinib in newly diagnosed brainstem glioma and recurrent high-grade glioma demonstrated tolerability, and suggested CNS penetration, but failed to show compelling efficacy as a PDGFRA directed therapy (Pollack et al., 2007). Other PDGFRA inhibitors, including Crenolanib and Dasatinib, have been explored in pHGG cohorts or preclinical models. However, none have received FDA approval for this indication, and results have largely been limited to safety or exploratory endpoints (Broniscer et al., 2018; Siegel et al., 2025; Tinkle et al., 2021).

Three MET inhibitors (METi), Crizotinib, Capmatinib, and Tepotinib, have been approved by the FDA for non-small cell lung cancer (NSCLC). Crizotinib, when combined with the PDGFRAi Dasatinib, was poorly tolerated in a phase I trial involving children with recurrent or progressive pHGG and DIPG (Broniscer et al., 2018). Capmatinib has demonstrated promising activity in preclinical glioma models (Zuckermann et al., 2024) but has not yet been evaluated in pediatric patients. Moreover, Capmatinib combined with Bevacizumab failed to show clear efficacy in adult high-grade glioma (Falchook et al., 2025). Tepotinib has shown encouraging intracranial activity in NSCLC brain metastases (Bestvina et al., 2022; Friese-Hamim et al., 2022) and in adult glioblastoma (Rodriguez et al., 2025).

Finally, four FGFR inhibitors (FGFRi), Erdafitinib, Pemigatinib, Infigratinib, and Futibatinib, have received FDA approval for non-CNS malignancies. Erdafitinib (Lee et al., 2023; Pant et al., 2023) (NCT03210714), Pemigatinib (Spanggaard et al., 2025) and Infigratinib (NCT01975701) have been investigated in CNS tumors. However, none currently hold an FDA indication for the treatment of pHGGs.

1.3.4. Therapeutic strategies to overcome the blood-brain barrier

The blood-brain barrier (BBB) is a highly specialized neurovascular interface that controls the exchange of substances between the systemic circulation and the CNS and represents a major obstacle to effective systemic therapy for pHGGs (Ajayi et al., 2026). Brain capillaries are composed of endothelial cells that are interconnected by complex tight junctions, which markedly restrict paracellular diffusion. These endothelial cells share a basal lamina with pericytes, providing structural support, and contributing to barrier integrity through tight regulation of transcytosis. Astrocytic end feet envelop approximately 90 % of brain capillaries and play a central role in maintaining BBB homeostasis. In addition, high expression of efflux transporters, which actively export many therapeutic agents from the CNS back into the circulation, further limits drug accumulation within brain tumors (Ajayi et al., 2026; Wu et al., 2023). As a result, numerous therapeutic strategies are currently being investigated to overcome BBB-mediated restrictions in drug delivery.

1.3.4.1. Intrathecal therapies

Convection enhanced delivery (CED) addresses BBB-related limitations by allowing direct intraparenchymal administration of therapeutic agents, thereby enabling elevated local drug concentrations while limiting systemic toxicity. In this approach, a catheter is stereotactically inserted into the brain parenchyma and drugs are infused slowly under controlled positive pressure. This generates convective bulk flow, which distributes the infused compound through the extracellular spaces of the brain tissue (Sperring et al., 2023).

The PNOC015 trial demonstrated the feasibility and safety of repeated CED administration of MTX110, an aqueous formulation of the HDACi Panobinostat, in children with newly diagnosed DIPG. This study provided evidence of effective intratumoral drug distribution and acceptable toxicity profiles (Mueller et al., 2023). In addition, CED delivery of a nanoliposomal formulation of Irinotecan has been evaluated in early phase pediatric studies, further supporting CED as a viable strategy for localized drug delivery in DIPG (Mueller et al., 2025; Narsinh et al., 2025).

An alternative approach for CNS drug administration is intrathecal delivery using Ommaya pumps. An Ommaya pump consists of an implantable reservoir connected to a ventricular catheter, enabling repeated administration of drugs or cell-based therapies directly into the cerebrospinal fluid. This method has been shown to be safe and well tolerated in children with brain tumors (Peyrl et al., 2014) and is routinely used in the clinical setting to deliver chemotherapeutic agents such as Topotecan (Blaney et al., 2013) as well as chimeric antigen receptor (CAR) T cell therapies (Monje et al., 2025).

1.3.4.2. Nanoparticle-based drug delivery strategies

Nanoparticle based drug delivery strategies seek to enhance therapeutic exposure in pHGGs by overcoming limited BBB penetration and reducing systemic toxicity (Power et al., 2022). Among the available nanoparticle platforms, liposomes, and lipid nanoparticles (LNPs) have been studied most extensively due to their favorable biocompatibility and their capacity to encapsulate small molecule drugs or nucleic acids (Hou et al., 2021; Khare et al., 2023; Zuberi et al., 2025).

Liposomal formulations have progressed furthest toward clinical translation and have been shown to be safely administered directly into the brain, supporting their feasibility for local drug delivery approaches in CNS tumors (Mueller et al., 2025; Wagner et al., 2008). By comparison, LNP-based strategies in pHGGs are still largely at the preclinical stage. Experimental studies indicate that LNPs are capable of delivering mRNA, siRNA, or gene editing components to tumor cells *in vivo*, highlighting their emerging potential as future therapeutic platforms (Cao et al., 2025; Rosenblum et al., 2020; Tong et al., 2025; Wang et al., 2025; Zhang et al., 2025; Zhao et al., 2024).

1.3.4.3. Focused ultrasound-mediated BBB disruption

Low intensity focused ultrasound (FUS) combined with microbubbles enables transient and spatially controlled opening of the BBB, thereby facilitating enhanced delivery of systemically administered therapeutics to brain tumors (Gorick et al., 2022; Zhu et al., 2024). Early first in-human studies have demonstrated the feasibility and safety of FUS-mediated BBB opening in patients, representing a major technological advance in non-invasive approaches to CNS drug delivery (Abrahao et al., 2019; Chen et al., 2023). This strategy has also been successfully applied in patients with DMG (Wu et al., 2025). Ongoing clinical trials are currently evaluating FUS in combination with the chemotherapeutic agents Doxorubicin and Etoposide in patients with DMG (NCT05630209, NCT05762419).

Importantly, BBB opening alone is not sufficient to ensure therapeutic efficacy, as clinical benefit depends critically on the selection of the systemic agent and the underlying tumor biology.

1.3.5. Immunotherapeutic approaches

Among current immunotherapeutic strategies, chimeric antigen receptor (CAR) T cell therapy has demonstrated the most compelling early clinical activity in pHGGs. CAR T cells are genetically engineered T lymphocytes that express synthetic receptors combining an antigen-binding domain (typically derived from a monoclonal antibody) with intracellular T cell signaling

domains, enabling major histocompatibility complex (MHC)-independent recognition and targeted killing of tumor cells (Sterner & Sterner, 2021). Phase I clinical trials in patients with DMG have evaluated GD2-CAR T cells (Lin et al., 2024; Monje et al., 2025) as well as B7-H3 CAR T cells (Vitanza et al., 2025), with early results indicating encouraging clinical and radiographic responses.

Immune checkpoint inhibition (ICI) has also been explored in pediatric cancers. ICI is an immunotherapeutic strategy that enhances antitumor immune responses by blocking inhibitory receptor-ligand interactions that physiologically restrain T cell activation, thereby restoring cytotoxic T cell function against tumor cells (Pardoll, 2012; Ribas & Wolchok, 2018). A pediatric clinical trial investigating the combination of Nivolumab, a programmed cell death protein 1 (PD-1) inhibitor, and Ipilimumab, a cytotoxic T lymphocyte associated protein 4 (CTLA-4) inhibitor, failed to improve survival in children with newly diagnosed DIPG and other high-grade CNS malignancies (Dunkel et al., 2023). In contrast, treatment with Nivolumab in pediatric cancers characterized by high tumor mutational burden and mismatch repair deficiency resulted in durable responses and prolonged survival, highlighting the importance of molecular context for checkpoint inhibitor efficacy (Das et al., 2023).

Therapeutic cancer vaccines represent an emerging immunotherapeutic strategy in pHGGs, with the goal of eliciting tumor specific T cell responses against shared or tumor restricted antigens. The most advanced vaccine approach in this setting targets the H3K27M neoantigen, which is present in the majority of DMGs and absent from normal tissues (Ochs et al., 2017). Subsequent early phase clinical studies demonstrated that vaccination with H3K27M-derived peptides is feasible, induces robust antigen-specific immune responses, and is associated with prolonged survival in a subset of adult patients with DMG (Boschert et al., 2024; Grassl et al., 2023; Hotchkiss et al., 2024).

1.3.6. Combination treatments for pHGGs

Monotherapies frequently fail to achieve durable clinical benefits. Tumor cell plasticity enables dynamic adaptation to therapeutic pressure through transcriptional reprogramming, epigenetic remodeling, and activation of compensatory signaling pathways (Meacham & Morrison, 2013; Shaffer et al., 2017; Sharma et al., 2010). Consequently, resistant cell populations frequently emerge, limiting long-term efficacy. This adaptive capacity provided a strong rationale for the development of combination treatment strategies in recent years.

A central objective of combination cancer therapies is to achieve synergistic interactions between treatment modalities, whereby the combined antitumor effect exceeds the additive activity of individual agents, resulting in enhanced therapeutic efficacy (Bukowska et al., 2014; Metselaar et al., 2021). In addition to synergy, combination strategies enable simultaneous targeting of multiple biological pathways and cellular subpopulations within tumors, thereby addressing intratumoral heterogeneity and reducing the likelihood of resistance development (Palmer & Sorger, 2017). Moreover, when robust synergistic interactions are achieved, combination regimens may permit dose reductions of individual agents while maintaining efficacy, potentially limiting treatment-related toxicities, and adverse effects (Bukowska et al., 2014; Metselaar et al., 2021).

1.3.6.1. Targeted therapy with RT

For patients with DMG, RT remains the primary therapeutic option, yet is largely palliative. This has driven growing interest in strategies aimed at improving the therapeutic impact of RT in this patient population. To date, extensive preclinical and clinical efforts have evaluated a wide range of combination approaches incorporating RT.

RT exerts its antitumor effects primarily through induction of DNA damage, and unrepaired lesions ultimately trigger tumor cell death. This mechanism creates opportunities to enhance RT efficacy by targeting DNA damage response pathways and apoptosis signaling using small molecule inhibitors. Multiple targeted agents have demonstrated radiosensitizing potential in preclinical models of pHGGs. These include the PARP inhibitor (PARPi) Olaparib which enhances RT-induced DNA damage and impairs DNA repair capacity in pediatric glioma models (Vuurden et al., 2011). More recently, H3K27M-altered DMGs have been shown to exhibit HR deficiency, rendering these tumors particularly sensitive to combined PARP inhibition and RT (Guo et al., 2025). Similarly, inhibition of the DNA damage response kinase ataxia-telangiectasia mutated (ATM) using the brain-penetrant inhibitor AZD1390 increases radiation sensitivity by disrupting DSB repair and promoting tumor cell apoptosis (Xie et al., 2023). In addition, dual inhibition of anti-apoptotic B cell lymphoma-2/-extra large (BCL-2/-XL) proteins using Navitoclax synergizes with irradiation to induce apoptosis in preclinical models of H3K27M-altered DMGs (Vardon et al., 2025). However, clinical translation has so far been disappointing. The PARPi Veliparib administered concurrently with RT did not improve survival outcomes in children with newly diagnosed pHGGs in a phase 2 trial. Notably, tumors harboring H3K27M mutations were excluded from this study, restricting applicability to DMGs (Karajannis et al., 2024). Similarly, concomitant treatment with the Wee1 kinase inhibitor Adavosertib and RT in DIPG patients was feasible and well tolerated but failed to significantly

improve overall survival compared with historical controls (Mueller et al., 2022). In contrast, a phase 1/2 study demonstrated that post-RT administration of the CDK4/6 inhibitor Ribociclib in DIPG patients was pharmacokinetically feasible and biologically active; however, the trial design did not directly assess Ribociclib as a radiosensitizer (DeWire et al., 2020).

Given the prominent role of epigenetic dysregulation in many pHGGs, epigenetic modulators such as HDACi have also been explored as radiosensitizing agents. Quisinostat has shown encouraging activity *in vitro* and in preclinical tumor models (Cascio et al., 2023), while Panobinostat (Monje et al., 2023) and Valproic Acid (Su et al., 2020) have already advanced into clinical evaluation in combination with RT, although without demonstrating a significant clinical benefit.

In addition, targeting oncogenic drivers in conjunction with RT has demonstrated efficacy in selected molecular subtypes. In MET-driven IHG, the METi Capmatinib has been successfully validated as a radiosensitizer in preclinical models (Zuckermann et al., 2024).

In adult brain tumors, RT combined with chemotherapeutic agents, particularly TMZ, represents a standard of care and has been shown to significantly prolong patient survival (Stupp et al., 2005). In contrast, although TMZ based regimens have been extensively evaluated in pediatric patients, treatment outcomes remain poor relative to adult benchmarks (Jakacki et al., 2016).

1.3.6.2. Immunotherapy with RT

Ionizing radiation can modulate the tumor microenvironment by promoting the release of tumor-associated antigens and danger signals, enhancing antigen presentation, and altering chemokine secretion, and vascular permeability. Together, these effects may improve immune cell recruitment and convert immunologically cold tumors into a state that is more permissive to immunotherapeutic interventions (Persson et al., 2022). DMGs are characterized by low immune cell infiltration and a low tumor mutational burden, resulting in limited neoantigen presentation at the cell surface and thereby restricting the efficacy of immune checkpoint inhibitor monotherapy (Messiaen et al., 2023; Price et al., 2021). Nevertheless, a clinical study conducted in 2018 evaluated RT in combination with the PD-1 inhibitor Nivolumab, and reported a trend toward improved survival in patients with recurrent DIPG (Kline, Liu, et al., 2018).

Preclinical studies in adult glioblastoma multiforme (GBM) further support the potential of combining RT with immunotherapy. In murine models bearing orthotopic brain tumors, Anti-PD-1 blockade administered together with RT resulted in long-term survival benefits (Zeng et al., 2013). In addition, CAR T cell therapies have demonstrated synergistic activity when combined with RT in GBM models, including GD2-CAR T cells (Murty et al., 2020) and NKG2D-CAR T cells (Weiss et al., 2018). To date, systematic evaluation of these combination strategies in pHGGs remains limited.

It is important to note that many targeted therapies have been tested in combination with RT, often being administered sequentially after irradiation, rather than being formally assessed as radiosensitizers when given concurrently with RT. Despite encouraging preclinical data, combination approaches evaluated in clinical studies have thus failed to produce meaningful improvements in survival or overall clinical outcomes in pHGGs (Metselaar et al., 2021). Accordingly, no combination strategies involving systemic immunotherapies or targeted agents in conjunction with RT are currently approved as first line treatments for pHGGs.

2. Aims and objectives

2.1. Comparing the radiosensitization potential of various compound classes in pediatric-type diffuse high-grade glioma

pHGGs remain among the most lethal pediatric brain tumors, and current standard therapies, including RT for DMGs, are largely palliative. Therefore, I aimed to contribute to the improvement of RT-based treatment strategies for these patients. Despite extensive preclinical and clinical efforts, combination therapies incorporating RT have not led to meaningful improvements in clinical outcomes. Moreover, targeted therapies have not been systematically evaluated as radiosensitizers in pHGGs, and their potential use as first-line combination partners with RT remains largely unexplored.

The primary aim of this project was to systematically identify, evaluate, and compare targeted compounds that enhanced the efficacy of RT in pHGGs.

To achieve this aim, I first performed high-throughput combination screening using a curated library of FDA-approved drugs in combination with RT across a diverse panel of patient-derived pHGG cell models, alongside non-malignant control cells, to identify potential radiosensitizing agents.

As a further objective, I validated the identified candidate compounds *in vitro* using multiple orthogonal readouts, including cell viability, apoptosis induction, long-term growth suppression, and DNA damage responses.

Beyond *in vitro* validation, I aimed to test promising drug+RT combinations in *in vivo* xenograft models to assess therapeutic efficacy under physiologically relevant conditions.

In addition, I evaluated the pharmacokinetic properties of selected compounds *in vivo* to determine whether limited bioavailability or blood-brain barrier penetration constrained radiosensitization efficacy despite robust *in vitro* activity.

2.2. Overcoming ALK inhibitor resistance in ALK-fusion infant-type hemispheric glioma

Despite inducing robust initial responses, treatment with the ALK inhibitor Lorlatinib has increasingly been associated with the development of acquired resistance in ALK-driven infant-type hemispheric gliomas (IHGs).

The overarching aim of this project was to elucidate the mechanisms underlying acquired resistance to Lorlatinib in ALK-fusion-driven IHG, with the long-term goal of identifying rational combinatorial treatment strategies that could improve therapeutic durability.

To address this aim, I pursued several specific objectives.

First, I established and characterized stable *in vitro* and *in vivo* models of Lorlatinib resistance through prolonged drug exposure, thereby enabling the systematic investigation of resistance-associated phenotypes.

Second, I functionally characterized the resistant state, with a particular focus on the regulation of proliferation and apoptosis under continued ALK inhibition. This included a comparative analysis with an additional ALK inhibitor to determine whether resistance mechanisms were compound-specific or class-wide.

A further objective was to define transcriptional programs associated with acquired resistance by performing bulk RNA sequencing of resistant tumor models and identifying enriched signaling pathways that could support tumor survival under ALK inhibition.

Based on these findings, I aimed to identify and functionally validate therapeutic vulnerabilities of resistant tumor cells through targeted drug testing.

Finally, I sought to prioritize candidate combinatorial treatment strategies for subsequent evaluation in preclinical pHGG mouse models, thereby providing a translational framework for overcoming ALK inhibitor resistance in this patient population.

3. Materials and Methods

3.1. Materials

3.1.1. Cells

Cell cultures	Alteration	Specie	Supplier	Culture conditions
SU-DIPG-XIII (13)	H3.3 K27M	Human PDX	Michelle Monje, Stanford University, USA	TSM, TrypLE
HSJD-DIPG-007	H3.3 K27M	Human PDX	Ángel Montero Carcaboso, Sant Joan de Déu Barcelona Hospital, Spain	TSM, TrypLE
SU-DIPG-XVII (17)	H3.3 K27M	Human PDX	Michelle Monje, Stanford University, USA	TSM, TrypLE
SU-DIPG-XIX (19)	H3.3 K27M	Human PDX	Michelle Monje, Stanford University, USA	TSM, TrypLE
SU-DIPG-XXI (21)	H3.1 K27M	Human PDX	Michelle Monje, Stanford University, USA	TSM, TrypLE
SU-DIPG-IV (4)	H3.1 K27M	Human PDX	Michelle Monje, Stanford University, USA	TSM, TrypLE
SJ-GBM2	H3 WT	Human PDX	Peter J Houghton, St Jude, Memphis, USA	TSM, TrypLE
HSJD-GBM-001	H3 WT	Human PDX	Ángel Montero Carcaboso, Sant Joan de Déu Barcelona Hospital, Spain	TSM, TrypLE
HSJD-GBM-002	H3 G34R	Human PDX	Ángel Montero Carcaboso, Sant Joan de Déu Barcelona Hospital, Spain	TSM, TrypLE
NSC	Non-malignant	Human, iPSC-derived	Tuyu Zheng, DKFZ Heidelberg, Germany	DMEM/F-12, Accumax
HEK 293T	Non-malignant	Human	ATCC, Manassas, USA	DMEM, Trypsin
SJ-DIPGx7	H3.3 K27M	Human PDX	Suzanne Baker, St Jude Children's Research Hospital, Memphis, USA	TSM, TrypLE
SU-DIPG-VI (6)	H3.3 K27M	Human PDX	Michelle Monje, Stanford University, USA	TSM, TrypLE
BI#190	PPP1CB::ALK, Trp53 KO	Mouse (CD1)	Britta Ismer, DKFZ Heidelberg, Germany	TSM, Accumax

3.1.2. Cell culture reagents

Product	Supplier	Catalogue number
Accumax, Cell Aggregate Dissociation	Life Technologies	00-4666-56
Antibiotic-Antimycotic	VWR	HYCLSV30079.01
B-27 Supplement Minus Vitamin A (50x)	Life Technologies	12587001
CHIR-99021	Axon-Medchem	1386
Chroman1	MedChemExpress	HY-15392
Deoxyribonuclease I, 100 mg	Worthington	LS002007
DMEM/F-12	Life Technologies	11320074
Dulbecco's Balanced Salt Solution (DPBS)	Gibco	14190250
Emricasan	Selleckchem	S7775
FBS Superior	Sigma-Aldrich	S0615
FGF2	Peprotech	100-18B
GlutaMAX Supplement	Life Technologies	35050061
Heparin Solution, 0.2%	Sigma-Aldrich	H3149-10KU
HEPES Buffer Solution	Life Technologies	15630056
L-Glutamine (200 mM)	Life Technologies	25030081
MEM Non-Essential Amino Acids Solution 10 mM (100x)	Life Technologies	11140035
MgCl2 (1M), 100 ml	Life Technologies	AM9530G
Neurobasal-A Medium	Life Technologies	10888022
Penicillin-Streptomycin (10.000 U/ml)	Life Technologies	15140122
Poly-Amine Supplement (1000x)	Sigma	P8483
Recombinant Human Epidermal Growth Factor (hEGF)	Peprotech	AF-100-15
Recombinant Human Fibroblast Growth Factor (hFGF)	Peprotech	AF-100-18B
Recombinant Human PDGF-AA	Peprotech	100-13A
SB-525334	Selleckchem	S1476
Sodium Pyruvate, 100 mM	Life Technologies	11360039
Synth-a-freeze cryopreservation medium	Thermo Fisher Scientific	A1254201
Trans-ISRIB	Tocris	5284
Trypan Blue Dye	BioRad	1450013
TrypLE Express Enzyme (1x), no phenol red	Life Technologies	12604013
Trypsin-EDTA Solution	Sigma-Aldrich	T4049

3.1.3. Mice

Mouse strain	Supplier	Immune status
Crl:CD1 (CD1)	Janvier Labs, France	Immunocompetent
Crl:CD1-Foxn1nu (CD1 nude)	Charles River, Germany	Immunocompromised
NOD-*Prkdc*^{scid}-*IL2rg*^{Tm1}/Rj (NXG)	Janvier Labs, France	Immunodeficient
NOD-*Rag2*^{tm1}-*Il2rg*^{tm1}/Rj (NRG)	Janvier Labs, France	Immunodeficient

3.1.4. Reagents, kits and dyes

Product	Supplier	Catalogue number
4% PFA in PBS	Santa Cruz	Sc-281692
ABC kit	Vector Laboratories	PK-6100
AllPrep DNA/RNA Mini Kit	Qiagen	80204
Annexin V binding buffer	BioLegend	422201
Annexin V-FITC (90 µg/ml)	BioLegend	640906
CellTiter-Glo	Promega	G7572
Click-iT Plus EdU Alexa Fluor 647 Flow Cytometry Kit	Invitrogen, Thermo Fischer Scientific	C10635
DAB kit	HIGHDEF® DAB Chromogen/Substrate Set	ENZ-ACC105-0200
donkey a-rabbit	Jackson ImmunoResearch	711-065-152
Eukitt mounting medium	Orsatec GmbH	6.32.01.0001.04.01.2
PE Mouse Anti-H2AX (pS139) (50µg/ml)	BD Biosciences	562377
PE Mouse IgG1 k Isotype control (0.2mg/ml)	BD Biosciences	554680
Propidium Iodide Solution, 0.5mg/ml	BioLegend	B283508
rabbit a-Ki67	Abcam	AB15580
RNA ScreenTape	Agilent Technologies	5067-5576
RNA ScreenTape Ladder	Agilent Technologies	5067-5578
RNA ScreenTape Sample Buffer	Agilent Technologies	5067-5577
Ultrapure Water	Invitrogen	10977-049

3.1.5. Consumables

Product	Supplier	Catalogue number
10 ml Clear Advantage Reagent Reservoir	Integra Biosciences	4332
14 ml Polypropylene Round-Bottom Tube	Falcon	352059

25cm2 Flask, Ultra-Low Attachment Surface	Corning	4616
384U PrimeSurface® 3D Culture Spheroid White Plates	S-Bio	MS-9384W
5 ml Polystyrene Round-Bottom Tube	Falcon	352054
5 ml Polystyrene Round-Bottom Tube with Cell-Strainer Cap	Falcon	352235
75 cm2 Flask, Ultra-Low Attachment Surface	Corning	3814
Bacillol AF Bode	Hartmann	15062
Bepanthen eye cream	Bayer	81552983
Cell Strainer 40 µm	Falcon	352340
Cellstar 10 ml serological pipette	Greiner Bio-One	607180/10 ml
Cellstar 25 ml serological pipette	Greiner Bio-One	760180/25 ml
Cellstar 5 ml serological pipette	Greiner Bio-One	606180/5 ml
Cellstar 50 ml serological pipette	Greiner Bio-One	768180/50 ml
Centrifuge tube 15 ml	TPP	91015
Centrifuge tube 50 ml	TPP	91050
Costar 6 Well Plate, Ultra-Low Attachment Surface	Corning	3471
Costar 96 Well Plate, Round Bottom, Ultra-Low Attachment Surface	Corning	7007
Costar 96 Well Plate, Ultra-Low Attachment Surface	Corning	3474
CRYO.S	Greiner Bio-One	122277
Disposable Scalpel No 23	Feather	02.001.30.023
Dual-Chamber Cell Counting Slides	BioRad	1450011
Embedding cassettes: Biopsie-Einbettkassetten Swingsette™	Carl Roth	XY29.1
Histoacryl (1x)	B. Braun	1050044
Inject-F Luer Solo 1m syringe	B. Braun	9166017V
Isofluran	CP-Pharma	AP/DRUGS/220/96
Microlance 3 16G	BD Biosciences	300637
Microvette® 500 Lithium Heparin LH, 500 µl	SARSTEDT AG & Co.	2.013.045.100
Nalgene Filtration Products	Thermo Fisher Scientific	567-0010
Omican 100	B. Braun	9151141S
PCR SingleCap 8er SoftStrips 0.2 ml	Biozym	710971
Petri dish, 10 cm	Greiner Bio-One	633180
Petri dish, 15 cm	Greiner Bio-One	639161
Petri dish, 6 cm	Greiner Bio-One	628102
Safe-Lock Tubes 1.5 ml	Eppendorf	12682
Safe-Lock Tubes 2.0 ml	Eppendorf	12776

Stericup Quick Release	Merck	S2GPU05RE
Stericup Receiver Flask 500ml	Merck	S200B05RE
Steritop 45 mm Neck Size	Merck	S2GPT05RE
Epredia™ SuperFrost Plus™ microscope slides	Thermo Fisher Scientific	10149870
White bottom 96-well plates	Greiner Bio-One	655073

3.1.6. Drugs

Drug	Supplier	Catalogue number
A-1331852	Selleckchem	S7801
Alpelisib	MedChemtronica AB	HY-15244
AZD4320	MedChemtronica AB	HY-112416
Bortezomib	BIOZOL DIAGNOSTICA	SEL-S1013
Cobimetinib	MedChemExpress	HY-13064
Crizotinib	MedChemtronica AB	HY-50878
Entinostat	BIOZOL DIAGNOSTICA	SEL-S1053
Everolimus	MedChemtronica AB	HY-10218
Galunisertib	MedChemtronica AB	HY-13226
Lorlatinib	MedKoo Biosciences	406533
LP-118	Newave Pharmaceuticals	collaboration
Marizomib	MedChemExpress	HY-10985
Navitoclax	MedChemtronica AB	HY-10087
Panobinostat	MedChemtronica AB	HY-10224
Pelcitoclax (APG-1252-M1)	Ascentage Pharma	collaboration
Quisinostat	BIOZOL DIAGNOSTICA	SEL-S1096
Romidepsin	MedChemExpress	HY-15149
Silibinin	Sigma-Aldrich Chemie	S0417
Staurosporine	Biomol	Cay81590
Trametinib	MedChemtronica AB	HY-10999
Valproic acid (VPA)	MedChemExpress	HY-10585

3.1.7. Solvents

Product	Supplier	Catalogue number
Dimethyl-sulfoxide (DMSO)	Sigma-Aldrich	D2653-5X
D-Luciferin, Potassium Salt	Abcam	ab143655
Glucose 40%	B. Braun	2357742
Hydrochloric acid solution (1N)	Sigma-Aldrich	H9892
Hydroxypropyl-β-Cyclodextrin	Santa Cruz	sc-288158
Metapyrin (Metamizol)	Serumwerk Bernburg AG	3100197.00.00
NaCl 0.9%	B. Braun	5/12606228/0315
Polyethylenclycol 300 (PEG300)	Carl Roth	2632.1

Polyethylenclycol 400 (PEG400)	Carl Roth	0144.1
Tween80	Fisher BioReagents	152160

3.1.8. Devices and machines

Device or machine	Supplier
Automated Cell Counter TC20	BioRad
EclipseTi2 Microscope	Nikon
FACSAria Fusion	BD Biosciences
FACSCanto II	BD Biosciences
GloMax® Discover Microplate Reader	Promega
Heraeus Multifuge 3 s	Thermo Fisher Scientific
Histoscanner PrimeHisto XE	Pacific Image Electronics
In Vivo Imaging System (IVIS) Lumina LT Series III	Caliper Life Sciences, Perkin Elmer
Isofluran Vet. Med. Vapor	Drägerwerk AG
IVC Racks and cages	Tecniplast
LSRFortessa	BD Biosciences
Microtome	Leica Biosystems
Mithras LB 940 Multimode Microplate Reader	Berthold Technologies
MultiRad225	Precision X-Ray
NanoDrop Spectrophotometer	Thermo Fisher Scientific
SmART+	Precision X-Ray
Stereotactic frame	World Precision Instruments
TapeStation 4150	Agilent Technologies
ThermoLux Wärmeunterlagen	Witte + Sutor GmbH
UltraMicroPump III (UMP3)	World Precision Instruments
UMP3 UltraMicroPump	World Precision Instruments
Vacusip	Integra
XGI-8 Gas Anesthesia System	Caliper Life Sciences

3.1.9. Softwares

Software	Version	Supplier
Agilent TapeStation Software 5.1	5.1	Agilent Technologies
BD FACS Diva	9.9	BD Biosciences, Franklin Lakes, USA
BioRender 2025	2025	Science Suite Inc., Toronto, Canada

ChatGPT	GTP-5.2	OpenAI
EndNote 20.0.1	20.0.1	Clarivate Analytics
FlowJo v10.10.0	v10.10.0	FlowJo LLC, Ashland, USA
GraphPad Prism	10	GraphPad Software Inc., Boston, USA
ImageJ FIJI	1.54f	National Institute of Health, Bethesda, USA
iTREX	2023	DKFZ, Heidelberg, Germany
Living Image software v4.5.2	v4.5.2	Caliper Life Sciences, Perkin Elmer
Microsoft Office Standard	2021	Microsoft, Redmond, USA
NIS Elements Imaging Software	6.10.02	Nikon
Perplexity	2025	Perplexity AI, Inc.
R2	2024	Academic medical center (AMC), Amsterdam, Netherlands
Smart+ software	1.20.8	Precision X-Ray

3.2. Methods

3.2.1. Cell culture

pHGG tumor spheres were cultured in serum-free tumor sphere medium (TSM) supplemented with B-27, heparin, hEGF, hFGF and hPDGF-AA (working TSM) (Lin & Monje, 2017) in ultra-low attachment (ULA) vessels (Corning). TSM base (without supplements) was used for washing. TSM was prepared according to Table 1.

Table 1: Composition of the TSM media

Components of the TSM base	**End concentration**
Neurobasal-A	47.5 %
DMEM/F-12	47.5 %
HEPES Buffer	1 %
Sodium Pyruvate	1 %
MEM non-essential amino acids	1 %
GlutaMAX-I Supplement	1 %
Antibiotic-antimycotic	1 %
Supplements for working TSM	
B-27	2 %
Heparin	2 µg/ml
hEGF	20 ng/ml
hFGF	20 ng/ml
hPDGF-AA	10 ng/ml

Cells were splitted once or twice a week (when the sphere center was getting dark) using eighter Accumax or TrypLE for 5 min at 37 °C, afterwards mechanically dissociated by pipetting, and washed with TSM base. Cells that did not entirely dissociate, were additionally incubated with 10 µl/ml DNase I and 1 µl/ml $MgCl_2$ for 5 min at room temperature.

HEK293T cells were cultured as spheres in DMEM supplemented with 10 % FBS, 1 % L-Glutamine, and 1 % penicillin-streptomycin in ULA vessels. Cells were splitted by 5 min incubation with Accumax at 37 °C, mechanically dissociated by pipetting, and washed with media.

NSCs were cultured as spheres in NSC media (Table 2) in ULA vessels. Media was changed every day. Cells were splitted by 5 min incubation with Accumax at 37 °C, mechanically dissociated by pipetting and washed with media. After each splitting, CEPT was added to the culture wells to increase viability. CEPT not used during the drug screen.

Table 2: Composition of the NSC media

Components of NSC media	**End concentration**
DMEM/F-12	Base
B-27	2 %
GlutaMAX-I Supplement	1 %
MEM non-essential amino acids	0.5 %
CHIR-99021	1.5 µM
SB-525334	2.5 µM
FGF2	40 ng/ml
EGF	40 ng/ml
hLIF	5 ng/ml
Heparin	2 µg/ml
CEPT components	
Poly-Amine Supplement	1 µl/ml
CET master mix (2.8 mM Trans-ISRIB, 200 µM Chroman1, 6 mM Emricasan)	0.25 µl/ml

All cells were counted in a 1:1 dillution in TrypanBlue using the Automated Cell Counter TC20 (BioRad). Cells were centrifuged at 300 xg for 5 min, resuspended in the respective media and then seeded in cell culture vessels. Media was changed 2-3x per week, if not mentioned otherwise. Cells were cryopreserved in Synth-a-freeze freezing medium (Thermo Fisher Scientific), and stored in a liquid nitrogen tank at -196 °C.

3.2.2. Inhibitor treatment

For *in vitro* experiments, all drugs were diluted in DMSO to a 10 mM concentration and stored at -20 °C. This stock was then diluted in TSM to the respective concentrations needed in each assay. Dimethyl sulfoxide (DMSO) was used as the vehicle control in all assays. Control cells were treated with an equivalent concentration of DMSO corresponding to the highest drug concentration used.

3.2.3. Irradiation (*in vitro*)

Cell were irradiated with X-ray irradiation using the MultiRad 225 (Precision X-Ray). The cells were irradiated 2 h after drug exposure on shelf 4 of the machine through a 0.5 mm copper filter at the settings of 200 kV, 17.8 mA and a dose rate of 215.1 cGy/min. The irradiation time to reach 0.5-30 Gy was chosen according to internal dosimetry results.

3.2.4. Drug screening

The drug library consisted of 90 FDA-approved drugs (Figure 2) and was designed, and the drug plates provided by the Translational Drug Screening Unit at the DKFZ (KITZ core library 2022) (Peterziel et al., 2022). The drugs were printed in round-bottom ULA 384-well plates with opaque walls (S-Bio), and stored in an oxygen- and moisture-free environment at room temperature. Each drug was tested in 5 increasing concentrations. Cells were seeded into these plates at a density of 500 cells/well and then irradiated 2 h after drug exposure at two irradiation doses, according to the radiosensitivity of each cell line. After 72 h incubation at 37 °C, a cell viability assay was performed as readout. To quantify the radiosensitizing effect, the "Coefficient of Drug Interaction" (CDI) was calculated according to the following formula: $CDI = \frac{(DrugRT)}{(Drug)\ x\ (RT)}$. CDI values < 1 are considered as synergistic, values ~ 1 are considered as additive and values > 1 are considered as antagonistic (Cao & Zhen, 1989; Chen et al., 2014; Xu et al., 2007).

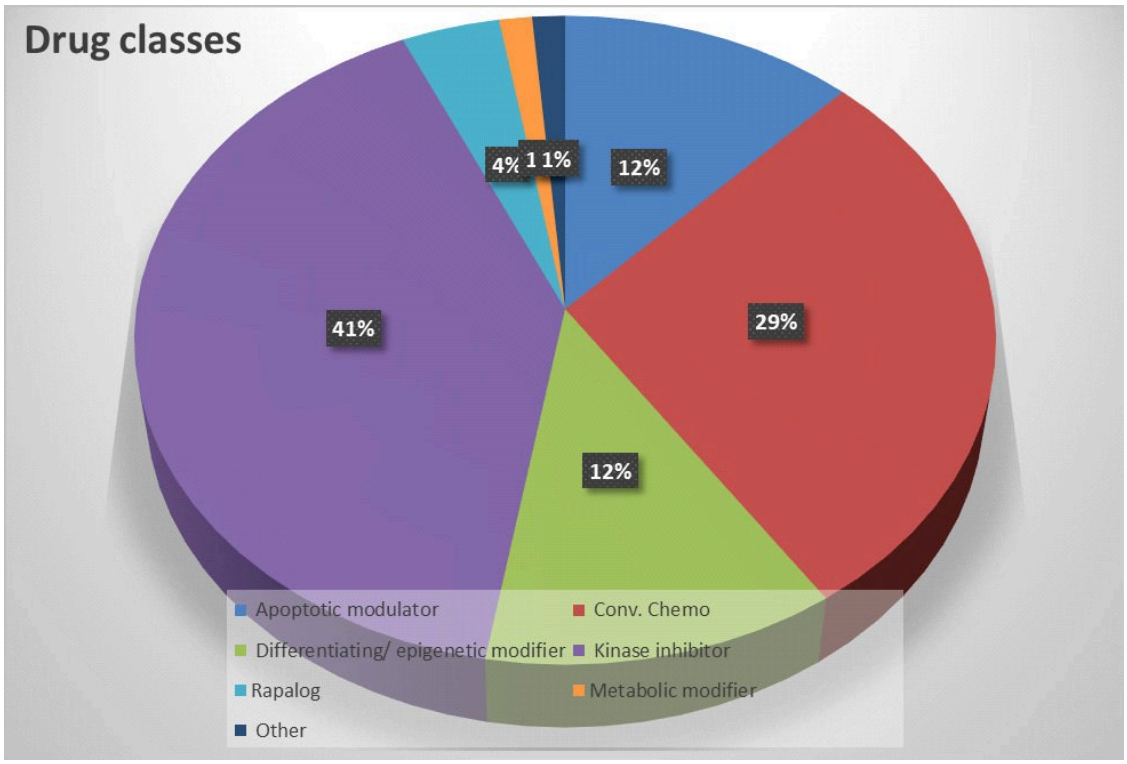


Figure 2: Composition of the drug library used for the drug+RT screening (provided by the Translational Drug Screening Unit 2022).

3.2.5. Cell viability assays

Cells were treated with the drugs, DMSO (negative control) and Staurosporine (positive control), and irradiated using the MultiRad 225. After 72 h of incubation at 37 °C, CellTiterGlo-Reagent (CTG, Promega) was added to the cells in a 1:2 ratio (1 part CTG : 2 parts cell

suspension). The plates were incubated for 15 min in room temperature protected from light. The solution was transferred to opaque plates and luminescence was measured at the Mithras (Berthold Technologies) or the GloMax Discover (Promega) plate reader at 0.3 sec integration time.

3.2.6. Apoptosis assays

100,000 cells were treated with drugs and irradiation, and incubated for 72 h at 37 °C. The cells were harvested, dissociated, and incubated with a 1:100 dillution of AnnexinV (Biolegend) in AnnexinV-binding buffer (Biolegend) for 15 min at room temperature in the dark. Afterwards, AnnexinV-binding buffer was added to the cells and the cell solution was filtered into FACS tubes. Propidium iodide (PI, Biolegend) was added in a 1:200 dilution shortly before acquisition at BD Fortessa. Data was analyzed using FlowJo.

3.2.7. Long-term growth inhibition assays

Cells were seeded into round-bottom ULA 96-well plates (Corning), treated with drugs, and centrifuged at 100 G for 5 min. 2 h after the drug exposure cells were irradiated and incubated at 37 °C. The plate was imaged at different time points using the EclipseTi2 microscope (Nikon). The area of each sphere was determined using ImageJ.

3.2.8. yH2AX staining

200,000 cells were seed into ULA 6-well plates and treated with the drug for 24 h before irradiation. At different timepoints after irradiation, cells were collected into FACS tubes and dissociated. To fix the cells, the pellet was resuspended in 4 % PFA in PBS (Santa Cruz) and incubated at room temperature for 15 min. Cells were washed with PBS, resuspended in permeabilization buffer (PBS + 2 % FBS + 0.1 % TritonX-100), and incubated at room temperature for 15 min. Afterwards the antibodies were diluted in permeabilization buffer to a final concentration 1:100 for Anti-γH2AX and 1:400 for the isotype control, added to the cell solution, and incubated for 1 h at room temperature protected from light. Cells were washed twice with permeabilization buffer and resuspended in wash buffer (PBS + 2 % FBS). The samples were acquired at BD Fortessa and analyzed using FlowJo.

3.2.9. RNA isolation

RNA was isolated from fresh-frozen tumor-tissue, cryo-preserved tumor cells and cell pellets according to the manufacturer's instructions of the AllPrep DNA/RNA/Protein Mini Kit (Qiagen). The quality of the samples was analyzed using the TapeStation 4150 (Agilent Technologies) according the the manufacturer's instructions (Agilent Technologies).

3.2.10. Bulk RNA sequencing

Library preparation and RNA sequencing were performed by the Next Generation Sequencing Core Facility at the DKFZ. Total RNA libraries were generated using the TruSeq Stranded mRNA Library Preparation Kit (Illumina). Sequencing was carried out on an Illumina NovaSeq 6000 platform using 100 bp paired-end reads (S4 flow cell). Downstream data analysis was performed using the R2: Genomics Analysis and Visualization Platform (Academic Medical Center, Amsterdam, Netherlands).

3.2.11. EdU assay

200,000 cells were seed into ULA 6-well plates and treated with the drug for 24 h. The staining was performed according to the manufacturer's instructions of the "Click-iT EdU Flow Cytometry Cell Proliferation Assay Kit" (Thermo Fisher Scientific).

In short, EdU was added to the cells to a final concentration of 10 µM and incubated at 37 °C for 45 min. Cells were transferred to FACS tubes and dissociated. To fix the cells, the pellet was resuspended in 4 % PFA in PBS (Santa Cruz) and incubated at room temperature for 15 min. Cells were washed with PBS, resuspended in saponin buffer (Thermo Fisher Scientific), and incubated at room temperature for 15 min. The Click-iT reaction cocktail (Thermo Fisher Scientific) was prepared according to the manufacturer's instructions, added to the cell solution, and incubated for 30 min at room temperature protected from light. Cells were washed with saponin buffer and resuspended in saponin buffer. The samples were acquired at BD Fortessa and the data analyzed using FlowJo.

3.2.12. Mice and ethical compliance

All animal experiments were conducted in accordance with legal and ethical regulations approved by the corresponding authorities in Baden-Württemberg, Germany (Regierungspräsidium Karlsruhe). The experiments performed in this dissertation were approved in the following animal protocols: G293/20, G138/21, and G167/23. Animals were housed in individually-ventilated cages (IVC) in a temperature-controlled facility with a 12 h : 12 h light-dark cycle, and water and food *ad libitum*. Mice were monitored daily for their health status, tumor-related, and treatment-related symptoms. When the mice showed symptoms listed in the termination criteria of the corresponding animal protocol, the mice were euthanized.

3.2.13. Intracranial transplantation

7–9-week-old, female mice were orthotopically transplanted with 200,000-500,000 luciferase-GFP-labelled pHGG cells. 24 h before surgery, the mice received metamizole (800 mg/kg)

analgesia via the drinking water. Perioperative metamizole (200 mg/kg) analgesia was administered subcutaneously. During the whole surgery, the mice were anesthetized by inhalation anesthesia of 1.5-2.5 % isoflurane. Eye cream (Bepanthen) was applied to eyes to prevent corneal drying and mice were fixed in a stereotactic frame on a heating pad. After a negative toe reflex test, a small incision (~5 mm) was cut on the midline scalp to expose the skull. Using a 16 G cannula, a small hole was drilled at the designated coordinates (Table 3, Figure 3). A Hamilton needle was inserted into through the hole at the designated depth (Table 3) and the cell suspension (4 µl) was slowly injected into the brain (1400-1800 MDN). After carefully removing the needle, the incision was closed using tissue adhesive (Histoacryl, B.Braun). Mice were placed into clean IVC for recovery and received metamizole (800 mg/kg) analgesia via the drinking water for additional two days. Mice were marked by ear punches. The health status of the mice was monitored daily.

Table 3: Injection coordinates for the intracranial transplantation of pHGG cells.

Injection location	**Starting point**	**Coordinates on the skull**	**Injection depth**	**Injection pace**
Brainstem	Lambda	1 mm posterior	4-4.5 mm deep	1400 MDN
Thalamus	Bregma	2 mm posterior, 1 mm mediolateral	2.5 mm deep	1800 MDN

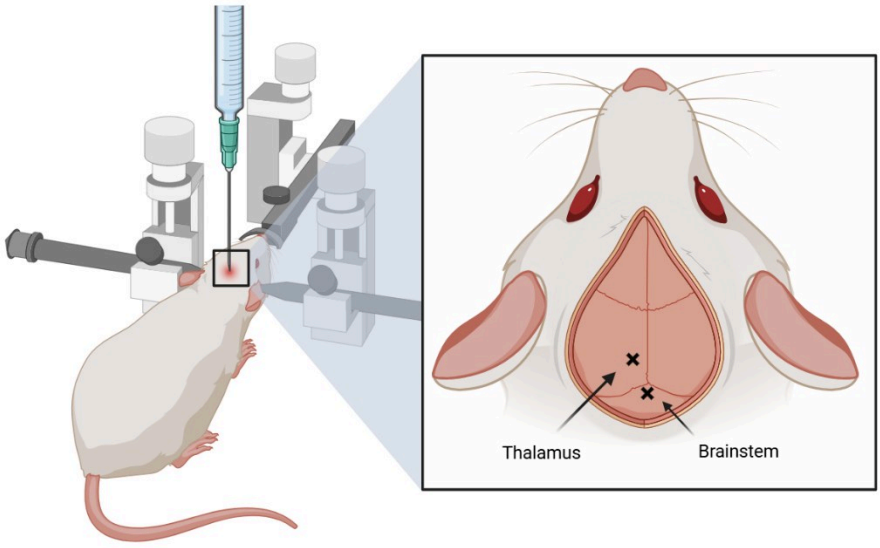


Figure 3: Injection coordinates for the intracranial transplantation of pHGG cells.
Mice were fixed in a stereotactic frame and a small incision was cut to expose the skull. The injection sites on the skull are schematically indicated with an "X".

3.2.14. Bioluminescence imaging (IVIS)

Tumor engraftment and progression were monitored by bioluminescence signal of the luciferase activity of the transplanted pHGG cells. Mice were anesthetized by inhalation anesthesia of 1.5-2.5 % isoflurane and eyes covered with eye cream (Bepanthen). Mice were intraperitoneally (i.p.) injected with with 150 mg/kg D-Luciferin solution, and after 10 min of incubation time, the mice were imaged for 5 min in the In Vivo Imaging System Lumina LT Series III (Perkin Elmer) machine. For the imaging of brains *ex vivo*, the brains were placed in a 12-well cell culture plate containing 1 ml PBS. 100 µl D-Luciferin was added shortly before acquisition to the PBS. Brains were imaged for 15-30 seconds. Data were analyzed using the Living Image software (Perkin Elmer).

3.2.15. Irradiation (*in vivo*)

Mice were treated with whole brain X-ray irradiation using the SmART+ irradiation device (Precision oncology) in collaboration with Ina Kurth, Mareike Roscher, and Rosemarie Euler-Lange (Morszeck Pre-Clinical-Trial Unit, DKFZ). Mice were anesthetized by inhalation anesthesia of 1.5-2.5 % isoflurane and eyes covered with eye cream (Bepanthen). Mice were placed in the instrument and a CT scan was used to position the mouse correctly to the treatment plan, which was prepared beforehand according to the mouse strain and age. Two radiation beams were positioned at 90° and 270° around the head (Figure 4 A) with the isocenter of the radiation beam positioned above the head to cover the whole brain and spare ventral head and neck tissue (Figure 4 B). Using a circular collimator of 25 mm diameter, mice were irradiated at daily (only on weekdays) fractions (fx) of 0.5 Gy/day or 2 Gy/day until the cumulative total dose was achieved.

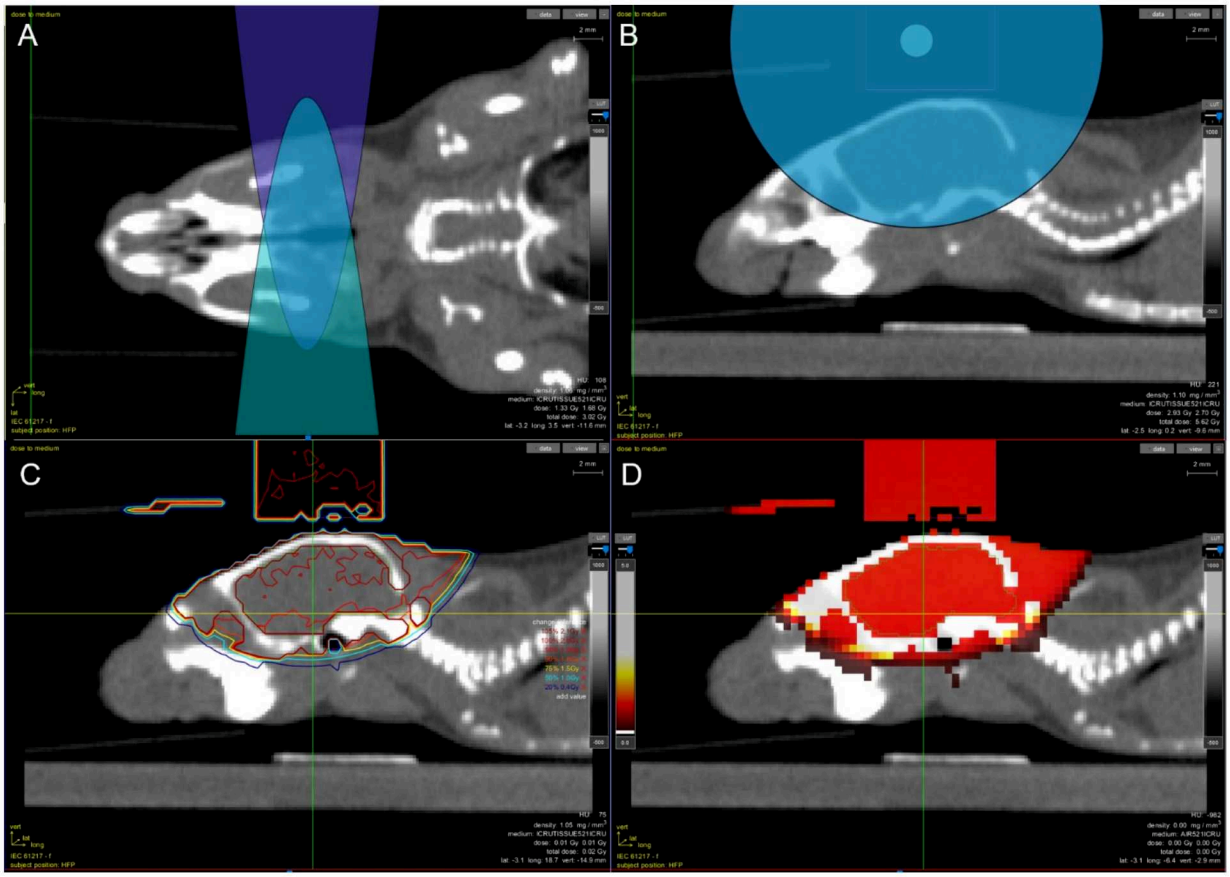


Figure 4: Positioning of the two irradiation beams for the whole-brain irradiation with the SmART+ machine. Dark blue and turquoise display the two irradiation beams (A), in light blue the overlapping area of the two beams is shown (A, B). Only the overlapping area is receiving the complete dose of 2 Gy/fx/day, as shown in red (C, D).

3.2.16. Drug treatment

The mice were treated with the drugs daily (only on weekdays) by oral gavage (oral), intraperitoneal (i.p.) or intravenous (i.v.) injection according to the following Table 4. Drugs were prepared for one week and stored at 4 °C for this time period. Drug formulations and concentrations were selected based on prior reports demonstrating efficacy and acceptable tolerability (referenced in Table 4).

Table 4: Formulation and application of the drugs used in the in vivo experiments.

Drug class	Drug	Dose	Vehicle	Application route	Application frequency	Reference
Proteasomei	Marizomib	150 µg/kg	1 % DMSO in PBS	i.p.	2x week	(Manton et al., 2016; Vlashi et al., 2010)
Proteasomei	Marizomib	150 µg/kg	1 % DMSO in PBS	i.v.	2x week	(Lin et al., 2019)

MEKi	Cobimetinib	15 mg/kg	5 % DMSO, 30% PEG300, 5 % Tween80, 60 % water	oral	2x week	(Kawakami et al., 2016)
MEKi	Cobimetinib	10 mg/kg	5 % DMSO, 30 % PEG300, 5 % Tween80, 60 % water	oral	5x week	(Han et al., 2020)
MEKi	Trametinib	1 mg/kg	5 % DMSO, 10 % Hydroxypropyl-β-Cyclodextrin, 85 % PBS	oral	5x week	(Izquierdo et al., 2022)
HDACi	Romidepsin	1 mg/kg	2 % DMSO, 2 % Tween80, 48 % PEG300, 48 % water	i.p.	5x week	(Noll et al., 2023)
HDACi	Valproic acid (VPA)	200 mg/kg	PBS	i.p.	5x week	(Enshaeieh et al., 2021)
HDACi	Panobinostat	5 mg/kg	2.5 % DMSO, 5 % PEG400, 5 % Tween80, 87.5 % saline	i.p.	5x week	(Hennika et al., 2017)
BCLi	AZD-4320	10 mg/kg	10 % DMSO, 40 % PEG300, 5 % Tween80, 45 % saline	i.v.	1x week	(Balachander et al., 2020)
ALKi	Lorlatinib	10 mg/kg	0.14 % HCL in water	oral	5x week	(Zou et al., 2015)

3.2.17. Processing of endpoint samples

When the mice reached endpoint criteria symptoms, as listed in the according animal protocol, the mice were euthanized with increasing CO_2 concentrations and subsequently decapitated. The brain was isolated and cut sagittally into two halves. For histological analysis, the brain halves were fixed in formalin and, after 24 h incubation at 4 °C, dehydrated, and embedded in paraffin (FFPE). For cryopreservation of the tumor cells, the tumor region was isolated from the brain, mechanically dissociated in TSM with a pipette, filtered through a 40 µm filter (Falcon), and frozen in Synth-a-freeze freezing media (Thermo Fisher Scientific). To generate fresh frozen samples, the tumor region was isolated, immediately frozen in liquid nitrogen and stored at -80 °C.

3.2.18. Pharmacokinetic analysis

For the pharmacokinetic analysis the mice were treated once with the drugs (Table 4) and sacrificed at different time points (30 min - 24 h) after drug administration. Blood samples were collected by heart puncture of the left ventricle using an insulin syringe Omican 100 (B. Braun). Blood was collected in Lithium-Heparin capillary blood tubes (Microvette 500 µl, Sarstedt), centrifuged at 1600 xg for 10 min at 4 °C, and plasma was isolated and immediately frozen in liquid nitrogen. The mouse was subsequently perfused manually by injecting PBS with a 20 ml syringe through the left ventricle through the whole vascular system of the mouse. Afterwards, the perfused brain was collected, sagittally cut in halves, and frozen in liquid nitrogen. Samples were stored at -80 °C until analysis.

The mass spectrometry analysis was performed in collaboration with Jürgen Burhenne and Kevin Steimel (Department of Clinical Pharmacology and Pharmacoepidemiology, Heidelberg University Hospital). The plasma and brain tissue samples were subjected to protein precipitation with 38 % acetonitrile in methanol to deplete proteins present in the samples. The protein-depleted extracts were subsequently injected into the UPLCMS/MS system (Waters) consisting of an Acquity UPLC I-Class® System, a Xevo TQS triple-stage quadrupole mass spectrometer, and a Z-spray heated electrosprayionization source. The eluent A consisted of 5 % acetonitrile in water with 0.1 % formic acid and eluent B consisted of acetonitrile with 0.1 % formic acid. The separation column Acquity UPLC Peptide BEH C18 was used.

3.2.19. Immunohistochemistry and Hematoxylin-Eosin staining

The brains were cut sagitally and fixed with formalin at 4 °C for 24 h up to a week. The brains were then transferred into an embedding cassette and dehydrated according to the following protocol:

Solution	Time	Speed (rpm)
10% Formalin	30 min	60
70% Ethanol	30 min	70
80% Ethanol	4 h	70
90% Ethanol	10 h	70
100% Ethanol	7 h	70
100% Ethanol	7 h	70
100% Ethanol	4 h	70
100% Ethanol	6 h	70
Xylene	6 h	70
Xylene	6 h	60
Paraffin	4 h	60
Paraffin	4 h	60

The dehydrated samples were embedded in paraffin and cut into 5 µm thick sections using a microtome (Leica Biosystems). The sections were mounted on SuperFrost Plus microscope slides (Epredia) and dried overnight at 37°C. The next day, FFPE samples were deparaffinized using the following protocol:

Solution	**Time x Repeats**
Xylene	10 min x 2
100% Ethanol	5 min x 2
95% Ethanol	5 min
70% Ethanol	5 min
Water or PBS	5 min

For the H&E staining the deparaffinized samples were stained with Hematoxylin and Eosin (H&E) according to the following protocol:

Solution	**Time**
Hematoxylin	7 min
Tap water	2 min
Eosin	3 min
Tap water	Rinse

For the Ki67 staining, the deparaffinized samples were incubated with citrate buffer at 100 °C for 20 min for antigen retrieval. Then, the samples were washed, and the sections blocked with 10 % donkey serum for 1 h, followed by incubation with the primary antibody (rabbit anti-Ki67 1:1000) overnight at 4 °C. After washing, the sections were incubated with the secondary antibody (donkey anti-rabbit 1:400) for 1 h at room temperature. After washing, samples were incubated with ABC kit (Vector Laboratories) according to manufacturer's instructions for 30 min. Sections were rinsed with PBS and incubated with the DAB kit (HIGHDEF® DAB Chromogen/Substrate Set) according to manufacturer's instructions for 10 min. After washing with tap water, the sections were counterstained with Hematoxylin (1:10 dilution) for 1-2 min and rinsed with tap water.

After the staining, the sections were dehydrated again according to the following protocol:

Solution	**Time x Repeats**
70 % Ethanol	1 min
95 % Ethanol	1 min
100 % Ethanol	1 min x 2
Xylene	2 min x 2

The stained sections were mounted with 200-300 µL Eukitt mounting medium (Orsatec) and dried overnight. The sections were imaged with a Histoscanner (Pacific Image Electronics).

3.2.20. Graphs and statistical analysis

All graphs were plotted and statistical analysis performed using GraphPad Prism 10. Data are represented by mean ± standard deviation (SD). For comparisons between two independent groups, an unpaired two-tailed Student's t-test was used. For experiments involving two independent variables, a two-way analysis of variance (ANOVA) was applied to assess main effects and interactions between factors. When significant effects were detected, post-hoc Sidak's or Tukey's multiple-comparison tests were performed. For dose-response analysis, a non-linear regression with a variable slope (four parameters) was performed. For survival analyses, survival curves were generated using the Kaplan-Meier method, and differences between groups were assessed using the log-rank (Mantel-Cox) test. The survival graphs in this thesis show symptom free survival, not overall survival.

P-values below 0.05 were considered as statistically significant. Statistical significance is indicated in the figures as following: $p < 0.05$ (*), $p < 0.01$ (**), $p < 0.001$ (***), and $p < 0.0001$ (****). If not indicated otherwise, only statistically significant comparisons are shown in the figures. All experiments were performed with at least 3 independent replicates (n).

3.2.21. Illustrations and figure design

All illustrations were generated using BioRender (https://app.biorender.com/) and figures assembled with Microsoft PowerPoint.

3.2.22. Use of artificial intelligence

To improve the language and readability of this thesis I used ChatGPT (GPT-5.2) and Periplexity. I reviewed every text after the usage of these tools and take full responsibility for the content of this thesis.

4. Results

4.1. Comparing the radiosensitization potential of various compound classes in pediatric-type diffuse high-grade glioma

4.1.1. Heterogeneous intrinsic radiosensitivity across PDX-derived pHGG cell models

To assess the intrinsic radiosensitivity of patient-derived xenograft (PDX)-derived pHGG cells, I measured cell viability following exposure to increasing doses of X-ray irradiation. The tested pHGG models exhibited substantial heterogeneity in their response to radiotherapy, with some exhibiting marked reductions in cell viability, indicative of increased radiosensitivity (Figure 5 A), whereas others showed little (less than 50 %) to no decrease in viability even at doses up to 30 Gy, consistent with a more radioresistant phenotype (Figure 5 B).

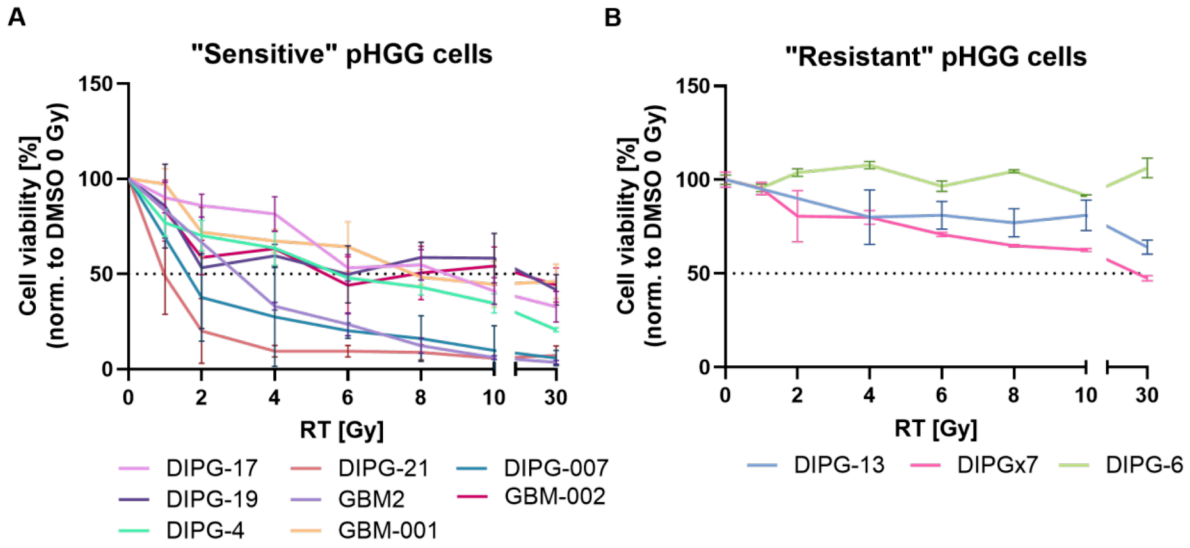


Figure 5: Radiosensitivity of PDX-derived pHGG cell cultures.
Cell viability was assessed 3 days after treatment with increasing doses of X-ray RT. According to their response to up to 30 Gy, cells were grouped into A) 'Sensitive' (more than 50 % cell viability reduction over the tested RT doses) and B) 'Resistant' cells (less than 50 % cell viability reduction over the tested RT doses). Mean ± SD, n=3.

4.1.2. Comprehensive drug+RT screening identifies potential radiosensitizers for pHGG cells

Based on the individual radiosensitivity profiles of the pHGG cells (Figure 5), I evaluated the radiosensitizing potential of approximately 90 FDA-approved compounds across nine pHGG cell cultures representing distinct histone alteration subtypes (WT, H3K27M, H3G34R), as well as two non-malignant control cell types (NSC and HEK). For each condition, the *Best CDI* (defined as the lowest CDI across all tested drug concentrations) was calculated and visualized as heatmap (Figure 6), where darker colors indicate lower CDI values and stronger radiosensitizing effects. Overall, marked differences in treatment sensitivity were observed

between cell models, with some cultures showing generally higher sensitivity to radiosensitization (e.g. DIPG-21), whereas others exhibited limited responses (e.g. NSCs at 1 Gy).

To identify compounds with consistent radiosensitizing activity across models, I summed the *Best CDI* values across all tested cells (*Best CDI Sum*) and ranked them in ascending order (Table 5). The top-performing compounds predominantly belonged to the following classes: BCL-2 family inhibitors (BCLi), MEK inhibitors (MEKi), HDAC inhibitors (HDACi), and proteasome inhibitors (Proteasomei). These compounds are indicated by red arrows in Figure 6. Staurosporine, a broad-spectrum protein kinase inhibitor, exhibited the strongest overall effect, consistent with its widespread use as a positive control for apoptosis and general cell death induction (Lawrie et al., 1997; Malsy et al., 2019; Xue et al., 2003).

To assess selectivity for pHGG cells, I compared the ranking of most efficient drugs from pHGG cultures with those from control cells. Several shared top hits were observed in NSCs (Navitoclax, A-1331852, Trametinib, Entinostat), whereas only one shared top hit was identified in HEK cells (Bortezomib) (Table 6), indicating that the majority of compounds exerted stronger radiosensitizing effects in pHGG cells than in non-malignant controls.

In the subsequent experiments, I primarily focused on H3K27M-driven DMGs, as this pHGG entity is associated with the most limited therapeutic options, largely restricted to RT, although the initial screening was performed across a collection of H3K27M, H3G34R, and H3WT tumors. Notably, the top scoring drug candidates were largely consistent across all pHGG entities. Based on this, all subsequent *in vitro* and *in vivo* validation experiments were conducted exclusively in H3K27M-driven models.

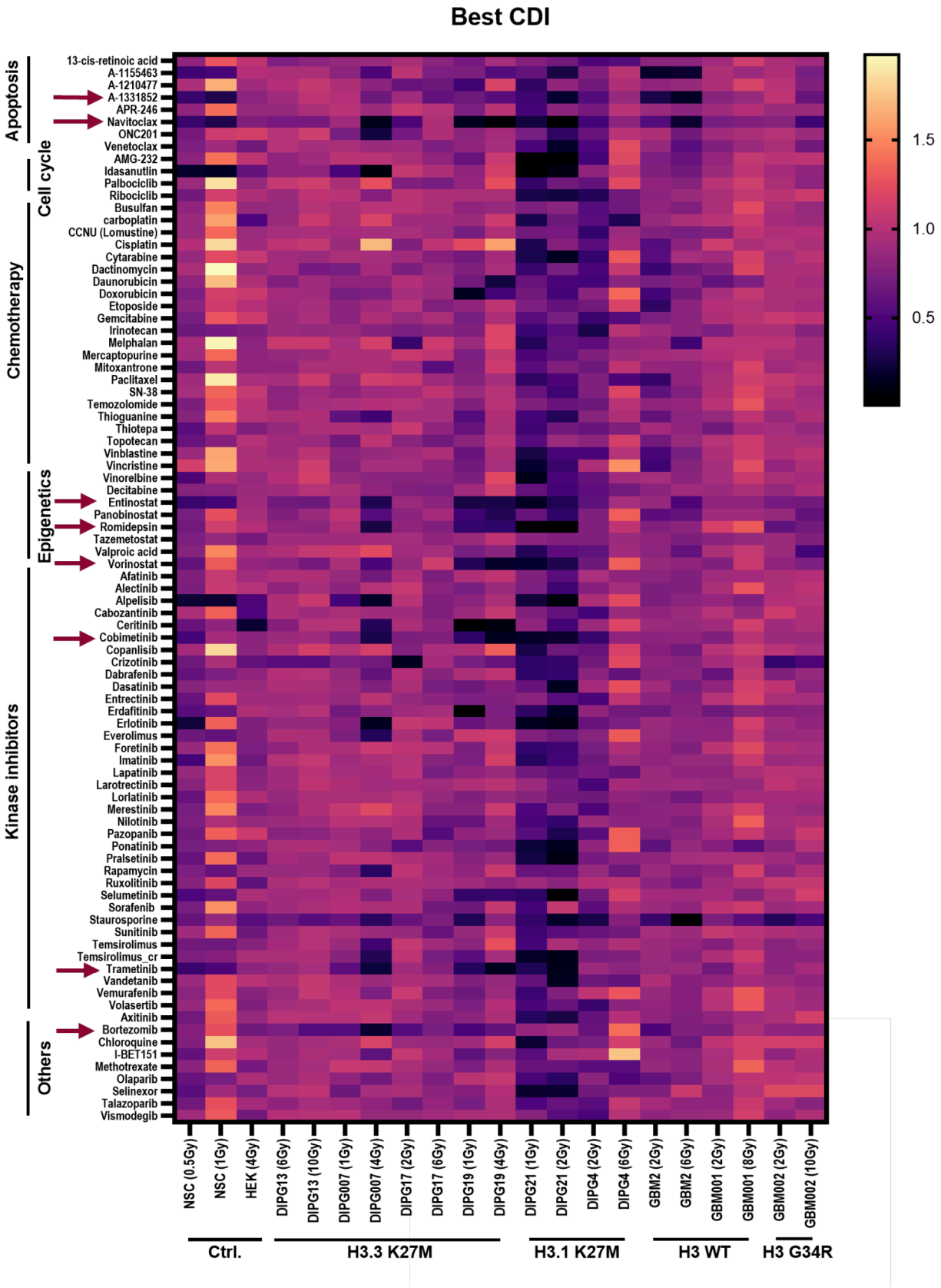


Figure 6: Heatmap of the Best CDI of all tested cells in the drug+RT screens.
Cells were irradiated with two RT doses 2 h after being in contact with the drug. After 3 days of incubation, the cell viability was assessed and the Best CDI (lowest CDI among all tested drug concentrations) was calculated. Cells were grouped according to their histone alteration (X-axis), and drugs grouped according to their mechanism of action (Y-axis). Drug candidates showing low Best CDIs among all tested cells are highlighted with a red arrow.

Table 5: Ranking of the drug candidates according to the Best CDI Sum in pHGG cells.
The Best CDI Sum was normalized to the number of tested cells. Drugs that I selected for further testing are displayed in bold.

Rank	Best CDI Sum	Drugs	Drug class
1	0,49	Staurosporine	Unselective kinase inhibitor
2	0,50	**Navitoclax**	BCL-2/-XL inhibitor
3	0,62	**Entinostat**	HDAC inhibitor
4	0,64	**Cobimetinib**	MEK1/2 inhibitor
5	0,66	**Trametinib**	MEK1/2 inhibitor
6	0,67	Crizotinib	ALK/MET/ROS inhibitor
7	0,67	**A-1331852**	BCL-XL inhibitor
8	0,69	**Romidepsin**	HDAC inhibitor
9	0,69	Erdafitinib	FGFR inhibitor
10	0,70	**Bortezomib**	Proteasome inhibitor
11	0,71	A-1155463	BCL-XL inhibitor
12	0,72	Vorinostat	HDAC inhibitor
13	0,73	Erlotinib	EGFR inhibitor
14	0,73	Daunorubicin	Anthracycline, chemotherapy
15	0,73	**Panobinostat**	HDAC inhibitor

Table 6: Ranking of the drug candidates according to the Best CDI Sum in non-malignant control cells.
The Best CDI Sum was normalized to the number of tested cells. Drugs that are also identified in pHGGs are displayed in bold.

Rank	Best CDI Sum HEK	Drugs HEK	Best CDI Sum NSC	Drugs NSC
1	0,20	Ceritinib	0,16	Idasanutlin
2	0,49	Alpelisib	0,21	Alpelisib
3	0,51	Carboplatin	0,35	**Navitoclax**
4	0,51	Cabozantinib	0,35	**A-1331852**
5	0,56	Staurosporine	0,44	**Entinostat**
6	0,59	Ruxolitinib	0,46	**Trametinib**
7	0,60	Crizotinib	0,46	A-1155463
8	0,62	Idasanutlin	0,57	Selumetinib
9	0,62	Pralsetinib	0,59	Erdafitinib
10	0,65	Sunitinib	0,64	Everolimus
11	0,65	Imatinib	0,66	Temsirolimus
12	0,69	Vismodegib	0,67	Dabrafenib
13	0,69	**Bortezomib**	0,67	Irinotecan
14	0,69	Venetoclax	0,68	Olaparib
15	0,69	Tazemetostat	0,69	Rapamycin

4.1.3. Selected compounds exhibit nanomolar potency in pHGG cells

To validate the most effective compounds identified in the drug screen, I assessed the effects of single-agent treatment in two H3K27M pHGG cell cultures (Figure 7 and Supplementary figure 1). Most compounds exhibited IC50 values in the nanomolar range, whereas BCLi showed IC50 values above 10 µM.

Given that BBB penetration of several compounds from the primary screen, namely Entinostat (Hooker et al., 2010), Navitoclax (Greenberg et al., 2024; Riessland et al., 2024), A-1331852 (Wang et al., 2020), Romidepsin (Belayet et al., 2022), Trametinib (Vaidhyanathan et al., 2014), Cobimetinib (Choo et al., 2014), and Bortezomib (Huehnchen et al., 2020) is limited or insufficiently characterized, I included additional compounds from the corresponding drug classes in subsequent experiments, namely Marizomib (Proteasomei) (Lin et al., 2019), Quisinostat (HDACi) (Cascio et al., 2023), Pimasertib (MEKi) (de Gooijer et al., 2018), Panobinostat (HDACi) (Hennika et al., 2017) that have demonstrated improved BBB penetrance.

At present, no BBB penetrant BCLi has been described. In addition, BCLis, particularly dual BCL-2/-XL inhibitors such as Navitoclax, have been associated with severe dose limiting toxicities, including thrombocytopenia, which is attributed to BCL-XL inhibition in platelets (Wilson 2010, Gandhi 2011). To mitigate this limitation, I included alternative BCLis with improved systemic tolerability, specifically Pelcitoclax (Lakhani et al., 2024), LP-118 (Ravikrishnan et al., 2025), and AZD4320 (Balachander et al., 2020), in subsequent experiments.

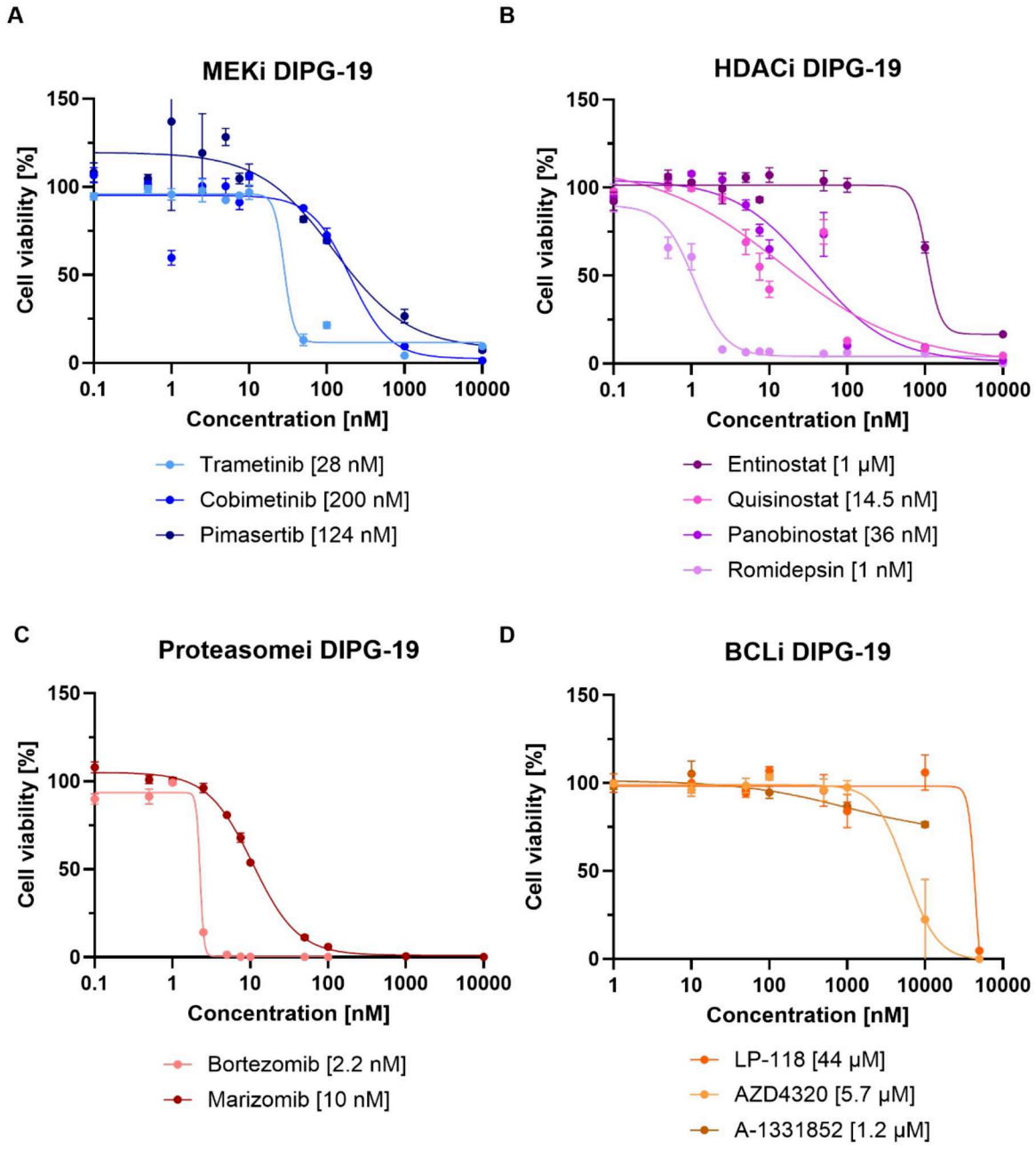


Figure 7: Drug response curves of selected drug candidates in DIPG-19 (H3K27M).
The cell viability of the pHGG cells was assessed 3 days after incubation with increasing drug concentrations, and a non-linear regression curved was fitted to the data to determine the IC50. The respective IC50 are displayed in brackets after the drug name. A) MEK inhibitors (MEKi), B) HDAC inhibitors (HDACi), C) Proteasome inhibitors (Proteaseomei), and D) BCL-2 family inhibitors (BCLi). Mean ± SD, n=3.

4.1.4. Selected compounds induce radiosensitization in pHGG cells as determined by cell viability assays

I evaluated radiosensitization by the selected compounds in cell viability assays using concentrations around their respective IC50 values (< IC50, ~ IC50, > IC50) in three H3K27M-driven pHGG cell cultures (DIPG-007, DIPG-19 and DIPG-21). Combination treatment at concentrations around the IC50 (comparisons shown in Figure 8 - Figure 11) resulted in a significant reduction in cell viability in DIPG-007 cells for nearly all tested compounds when compared with either drug or RT alone. In contrast, Pimasertib, A-1331852, and Bortezomib did not show a significant combinatorial efficacy compared with RT alone in DIPG-007 cells, but demonstrated radiosensitization in DIPG-19 (Supplementary figure 2 - Supplementary figure 5) and DIPG-21 (Supplementary figure 6 - Supplementary figure 8).

As the IC50 values of BCL inhibitors exceeded clinically achievable plasma concentrations in patients (4-6 µM; Wilson 2010, Roberts 2015), and thus surpassed levels predicted to be achievable within the brain (Greenberg et al., 2024), lower concentrations ranging from 50 to 1000 nM were tested instead, with AZD-4320 showing radiosensitization at 500 nM (Figure 10). In contrast, LP-118 did not affect cell viability either as a single agent or in combination with RT in any of the tested cell cultures (Figure 10 and Supplementary figure 4).

Most of these findings were consistent across all tested cell lines (Supplementary figure 2 - Supplementary figure 8).

As a metric for combinatorial efficacy, I calculated the *Best CDIs* for each drug+RT combination and visualized them in a heatmap (Figure 12). Consistent with earlier results (Figure 6), DIPG-21 cells exhibited the highest overall sensitivity to combination treatments. Among HDAC inhibitors, Panobinostat and Romidepsin yielded the lowest *Best CDI* values, while Cobimetinib and Trametinib performed best among MEK inhibitors. Both proteasome inhibitors, Bortezomib and Marizomib, showed comparable radiosensitization, and AZD-4320 was the most effective BCL-2 family inhibitor based on *Best CDI*. Notably, no antagonistic effects were observed for any of the tested drug+RT combinations, which revalidated the findings of the drug screen.

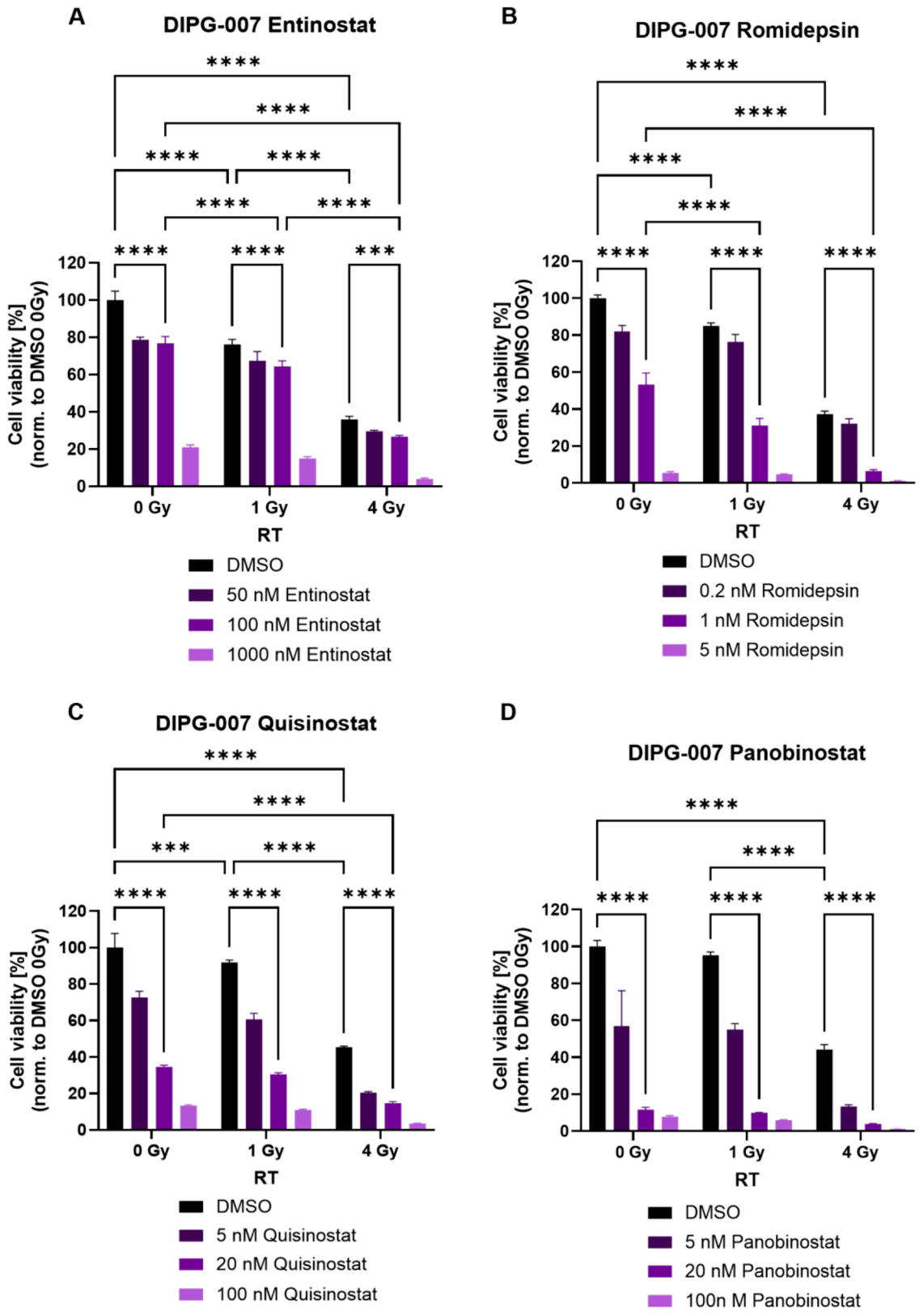


Figure 8: Cell viability assays after HDACi and RT combination treatment in DIPG-007 cells.
Cells were irradiated 2 h after being in contact with the drugs and their cell viability was assessed after 3 days of incubation. Cells were tested at 0 Gy and at two RT doses (~ 60 % viability and ~ 40 % viability after RT), as well as in three drug concentrations (< IC50, ~ IC50, > IC50). Statistics of only selected comparisons at IC50 are shown. Mean ± SD, n=3.

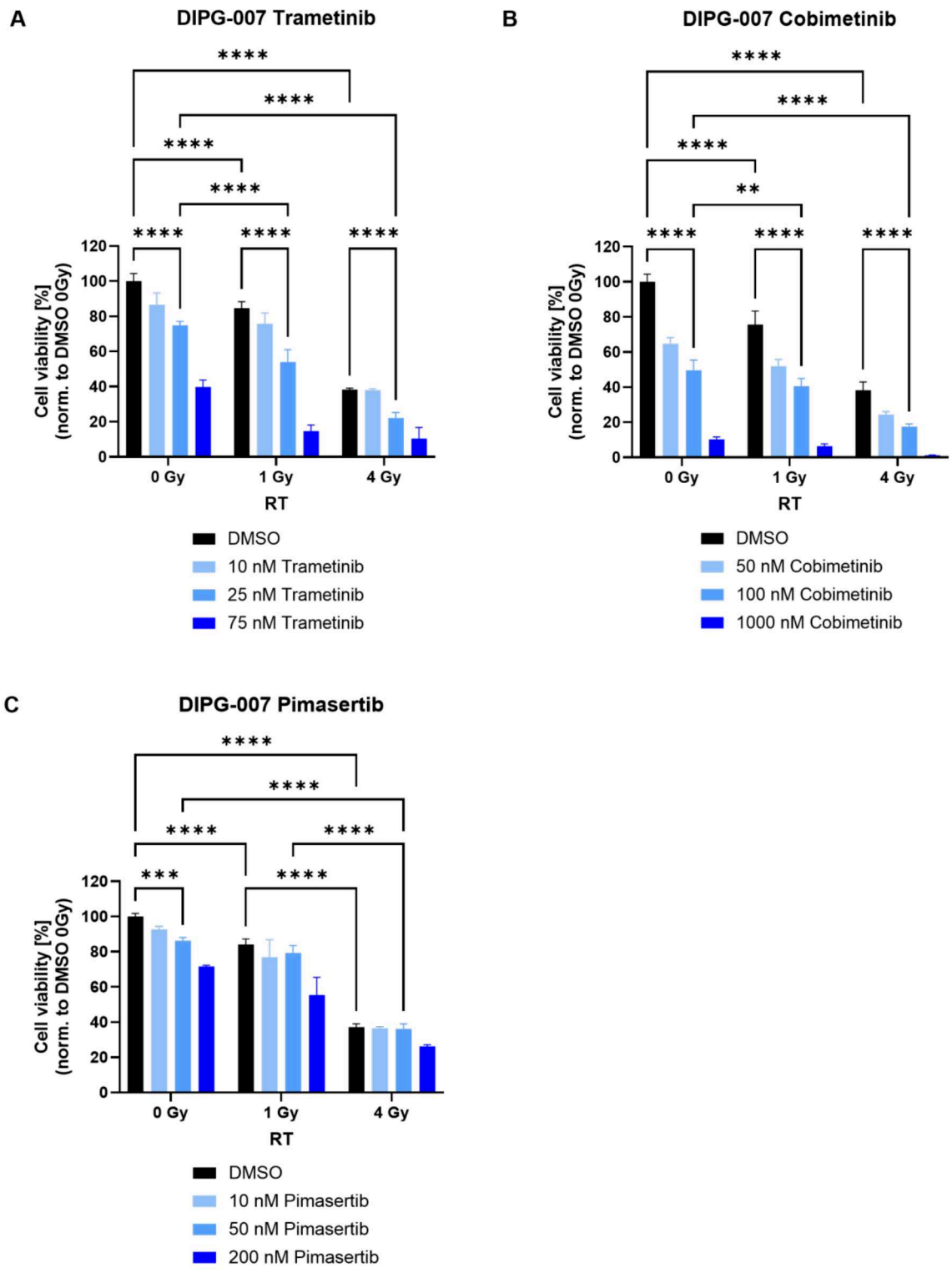


Figure 9: Cell viability assays after MEKi and RT combination treatment in DIPG-007 cells.
Cells were irradiated 2 h after being in contact with the drugs and their cell viability was assessed after 3 days of incubation. Cells were tested at 0 Gy and at two RT doses (~ 60 % viability and ~ 40 % viability after RT), as well as in three drug concentrations (< IC50, ~ IC50, > IC50). Statistics of only selected comparisons at IC50 are shown. Mean ± SD, n=3.

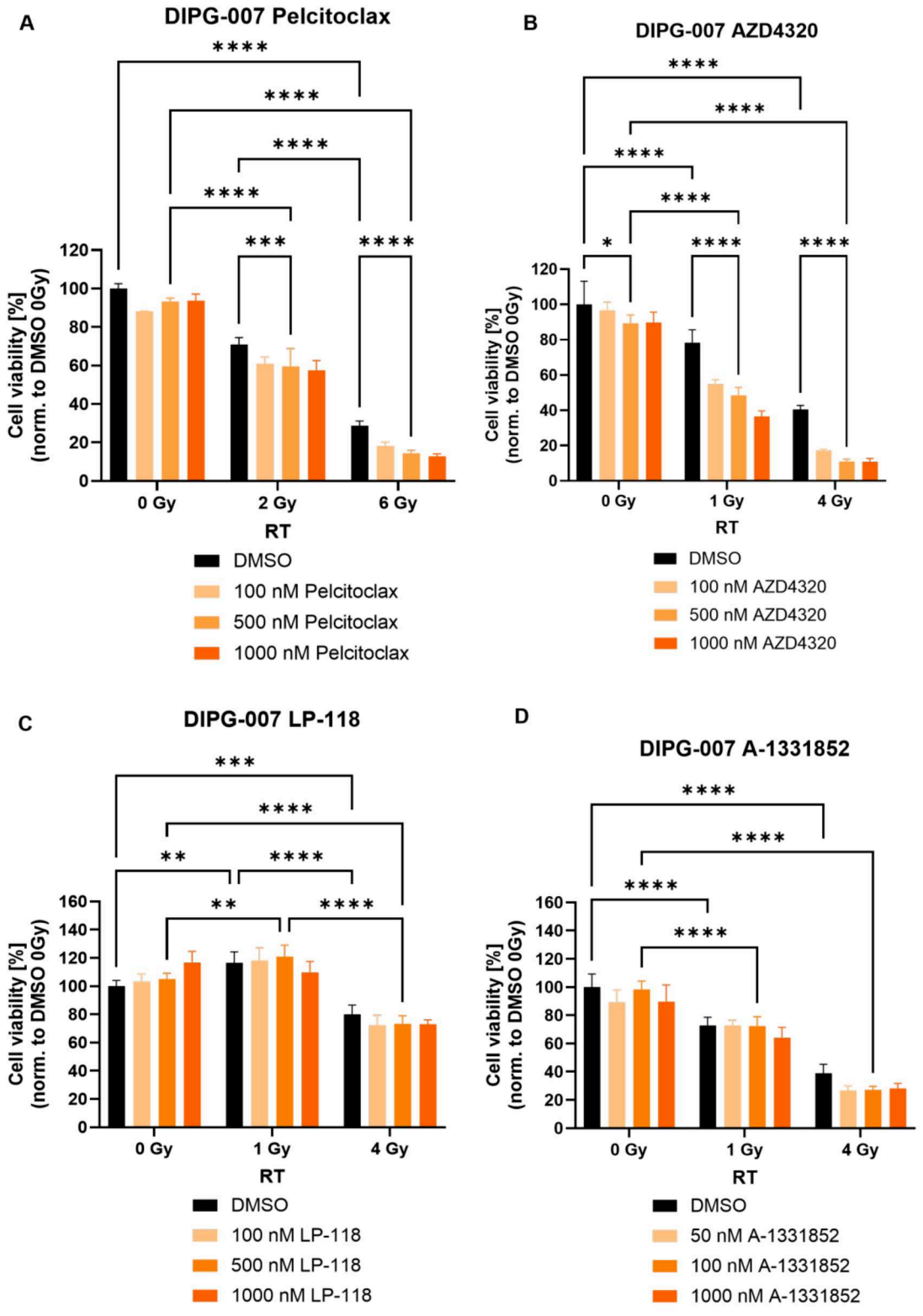


Figure 10: Cell viability assays after BCLi and RT combination treatment in DIPG-007 cells.
Cells were irradiated 2 h after being in contact with the drugs and their cell viability was assessed after 3 days of incubation. Cells were tested at 0 Gy and at two RT doses (~ 60 % viability and ~ 40 % viability after RT), as well as in three drug concentrations (< IC50, ~ IC50, > IC50). Statistics of only selected comparisons at IC50 are shown. Mean ± SD, n=3.

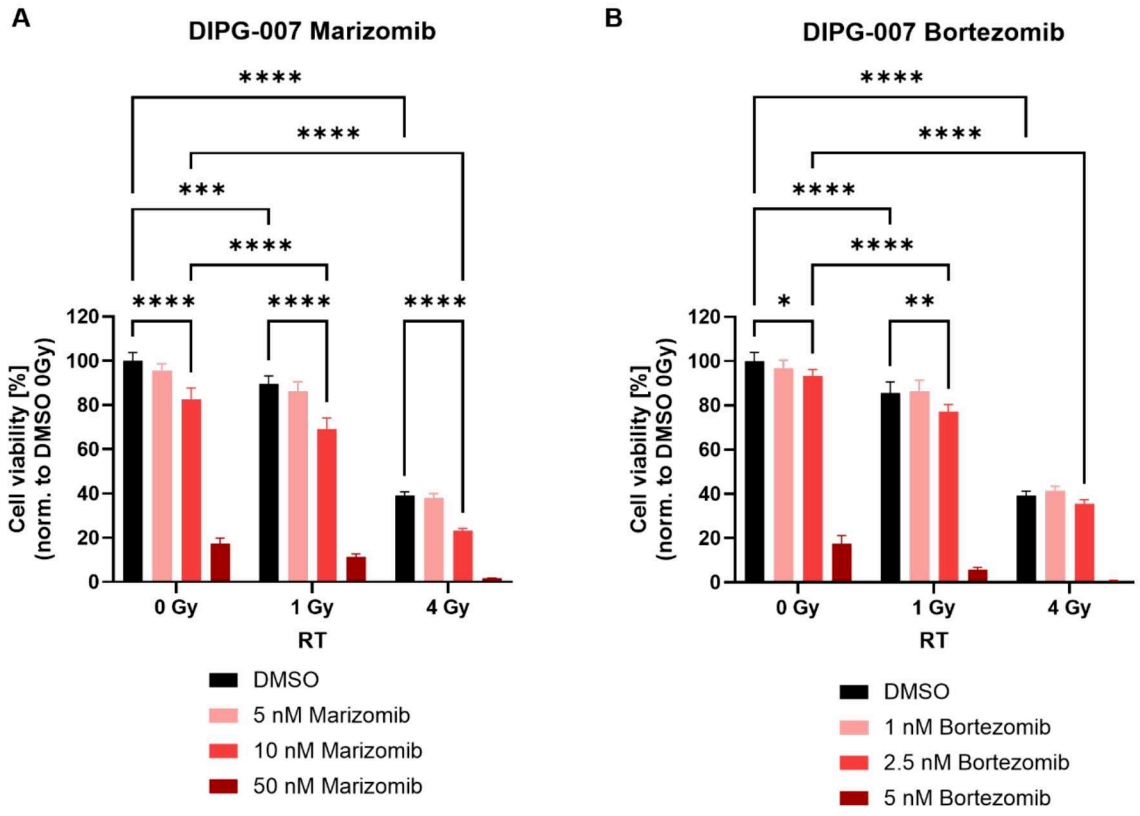


Figure 11: Cell viability assays after Proteasomei and RT combination treatment in DIPG-007 cells.
Cells were irradiated 2 h after being in contact with the drugs and their cell viability was assessed after 3 days of incubation. Cells were tested at 0 Gy and at two RT doses (~ 60 % viability and ~ 40 % viability after RT), as well as in three drug concentrations (< IC50, ~ IC50, > IC50). Statistics of only selected comparisons at IC50 are shown. Mean ± SD, n=3.

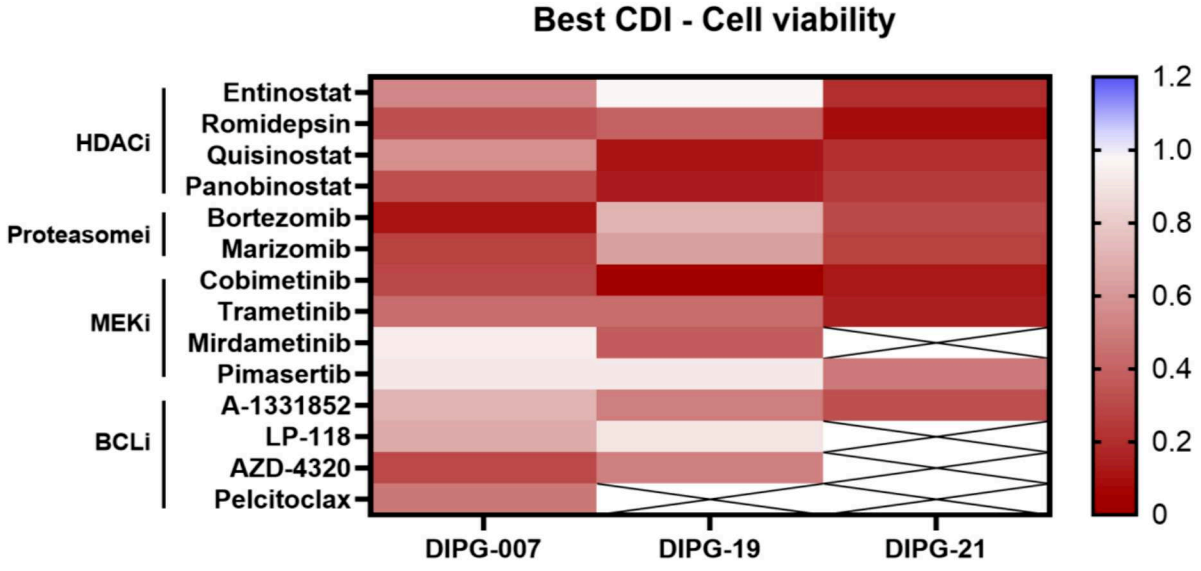


Figure 12: Heatmap comparing the Best CDIs of the tested drug+RT combinations of the cell viability assays in different pHGG cell cultures (X-axis).
Drugs are grouped according to their mechanism of action (Y-Axis). Low Best CDIs (dark red) indicate a synergistic drug+RT effect, Best CDIs around 1 (white) indicate an additive drug+RT effect while Best CDIs above 1 (blue) indicate an antagonistic effect.

4.1.5. Drug+RT combination treatment enhances apoptosis in pHGG cells

A limitation of cell viability assays is that they quantify total cellular adenosine triphosphate (ATP) levels and therefore cannot distinguish between cell death and growth arrest. To address this limitation, I assessed induction of cell death by flow cytometry (Figure 13).

Significantly increased proportions of apoptotic cells were observed upon combination treatment with 4 Gy irradiation and 500 nM AZD-4320, 25 nM Trametinib, or 1 nM Romidepsin, respectively, compared with both RT alone and drug-only treatment. In contrast, treatment with 10 nM Marizomib or 100 nM Cobimetinib in combination with 4 Gy did not result in a significant increase in apoptotic cells compared to RT alone.

Combinatorial efficacy was further quantified by calculating the *Best CDI* for each drug+RT condition (Figure 14). Romidepsin, Trametinib, and Marizomib exhibited the lowest *Best CDI* values, indicating the strongest effects on apoptosis induction in DIPG-007 and DIPG-19 cells. These results indicate, that the selected drug+RT combination treatments not only reduce cell viability, but also induce cell death in pHGG cells.

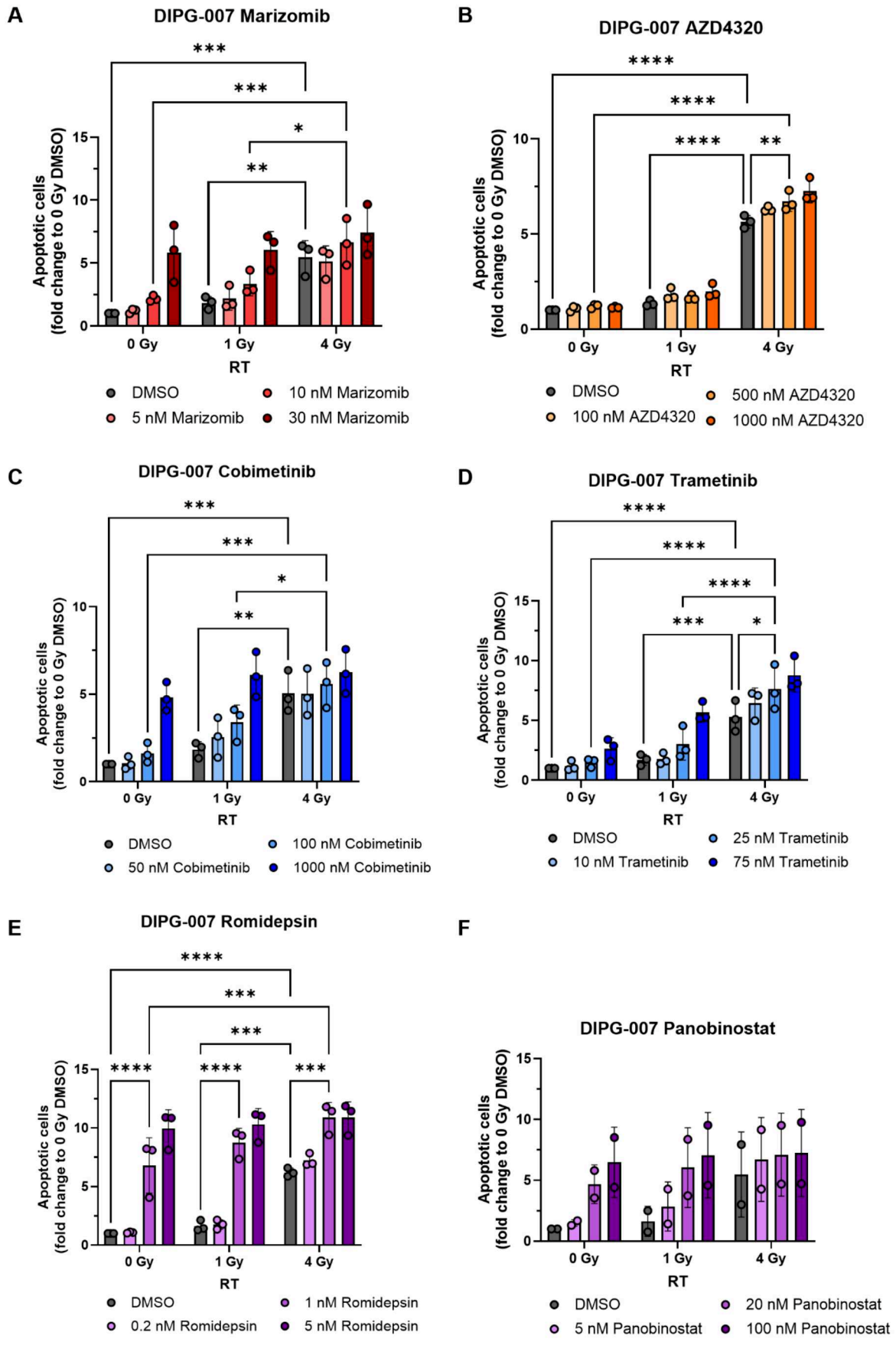


Figure 13: Apoptosis induction after drug+RT combination treatment in DIPG-007 cells.

Cells were treated with drug+RT combinations for 3 days, stained with AnnexinV+PI and acquired by flow cytometry. A) Proteasomei Marizomib (n=3), B) BCLi AZD4320 (n=3), C) MEKi Cobimetinib (n=3), D) MEKi Trametinib (n=3), E) HDACi Romidepsin (n=3), and F) HDACi Panobinostat (n=2). All AnnexinV positive cells were identified as apoptotic cells. Cells were tested at 0 Gy and at two RT doses (~ 60 % viability and ~ 40 % viability after RT), as well as in three drug concentrations (< IC50, ~ IC50, > IC50). Statistics of only selected comparisons at IC50 are shown. Mean ± SD.

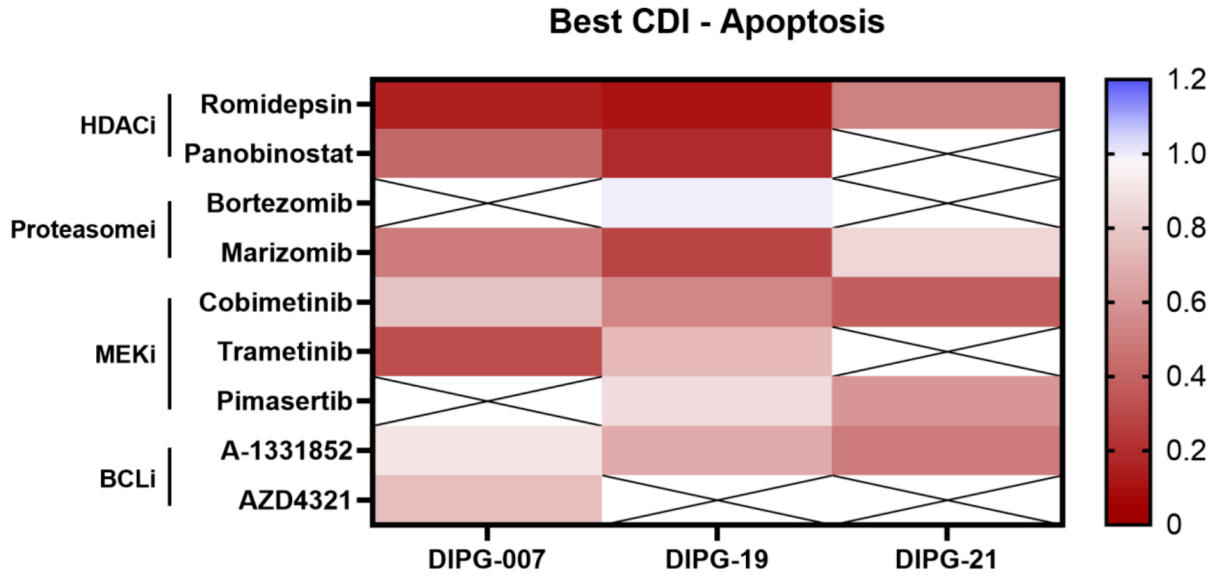


Figure 14: Heatmap comparing the Best CDI of the tested drug+RT combinations of the apoptosis assays of different pHGG cell cultures (X-axis).
Drugs are grouped according to their mechanism of action (Y-Axis). Low Best CDIs (dark red) indicate a synergistic drug+RT effect, Best CDIs around 1 (white) indicate an additive drug+RT effect while Best CDIs above 1 (blue) indicate an antagonistic effect.

4.1.6. Drug+RT combination treatment leads to long-term growth inhibition in pHGG cells

Clonogenic assays are commonly used in radiobiology to assess whether a cell retains the ability to undergo unlimited rounds, thereby forming a macroscopic colony (typically over one to three weeks), which defines clonogenic capacity (Franken et al., 2006; Munshi et al., 2005). I attempted to establish this assay for pHGG cell cultures but was unsuccessful. Clonogenic assays are typically performed using adherent cells that are fixed and stained at the experimental endpoint. However, pHGG cultures do not grow robustly under adherent conditions. When cells were seeded sparsely as single cells in matrigel to allow separation of colonies for counting, the cells failed to survive and did not form colonies even under untreated conditions (data not shown).

To nevertheless assess long-term effects of the combination treatment in pHGG cells, I analyzed long-term growth inhibition by monitoring single tumor spheres over a 14-day period, with sphere size measured at four defined time points. Although this approach does not directly measure clonogenic capacity, as single cells were not seeded and tested for colony formation, it allowed monitoring of reproductive cell death over a period of 14 days following treatment (Figure 15 and Figure 16).

As shown for DIPG-007 in Figure 15 and Figure 16, Cobimetinib monotherapy already resulted in a significant inhibition of sphere growth compared with DMSO-treated controls, whereas Marizomib showed a modest, non-significant trend toward reduced sphere size. Consistent with previous findings (Figure 10 A), Pelcitoclax alone (at 500 nM) did not affect sphere growth.

Irradiation with 4 Gy alone significantly reduced sphere size, while the addition of Marizomib, Cobimetinib, or Pelcitoclax to RT showed a trend toward further growth inhibition, although these effects did not reach statistical significance in DIPG-007. In contrast, in DIPG-19 cells, Pelcitoclax combined with radiotherapy led to a significant reduction in sphere size compared with radiotherapy and drug monotherapy (Supplementary figure 9 and Supplementary figure 10). Similarly, in DIPG-17 cells, Cobimetinib combined with radiotherapy induced a significant reduction in sphere growth relative to both single treatments (Supplementary figure 11 and Supplementary figure 12).

These results show, that the selected drug+RT combinations affect the long-term growth of pHGG cells.

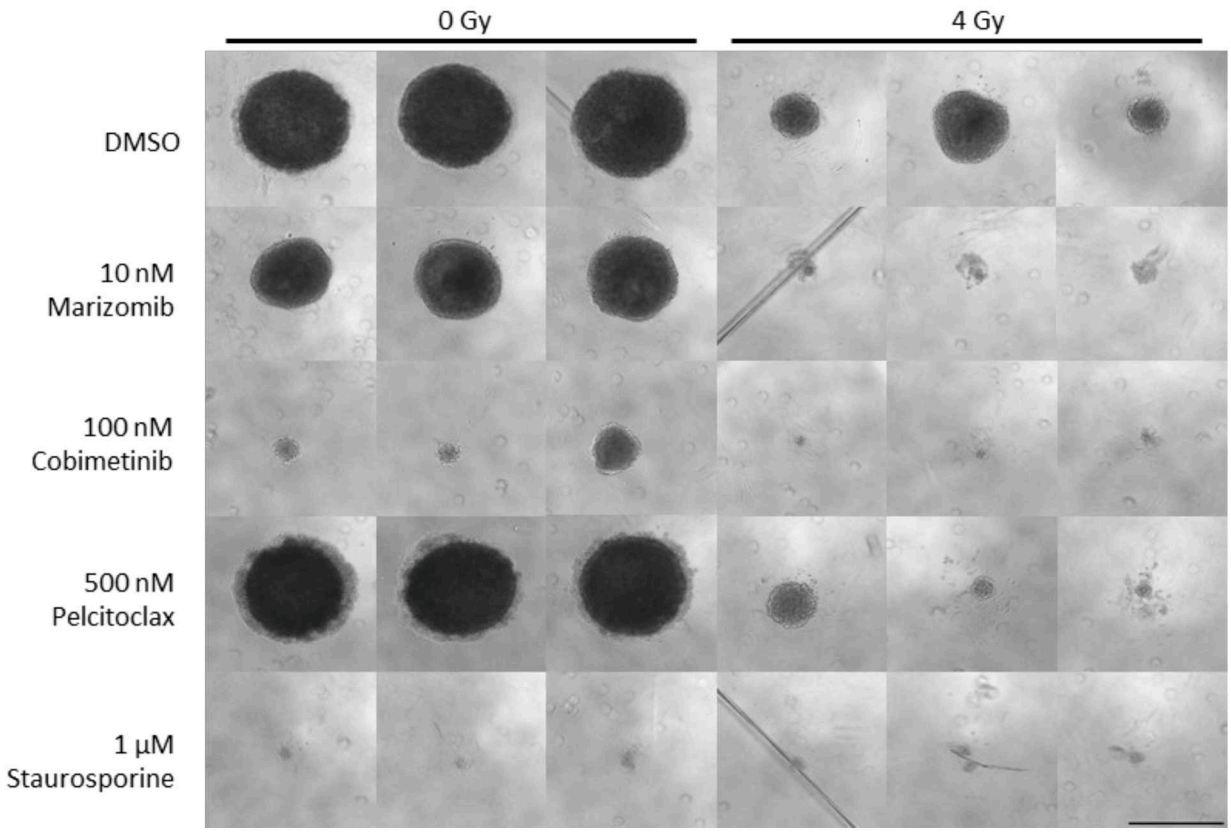


Figure 15: Representative pictures of the long-term growth inhibition assay in DIPG-007 spheres at day 14. Pictures were taken at brightfield 10x magnification using the Nikon EclipseTi2 microscope. The scale bar represents 1mm. Three independent technical replicates are shown. DMSO served as negative control and Staurosporine as positive control.

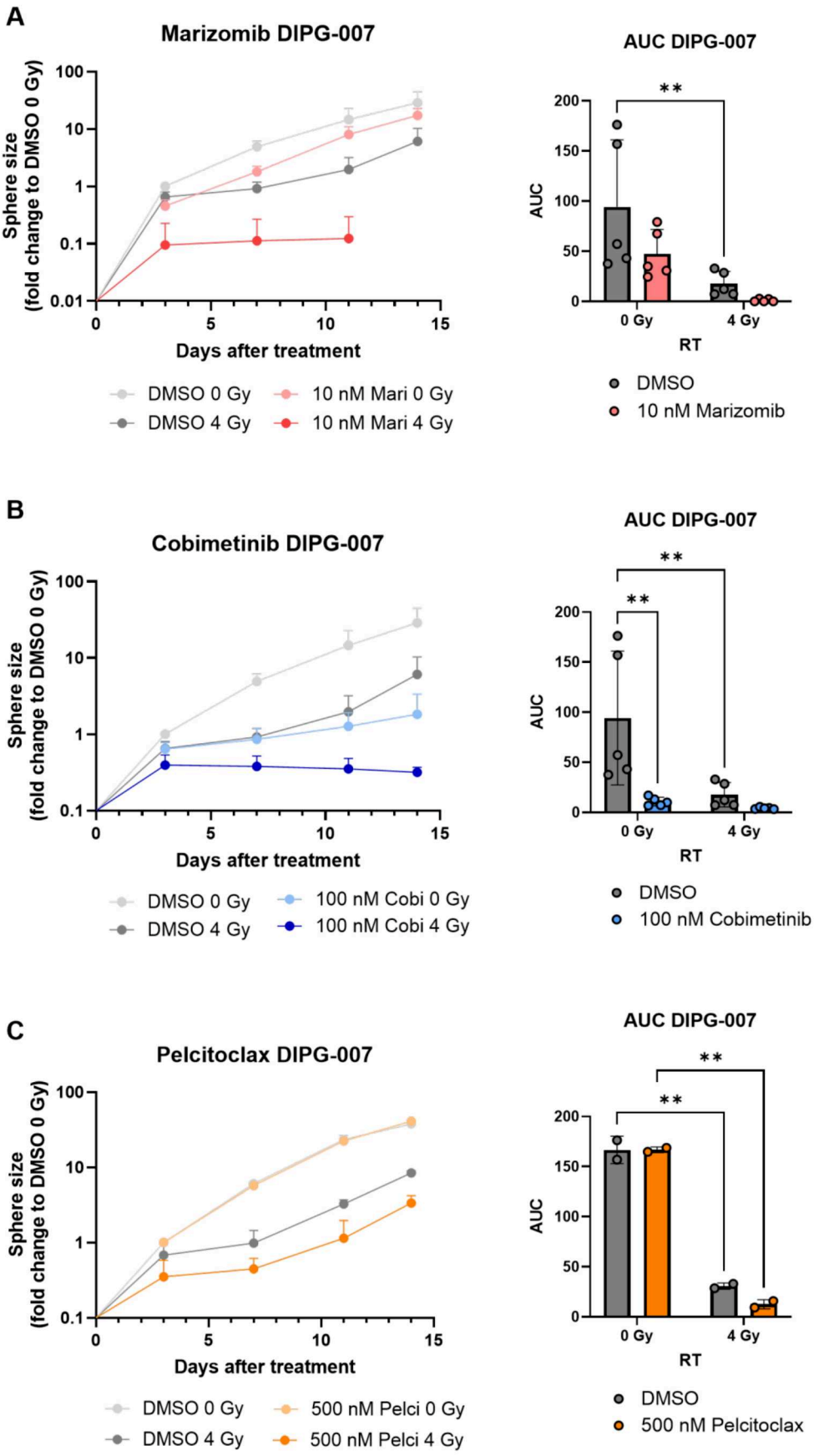


Figure 16: Quantification of the sphere size of the long-term growth inhibition assays in DIPG-007 cells.

The area of each sphere was assessed on day 3, 7, 11, and 14 after drug+RT treatment. The area under the curve (AUC) was then calculated for each biological replicate. Sphere size over time (left) and respective AUC (right) after A) Marizomib+RT treatment (n=5), B) Cobimetinib+RT treatment (n=5), and C) Pelcitoclax+RT treatment (n=2). Mean ± SD.

4.1.7. Candidate compounds differentially influence radiotherapy-induced DNA double-strand breaks

Some radiosensitizers have been shown to amplify RT-induced DNA double-strand breaks (DSBs) or to prolong their persistence in cancer cells (Geng et al., 2006; Löser et al., 2010; Zuckermann et al., 2024).

To determine whether the selected drug candidates enhance RT-induced DNA DSBs in pHGG cells, DNA DSB formation was quantified by γH2AX staining using flow cytometry following combination treatment. In the absence of irradiation (0 Gy), low proportions of γH2AX-positive cells were observed across all treatment conditions. In contrast, 90 min after irradiation with 2 Gy, the proportion of γH2AX-positive cells increased to approximately 40 % in DMSO-treated controls. The addition of Marizomib, Cobimetinib, Pelcitoclax, or Romidepsin to RT did not result in a significant further increase in γH2AX formation at the 90 min time point in the tested cells (Figure 17 A).

To determine whether combination treatment affected DNA DSB persistence, I analyzed γH2AX levels at multiple time points following irradiation (Figure 17 B-E). Marizomib and Pelcitoclax did not alter the proportion of γH2AX-positive cells at any assessed time point. Cobimetinib showed a trend toward reduced γH2AX positivity at 1 h and 4 h after RT, whereas Romidepsin appeared to increase the persistence of γH2AX-positive cells from 4 h to 24 h post-irradiation. Statistical analysis was not performed for these experiments, as they were conducted only once.

Together, these results suggest that the observed radiosensitizing effect may involve mechanisms downstream of the immediate DNA damage response.

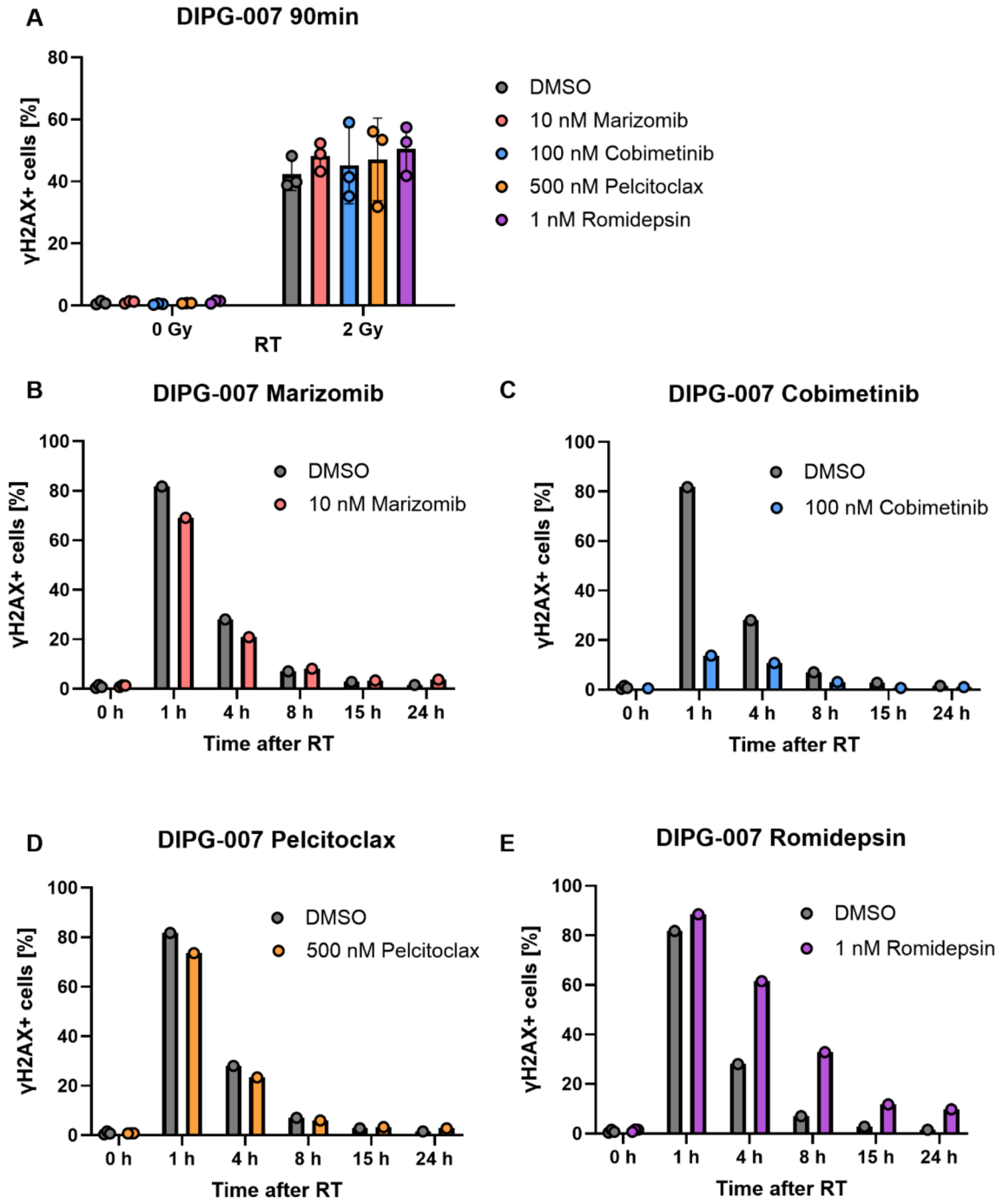


Figure 17: Effects of drug+RT treatment on RT-induced DNA double-strand breaks (DSB).
The amount of RT-induced DNA DSBs were assessed A) 90 min (n=3) and B)-E) 1 h-24 h (n=1) after RT by γH2AX staining via flow cytometry. Mean ± SD.

4.1.8. NXG mice are unable to tolerate fractionated whole-brain irradiation

In preparation for the preclinical evaluation of the selected drug+RT combinations, I aimed to establish orthotopic pHGG xenograft models. To prevent immune mediated rejection of PDX-derived human tumor cells after transplantation, the use of immunodeficient or immunocompromised mouse strains is required. NSG mice are most commonly used for this purpose, as they are profoundly immunodeficient and therefore provide optimal conditions for human tumor cell engraftment. However, NSG mice harbor the *Prkdc*^{scid} mutation, which disrupts the catalytic subunit of the DNA-PK and impairs DNA repair via the NHEJ pathway (Jeggo, 1998). As a consequence, these mice are markedly more radiosensitive than other mouse strains (Pearson et al., 2008; Saki et al., 2019).

A previous study demonstrated that NSG mice tolerate 10 Gy RT delivered in five daily fractions of 2 Gy without histological signs of brain toxicity; however, animals were only monitored for up to 72 h after RT (Saki et al., 2019). To assess tolerance to fractionated whole-brain RT at higher doses, I exposed NXG mice, an alternative to NSG mice with identical genetic characteristics (Finesso et al., 2023), to fractionated irradiation regimens of 10, 20, or 30 Gy delivered at 2 Gy per fraction (fx) per day, as well as 10 Gy delivered at 0.5 Gy/fx per day. During the irradiation period, mice receiving 2 Gy/fx exhibited significant weight loss exceeding 20 % of body weight across all dose groups. Consequently, irradiation was discontinued at 18 Gy in the cohorts intended to receive 20 Gy and 30 Gy total dose, and the animals were sacrificed. Mice treated with 0.5 Gy/fx (10 Gy total) tolerated the irradiation phase without apparent adverse events. However, during the subsequent observation period, animals developed acute weight loss exceeding 20 % body weight and were therefore sacrificed as well (Figure 18).

Given that effective RT doses for treating pHGG xenografts *in vivo* typically range between 10 and 20 Gy (Husband et al., 2021), NSG or NXG mice were considered unsuitable for subsequent experiments.

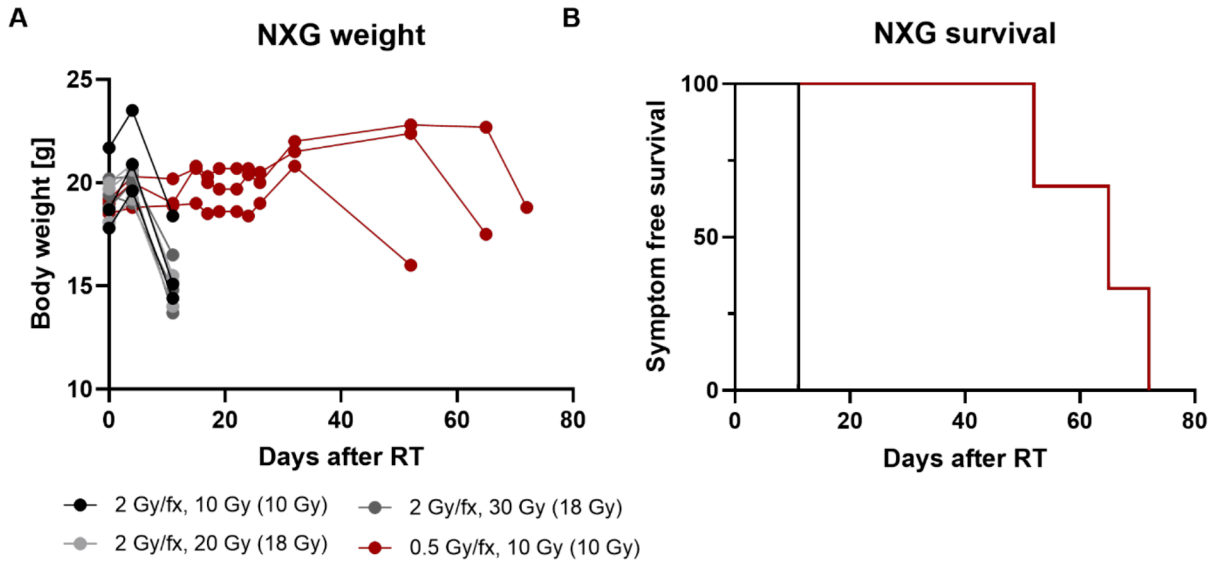


Figure 18: Fractionated whole-brain RT causes severe toxicities in immunodeficient NXG mice.
NXG mice were exposed to fractionated whole-brain irradiation as indicated and afterwards the A) weight and B) survival monitored. Fx: fraction. RT dose in brackets represents the received RT dose at endpoint. n=3 mice per group.

4.1.9. Orthotopic pHGG xenografts exhibit model-dependent engraftment and growth behavior

Based on the results shown in Figure 18, alternative mouse strains with greater tolerance to irradiation were required. I selected CD1 nude and NRG mice for the subsequent *in vivo* experiments, as both strains lack an intact immune system but also exhibit higher irradiation tolerance than NSG or NXG mice.

CD1 nude mice carry a mutation in the *Foxn1* gene, resulting in thymic aplasia and T cell deficiency (Corbeaux et al., 2010). Importantly, these mice retain intact DNA repair pathways and display radiosensitivity profiles comparable to wild type mice. Previous studies have shown that CD1 nude mice tolerate RT doses of up to 54 Gy (Husband et al., 2021). However, because they lack only T cells, their degree of immunodeficiency is limited, and they are therefore classified as immunocompromised rather than fully immunodeficient (Chen et al., 2022).

As an alternative, NRG mice harbor a *Rag1* knockout, which prevents V(D)J recombination and eliminates mature B and T cells, rendering these animals fully immunodeficient. Importantly, this mutation does not affect core DNA repair mechanisms in non-hematopoietic tissues, resulting in greater radioresistance compared with NSG or NXG mice (Pearson et al., 2008). Previous studies have shown that NRG mice tolerate RT doses of up to 24 Gy (Maeda et al., 2017; Pearson et al., 2008). As CD1 nude mice generally demonstrate higher irradiation

tolerance than NRG mice, I prioritized CD1 nude mice for the establishment of pHGG xenograft models and used NRG mice only in cases where tumor engraftment failed in CD1 nude mice.

I transplanted DIPG-007, DIPG-19, DIPG-17, and DIPGx7 cells into the brainstem of CD1 nude mice, where gradual tumor growth was observed in all models, with latencies ranging from 60 to 300 days, as assessed by bioluminescence imaging (IVIS) (Figure 19). Since DIPG-21 cells failed to engraft in CD1 nude mice and DIPG-19 tumors exhibited comparatively long latencies (~300 days), I transplanted these cells additionally into immunodeficient NRG mice.

To assess potential effects of anatomic location on tumor growth, I transplanted DIPG-19 and DIPG-21 cells into the brainstem and the thalamus of NRG mice. DIPG-19 tumors transplanted into the brainstem showed growth dynamics comparable to those observed in CD1 nude mice (latency ~300 days), whereas thalamic implantation resulted in an apparent tumor growth delay (latency ~330 days). DIPG-21 cells did not engraft in the brainstem of NRG mice, and only one animal with thalamic implantation displayed a detectable tumor signal by the end of the observation period of 365 days.

Representative images of pHGG tumors in the brainstem of CD1 nude mice are shown in Figure 20. Tumors were identified by GFP and luciferase signals, which was possible due to stable labeling of the transplanted cells (Figure 20 A and B). In addition, fixed brain sections were stained with hematoxylin and eosin (H&E) and Ki67 to visualize tumor morphology and proliferating tumor cells, respectively (Figure 20 C and D).

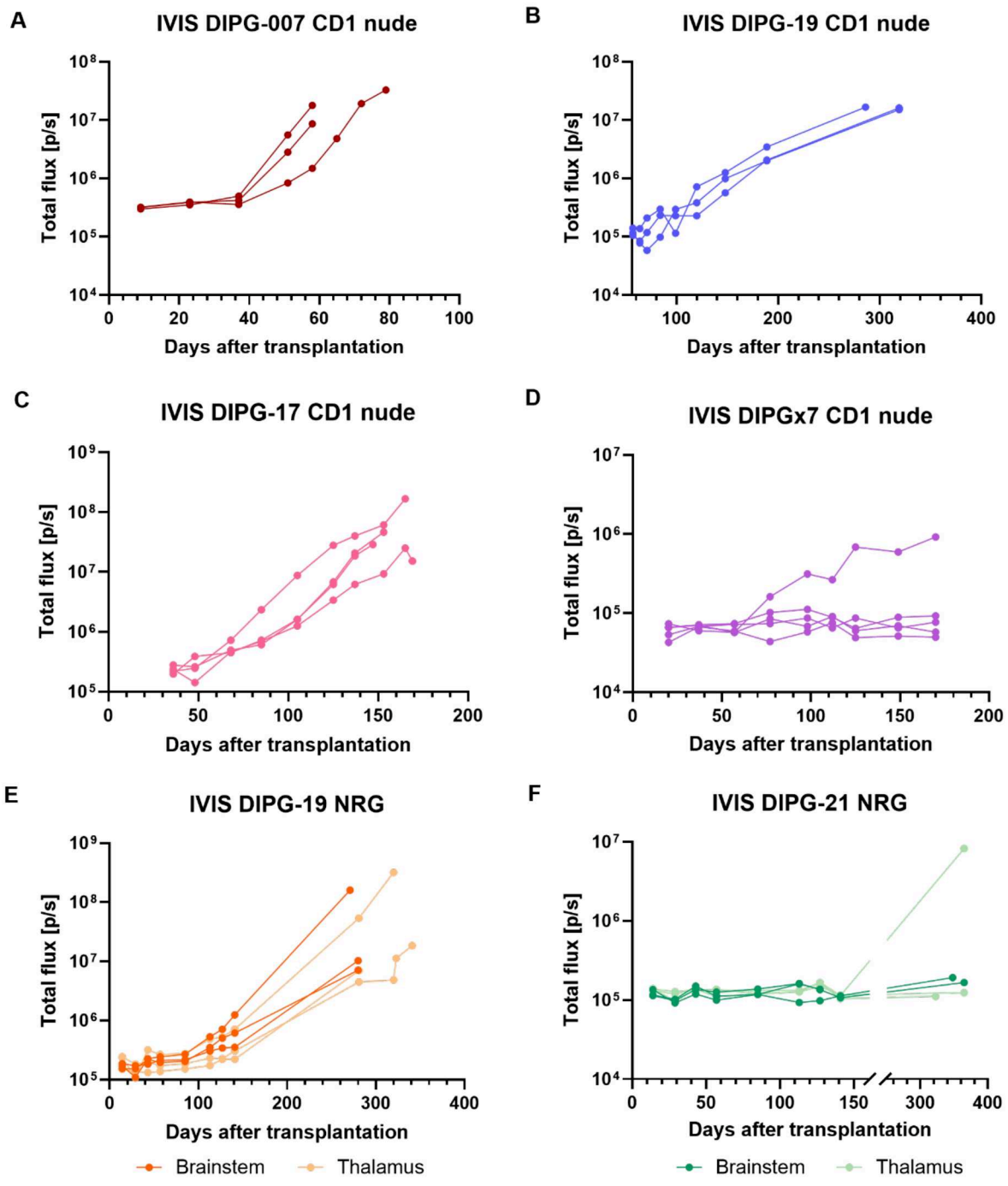


Figure 19: pHGG xenograft model establishment in CD1 nude and NRG mice.
pHGG cells (H3K27M) were intracranially transplanted into A)-D) CD1 nude mice or E)-F) NRG mice and their tumor signals were monitored by bioluminescence imaging (IVIS) over time. Each curve represents an individual mouse (n=3-5). The DIPGx7 experiment is still ongoing and all animals are still alive (day 170).

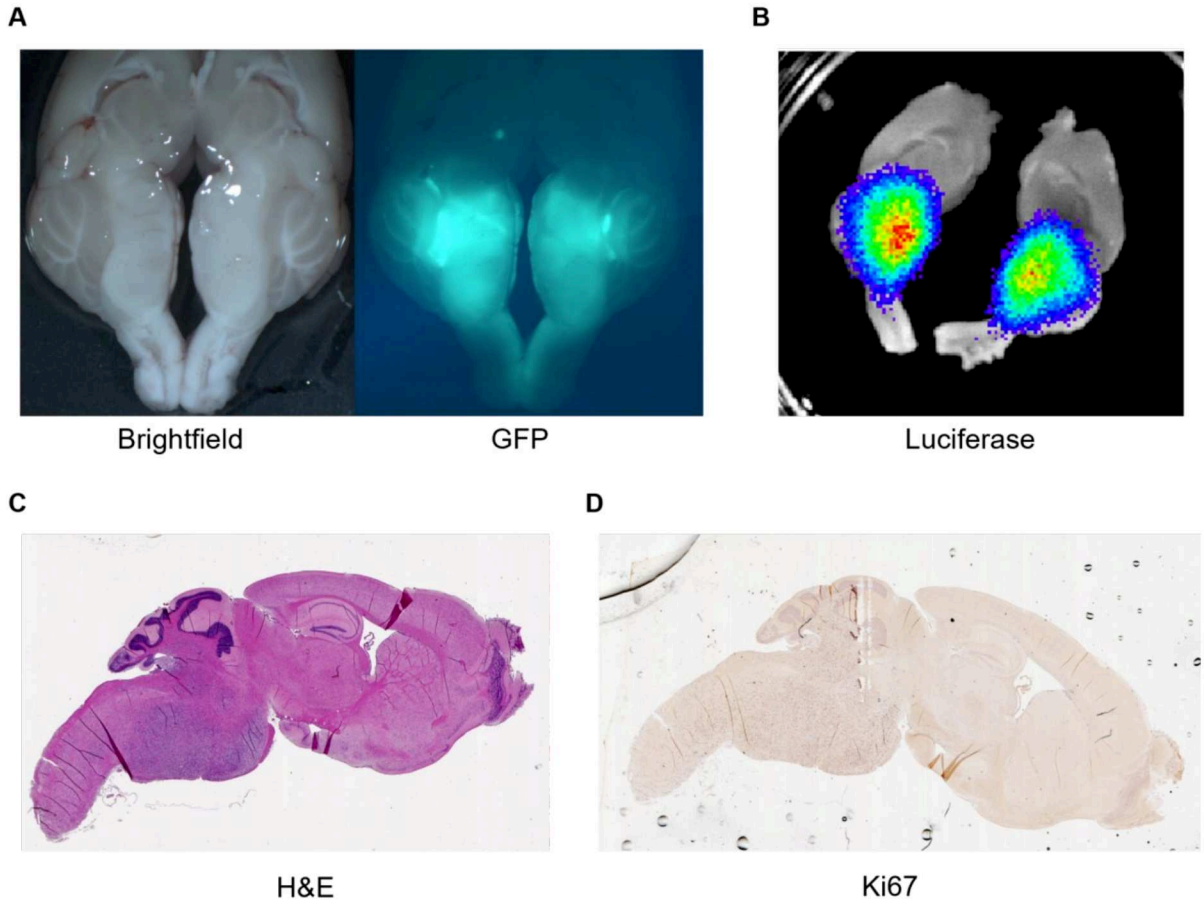


Figure 20: Representative pictures of pHGG tumors in the brainstem of CD1 nude mice.
A) Brightfield and GFP fluorescence images from a freshly dissected brain acquired using a 0.63x objective at 1x zoom at a fluorescence microscope. B) Luciferase signal of a freshly dissected brain captured by bioluminescence imaging (IVIS). C) H&E staining of a fixed brain sample. D) Ki67 staining of a fixed brain sample.

4.1.10. Fractionated radiotherapy delays tumor progression in the DIPG-007 xenograft model

To evaluate the intrinsic radiosensitivity of the DIPG-007 mouse model, I treated tumor-bearing mice with fractionated whole-brain irradiation using cumulative doses of 4, 8, or 12 Gy administered in 2 Gy fractions (reflecting the clinical use of ~1.8 Gy/fraction), followed by monitoring of tumor growth and latency (Figure 21). Mice receiving a total dose of 4 Gy showed tumor progression and latency comparable to non-irradiated controls, with a median latency of approximately 60 days (Figure 19 A). In contrast, irradiation with total doses of 8 Gy and 12 Gy resulted in slower tumor progression and prolonged survival, with median latencies of approximately 76 and 84 days, respectively.

The planned group size was three mice per treatment arm; however, I needed to exclude several animals from the experiment due to adverse events. None of the applied RT doses resulted in tumor regression or clearance, thereby defining a treatment window that allows for the addition of drug treatment and the evaluation of potential synergistic effects.

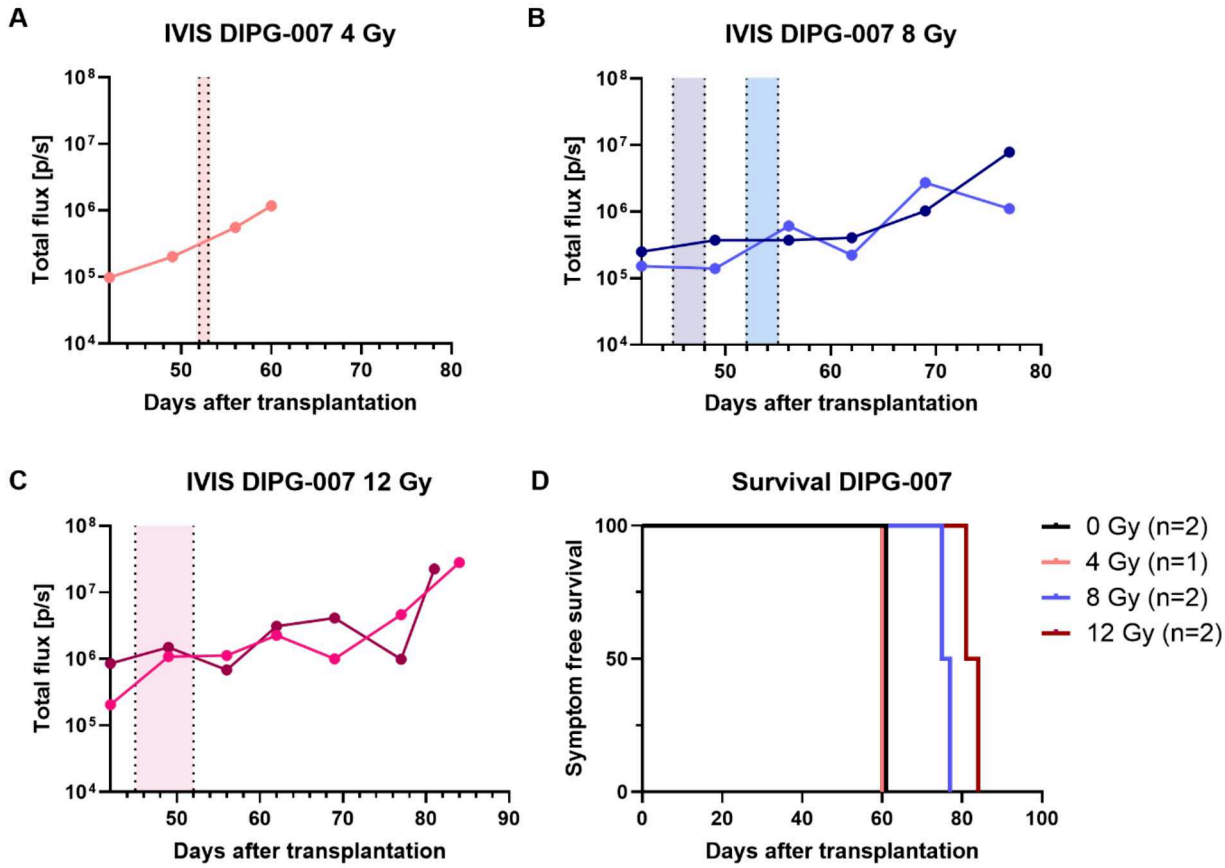


Figure 21: Radiosensitivity of the DIPG-007 mouse model in CD1 nude mice.
Mice harboring DIPG-007-induced brain tumors were irradiated with fractionated X-ray RT at 2 Gy/fraction/day up to total doses of A) 4 Gy, B) 8 Gy, and C) 12 Gy using the SmART+ machine. Tumor signals were monitored over time using bioluminescence imaging (IVIS). Each curve represents an individual animal. D) Survival of all the irradiated mice compared to the non-irradiated control animals from Figure 19 A.

4.1.11. Preclinical evaluation of the radiosensitizing potential of identified compounds in the DIPG-007 model

4.1.11.1. Preclinical investigation of Marizomib, Cobimetinib, and Romidepsin reveals no improvement of radiotherapy efficacy

Based on the previous *in vitro* and *in vivo* data, a preclinical study was conducted to evaluate the radiosensitizing effects of Marizomib (Mari), Cobimetinib (Cobi), and Romidepsin (Romi) *in vivo*. DIPG-007 cells were transplanted into the brainstem of CD1 nude mice, which were randomized on day 42 based on tumor burden into eight treatment groups. Drug and RT treatment was initiated on day 43 (Figure 22 A). Mice received fractionated whole-brain X-ray irradiation with a total dose of 12 Gy delivered over six days at 2 Gy/day, with a treatment break over the weekend. Drug administration was performed as outlined in Table 4 and continued until predefined endpoint criteria were reached.

Fractionated RT (12 Gy) significantly reduced tumor growth and prolonged survival (Marizomib vs. Marizomib+RT, p = **; Cobimetinib vs. Cobimetinib+RT, p = *) compared with the

corresponding drug-only treatment groups (Figure 22 B, C, E). In contrast, Marizomib and Cobimetinib monotherapy did not significantly affect tumor growth (Figure 22 B, C) or survival (Figure 22 E) compared with vehicle-treated controls. Furthermore, within the irradiated cohorts, no significant differences were observed between the combination treatments and vehicle+RT.

Romidepsin treatment, both as monotherapy and in combination with RT, resulted in significant toxicity in mice (Supplementary figure 13 D), despite the applied dose having been previously reported as well tolerated (Noll et al., 2023).

In the remaining treatment groups, individual mice were occasionally removed from the study due to body weight loss exceeding 20 %, in accordance with predefined endpoint criteria. Apart from these cases, no obvious treatment-associated body weight loss or signs of systemic toxicity were detected at the group level (Supplementary figure 13).

The absence of both single-agent activity and the drug+RT effects previously observed *in vitro* may indicate that the compounds failed to achieve adequate concentrations in the mouse brain, suggesting that the dosing regimens require further optimization.

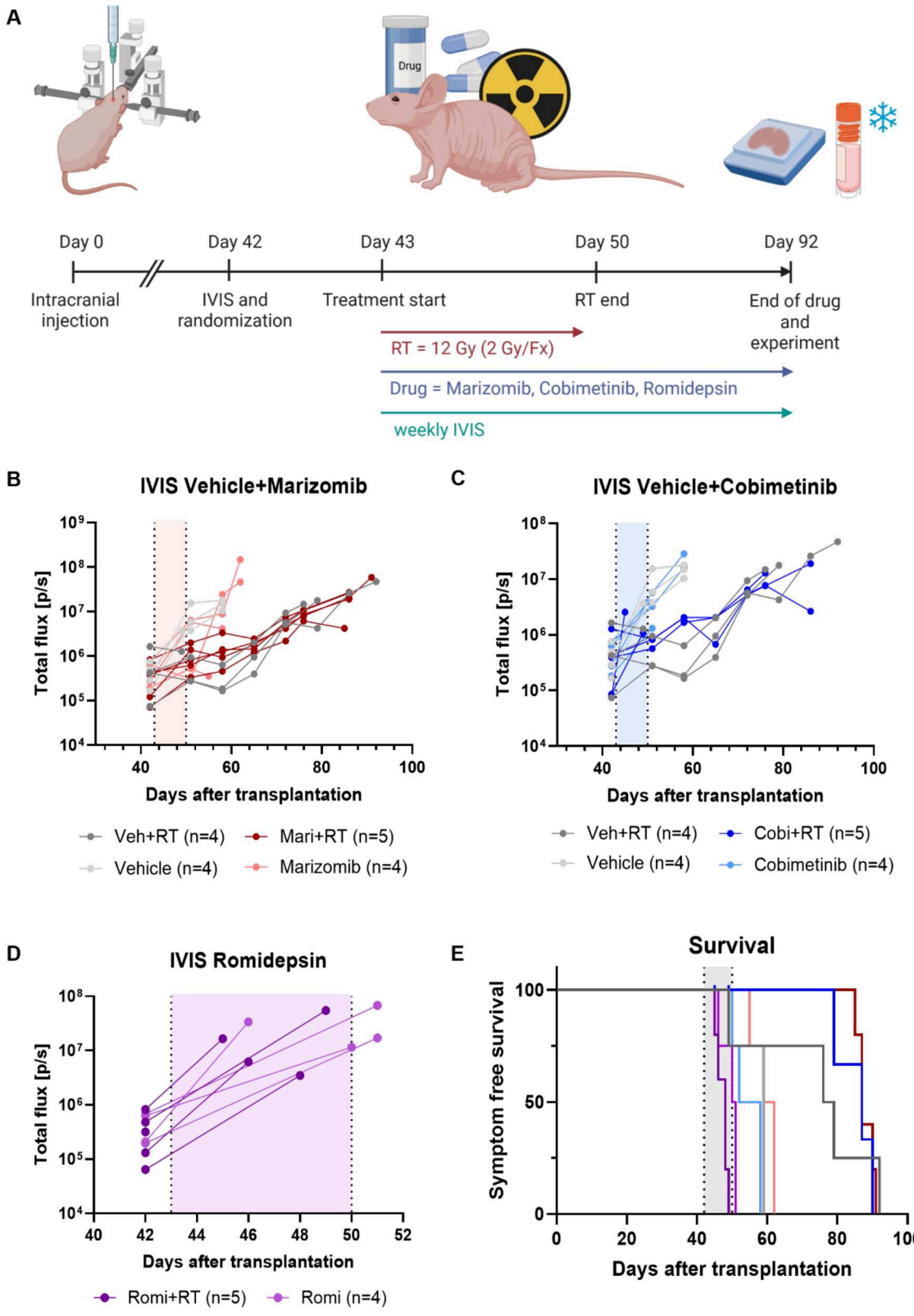


Figure 22: Preclinical evaluation of Marizomib (Mari, Proteasemei), Cobimetinib (Cobi, MEKi), and Romidepsin (Romi, HDACi) in combination with 12 Gy RT in the DIPG-007 mouse model.
A) Schematic illustration of the study. IVIS tumor signal of B) Marizomib-treated (150 µg/kg, i.p., 2x week), C) Cobimetinib-treated (15 mg/kg, oral, 2x week), and D) Romidepsin-treated (1 mg/kg, i.p., 5x week) mice in comparison to vehicle-treated mice. Vehicle of Romidepsin (i.p., 5x week) was used for all vehicle-treated animals. E) Survival of all the treatment groups within this study. The area between the dashed lines represents the RT treatment frame.

4.1.11.2. Optimized dosing strategies of Marizomib and Cobimetinib fail to enhance radiotherapy response *in vivo*

Given that Marizomib has been reported to be BBB penetrant in monkeys and rats (Di et al., 2016), and to reduce tumor growth as monotherapy in other DIPG (Lin et al., 2019) and GBM (Manton et al., 2016) models at comparable doses, I considered whether the intraperitoneal (i.p.) administration route used in this study (Manton et al., 2016; Vlashi et al., 2010) may have been suboptimal for intracranial tumor models. Intravenous (i.v.) administration could potentially improve brain drug exposure, which has been successfully applied by (Lin et al., 2019). Cobimetinib, although described as having limited BBB penetration (Choo et al., 2014), is currently under clinical investigation for the treatment of pLGG, where it has shown limited single agent activity (Trippett et al., 2022). In this context, I hypothesized that increasing the treatment frequency to daily dosing (Rosen et al., 2016) could enhance overall drug exposure and availability.

Given that mice treated with Romidepsin exhibited treatment-related toxicity, I sought an alternative HDACi with improved BBB penetration. The HDACi valproic acid, also referred to as valproate or VPA, has been detected in the cerebrospinal fluid of non-human primates (Stapleton et al., 2008) and in children with epilepsy (Löscher et al., 1988), thereby making it a suitable candidate for the subsequent experiments. Based on these considerations, I modified the drug administration regimens of Marizomib and Cobimetinib, and included VPA in a second preclinical trial (Figure 23).

The overall study design was comparable to the previous experiment (Figure 22), with the exception that treatment was initiated one week earlier, on day 36, to extend the post-treatment observation period. Tumor burden in this model was already approaching endpoint IVIS signal levels by day 43 and was associated with early mortality. As shown in Figure 23, none of the combination treatments resulted in delayed tumor progression or prolonged survival compared with vehicle+RT treatment. In both the vehicle- and VPA-treated groups, RT significantly extended survival (vehicle vs. vehicle+RT, p = *; VPA vs. VPA+RT, p = **). In the Marizomib and VPA treatment groups, individual mice were occasionally removed from the study due to body weight loss exceeding 20 %, in accordance with predefined endpoint criteria. Apart from these cases, no obvious treatment-associated body weight loss or signs of systemic toxicity were detected (Supplementary figure 14).

Given that the optimized dosing strategies did not improve study outcomes and still failed to demonstrate single-agent or combinatorial efficacy, these findings further support the hypothesis that limited BBB penetration of the selected compounds represents a major limiting factor.

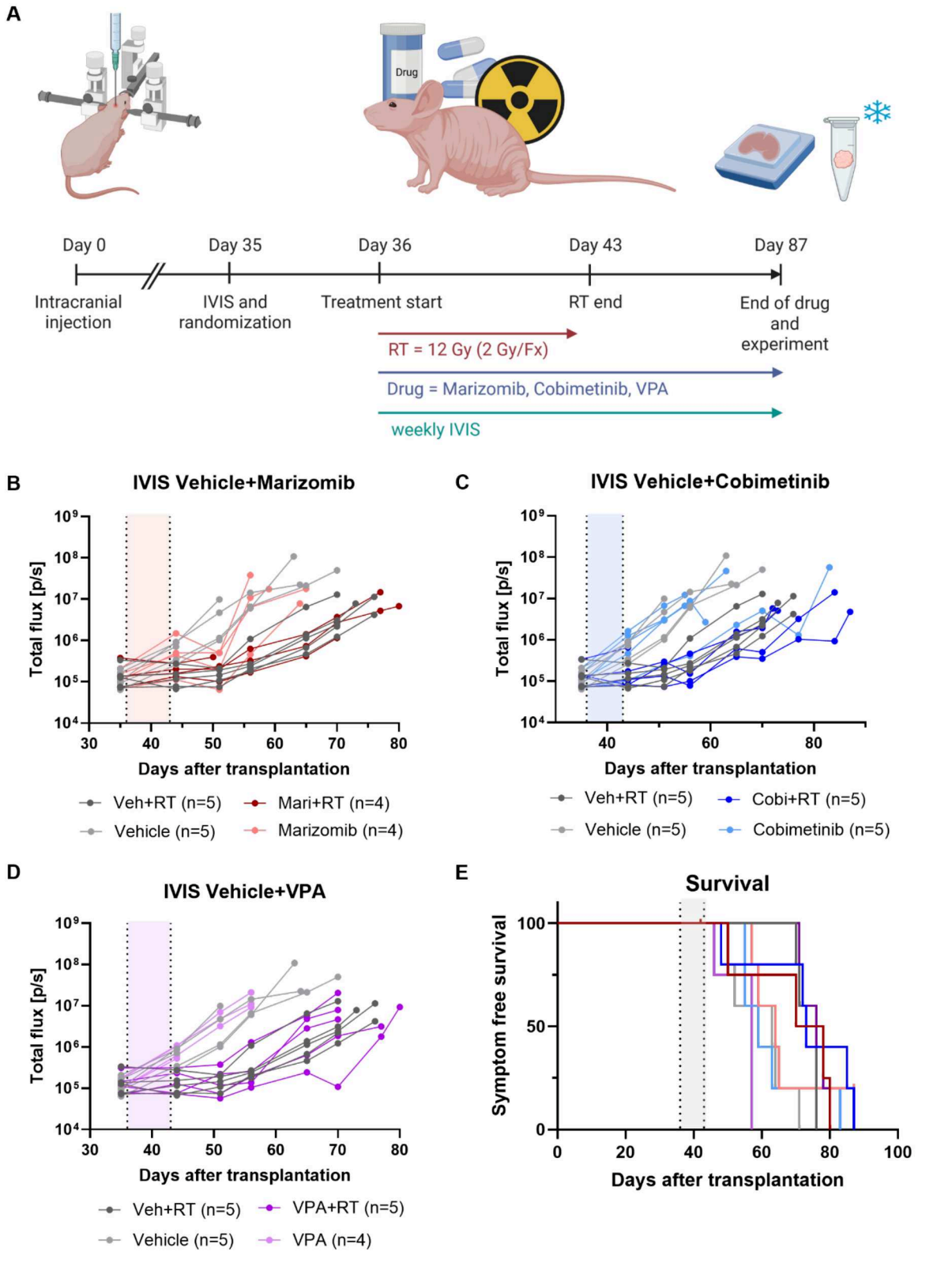


Figure 23: Preclinical evaluation of Marizomib (Mari, Proteasemei), Cobimetinib (Cobi, MEKi), and Valproic acid (VPA, HDACi) in combination with 12 Gy RT in the DIPG-007 mouse model.
A) Schematic illustration of the study. IVIS tumor signal of B) Marizomib-treated (150 µg/kg, i.v., 2x week), C) Cobimetinib-treated (10 mg/kg, oral, 5x week), and D) VPA-treated (200 mg/kg, i.p., 5x week) mice in comparison to vehicle-treated mice. Vehicle of Cobimetinib (oral, 5 x week) was used for all vehicle-treated animals. E) Survival of all the treatment groups within this study. The area between the dashed lines represents the RT treatment frame.

4.1.11.3. Limited brain exposure of candidate compounds correlates with lack of *in vivo* efficacy

Based on results observed in the preclinical studies (Figure 22 and Figure 23), I hypothesized that insufficient BBB penetration of the tested compounds contributed to the lack of efficacy. To assess brain exposure, I performed a pharmacokinetic analysis of Romidepsin and Cobimetinib. Each compound was administered once, and blood plasma and perfused brain tissue were collected at multiple time points post-administration. Drug concentrations were subsequently quantified by mass spectrometry.

For Romidepsin, the highest plasma concentrations were detected 30 min after administration, followed by a time-dependent decline (Figure 24 A). Romidepsin was not detectable in any of the analyzed brain samples. In contrast, Cobimetinib plasma concentrations remained relatively stable for up to 8 h and gradually decreased thereafter (Figure 24 B). Brain concentrations of Cobimetinib increased within the first 4 h after administration and remained stable up to 24 h, with peak levels observed at 8 h post-treatment. At peak brain concentrations, Cobimetinib reached approximately 30 % of the corresponding plasma levels.

The IC50 of Cobimetinib in DIPG-007 cells is approximately 100 nM, corresponding to a brain tissue concentration of ~53 ng/g. Cobimetinib concentrations in the brain remained slightly below this threshold, which may account for the lack of therapeutic efficacy observed in the first two preclinical studies (Figure 22 and Figure 23).

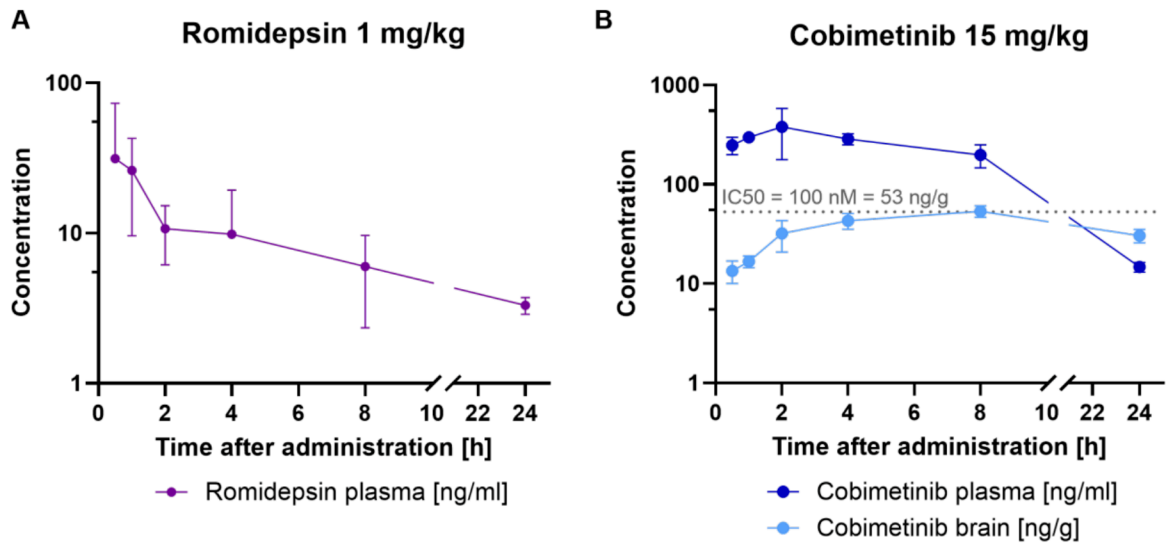


Figure 24: Pharmacokinetic (PK) analysis of Romidepsin and Cobimetinib in CD1 nude mice.
The concentration of A) Romidepsin (1 mg/kg, i.p.) and B) Cobimetinib (15 mg/kg, oral) was assessed in the blood plasma and brain tissue at different time points after drug administration to CD1 nude mice by mass spectrometry. Mean ± SD, n=3.

4.1.11.4. Preclinical evaluation of alternative MEKi and HDACi fail to improve radiotherapy efficacy *in vivo*

As a final attempt to validate the selected compound classes in intracranial pHGG models, I selected the BCLi AZD4320, the MEKi Trametinib, and the HDACi Panobinostat.

AZD4320 is a dual BCL-2/-XL inhibitor with high efficacy in hematological malignancies. Although AZD4320 exhibits a similar inhibition profile to Navitoclax, preclinical studies suggest a lower incidence of dose limiting thrombocytopenia compared with Navitoclax (Balachander et al., 2020).

Trametinib, similar to Cobimetinib, is a MEKi that showed high efficacy in the initial drug+RT screen as well as in subsequent *in vitro* validation experiments. Trametinib is currently under clinical investigation for pLGG and MAPK-driven pHGGs (Bouffet et al., 2023; Perreault et al., 2019), making it an attractive candidate for potential clinical translation.

Panobinostat, also known as LBH589, is a pan-HDACi that has demonstrated antitumor activity in preclinical pHGG models (Hennika et al., 2017) and is currently being evaluated in clinical trials for DIPG (Monje et al., 2023; Mueller et al., 2023). Although radiosensitizing effects of Panobinostat have been suggested in glioblastoma (Pont et al., 2015), prostate cancer (Xiao et al., 2013), and bladder cancer (Groselj et al., 2013), clinical evidence supporting a radiosensitizing effect in pHGGs remains limited.

In this study, I followed the treatment scheme shown in Figure 25 A, which was comparable to that used in the second preclinical trial (Figure 23).

Consistent with the previous two studies (Figure 22 and Figure 23), RT significantly prolonged survival across all treatment groups (vehicle vs. vehicle+RT, p = **; AZD vs. AZD+RT, p = *; Trametinib vs. Trametinib+RT, p = **; Panobinostat vs. Panobinostat+RT, p = **). Beyond the effect of RT, no additional reduction in tumor growth or improvement in survival was observed for any drug+RT combination compared with vehicle+RT (Figure 25 B-E).

In all treatment groups, individual mice were occasionally removed from the study due to body weight loss exceeding 20 %, in accordance with predefined endpoint criteria. Apart from these cases, no obvious treatment-associated body weight loss or signs of systemic toxicity were detected at the group level (Supplementary figure 15).

Despite strong *in vitro* activity, the absence of both single-agent and combinatorial efficacy across all three preclinical trials suggests that limited BBB penetration, and the resulting insufficient intratumoral drug exposure, represent a principal barrier when evaluating radiosensitizers in orthotopic pHGG models.

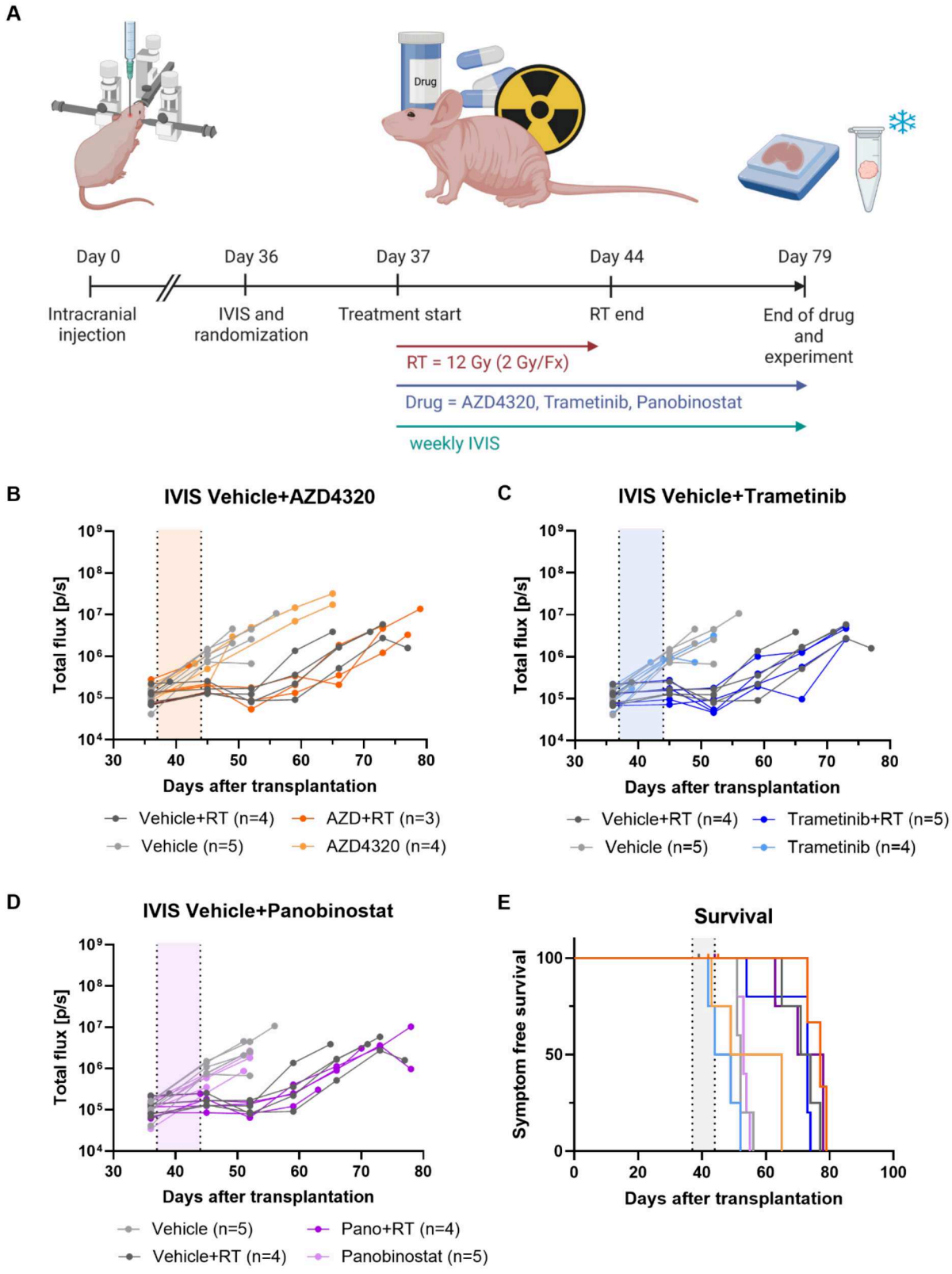


Figure 25: Preclinical evaluation of AZD4320 (AZD, BCLi), Trametinib (MEKi), and Panobinostat (Pano, HDACi) in combination with 12 Gy RT in the DIPG-007 mouse model.
A) Schematic illustration of the study. IVIS tumor signal of B) AZD4320-treated (10 mg/kg, i.v., 1x week), C) Trametinib-treated (1 mg/kg, oral, 5 x week), and D) Panobinostat-treated (5 mg/kg, i.p., 5x week) mice in comparison to vehicle-treated mice. Vehicle of Trametinib (oral, 5 x week) was used for all vehicle-treated animals. E) Survival of all the treatment groups within this study. The area between the dashed lines represents the RT treatment frame.

4.2. Overcoming ALK inhibitor resistance in ALK-fusion infant-type hemispheric glioma

4.2.1. Chronic Lorlatinib treatment induces stable Lorlatinib-resistance in PPP1CB::ALK-driven pHGG cells

To generate Lorlatinib-resistant cells, I continuously cultured PPP1CB::ALK-driven pHGG cells (BI#190) with either 10 nM Lorlatinib or DMSO as a vehicle control. After 10 weeks, I assessed the cell viability of both cell cultures to increasing concentrations of Lorlatinib (Figure 26 A).
Cells maintained under continuous DMSO treatment (DMSO cells) showed a dose-dependent reduction in viability in response to Lorlatinib teatment. In contrast, cells continuously cultured with Lorlatinib (Lorlatinib-resistant cells) displayed minimal changes in viability across the tested concentration range, indicating the development of drug resistance (Figure 26 B).
I repeated this procedure independently to establish three additional Lorlatinib-resistant cell populations (Res. cells 2, 3, and 5; Supplementary figure 16).

To evaluate the stability of resistance, I subsequently cultured each resistant cell population for 6 weeks in the absence of Lorlatinib under continuous DMSO treatment. Following this drug withdrawal period, I assessed cell viability of the cell cultures to either DMSO or 10 nM Lorlatinib treatment (Figure 27 A).
Treatment with 10 nM Lorlatinib reduced the viability of DMSO cells to approximately 50 % (Figure 27 B), consistent with earlier observations (Figure 26). In contrast, Lorlatinib-resistant cells that had been cultured under DMSO conditions did not show a reduction in viability upon Lorlatinib exposure (Figure 27 C-E), indicating that the resistant phenotype remained stable even in the absence of continued drug selection.
Interestingly, Lorlatinib-resistant cells maintained under continuous Lorlatinib treatment exhibited significantly higher viability upon exposure to 10 nM Lorlatinib compared to DMSO (Figure 27 C-E). These findings suggest that Lorlatinib treatment may confer a survival advantage to resistant cells.
Comparable results were observed after 3 (Supplementary figure 17) and 8 weeks (Supplementary figure 18) of continuous DMSO or Lorlatinib treatment.

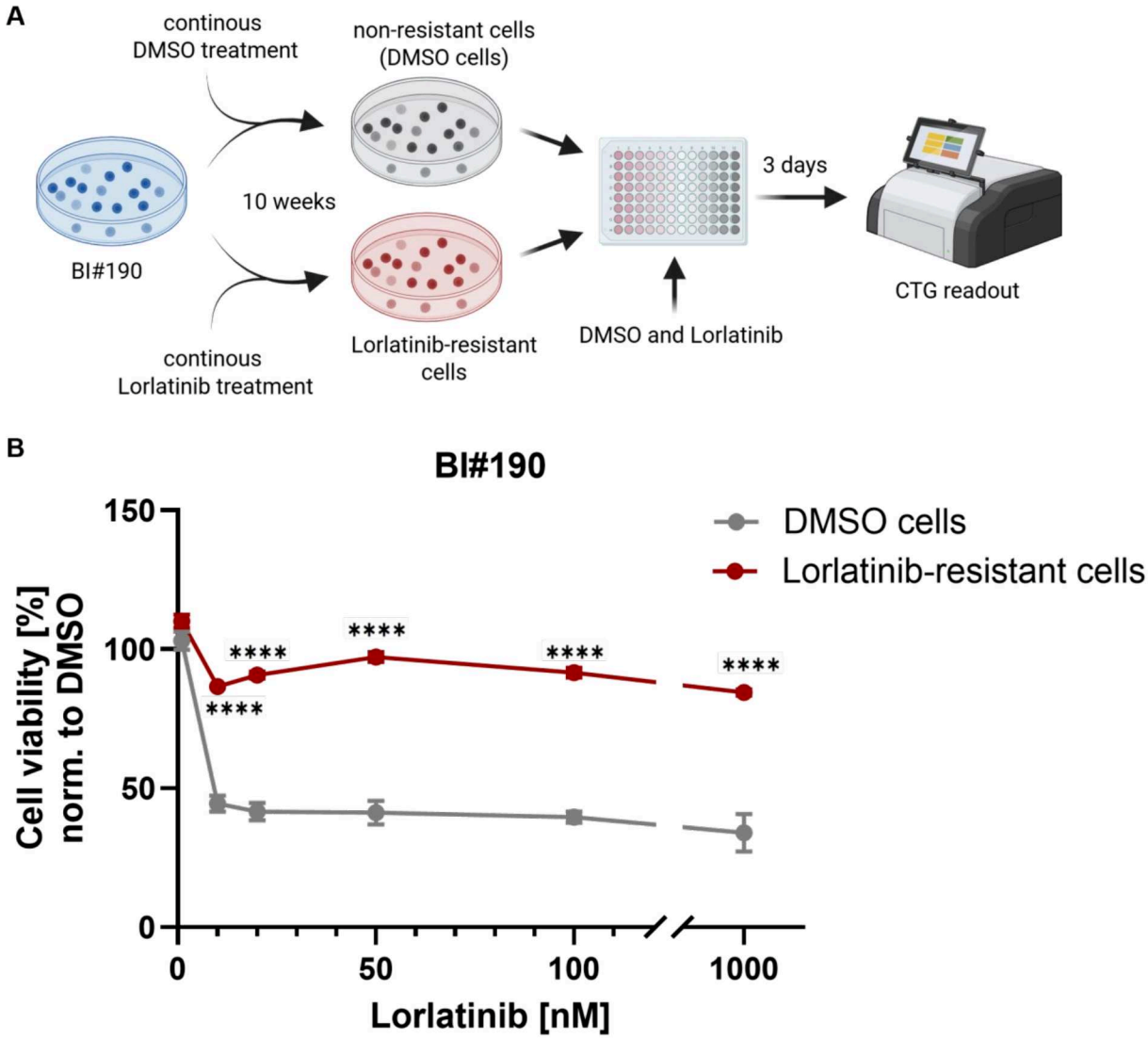


Figure 26: Generation of Lorlatinib-resistant cells in vitro.
A) *Experimental workflow. BI#190 cells were seeded into two wells and continuously cultured with either DMSO (DMSO cells) or 10 nM Lorlatinib (Lorlatinib-resistant cells). After 10 weeks, both cell cultures were seeded into 96-well plates and treated with either DMSO or increasing concentrations of Lorlatinib. After 3 days, the cell viability of both cell cultures was assessed by CellTiterGlo (CTG). B) Cell viability of DMSO cells and Lorlatinib-resistant cells in response to increasing concentrations of Lorlatinib. Mean ± SD, n=3.*

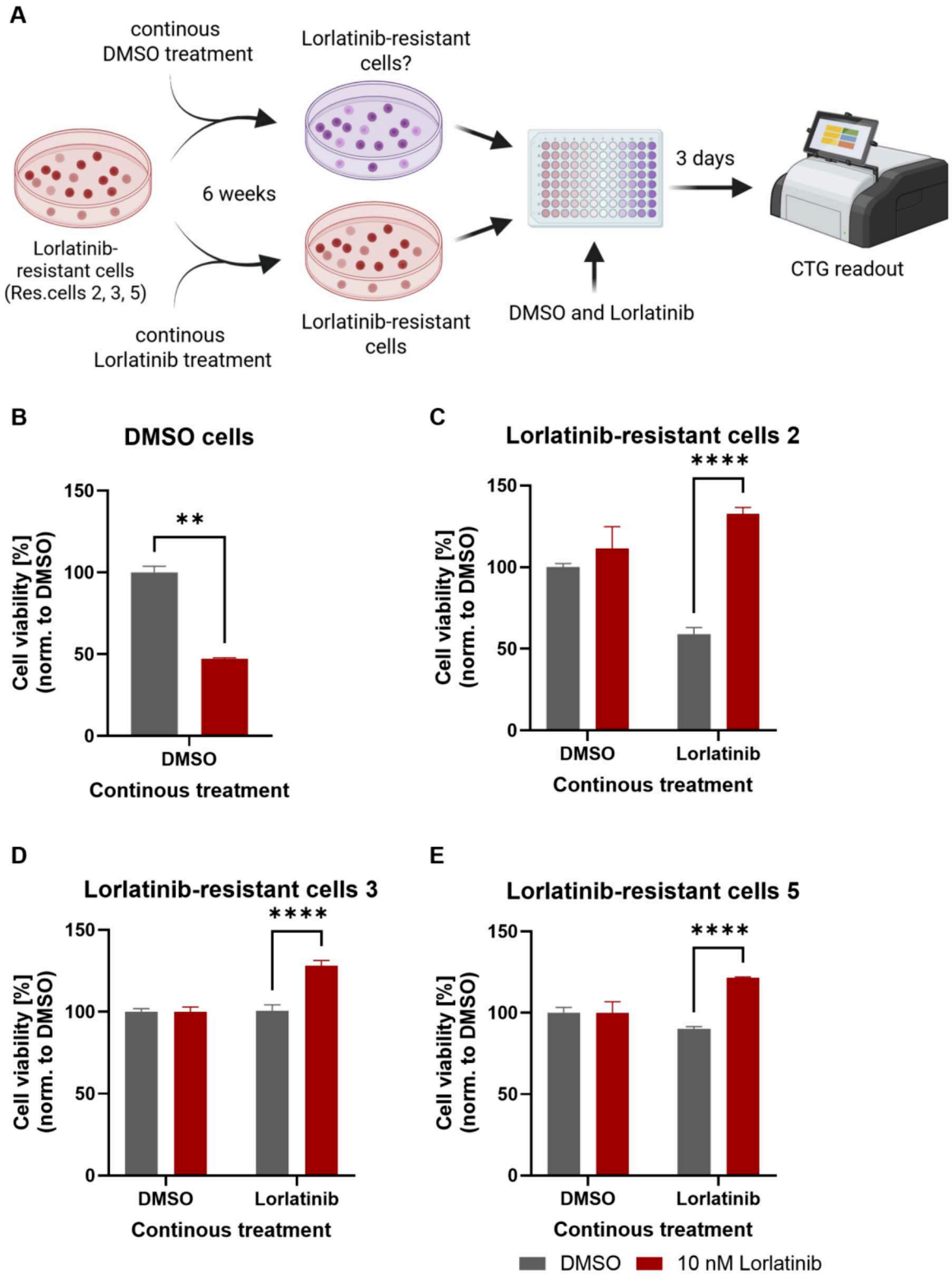


Figure 27: Lorlatinib resistance is stable even after Lorlatinib withdrawal.
A) *Experimental workflow. Lorlatinib-resistant cells were seeded into two wells and continuously cultured with either DMSO or 10nM Lorlatinib. After 6 weeks, both cell cultures were seeded into 96-well plates and treated with either DMSO or 10 nM Lorlatinib. After 3 days, the cell viability of both cell cultures was assessed by CellTiterGlo (CTG). B) Cell viability of DMSO cells in response to DMSO and 10 nM Lorlatinib treatment. C-E) Cell viability of Lorlatinib-resistant cells 2, 3, and 5 continuously cultured with DMSO or Lorlatinib for 6 weeks (X-axis), in response to DMSO and 10 nM Lorlatinib treatment after 3 days (grey and red respectively). Mean ± SD, n=3.*

4.2.2. ALK-inhibition enhances proliferation and inhibits apoptosis in Lorlatinib-resistant cells

Since Lorlatinib-resistant cells exhibited a higher cell viability upon treatment with 10 nM Lorlatinib compared with DMSO (Figure 27 C-E), I sought to investigate the underlying basis of this phenotype. I performed an EdU proliferation assay to assess DNA synthesis and found that Lorlatinib-resistant cells (Res.cells 2, 3, and 5) proliferated significantly more when treated with 10 nM Lorlatinib than with DMSO, as indicated by significantly increased EdU incorporation within 45 min (Figure 28 A).

In addition, I assessed cell death induction in response to 10 nM Lorlatinib treatment in resistant and non-resistant cells. In DMSO cells, exposure to 10 nM Lorlatinib significantly reduced the proportion of viable cells and increased the fraction of apoptotic cells compared with DMSO treatment (Figure 28 B). In contrast, in Lorlatinib-resistant cells (Res.cells 2, 3, and 5), no significant differences were detected in viable, apoptotic, or necrotic cell populations between Lorlatinib and DMSO treatment (Figure 28 C-E). These findings suggest that Lorlatinib treatment in resistant cells is associated with both increased proliferation and reduced cell death.

To determine whether this effect was specific to Lorlatinib, I exposed DMSO cells and Lorlatinib-resistant cells (Res.cells 2) to increasing concentrations of Crizotinib, an alternative ALK inhibitor. Crizotinib treatment resulted in a dose-dependent reduction in cell viability in DMSO cells (Figure 29). In contrast, Crizotinib significantly increased the viability of Res.cells 2 compared with DMSO cells over a concentration range of 1-400 nM, whereas higher Crizotinib concentrations appeared to be toxic to Res.cells 2 (Figure 29). These findings indicate that the increase in cell proliferation following ALK inhibition may reflect a class-wide mechanism rather than a Lorlatinib-specific effect.

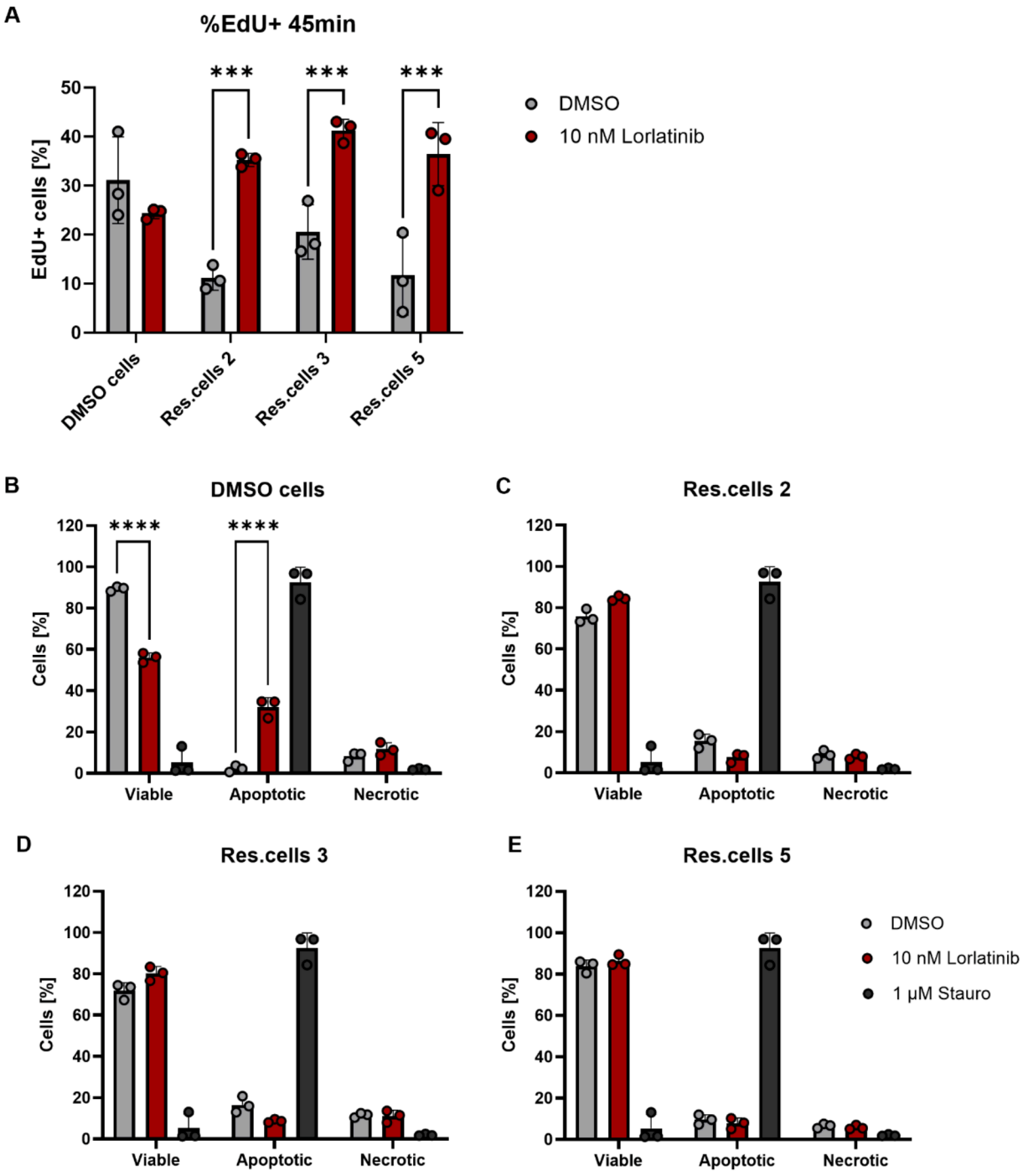


Figure 28: Lorlatinib treatment enhances proliferation and inhibits apoptosis in Lorlatinib-resistant cells.
A) EdU incorporation (within 45 min) into the DNA of DMSO cells and Lorlatinib-resistant cells (Res.cells 2, 3, 5) after 10 nM Lorlatinib and DMSO treatment was assessed by flow cytometry. B)-E) Cell death induction after 10 nM Lorlatinib and DMSO treatment in DMSO cells and Res.cells 2, 3, 5 was assessed by AnnexinV+PI staining using flow cytometry. Staurosporine (Stauro) served as positive control for cell death induction. Mean ± SD, n=3.

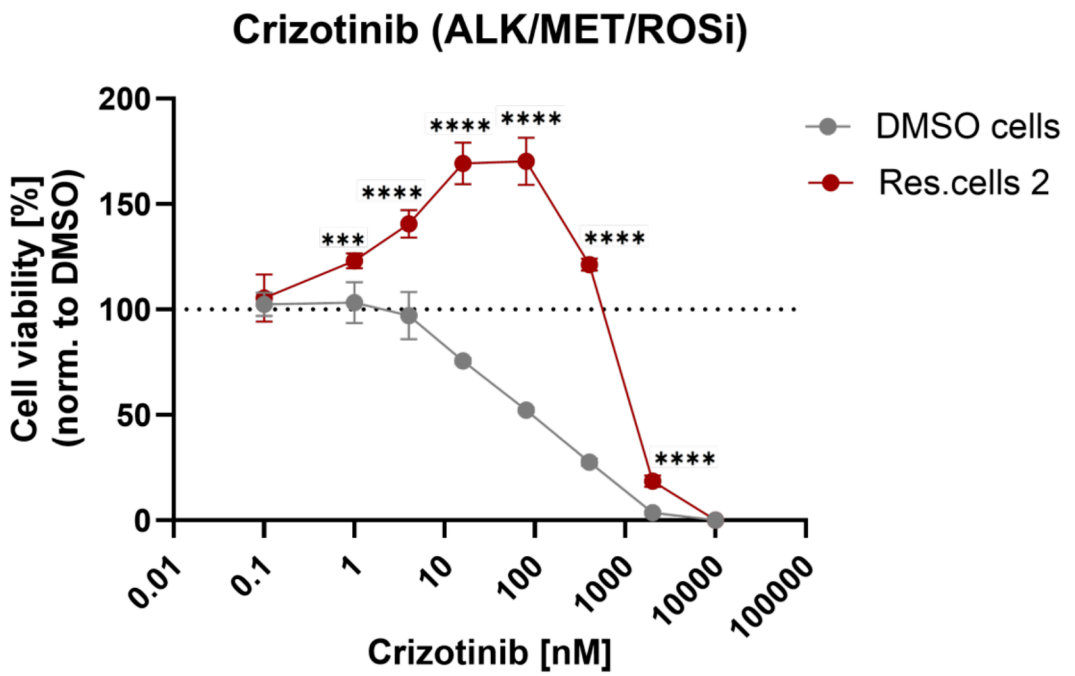


Figure 29: Effects of Crizotinib treatment on DMSO cells and Lorlatinib-resistant cells (Res.cells 2).
Cell viability of DMSO cells and Res.cells 2 in response to increasing Crizotinib concentrations. Mean ± SD, n=3.

4.2.3. Continuous Lorlatinib treatment suppresses tumor growth but does not induce stable resistance *in vivo*

To generate Lorlatinib-resistant tumors *in vivo*, I intracranially transplanted PPP1CB::ALK-driven pHGG cells (BI#190) into the thalamus of CD1 mice and randomized the animals into two treatment groups based on tumor burden. Beginning on day 7 post-transplantation, I initiated daily treatment (weekdays only) with 10 mg/kg Lorlatinib or vehicle. Treatment was continued until tumor signals remained below 1 × 10^6 p/s for five consecutive weeks, to assess whether resistance would emerge under continuous drug exposure, even in the absence of detectable tumor burden by bioluminescence imaging (IVIS) (Figure 30 A).

All vehicle-treated mice reached endpoint criteria within 17-21 days after transplantation and were sacrificed, whereas tumor signals in all Lorlatinib-treated animals declined below the detection threshold of 1 × 10^6 p/s (Supplementary figure 19 A). As no resistant tumors emerged during continuous treatment, I paused Lorlatinib administration for two weeks to assess potential tumor regrowth. Tumor recurrence was detected in four of eight Lorlatinib-treated animals, and I resumed Lorlatinib treatment in signal-dependent cycles. Treatment was reinitiated when tumor signals exceeded 2 × 10^6 p/s and paused when signals fell below 1 × 10^6 p/s. This treatment strategy has previously been shown to induce resistance to the

smoothened inhibitor Sonidegib in a preclinical model of sonic hedgehog medulloblastoma (Krausert et al., 2022).

Tumor signals fluctuated during these treatment cycles; however, resistant tumors could not be established within the permitted treatment period of up to 140 days (Figure 30 B-E). Tumor cells from three animals (AC008, AC009, AC010; Figure 30 B-D) were cryopreserved at endpoint, whereas one mouse (AC012) showed complete tumor clearance by the end of the observation period (Figure 30 E). Throughout the treatment period, no significant weight loss or other signs of toxicity were observed (Supplementary figure 19 B).

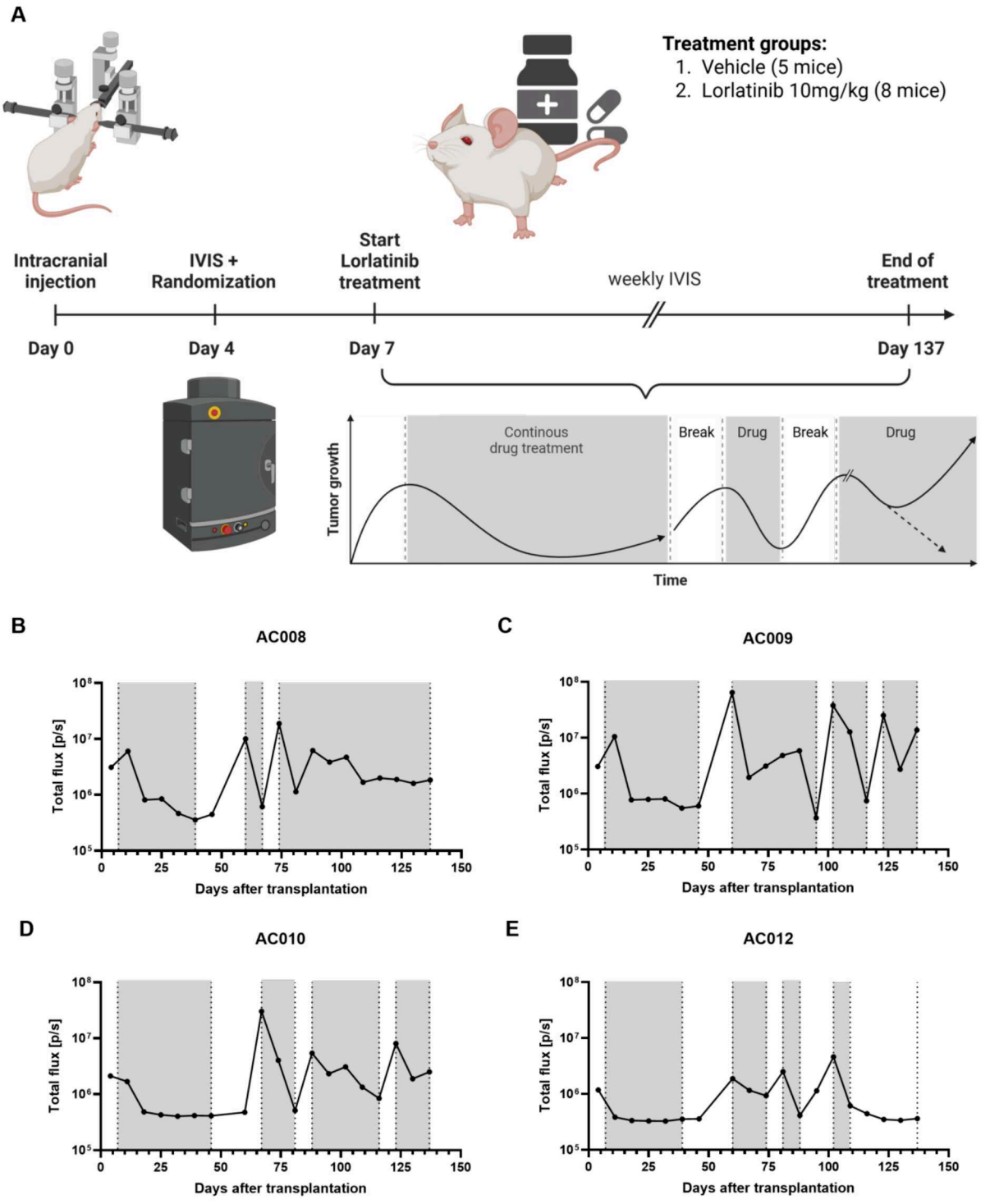


Figure 30: PPP1CB::ALK-driven pHGG cell-derived tumors are responsive to Lorlatinib treatment in vivo. A) Experimental layout. PPP1CB::ALK-driven pHGG cells were intracranially transplanted into the thalamus of CD1 mice. Mice were randomized according to their tumor signal on day 4 and were continuously treated with 10 mg/kg Lorlatinib or vehicle starting at day 7 until the tumor signal stayed below $1x10^6$ p/s for 5 consecutive weeks. After 2 weeks of treatment pause, Lorlatinib-treatment resumed in treatment cycles. Treatment was started when the tumor signal reached $2x10^6$ p/s and stopped when the tumor signal fell below $1x10^6$ p/s. B)-E) Tumor signal over time for each individual mouse (AC008, AC009, AC010, AC012).

4.2.4. Re-transplantation of Lorlatinib-pretreated tumors induces stable disease in Lorlatinib-treated mice

To assess whether Lorlatinib pre-treated tumor cells could still give rise to Lorlatinib-resistant tumors *in vivo*, I retransplanted tumor cells obtained from the previous experiment (Figure 30) into the thalamus of CD1 mice and reinitiated daily Lorlatinib treatment (10 mg/kg) on day 7 post-transplantation. Lorlatinib was administered continuously on weekdays until mice reached predefined endpoint criteria (Figure 31 A).

As shown in Figure 31 B-E, Lorlatinib treatment resulted in stable disease in all four mice, with tumor signals remaining above 1×10^7 p/s despite ongoing treatment. Mice AC026 and AC027 (Figure 31 A, B) reached endpoint criteria during weekend treatment pauses, whereas the tumor in AC028 exhibited rapid growth during a one-week interruption of Lorlatinib administration (Figure 31 C). AC032 was the only mouse to reach endpoint criteria during active Lorlatinib treatment (Figure 31 E). Throughout the experiment, no significant weight loss or other signs of treatment-related toxicity were observed (Supplementary figure 20).

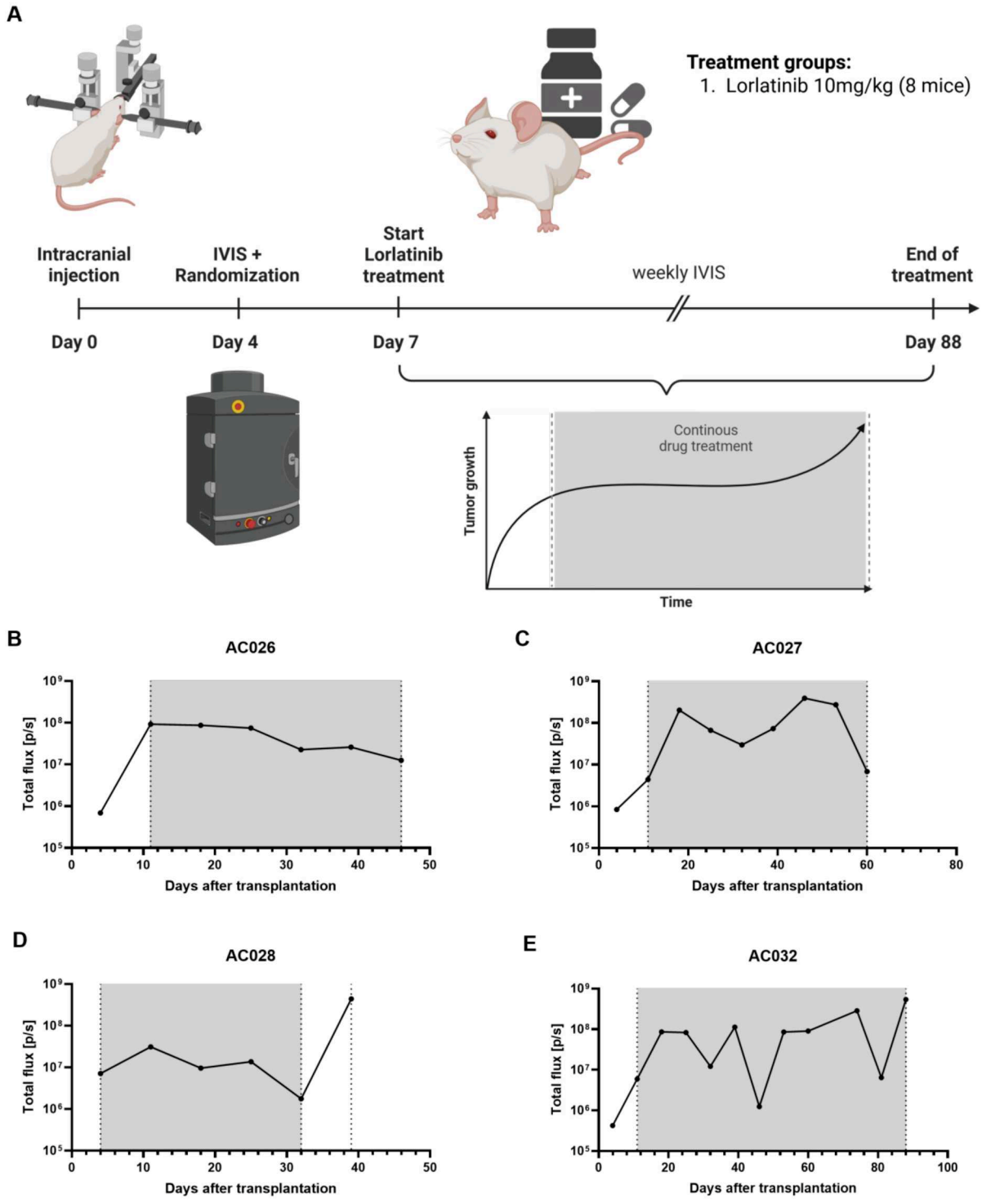


Figure 31: Lorlatinib-treatment induces stable disease in mice harboring tumors deriving from Lorlatinib pre-treated tumor cells.
A) Lorlatinib pre-treated tumor cells were re-transplanted into the thalamus of CD1 mice and were randomized on day 4. Daily Lorlatinib treatment (10 mg/kg) started on day 7 and was continuously administered every weekday until the mice developed endpoint criteria symptoms. B)-E) Tumor signal over time of each individual mouse (AC026, AC027, AC028, AC032).

4.2.5. Tumor-derived cells retain partial Lorlatinib sensitivity despite prior *in vivo* exposure

As the tumors did not appear to be fully resistant to Lorlatinib *in vivo*, I established cultures from these tumors and assessed their response to Lorlatinib *in vitro* using a cell viability assay. As shown in Figure 32, all tested tumor-derived cells exhibited a significant reduction in viability following Lorlatinib treatment compared with DMSO-treated controls.

Notably, all tumor-derived cells displayed significantly higher viability in response to Lorlatinib compared with the initially transplanted, Lorlatinib-naïve BI#190 cells. In this experiment, vehicle treated samples, rather than BI#190, would have represented the appropriate controls; however, no cryopreserved cells from these animals were available.

In addition, although not statistically significant, a trend toward reduced sensitivity to 10 nM Lorlatinib was observed in tumor cells derived from the second transplantation compared with those derived from the first transplantation.

Taken together, these data suggest that, while complete resistance did not emerge, *in vivo* Lorlatinib exposure may be associated with a partial decrease in drug sensitivity in ALK-driven tumor cells.

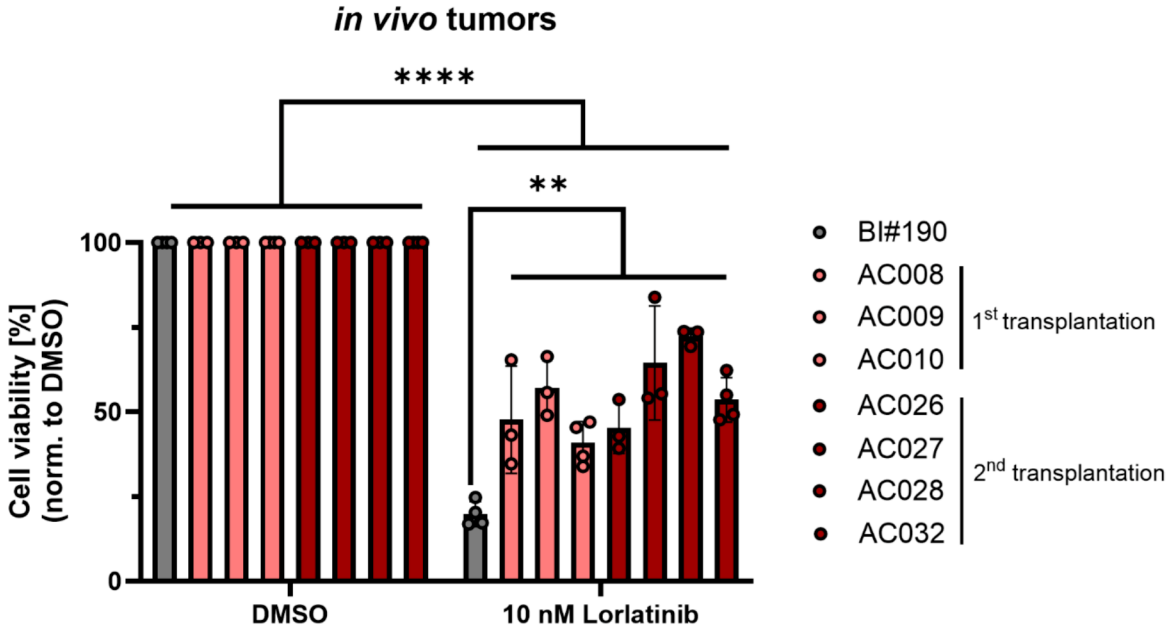


Figure 32: Lorlatinib pre-treated tumors respond less to Lorlatinib treatment in vitro compared to Lorlatinib-naïve cells.
Tumors derived from the mice of the previous two in vivo experiments (Figure 30 and Figure 31) and the initially transplanted, Lorlatinib-naïve cells (BI#190) were taken into culture and tested for their response to 10 nM Lorlatinib in vitro in a cell viability assay. Mean ± SD, n=3.

4.2.6. Bulk RNA sequencing reveals targetable vulnerabilities of Lorlatinib-resistant tumor cells

To characterize transcriptional changes associated with Lorlatinib resistance, I submitted RNA from all Lorlatinib-resistant cells generated *in vitro* and from all Lorlatinib-treated tumors for bulk RNA sequencing. Differential gene expression was observed when comparing vehicle-treated tumors (vehicle) with Lorlatinib-treated tumors, derived from the first and second transplantation (Lorl_1st Generation and Lorl_2nd Generation respectively), as well as DMSO cells (non res) with Lorlatinib-resistant cells (Lorl res cells).

In Lorlatinib-treated tumors upregulated gene signatures associated with TGFβ-driven epithelial-to-mesenchymal transition (EMT) and ALK bypass signaling pathways were identified (Figure 33 A, B). In contrast, analysis of the *in vitro* samples revealed upregulation of genes involved in PI3K-AKT-mTOR signaling alongside downregulation of pro-apoptotic gene expression (Figure 33 C, D).

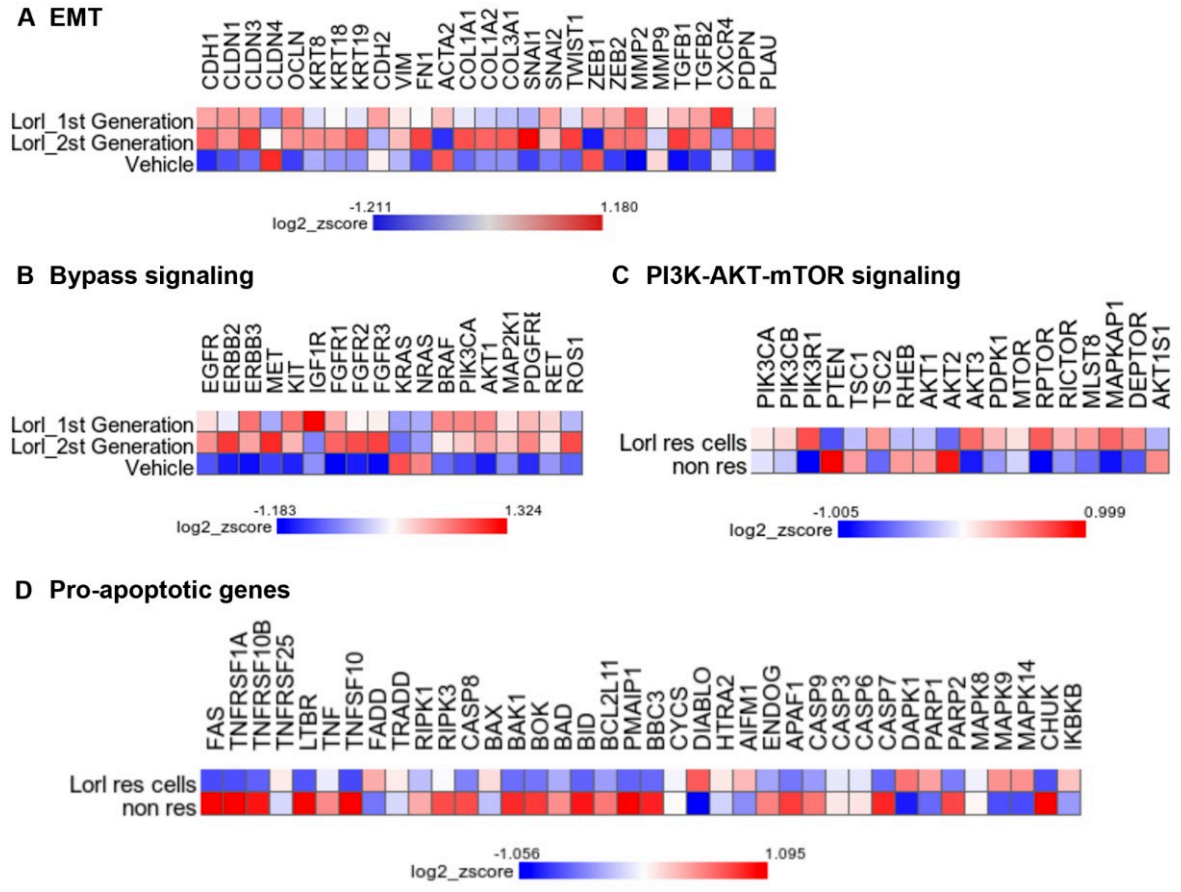


Figure 33: Bulk RNA sequencing analysis from Lorlatinib resistant cells and in vivo tumors.
A) Upregulation of genes involved in TGFβ-driven EMT (Taube et al., 2010) in Lorlatinib-treated tumors compared to vehicle-treated tumors in vivo. B) Upregulation of genes involved in ALK bypass signaling pathways (Wilson et al., 2015) in Lorlatinib-treated tumors compared to vehicle-treated tumors in vivo. 1st Generation represents the samples of the first transplantation and 2nd Generations represents the samples from the second transplantation. Vehicle represents samples from vehicle-treated animals. C) Upregulation of genes involved in PI3K-AKT-mTOR

signaling (Glaviano et al., 2023) in Lorlatinib-resistant cells (Lorl res cells) compared to non-resistant cells (non res). D) Down-regulation of pro-apoptotic genes (Elmore, 2007) in Lorlatinib-resistant cells (Lorl res cells) compared to non-resistant cells (non res). Selected representative genes for each pathway are shown.

4.2.7. Lorlatinib-resistant cells show selective vulnerability to BCL-2/-XL inhibition

To assess whether Lorlatinib-resistant cells display selective vulnerabilities to inhibition of pathways identified by RNA sequencing (Figure 33), I measured cell viability of Res.cells 2 and DMSO cells following exposure to increasing concentrations of selected inhibitors. In addition, I included 10 nM Lorlatinib in the treatments to evaluate whether resistant cells could be resensitized to Lorlatinib.

Treatment with Galunisertib, a TGFβ receptor inhibitor (TGFβRi), or Capmatinib, a MET inhibitor (METi), did not substantially affect cell viability in either Res.cells 2 or DMSO cells. Combination treatment with Galunisertib+Lorlatinib or Capmatinib+Lorlatinib resulted in viability levels in Res.cells 2 that were comparable to those observed with Lorlatinib treatment alone (Figure 34 A, B).

Treatment with the PI3Kα inhibitor (PI3Ki) Alpelisib did not differentially affect the viability of Res.cells 2 compared with DMSO cells (Figure 34 C). Although Everolimus, an mTOR inhibitor (mTORi), did not affect cell viability as a single agent, co-treatment with Everolimus and Lorlatinib reduced the Lorlatinib-associated increase in viability observed in Res.cells 2, restoring viability to baseline levels (Figure 34 D).

In contrast, Res.cells 2 exhibited increased sensitivity to AZD4320 and Navitoclax, both BCL-2/-XL inhibitors, at concentrations above 100 nM compared with DMSO cells (Figure 34 E, F). A similar trend was observed when AZD4320 was combined with Lorlatinib in Res.cells 2 (Figure 34 E), whereas this effect was not evident for the combination of Navitoclax and Lorlatinib (Figure 34 F).

These findings suggest that inhibition of BCL-2/-XL proteins represents a potential targetable vulnerability in Lorlatinib-resistant cells.

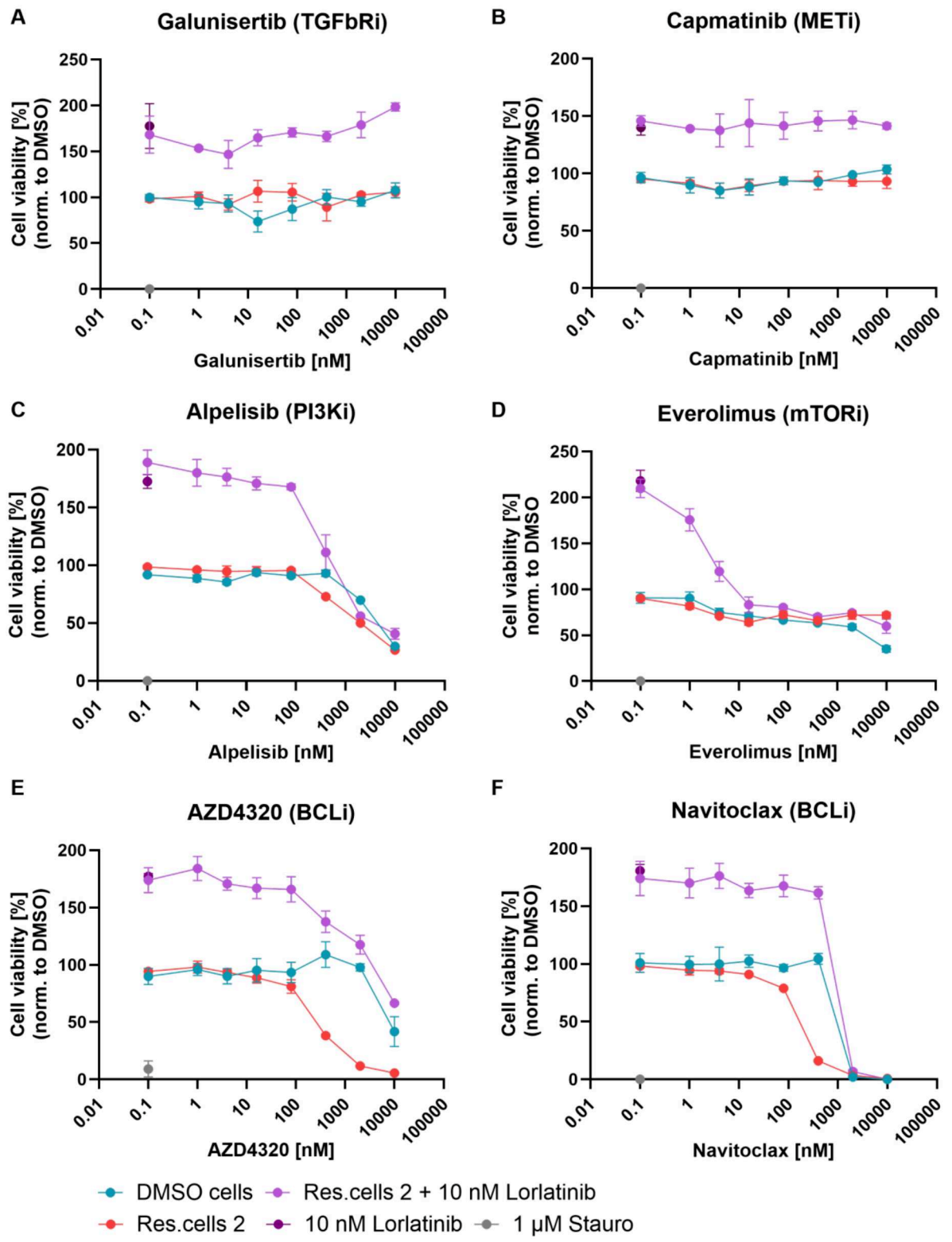


Figure 34: Combination treatment identified vulnerabilities of Lorlatinib-resistant cells (Res.cells 2). Cell viability assays after treating DMSO cells and Res.cells 2 with increasing concentrations of A) Galunisertib (TGFβRi), B) Capmatinib (METi), C) Alpelisib (PI3Ki), D) Everolimus (mTORi), E) AZD4320 (BCLi), and F) Navitoclax (BCLi). Staurosporine (Stauro) served as positive control for cell death. Mean ± SD, n=3.

5. Discussion

5.1. Comparing the radiosensitization potential of various compound classes in pediatric-type diffuse high-grade glioma

In DMG patients, RT constitutes the only available therapeutic option, yet its effects are restricted to palliation (Bartels et al., 2011; Jansen et al., 2012). This therapeutic limitation underscores the high interest in improving RT efficacy for these tumors. Accordingly, in this study, I aimed to assess which compounds or compound classes have the potential to function as radiosensitizers in this context.

I initiated this project with a comprehensive drug screen in combination with X-ray RT, testing a custom library of approximately 90 FDA-approved drugs for their radiosensitizing potential in nine different PDX-derived pHGG cell cultures and two non-cancer control cell lines. Through this approach, I identified four compound classes with high efficacy in combination with RT, namely MEKi, HDACi, BCLi, and Proteasomei. Drugs belonging to these classes consistently demonstrated the lowest CDIs, indicative of strong synergistic effects, across all tested cell models and showed higher efficacy in pHGG cells compared to control cells.
Interestingly, chemotherapeutic agents were generally less effective in inducing RT synergies than targeted agents. Given that chemotherapeutics, most prominently TMZ, but also CCNU and Vincristine, are commonly administered concomitantly with or following RT in the clinical setting (Jakacki et al., 2016; Mallick et al., 2015; Perwein et al., 2023), this observation was unexpected. However, as combinations of chemotherapy and RT have not led to significant improvements in clinical outcomes for pHGGs to date (Jakacki et al., 2016; Vanan & Eisenstat, 2014), these results are consistent with current clinical experience. Importantly, many chemotherapeutic agents used in pediatric pHGGs have not been systematically evaluated or specifically selected for this patient population, but are largely derived from adult treatment regimens (Chatwin et al., 2021).

Within these experiments, I was able to validate findings from previous studies identifying the BCL-2/-XL inhibitor Navitoclax (Vardon et al., 2025) as well as the HDACi Quisinostat (Cascio et al., 2023), and Panobinostat (Monje et al., 2023) as radiosensitizers in pHGGs. In contrast, despite promising results reported in earlier studies, the PARPi Olaparib (Guo et al., 2025; Vuurden et al., 2011) did not rank among the most effective compounds in my combined drug+RT screen (Figure 6, Table 5).
Guo et al. reported that H3K27M models exhibit deficiencies in the homologous recombination (HR) DNA repair pathway, rendering them sensitive to PARP inhibition and subsequent radiosensitization (Guo et al., 2025). As there is currently no evidence that all DMGs display

HR deficiencies, and as my drug+RT screen encompassed multiple pHGG entities, heterogeneity in DNA repair capacity may explain the observed discrepancy.

To investigate whether DNA repair mechanisms might be directly involved in mediating radiosensitization of the selected compounds, I assessed γH2AX levels, a marker of DNA DSBs, at multiple time points following combination treatment (Figure 17). I observed a trend toward increased and decreased DSB persistence after treatment with Romidepsin and Cobimetinib, respectively.

Romidepsin is an HDACi and is therefore involved in chromatin remodeling and epigenetic regulation. HDACi have previously been associated with increased DSB persistence (Geng et al., 2006). In contrast, the reduction in DSB persistence observed in Cobimetinib treated cells remains unclear. One possible explanation is that MEK inhibition frequently induces G1 arrest, which can reduce replication associated DNA damage signaling and alter γH2AX kinetics, as reported previously (Grabenbauer et al., 2018). In addition, inhibition of extracellular signal-related kinase (ERK) has been linked to enhanced DNA dependent protein kinase (DNA-PK) activation, which could accelerate DSB end joining and thereby reduce γH2AX persistence (Wei et al., 2013).

Although I did not observe major effects of the combination treatments on RT induced DNA DSB levels, this does not contradict the hypothesis that these drugs may act as effective radiosensitizers in pHGGs. Synergistic effects between drugs and RT can also arise from pathways downstream of direct DNA repair mechanisms, including apoptosis, cell cycle regulation, and growth factor signaling pathways such as MAPK signaling (Carrassa & Damia, 2017; Metselaar et al., 2021; Sriramulu et al., 2023), all of which are directly targeted by the drug candidates evaluated in this study.

For the *in vivo* validation of selected compounds, I have established three orthotopic pHGG mouse models in CD1 nude mice that are suitable for preclinical testing, namely DIPG-007 with a latency of approximately 60 days, DIPG-19 with a latency of approximately 300 days, and DIPG-17 with a latency of approximately 150 days (Figure 19).

DIPG-007 cells are widely used in pHGG models and have been shown to reliably engraft across multiple immunodeficient and immunocompromised mouse strains (’t Hart et al., 2023; Khan et al., 2021; Xu et al., 2021). In addition, DIPG-17 has been successfully transplanted into NSG mice (Ishida et al., 2021), and DIPGx7 has been engrafted in CD1 nude mice (Patel et al., 2019). In contrast, no published reports are currently available describing successful transplantation of DIPG-19 or DIPG-21.

Using the DIPG-007 model, I conducted the first preclinical trial applying a total RT dose of 12 Gy with concomitant treatment with Marizomib (Proteasomei), Cobimetinib (MEKi), and Romidepsin (HDACi). As all three inhibitors showed promising results in the *in vitro* validation experiments and have previously been evaluated in clinical studies for brain tumors (Iwamoto et al., 2011; Roth et al., 2024; Trippett et al., 2022), I selected them for initial *in vivo* testing. Unfortunately, none of the tested drugs showed a significant effect either as monotherapy or in combination with RT on tumor growth or survival when compared with vehicle or vehicle+RT treated animals, respectively (Figure 22). Based on the hypothesis that limited BBB penetration of the selected compounds contributed to the lack of efficacy, I performed a second preclinical trial using an adjusted treatment schedule for Marizomib and Cobimetinib, and included an alternative BBB penetrant HDACi (VPA). Despite these modifications, none of the tested drugs showed a significant effect either as monotherapy or in combination with RT when compared with vehicle or vehicle+RT treated animals, respectively (Figure 23).

It remained unclear whether drug concentrations were still insufficient and/or whether BBB penetration was inadequate to affect DIPG cells *in vivo*. To address this, I performed a pharmacokinetic study measuring Cobimetinib and Romidepsin concentrations in blood plasma and brain tissue of CD1 nude mice at multiple time points after drug administration. The plasma concentration time profile of Cobimetinib in CD1 nude mice closely recapitulated the pharmacokinetic profile reported in humans, reaching peak levels at approximately 2 h after administration, maintaining relatively stable concentrations up to 8 h, and subsequently declining over time (Rosen et al., 2016). Similarly, the plasma concentration profile of Romidepsin in CD1 nude mice resembled that observed in humans, with peak concentrations shortly after administration followed by a rapid decrease in plasma levels (Connolly et al., 2020). Together with the Cobimetinib brain and plasma exposure data, these findings suggest that both drugs exhibit broadly comparable pharmacokinetic patterns in mice and humans.

Cobimetinib reached a maximum of approximately 30 % of its plasma concentration in the brain. However, these Cobimetinib concentrations appeared insufficient to effectively target DIPG-007 tumor cells *in vivo*, as Cobimetinib levels in the brain remained below the IC50 threshold of ~53 ng/g for most of the observation period (Figure 24).

Romidepsin was detectable only in blood plasma and was absent from brain samples. This may be explained by the combination of a relatively low administered dose of Romidepsin at 1 mg/kg and its high molecular weight exceeding 500 Da, both of which likely limit sufficient BBB penetration. Most small molecules cross the BBB via passive lipid mediated

transmembrane diffusion (Oldendorf, 1974). Thus, drug molecular weight is inversely correlated with BBB penetration. Compounds with molecular weights above 400 Da are generally considered to have poor BBB penetrance, although compounds exceeding 600 Da have been reported to cross the BBB in sufficient amounts to affect CNS function (Pan & Kastin, 2001). This highlights that BBB penetration is influenced by additional factors, including lipid solubility, charge, tertiary structure, protein binding, efflux transporter interactions such as P-glycoprotein (P-gp), and active carrier or receptor mediated transport mechanisms (Banks, 2009; Pardridge, 2005).

While Marizomib has not been reported to be a substrate of the efflux transporter P-gp, encoded by the *ABCB1* gene (or historically *MDR1*) (Obaidat et al., 2011), both Cobimetinib (Choo et al., 2014) and Romidepsin (Xiao et al., 2005) have been described as P-gp substrates. P-gp is an ATP-dependent efflux transporter enriched at the luminal membrane of brain microvascular endothelial cells constituting the BBB (Erickson et al., 2018). By actively exporting a broad range of lipophilic and amphipathic substrates back into the circulation, P-gp limits CNS exposure to many therapeutic compounds (Chai et al., 2022; Paul et al., 2025). This may further explain why Cobimetinib and Romidepsin do not reach substantial concentrations in the brain and suggests that modulating P-gp activity could represent a strategy to enhance BBB exposure of these drugs.

Pharmacological inhibition of P-gp has been shown to substantially increase brain exposure of P-gp substrate drugs in preclinical models (Kemper et al., 2003; Lemaire et al., 1996). In humans, third generation P-gp inhibitors such as Tariquidar have been shown to inhibit P-gp at the BBB and increase brain uptake of model substrates (Abraham et al., 2009; Wagner et al., 2009). However, the magnitude and duration of BBB inhibition appear more limited than in rodents (Bauer et al., 2012), and clinical co-administration to enhance CNS drug delivery has not become routine practice.

An additional factor influencing *in vivo* efficacy and BBB penetration is the ratio of free unbound drug to protein- or lipid-bound drug. In most cases, only the free unbound fraction is pharmacologically active, capable of interacting with molecular targets, and diffusing across biological membranes (Smith et al., 2010). As I did not assess free drug fractions in this study, it is possible that a substantial proportion of the administered compounds was protein bound, thereby limiting effective BBB penetration and single agent activity.

Considering its promising results in multiple preclinical and early clinical studies (Boccellato et al., 2021; Bota et al., 2021; Di et al., 2016; Lin et al., 2019; Mason et al., 2019), Marizomib advanced to a phase 3 clinical trial in which it was evaluated in combination with RT+TMZ followed by TMZ maintenance therapy in patients with newly diagnosed glioblastoma (Roth et

al., 2024). In this trial, the addition of Marizomib to RT+TMZ did not improve overall survival compared with standard RT+TMZ treatment and was associated with increased toxicity. It is important to note that this study was conducted in adult patients and that Marizomib was not evaluated in combination with RT alone, which was the treatment strategy pursued in my study. Based on the current literature, I do not have a definitive explanation for the lack of efficacy of Marizomib either as monotherapy or in combination with RT in my experiments. Given that Marizomib has previously been shown to reduce tumor growth and prolong survival in other DIPG models when administered as monotherapy at comparable doses, formulations, and administration routes (Lin et al., 2019), it is possible that the DIPG-007 model exhibits differential responses to treatment *in vivo* compared with *in vitro* conditions and relative to the DIPG models used in earlier studies.

Beyond proteasome inhibition, modulation of apoptotic signaling has also been proposed as a strategy to enhance radiation responses. BCLi have previously been proposed as radiosensitizers in several tumor entities (Lee et al., 2022; O'Steen et al., 2017; Pesch et al., 2022), based on their ability to lower the apoptotic threshold following RT-induced DNA damage (Delbridge et al., 2016). In the context of DMG, Navitoclax has recently been evaluated in combination with RT in a preclinical model (Vardon et al., 2025). In this study, RT was shown to induce a senescent phenotype in DMG cells, and Navitoclax exerted senolytic activity in these RT-induced senescent cells. However, despite this mechanistic rationale, the authors did not observe a robust radiosensitizing effect of Navitoclax *in vivo*, suggesting that induction of senolysis alone may be insufficient to confer a meaningful therapeutic benefit in DMG (Vardon et al., 2025).

Given the well-documented dose-limiting systemic toxicities of Navitoclax, particularly thrombocytopenia (Wilson et al., 2010), AZD4320 was selected as an alternative dual BCL-2/-XL inhibitor in this study. While AZD4320 itself has not entered clinical trials, a dendrimer-conjugated formulation, AZD0466, consisting of AZD4320 linked to a PEGylated dendrimer, has been clinically evaluated in hematological malignancies (NCT04865419) (Arslan et al., 2023). However, this study was terminated due to insufficient clinical benefit, and AZD0466 is currently not commercially available for research purposes.

As already discussed for the other compounds, a plausible explanation for the absence of radiosensitization in my experiment with AZD4320, might be insufficient intratumoral drug exposure resulting from limited BBB penetration. Consistent with this hypothesis, Navitoclax has been reported to achieve only low concentrations in rodent brain tissue (~42 nM total brain concentration), indicating restricted CNS delivery (Greenberg et al., 2024). Because BCLis generally have relatively high molecular weights and are substrates of efflux transporters

(Vogler et al., 2011), it is likely that effective target engagement within brainstem tumors may not have been achieved under the dosing conditions used.

In addition to apoptotic pathway modulation, epigenetic therapies have also been investigated as radiosensitizers. The pan-HDAC inhibitor Panobinostat has demonstrated radiosensitizing activity in several tumor entities, primarily through enhancement of radiation-induced DNA damage and impaired DNA repair (Chinnaiyan et al., 2005; Groselj et al., 2013). However, comparable evidence in pHGGs, including DMGs, remains limited. Although Panobinostat showed strong anti-tumor activity *in vitro* and was identified as a promising therapeutic candidate in large-scale functional screening studies of DIPG (Grasso et al., 2015), it did not elicit meaningful single-agent activity *in vivo* in preclinical DIPG models (Hennika et al., 2017). Consistent with these preclinical observations, clinical evaluation of Panobinostat in children with progressive DMG did not demonstrate significant therapeutic benefit, although treatment was generally tolerable (Monje et al., 2023). Only isolated case reports describing concomitant use in progressive disease have been published, suggesting that the combination is feasible and can be administered without unexpected acute toxicity, although no clear evidence of efficacy has been observed (Wang et al., 2017).
Similarly, the HDAC inhibitor valproic acid (VPA) has been explored as a potential radiosensitizer. In the DMG model tested here, I did not observe combinatorial efficacy between VPA and RT, indicating limited radiosensitizing activity under the tested conditions. This finding is consistent with clinical evidence, which has not demonstrated a clear therapeutic benefit of VPA as a radiosensitizer in DMGs. Although a systematic review and meta-analysis in HGG reported an association between concomitant VPA use during radiotherapy and improved overall survival (Sullivan et al., 2023), a phase 2 clinical trial in children with newly diagnosed DIPG or HGG demonstrated that VPA administered during RT was feasible and well tolerated, but did not improve survival outcomes (Su et al., 2020).

Additionally, inhibition of oncogenic signaling pathways such as MAPK has also been explored as a radiosensitization strategy. Even though the MEK inhibitors Cobimetinib and Trametinib have not been systematically evaluated as radiosensitizers in pHGGs, preclinical evidence from non-CNS tumor models suggests that MEK pathway inhibition can enhance radiation responses. Radiosensitizing effects have been reported in pancreatic cancer (Estrada-Bernal et al., 2015), melanoma (Schick et al., 2015), and non-small cell lung cancer (Kim et al., 2021), where MEK inhibition was shown to augment radiation-induced DNA damage, impair repair signaling and increase apoptotic cell death. In adult glioblastoma, however, results have been inconsistent, with several studies suggesting that radiosensitization by MEK inhibition is highly

context-dependent and influenced by tumor genotype and MAPK pathway activation status (Essien et al., 2022; Houweling et al., 2023).
More recently, the MEK inhibitor Mirdametinib has been shown to act as a radiosensitizer in NF1-deficient glioblastoma models, where combined treatment enhanced RT-induced cytotoxicity and impaired DNA damage repair signaling (Ioannou et al., 2024). However, whether these findings can be extrapolated to DMG or other pHGG subtypes remains unclear, as MAPK pathway dependency and NF1 alterations are not uniformly present in these tumors.

Overall, this study demonstrates that several targeted compound classes exhibit strong radiosensitizing effects in pHGG models *in vitro*, yet these effects do not translate *in vivo*, primarily due to inadequate CNS drug exposure. Taken together, limited BBB penetration likely represents a major constraint in these orthotopic models, although this hypothesis will require confirmation through dedicated pharmacokinetic analyses. These findings indicate that effective radiosensitization strategies for DMG will require not only biologically potent agents but also optimization of drug delivery to achieve sufficient intratumoral concentrations.

5.1.1. Outlook and future directions

Building on the preclinical insights generated in this study, future efforts aim to advance the translational potential of radiosensitization strategies for pHGGs, as outlined in the following section.

So far, the *in vivo* studies have been conducted in a single pHGG model, primarily due to the long tumor latencies associated with orthotopic pHGG xenografts. To strengthen the generalizability of my findings, it would be valuable to evaluate the tested combination therapies in additional models that I have established, such as DIPG-19, which appears sensitive to combination treatment *in vitro*. I am currently assessing the inherent radiosensitivity of this model as a prerequisite for future preclinical studies.

An additional limitation is that the PDX-derived cell cultures used in this study have been extensively passaged *in vitro* and may no longer fully recapitulate the original intratumoral heterogeneity of the patient tumors. The use of freshly derived PDX-tumor material would therefore be advantageous, although the availability of such samples is generally limited. Moreover, testing combination therapies in immunocompetent models would better capture the contribution of the immune system to treatment response. While autochthonous H3-mutant models are available, these models frequently harbor additional alterations such as PDGFRA amplification or mutation, which substantially influence tumor biology and complicate

interpretation (Pathania et al., 2017). My laboratory is actively involved in the generation of autochthonous and syngeneic pHGG models using *in utero* electroporation, some of which have recently been published (Schoof et al., 2026). However, despite extensive efforts, a model in which H3K27M alone is sufficient to drive tumorigenesis has not yet been established.

Given that limited BBB permeability appears to be a major constraint in the *in vivo* studies, future work will focus on establishing subcutaneous pHGG models to test the identified combination therapies as a proof of principle. This approach would allow assessment of treatment efficacy in an *in vivo* setting independent of BBB-related limitations. In addition, intranasal drug delivery could be explored, as it enables direct nose-to-brain transport while bypassing the BBB. In rodent models, drug delivery via the olfactory pathway primarily targets frontal brain regions, whereas the trigeminal nerve pathway allows access to the brainstem, pons, and cerebellum (Crowe et al., 2018; Dhuria et al., 2010), as demonstrated for nanoliposomal SN-38 (Sasaki et al., 2022).

Even if efficacy were observed using these approaches, direct clinical translation would remain challenging. However, several strategies exist to enhance drug delivery to the brain in patients, including CED and Ommaya reservoirs. Both approaches have been applied in pediatric brain tumor patients (Blaney et al., 2013; Monje et al., 2025; Mueller et al., 2025; Mueller et al., 2023; Narsinh et al., 2025; Peyrl et al., 2014). Another promising strategy is FUS-mediated BBB opening, which enables localized and transient increases in BBB permeability, and has recently been evaluated clinically in combination with Panobinostat (Wu et al., 2025). In addition, encapsulation of drugs into liposomal formulations, potentially combined with surface modifications to enhance BBB extravasation and tumor specificity, represents another avenue that could be exploited in the future.

Beyond conventional X-ray RT, particle therapies have increasingly been implemented in pediatric oncology over recent years. These modalities are currently available only at specialized centers, including the Heidelberg Ion Beam Therapy Center (HIT), where particle therapy is routinely applied and studied in patients (Rieken et al., 2012). At present, there was no strong rationale to incorporate particle therapy into this project. While particle therapies reduce off target toxicities and induce more complex DNA damage compared with X-ray RT, the drug screen identified compound classes that primarily affect downstream pathways such as apoptosis, cell cycle regulation, proliferation, and proteasome function rather than direct DNA repair. As these processes are similarly engaged following particle therapy, differential radiosensitization was not expected. Nevertheless, if future evidence suggests modality-

specific differences, the experimental pipeline established in this thesis could be readily adapted to proton or carbon ion irradiation.

Finally, a key future goal is to mechanistically understand why certain compounds or compound classes exhibit superior radiosensitizing activity in pHGGs. Transcriptomic profiling by RNA sequencing of treated *in vitro* or *in vivo* tumors could provide insights into treatment induced transcriptional changes and identify affected molecular pathways.

5.1.2. Conclusion

Within this project, I established a comprehensive preclinical pipeline for the identification and evaluation of novel radiosensitizers for pHGGs, with a particular focus on DMGs. Through extensive *in vitro* drug screening, I identified several compounds and compound classes with strong radiosensitizing potential. In parallel, I established novel immunodeficient pHGG mouse models, thereby providing a foundation for future preclinical studies beyond the scope of this project. Furthermore, I systematically evaluated a total of seven drugs across three preclinical studies and identified limited BBB penetration as the primary barrier to successful *in vivo* validation. Importantly, multiple clinically applicable strategies to enhance BBB permeability are available and represent promising avenues for future investigation.

Taken together, this work represents the first comparative approach to systematically identify and evaluate radiosensitizers, across *in vitro* and *in vivo* models, for these still incurable pediatric brain tumors. Although limited BBB penetration and model availability prevented successful validation of the selected drug candidates thus far, the strategy of repurposing FDA-approved drugs holds substantial potential to improve RT outcomes for patients with pHGGs.

5.2. Overcoming ALK inhibitor resistance in ALK-fusion infant-type hemispheric glioma

ALK-driven IHGs are commonly treated with ALKi, such as Lorlatinib, which often induce robust initial clinical responses. However, acquired treatment resistance frequently emerges, limiting long-term therapeutic efficacy. Evidence for this comes both from pre-clinical and clinical observations. Lorlatinib resistance has been described in preclinical models in which Lorlatinib was initially highly effective in eliminating PPP1CB::ALK-driven tumor cells, but tumors rapidly recurred after treatment cessation (Clarke et al., 2020). In addition, a recent clinical case report described disease progression during Lorlatinib treatment following an initial response, with the patient ultimately succumbing to the disease within 15 months after diagnosis (Wilson et

al., 2025). Together, these findings underscore the urgent need to understand the mechanisms underlying Lorlatinib resistance in order to improve therapeutic options for affected children.

To investigate this, I generated Lorlatinib-resistant tumor cells *in vitro* that maintained stable resistance even after drug withdrawal (Figure 27). Acquired drug resistance is often transient and can be lost upon treatment cessation (Sale et al., 2019), which does not appear to be the case in this model. Notably, I observed a paradoxical phenotype in which Lorlatinib-resistant cells not only failed to undergo apoptosis upon Lorlatinib treatment, but instead displayed increased proliferation compared with DMSO-treated controls (Figure 28).
This observation suggests that, following acquisition of resistance, Lorlatinib exposure may create a selective fitness advantage in this cellular state. This phenotype resembles the concept of 'drug addiction' in which resistant cells exhibit enhanced fitness in the presence of the inhibitor, whereas drug withdrawal reduces cellular fitness and/or induces cell death. This phenotype has been described in ALK-driven anaplastic large-cell lymphoma (ALCL) models with acquired resistance to ALK TKIs, where withdrawal triggered a detrimental signaling program rather than restoring baseline growth. This TKI-addiction was attributed to STAT1 overactivation upon withdrawal, switching on a tumor-suppressive transcriptional program and attenuating oncogenic STAT3 signaling (Rajan et al., 2020). Further, drug addiction has been documented in BRAF-mutant melanoma after acquired resistance to Vemurafenib, where drug withdrawal led to toxic MAPK-ERK pathway hyperactivation (Das Thakur et al., 2013). A related shift from dependence on oncogenic signaling to dependence on continued inhibitor exposure has also been reported in EGFR-mutant lung cancer under intensive EGFR and MET inhibition (Suda et al., 2012).
Mechanistically, resistant cells seem to become adapted to an 'optimal' signaling window such that excessive pathway output upon drug withdrawal becomes deleterious (Sale et al., 2019). More broadly, chronic kinase inhibition can rewire feedback regulation and pathway cross-talk, enabling compensatory activation across MAPK, PI3K-AKT, and JAK-STAT pathways (Yesilkanal et al., 2021). To the best of my knowledge, a comparable 'drug addiction' phenotype has not been reported in IHGs yet.

To investigate transcriptional changes induced by chronic Lorlatinib treatment, I performed bulk RNA sequencing on all *in vitro* and *in vivo* Lorlatinib-resistant samples, including their respective non-resistant control counterparts.
According to the literature, common 'on target' resistance mechanisms to Lorlatinib include mutations within the ALK RTK domain, primarily described in NSCLC. These mutations have been systematically summarized by Poei et al. and include L1198F, G2032R, D1203N,

G1123D, C1156Y plus L1198F, G1202R plus L1196M, and I1171N plus D1203N (Poei et al., 2024). In addition, a study from 2021 demonstrated that Gilteritinib can overcome Lorlatinib resistance mediated by the double mutant I1171N and F1174I in ALK (Liang et al., 2021). None of these mutations were detected in the RNA sequencing data of the resistant samples based on read alignment to the reference genome (data not shown). However, as variant calling is more robust and established using whole-genome sequencing (WGS) data, the presence of stable genomic alterations will be assessed by WGS. Moreover, while ALK amplification has been reported as a resistance mechanism following acquired resistance to Crizotinib (Katayama et al., 2012), it has not been identified as a mechanism of acquired resistance to second- or third-generation ALKi (Gainor et al., 2016). Taken together, these findings suggest that 'off target' resistance mechanisms are likely the predominant drivers of Lorlatinib resistance in ALK-driven IHGs, but still have to be further investigated.

RNA sequencing analysis revealed differential regulation of genes associated with TGFβ-driven epithelial-to-mesenchymal transition (EMT), RTK signaling including MET, EGFR, and HER2/3, PI3K-AKT-mTOR signaling, and apoptosis regulation (Figure 33). These findings are consistent with a previous study demonstrating that TGFβ-driven EMT mediates ALKi resistance in NSCLC and can be reversed by inhibition of the TGFβ receptor (TGFβR) using Silibinin (Verdura et al., 2022).

EMT is a biological process in which epithelial cells progressively lose epithelial characteristics such as stable cell-cell adhesion, apical-basal polarity, and expression of epithelial markers, while acquiring mesenchymal traits including increased migratory capacity, invasiveness, and mesenchymal marker expression (Allgayer et al., 2025; Yang et al., 2020). Although classical EMT does not occur in brain tumors due to their non epithelial origin (Iser et al., 2019; Laurenge et al., 2023), brain tumors can adopt mesenchymal-like transcriptional programs and upregulate mesenchymal markers such as N cadherin, fibronectin, vimentin, Snail, Twist, and Zeb (Figure 33).

In NSCLC, ALKi resistance has been linked to activation of bypass signaling pathways involving multiple RTKs including IGF1R, EGFR, KIT, MET, and HER2/3. In line with this, I observed upregulation of several RTKs in my Lorlatinib-resistant samples. Notably, MET amplification is a frequent resistance mechanism in patients relapsing on Lorlatinib (Dagogo-Jack et al., 2020), and combined inhibition of ALK and MET has demonstrated moderate antitumor activity in ALK rearranged NSCLC with acquired MET amplification (Dagogo-Jack et al., 2023). In addition, dependency on RAS-MAPK signaling has been identified as a hallmark of EML4::ALK-driven lung adenocarcinoma (Hrustanovic et al., 2015), providing a rationale for

combined ALKi and MEKi treatment strategies that are currently under clinical investigation (NCT04005144, NCT03202940).

I further identified upregulation of components of the PI3K-AKT-mTOR signaling pathway in Lorlatinib resistant cells compared with non-resistant controls (Figure 33 C). In EML::ALK-driven NSCLC, EGFR-PI3Kβ mediated reactivation of MAPK and PI3K-AKT signaling under ALK inhibition has been described as a mechanism conferring ALKi resistance, and combined inhibition of ALKi and PI3Kβi was shown to overcome this effect (Talwelkar et al., 2023). These findings are supported by earlier work identifying sustained PI3K-AKT signaling as a mediator of ALKi resistance in NSCLC and demonstrating efficacy of combined ALKi and PI3K inhibitor treatment *in vitro* and *in vivo* (Yang et al., 2014). Moreover, reactivation of MAPK and PI3K-AKT signaling under ALK inhibition has been linked to insufficient accumulation of the pro-apoptotic protein BIM (*BCL2L11*) and impaired apoptosis induction in ALK-driven NSCLC models. In this context, combined inhibition of ALKi and MCL-1 inhibitor restored apoptosis (Martín et al., 2025). Consistent with these findings, I observed downregulation of pro-apoptotic genes in Lorlatinib-resistant compared with non-resistant cells, supporting the hypothesis that apoptosis suppression contributes to ALKi resistance in ALK-driven brain tumors and may represent a therapeutically exploitable vulnerability.

As combinatorial treatment strategies have already been explored to overcome ALKi resistance in NSCLC, I applied a similar approach to my Lorlatinib-resistant ALK-driven IHG models *in vitro*. I assessed whether targeting the identified vulnerabilities, including TGFβR-mediated mesenchymal programs, RTK bypass signaling via MET, apoptosis regulation, and PI3K-AKT signaling, was sufficient to selectively reduce viability of Lorlatinib-resistant cells compared with non-resistant DMSO cells. In addition, I tested whether inhibition of these pathways could resensitize resistant cells to Lorlatinib by combining pathway specific inhibitors with ALK inhibition.

So far, I did not observe a differential response between resistant cells (Res.cells 2) and DMSO cells following treatment with the TGFβR inhibitor (TGFβRi) Galunisertib, the METi Capmatinib, the PI3Ki Alpelisib, and the mTORi Everolimus (Figure 34), suggesting that these pathways are unlikely to represent dominant resistance liabilities in this model. A possible explanation for the lack of efficacy of Galunisertib and Capmatinib is that the corresponding pathways were primarily identified in the *in vivo* resistant samples rather than in the *in vitro* resistant cells in which these inhibitors have been tested so far. Bulk RNA sequencing of whole tumors can capture additional transcriptional programs arising from the tumor microenvironment and cellular heterogeneity, and may therefore yield more complex signatures than RNA sequencing

of a cell culture model with a comparatively homogeneous genetic background. Therefore, subsequent drug testing was prioritized based on the *in vitro* findings.

In contrast, Res.cells 2 appeared more susceptible to BCL-2/-XL inhibition using AZD4320 and Navitoclax compared with non-resistant cells (Figure 34), revealing a potential vulnerability of Lorlatinib-resistant cells. This is consistent with previous reports in NSCLC indicating that resistance to ALK inhibition can involve adaptive rewiring of apoptotic signaling. In Lorlatinib-resistant NSCLC models, activation of EGFR signaling has been shown to promote survival through modulation of the anti-apoptotic protein BCL-XL (Katayama et al., 2023). Similarly, Alectinib resistance in ALK-rearranged NSCLC has been associated with activation of yes-associated protein 1 (YAP1), which transcriptionally upregulates anti-apoptotic proteins including MCL-1 and BCL-XL (Tsuji et al., 2020). Notably, both studies demonstrated therapeutic efficacy of combination strategies targeting upstream survival pathways (EGFR inhibition + Lorlatinib, or YAP1 inhibition + Alectinib), rather than directly inhibiting BCL-2 family proteins.
However, it is important to note that much of the mechanistic insight discussed here is derived from studies in NSCLC, as although ALKi resistance has been reported in pediatric brain tumors, the underlying resistance mechanisms in this context remain largely unexplored. To the best of my knowledge, there is no direct evidence demonstrating dependence on BCL-2 family anti-apoptotic signaling in Lorlatinib-resistant pHGG models. Therefore, the increased sensitivity of Res.cells 2 to combined BCL-2/-XL inhibition may represent a previously unrecognized therapeutic vulnerability that warrants mechanistic validation.

5.2.1. Outlook and future directions

In the future, I aim to mechanistically dissect why Lorlatinib treatment exerts a tumor promoting effect in Lorlatinib-resistant cells. As a first step, I plan to perform ALK knock-down using siRNA to determine whether this phenotype is ALK-dependent or reflects an intrinsically uncoupled mechanism. Depending on the outcome, I will further investigate which downstream pathways mediate this effect and whether they reveal targetable vulnerabilities that could overcome the resistant state.

In parallel, WGS represents a complementary approach to elucidate the molecular basis of the stable Lorlatinib resistance observed in these ALK-driven pHGG cells. While transcriptome analysis did not reveal consistent resistance-associated changes, WGS would enable unbiased detection of genomic alterations, including ALK kinase domain mutations and copy

number changes, that may contribute to resistance and cannot be comprehensively or reliably characterized using RNA-sequencing data alone.

To validate these observations *in vivo*, I plan to transplant the *in vitro* Lorlatinib-resistant cells into mice to generate an *in vivo* Lorlatinib-resistant model. Using this model would enable evaluation of combination strategies identified *in vitro*, for example BCL-2/-XL inhibition, to determine whether these approaches can restore therapeutic responses *in vivo*. In addition, it would be informative to test whether early combination treatment compared with Lorlatinib monotherapy can prevent or delay the emergence of Lorlatinib resistance *in vivo*.

To strengthen the functional validation of candidate combinations, I will extend the analysis beyond cell viability by assessing proliferation and apoptosis to confirm the underlying cellular response phenotypes. Mechanistically, bulk RNA sequencing, western blot analyses of key pathway components, and rescue experiments could be used to elucidate the molecular mechanism underlying the tumor promoting response to ALK inhibition.

Finally, as RTKi resistance has also been reported in other RTK-driven IHG entities, including NTRK-driven IHG (Cocco et al., 2018; Drilon et al., 2018), I will consider applying this experimental pipeline to additional preclinical IHG models.

5.2.2. Conclusion

Lorlatinib treatment, despite inducing robust initial responses, has increasingly been associated with acquired resistance in ALK-driven IHGs. In this study, I generated Lorlatinib-resistant IHG models *in vitro* and *in vivo* and comprehensively characterized the resulting ALKi resistance phenotype. I identified a previously undescribed tumor promoting effect of Lorlatinib treatment in Lorlatinib-resistant , which may have important implications for the clinical use of ALKi. In addition, I explored potential combination treatment strategies, thereby providing a foundation for future efforts to overcome ALKi resistance in patients with IHG.

6. References

't Hart, E., Bianco, J., Besse, H. C., Chin Joe Kie, L. A., Cornet, L., Eikelenboom, K. L., van den Broek, T. J. M., Derieppe, M., Su, Y., Hoving, E. W., Ries, M. G., & van Vuurden, D. G. (2023). Towards Standardisation of a Diffuse Midline Glioma Patient-Derived Xenograft Mouse Model Based on Suspension Matrices for Preclinical Research. *Biomedicines*, *11*(2), 527. https://doi.org/10.3390/biomedicines11020527

Abraham, J., Edgerly, M., Wilson, R., Chen, C., Rutt, A., Bakke, S., Robey, R., Dwyer, A., Goldspiel, B., Balis, F., Van Tellingen, O., Bates, S. E., & Fojo, T. (2009). A Phase I Study of the P-Glycoprotein Antagonist Tariquidar in Combination with Vinorelbine. *Clinical Cancer Research*, *15*(10), 3574-3582. https://doi.org/10.1158/1078-0432.CCR-08-0938

Abrahao, A., Meng, Y., Llinas, M., Huang, Y., Hamani, C., Mainprize, T., Aubert, I., Heyn, C., Black, S. E., Hynynen, K., Lipsman, N., & Zinman, L. (2019). First-in-human trial of blood–brain barrier opening in amyotrophic lateral sclerosis using MR-guided focused ultrasound. *Nature Communications*, *10*(1), 4373. https://doi.org/10.1038/s41467-019-12426-9

Ahmed, M., Sieben, A., Genechten, T. V., Libbrecht, S., Gilis, N., Praeter, M. D., Fricx, C., Calò, P., Campenhout, C. V., D'Haene, N., Witte, O. D., Kempen, L. C. V., Lammens, M., Salmon, I., Lebrun, L., Ahmed, M., Sieben, A., Genechten, T. V., Libbrecht, S., . . . Lebrun, L. (2024). Rare Oncogenic Fusions in Pediatric Central Nervous System Tumors: A Case Series and Literature Review. *Cancers*, *16*(19). https://doi.org/10.3390/cancers16193344

Ajayi, E. D., Elazazy, M., Abouzid, K., & Ali, H. I. (2026). Breaking barriers: Medicinal chemistry strategies and advanced in-silico approaches for overcoming the BBB and enhancing CNS penetration. *Eur J Med Chem*, *301*, 118219. https://doi.org/10.1016/j.ejmech.2025.118219

Allgayer, H., Mahapatra, S., Mishra, B., Swain, B., Saha, S., Khanra, S., Kumari, K., Panda, V. K., Malhotra, D., Patil, N. S., Leupold, J. H., & Kundu, G. C. (2025). Epithelial-to-mesenchymal transition (EMT) and cancer metastasis: the status quo of methods and experimental models 2025. *Molecular Cancer*, *24*(1), 167. https://doi.org/10.1186/s12943-025-02338-2

Andrade, A. F., Chen, C. C. L., & Jabado, N. (2023). Oncohistones in brain tumors: the soil and seed. *Trends in Cancer*, *9*(5), 444-455. https://doi.org/10.1016/j.trecan.2023.02.003

Arslan, S., Marconi, G., Martinelli, G., Fleming, S., Curti, A., Dinner, S. N., Blachly, J. S., Della Porta, M. G., Bajel, A., Sauer, T., Crysandt, M., Pigneux, A., Fransecky, L., Baldus, C. D., Konopleva, M. Y., Marmor, Y., Sharma, S., Elgeioushi, N., Cheung, P., . . . Jain, N. (2023). Safety and Tolerability of AZD0466 As Monotherapy for Patients with Advanced Hematologic Malignancies. Results from a Phase I/II Trial. *Blood*, *142*(Supplement 1), 5907. https://doi.org/10.1182/blood-2023-179168

Bagchi, A., Chiang, J., Pinto, S., Dhanda, S., & Gajjar, A. (2025). Infant-Type Hemispheric Gliomas: A Review of Clinical, Radiologic, Histopathologic, and Molecular Features. *Journal of the National Comprehensive Cancer Network*, *23*(11). https://doi.org/10.6004/jnccn.2025.7064

Balachander, S. B., Criscione, S. W., Byth, K. F., Cidado, J., Adam, A., Lewis, P., Macintyre, T., Wen, S., Lawson, D., Burke, K., Lubinski, T., Tyner, J. W., Kurtz, S. E., McWeeney, S. K., Varnes, J., Diebold, R. B., Gero, T., Ioannidis, S.,

Hennessy, E. J., . . . Gibbons, F. D. (2020). AZD4320, A Dual Inhibitor of Bcl-2 and Bcl-xL, Induces Tumor Regression in Hematologic Cancer Models without Dose-limiting Thrombocytopenia. *Clinical Cancer Research*, *26*(24), 6535-6549. https://doi.org/10.1158/1078-0432.CCR-20-0863

Banks, W. A. (2009). Characteristics of compounds that cross the blood-brain barrier. *BMC Neurology*, *9*(1), S3. https://doi.org/10.1186/1471-2377-9-S1-S3

Bartels, U., Hawkins, C., Vézina, G., Kun, L., Souweidane, M., & Bouffet, E. (2011). Proceedings of the diffuse intrinsic pontine glioma (DIPG) Toronto Think Tank: advancing basic and translational research and cooperation in DIPG. *Journal of Neuro-Oncology*, *105*(1), 119-125. https://doi.org/10.1007/s11060-011-0704-4

Bauer, M., Zeitlinger, M., Karch, R., Matzneller, P., Stanek, J., Jäger, W., Böhmdorfer, M., Wadsak, W., Mitterhauser, M., Bankstahl, J. P., Löscher, W., Koepp, M., Kuntner, C., Müller, M., & Langer, O. (2012). Pgp-Mediated Interaction Between (R)-[11C]Verapamil and Tariquidar at the Human Blood–Brain Barrier: A Comparison With Rat Data. *Clinical Pharmacology & Therapeutics*, *91*(2), 227-233. https://doi.org/10.1038/clpt.2011.217

Belayet, J. B., Beamish, S., Rahaman, M., Alanani, S., Virdi, R. S., Frick, D. N., Rahman, A. F. M. T., Ulicki, J. S., Biswas, S., Arnold, L. A., Roni, M. S. R., Cheng, E. Y., Steeber, D. A., Frick, K. M., & Hossain, M. M. (2022). Development of a Novel, Small-Molecule Brain-Penetrant Histone Deacetylase Inhibitor That Enhances Spatial Memory Formation in Mice. *Journal of Medicinal Chemistry*, *65*(4), 3388-3403. https://doi.org/10.1021/acs.jmedchem.1c01928

Bentayebi, K., Suwan, K., Ibrahimi, A., Sara, L., Ouadghiri, M., Aanniz, T., Amzazi, S., Belyamani, L., Hajitou, A., & Eljaoudi, R. (2024). Preclinical Evaluation of panobinostat and ONC201 for the treatment of diffuse intrinsic pontine glioma (DIPG). *Brain Disorders*, *13*, 100113. https://doi.org/10.1016/j.dscb.2023.100113

Bestvina, C. M., Patel, J. D., Le, X., Veillon, R., Anderson, I., Demedts, I., Garassino, M., Mazières, J., Morise, M., Smit, E., Eggleton, S. P., O'Brate, A., Otto, G., Bruns, R., Schumacher, K. M., & Paik, P. (2022). Intracranial Activity of Tepotinib in Patients (pts) With *MET* exon 14 (*MET*ex14) Skipping NSCLC Enrolled in VISION. *International Journal of Radiation Oncology*Biology*Physics*, *112*(2), e14-e15. https://doi.org/10.1016/j.ijrobp.2021.10.187

Blaney, S. M., Tagen, M., Onar-Thomas, A., Berg, S. L., Gururangan, S., Scorsone, K., Su, J., Goldman, S., Kieran, M. W., Kun, L., Boyett, J., & Stewart, C. (2013). A phase-1 pharmacokinetic optimal dosing study of intraventricular topotecan for children with neoplastic meningitis: A pediatric brain tumor consortium study. *Pediatric Blood & Cancer*, *60*(4), 627-632. https://doi.org/10.1002/pbc.24309

Blionas, A., Giakoumettis, D., Klonou, A., Neromyliotis, E., Karydakis, P., & Themistocleous, M. S. (2018). Paediatric gliomas: diagnosis, molecular biology and management. *Annals of Translational Medicine*, *6*(12), 251-251. https://doi.org/10.21037/atm.2018.05.11

Boccellato, C., Kolbe, E., Peters, N., Juric, V., Fullstone, G., Verreault, M., Idbaih, A., Lamfers, M. L. M., Murphy, B. M., & Rehm, M. (2021). Marizomib sensitizes primary glioma cells to apoptosis induced by a latest-generation TRAIL receptor agonist. *Cell Death & Disease*, *12*(7), 647. https://doi.org/10.1038/s41419-021-03927-x

Borsuk, R., Zhou, L., Chang, W.-I., Zhang, Y., Sharma, A., Prabhu, V. V., Tapinos, N., Lulla, R. R., & El-Deiry, W. S. (2021). Potent preclinical sensitivity to imipridone-

based combination therapies in oncohistone H3K27M-mutant diffuse intrinsic pontine glioma is associated with induction of the integrated stress response, TRAIL death receptor DR5, reduced ClpX and apoptosis. *American Journal of Cancer Research*, *11*(9), 4607-4623.

Boschert, T., Kromer, K., Lerner, T., Lindner, K., Haltenhof, G., Tan, C. L., Jähne, K., Poschke, I., Bunse, L., Eisele, P., Grassl, N., Mildenberger, I., Sahm, K., Platten, M., Lindner, J. M., & Green, E. W. (2024). H3K27M neoepitope vaccination in diffuse midline glioma induces B and T cell responses across diverse HLA loci of a recovered patient. *Science Advances*, *10*(5), eadi9091. https://doi.org/10.1126/sciadv.adi9091

Bota, D. A., Mason, W., Kesari, S., Magge, R., Winograd, B., Elias, I., Reich, S. D., Levin, N., Trikha, M., & Desjardins, A. (2021). Marizomib alone or in combination with bevacizumab in patients with recurrent glioblastoma: Phase I/II clinical trial data. *Neuro-Oncology Advances*, *3*(1), vdab142. https://doi.org/10.1093/noajnl/vdab142

Bouffet, E., Hansford, J. R., Garrè, M. L., Hara, J., Plant-Fox, A., Aerts, I., Locatelli, F., Lugt, J. v. d., Papusha, L., Sahm, F., Tabori, U., Cohen, K. J., Packer, R. J., Witt, O., Sandalic, L., Silva, A. B. P. d., Russo, M., & Hargrave, D. R. (2023). Dabrafenib plus Trametinib in Pediatric Glioma with BRAF V600 Mutations. *New England Journal of Medicine*, *389*(12), 1108-1120. https://doi.org/10.1056/NEJMoa2303815

Brada, M., Stenning, S., Gabe, R., Thompson, L. C., Levy, D., Rampling, R., Erridge, S., Saran, F., Gattamaneni, R., Hopkins, K., Beall, S., Collins, V. P., & Lee, S.-M. (2010). Temozolomide Versus Procarbazine, Lomustine, and Vincristine in Recurrent High-Grade Glioma. *Journal of Clinical Oncology*, *28*(30), 4601-4608. https://doi.org/10.1200/JCO.2009.27.1932

Broniscer, A., Jia, S., Mandrell, B., Hamideh, D., Huang, J., Onar-Thomas, A., Gajjar, A., Raimondi, S. C., Tatevossian, R. G., & Stewart, C. F. (2018). Phase 1 trial, pharmacokinetics, and pharmacodynamics of dasatinib combined with crizotinib in children with recurrent or progressive high-grade and diffuse intrinsic pontine glioma. *Pediatric Blood & Cancer*, *65*(7), e27035. https://doi.org/10.1002/pbc.27035

Bukowska, B., Gajek, A., & Marczak, A. (2014). Two drugs are better than one. A short history of combined therapy of ovarian cancer. *Contemporary Oncology/Współczesna Onkologia*, *19*(5), 350-353. https://doi.org/10.5114/wo.2014.43975

Cao, D., Hou, X., Wang, C., Wang, S., Liu, Z., Tian, M., Guo, K., Li, H., Kang, D. D., Zhong, Y., Xue, Y., Yu, C., Deng, B., & Dong, Y. (2025). Lipid nanoparticles for mRNA delivery in brain via systemic administration. *Science Advances*, *11*(33), eadw0730. https://doi.org/10.1126/sciadv.adw0730

Cao, S.-s., & Zhen, Y.-s. (1989). Potentiation of antimetabolite antitumor activity in vivo by dipyridamole and amphotericin B. *Cancer Chemotherapy and Pharmacology*, *24*(3), 181-186. https://doi.org/10.1007/BF00300240

Capper, D., Jones, D. T. W., Sill, M., Hovestadt, V., Schrimpf, D., Sturm, D., Koelsche, C., Sahm, F., Chavez, L., Reuss, D. E., Kratz, A., Wefers, A. K., Huang, K., Pajtler, K. W., Schweizer, L., Stichel, D., Olar, A., Engel, N. W., Lindenberg, K., . . . Pfister, S. M. (2018). DNA methylation-based classification of central nervous system tumours. *Nature*, *555*(7697), 469-474. https://doi.org/10.1038/nature26000

Carrassa, L., & Damia, G. (2017). DNA damage response inhibitors: Mechanisms and potential applications in cancer therapy. *Cancer Treat Rev*, *60*, 139-151. https://doi.org/10.1016/j.ctrv.2017.08.013

Cascio, C. L., Margaryan, T., Luna-Melendez, E., McNamara, J. B., White, C. I., Knight, W., Ganta, S., Opachich, Z., Cantoni, C., Yoo, W., Sanai, N., Tovmasyan, A., & Mehta, S. (2023). Quisinostat is a brain-penetrant radiosensitizer in glioblastoma.

Chai, A. B., Callaghan, R., Gelissen, I. C., Chai, A. B., Callaghan, R., & Gelissen, I. C. (2022). Regulation of P-Glycoprotein in the Brain. *International Journal of Molecular Sciences*, *23*(23). https://doi.org/10.3390/ijms232314667

Chambrelant, I., Eber, J., Antoni, D., Burckel, H., Noël, G., Auvergne, R., Chambrelant, I., Eber, J., Antoni, D., Burckel, H., Noël, G., & Auvergne, R. (2021). Proton Therapy and Gliomas: A Systematic Review. *Radiation*, *1*(3), 218-233. https://doi.org/10.3390/radiation1030019

Chatwin, H. V., Cruz Cruz, J., & Green, A. L. (2021). Pediatric high-grade glioma: moving toward subtype-specific multimodal therapy. *The FEBS journal*, *288*(21), 6127-6141. https://doi.org/10.1111/febs.15739

Chavaz, L., Bagchi, A., Dhanda, S. K., Toutain, F., Pfister, S. M., Sturm, D., Pietsch, T., Gielen, G. H., Waha, A., Clarke, M., Lu, C., Karremann, M., Benesch, M., Perwein, T., Nussbaumer, G., Kramm, C., Massimino, M., Biassoni, V., Vinci, M., . . . von Bueren, A. O. (2025). A Systematic Study of Molecular Diagnosis, Treatment and Prognosis in Infant-Type Hemispheric Glioma): An Individual Patient Data Meta-analysis of 164 patients. *Neuro-Oncology*, noaf264. https://doi.org/10.1093/neuonc/noaf264

Chen, J., Liao, S., Xiao, Z., Pan, Q., Wang, X., Shen, K., Wang, S., Yang, L., Guo, F., Liu, H. F., & Pan, Q. (2022). The development and improvement of immunodeficient mice and humanized immune system mouse models. *Front Immunol*, *13*, 1007579. https://doi.org/10.3389/fimmu.2022.1007579

Chen, L., Ye, H.-L., Zhang, G., Yao, W.-M., Chen, X.-Z., Zhang, F.-C., & Liang, G. (2014). Autophagy Inhibition Contributes to the Synergistic Interaction between EGCG and Doxorubicin to Kill the Hepatoma Hep3B Cells. *PLOS ONE*, *9*(1), e85771. https://doi.org/10.1371/journal.pone.0085771

Chen, Y.-H., Moore, D., Lee, C.-C., & Su, Y.-H. (2023). Focused ultrasound for brain metastases: an update on global clinical trials. *Journal of Neuro-Oncology*, *165*(1), 53-62. https://doi.org/10.1007/s11060-023-04492-3

Chinnaiyan, P., Vallabhaneni, G., Armstrong, E., Huang, S. M., & Harari, P. M. (2005). Modulation of radiation response by histone deacetylase inhibition. *Int J Radiat Oncol Biol Phys*, *62*(1), 223-229. https://doi.org/10.1016/j.ijrobp.2004.12.088

Choo, E. F., Ly, J., Chan, J., Shahidi-Latham, S. K., Messick, K., Plise, E., Quiason, C. M., & Yang, L. (2014). Role of P-Glycoprotein on the Brain Penetration and Brain Pharmacodynamic Activity of the MEK Inhibitor Cobimetinib. *Molecular Pharmaceutics*, *11*(11), 4199-4207. https://doi.org/10.1021/mp500435s

Clarke, M., Mackay, A., Ismer, B., Pickles, J. C., Tatevossian, R. G., Newman, S., Bale, T. A., Stoler, I., Izquierdo, E., Temelso, S., Carvalho, D. M., Molinari, V., Burford, A., Howell, L., Virasami, A., Fairchild, A. R., Avery, A., Chalker, J., Kristiansen, M., . . . Jones, C. (2020). Infant High-Grade Gliomas Comprise Multiple Subgroups Characterized by Novel Targetable Gene Fusions and Favorable Outcomes. *Cancer Discovery*, *10*(7), 942-963. https://doi.org/10.1158/2159-8290.CD-19-1030

Cocco, E., Scaltriti, M., & Drilon, A. (2018). NTRK fusion-positive cancers and TRK inhibitor therapy. *Nature Reviews Clinical Oncology*, *15*(12), 731-747. https://doi.org/10.1038/s41571-018-0113-0

Cohen, A. R. (2022). Brain Tumors in Children. *New England Journal of Medicine*, *386*(20), 1922-1931. https://doi.org/10.1056/NEJMra2116344

Connolly, R. M., Laille, E., Vaishampayan, U., Chung, V., Kelly, K., Dowlati, A., Alese, O. B., Harvey, R. D., Haluska, P., Siu, L. L., Kummar, S., Piekarz, R., Ivy, S. P., Anders, N. M., Downs, M., O'Connor, A., Scardina, A., Saunders, J., Rosner, G. L., . . . Team, f. t. E.-S. (2020). Phase I and Pharmacokinetic Study of Romidepsin in Patients with Cancer and Hepatic Dysfunction: A National Cancer Institute Organ Dysfunction Working Group Study. *Clinical Cancer Research*, *26*(20), 5329-5337. https://doi.org/10.1158/1078-0432.CCR-20-1412

Corbeaux, T., Hess, I., Swann, J. B., Kanzler, B., Haas-Assenbaum, A., & Boehm, T. (2010). Thymopoiesis in mice depends on a Foxn1-positive thymic epithelial cell lineage. *Proceedings of the National Academy of Sciences*, *107*(38), 16613-16618. https://doi.org/10.1073/pnas.1004623107

Crowe, T. P., Greenlee, M. H. W., Kanthasamy, A. G., & Hsu, W. H. (2018). Mechanism of intranasal drug delivery directly to the brain. *Life Sciences*, *195*, 44-52. https://doi.org/10.1016/j.lfs.2017.12.025

Dagogo-Jack, I., Kiedrowski, L. A., Heist, R. S., Lin, J. J., Meador, C. B., Krueger, E. A., Do, A., Peterson, J., Sequist, L. V., Gainor, J. F., Lennerz, J. K., & Digumarthy, S. R. (2023). Efficacy and Tolerability of *ALK*/*MET* Combinations in Patients With *ALK*-Rearranged Lung Cancer With Acquired *MET* Amplification: A Retrospective Analysis. *JTO Clinical and Research Reports*, *4*(8), 100534. https://doi.org/10.1016/j.jtocrr.2023.100534

Dagogo-Jack, I., Yoda, S., Lennerz, J. K., Langenbucher, A., Lin, J. J., Rooney, M. M., Prutisto-Chang, K., Oh, A., Adams, N. A., Yeap, B. Y., Chin, E., Do, A., Marble, H. D., Stevens, S. E., Digumarthy, S. R., Saxena, A., Nagy, R. J., Benes, C. H., Azzoli, C. G., . . . Hata, A. N. (2020). MET Alterations Are a Recurring and Actionable Resistance Mechanism in ALK-Positive Lung Cancer. *Clinical Cancer Research*, *26*(11), 2535-2545. https://doi.org/10.1158/1078-0432.CCR-19-3906

Das, A., Tabori, U., Sambira Nahum, L. C., Collins, N. B., Deyell, R., Dvir, R., Faure-Conter, C., Hassall, T. E., Minturn, J. E., Edwards, M., Brookes, E., Bianchi, V., Levine, A., Stone, S. C., Sudhaman, S., Sanchez Ramirez, S., Ercan, A. B., Stengs, L., Chung, J., . . . Morgenstern, D. A. (2023). Efficacy of Nivolumab in Pediatric Cancers with High Mutation Burden and Mismatch Repair Deficiency. *Clinical Cancer Research*, *29*(23), 4770-4783. https://doi.org/10.1158/1078-0432.CCR-23-0411

Das Thakur, M., Salangsang, F., Landman, A. S., Sellers, W. R., Pryer, N. K., Levesque, M. P., Dummer, R., McMahon, M., & Stuart, D. D. (2013). Modelling vemurafenib resistance in melanoma reveals a strategy to forestall drug resistance. *Nature*, *494*(7436), 251-255. https://doi.org/10.1038/nature11814

de Gooijer, M. C., Zhang, P., Weijer, R., Buil, L. C. M., Beijnen, J. H., & van Tellingen, O. (2018). The impact of P-glycoprotein and breast cancer resistance protein on the brain pharmacokinetics and pharmacodynamics of a panel of MEK inhibitors. *International Journal of Cancer*, *142*(2), 381-391. https://doi.org/10.1002/ijc.31052

Delbridge, A. R., Grabow, S., Strasser, A., & Vaux, D. L. (2016). Thirty years of BCL-2: translating cell death discoveries into novel cancer therapies. *Nat Rev Cancer*, *16*(2), 99-109. https://doi.org/10.1038/nrc.2015.17

DeWire, M., Fuller, C., Hummel, T. R., Chow, L. M. L., Salloum, R., de Blank, P., Pater, L., Lawson, S., Zhu, X., Dexheimer, P., Carle, A. C., Kumar, S. S., Drissi, R., Stevenson, C. B., Lane, A., Breneman, J., Witte, D., Jones, B. V., Leach, J. L., & Fouladi, M. (2020). A phase I/II study of ribociclib following radiation therapy in children with newly diagnosed diffuse intrinsic pontine glioma (DIPG). *Journal of Neuro-Oncology*, *149*(3), 511-522. https://doi.org/10.1007/s11060-020-03641-2

Dhuria, S. V., Hanson, L. R., & Frey, W. H. (2010). Intranasal delivery to the central nervous system: Mechanisms and experimental considerations. *Journal of Pharmaceutical Sciences*, *99*(4), 1654-1673. https://doi.org/10.1002/jps.21924

Di, K., Lloyd, G. K., Abraham, V., MacLaren, A., Burrows, F. J., Desjardins, A., Trikha, M., & Bota, D. A. (2016). Marizomib activity as a single agent in malignant gliomas: ability to cross the blood-brain barrier. *Neuro-Oncology*, *18*(6), 840-848. https://doi.org/10.1093/neuonc/nov299

Drilon, A. (2019). TRK inhibitors in TRK fusion-positive cancers. *Annals of Oncology*, *30*, viii23-viii30. https://doi.org/10.1093/annonc/mdz282

Drilon, A., Ou, S.-H. I., Cho, B. C., Kim, D.-W., Lee, J., Lin, J. J., Zhu, V. W., Ahn, M.-J., Camidge, D. R., Nguyen, J., Zhai, D., Deng, W., Huang, Z., Rogers, E., Liu, J., Whitten, J., Lim, J. K., Stopatschinskaja, S., Hyman, D. M., . . . Shaw, A. T. (2018). Repotrectinib (TPX-0005) Is a Next-Generation ROS1/TRK/ALK Inhibitor That Potently Inhibits ROS1/TRK/ALK Solvent- Front Mutations. *Cancer Discovery*, *8*(10), 1227-1236. https://doi.org/10.1158/2159-8290.CD-18-0484

Dunkel, I. J., Doz, F., Foreman, N. K., Hargrave, D., Lassaletta, A., André, N., Hansford, J. R., Hassall, T., Eyrich, M., Gururangan, S., Bartels, U., Gajjar, A., Howell, L., Warad, D., Pacius, M., Tam, R., Wang, Y., Zhu, L., & Cohen, K. (2023). Nivolumab with or without ipilimumab in pediatric patients with high-grade CNS malignancies: Safety, efficacy, biomarker, and pharmacokinetics—CheckMate 908. *Neuro-Oncology*, *25*(8), 1530-1545. https://doi.org/10.1093/neuonc/noad031

Elmore, S. (2007). Apoptosis: A Review of Programmed Cell Death. *Toxicologic Pathology*, *35*(4), 495-516. https://doi.org/10.1080/01926230701320337

Enshaeieh, M., Saadatnia, G., Babaie, J., Golkar, M., Choopani, S., & Sayyah, M. (2021). Valproic Acid Inhibits Chronic Toxoplasma Infection and Associated Brain Inflammation in Mice. *Antimicrobial Agents and Chemotherapy*, *65*(10), 10.1128/aac.01003-01021. https://doi.org/doi:10.1128/aac.01003-21

Erickson, M. A., Nicolazzo, J. A., & Banks, W. A. (2018). Commentary on the 2018 Named Series on blood-brain interfaces: Roles of neuroimmunomodulation in health and disease. *Brain Behav Immun*, *74*, 3-6. https://doi.org/10.1016/j.bbi.2018.08.016

Essien, E. I., Hofer, T. P., Atkinson, M. J., & Anastasov, N. (2022). Combining HDAC and MEK Inhibitors with Radiation against Glioblastoma-Derived Spheres. *Cells*, *11*(5), 775. https://www.mdpi.com/2073-4409/11/5/775

Estrada-Bernal, A., Chatterjee, M., Haque, S. J., Yang, L., Morgan, M. A., Kotian, S., Morrell, D., Chakravarti, A., & Williams, T. M. (2015). MEK inhibitor GSK1120212-mediated radiosensitization of pancreatic cancer cells involves

inhibition of DNA double-strand break repair pathways. *Cell Cycle*, *14*(23), 3713-3724. https://doi.org/10.1080/15384101.2015.1104437

Falchook, G. S., Battiste, J. D., Kalra, A., Shastry, M., Finney, L., Hoekstra, S. J., Shih, M. G., & Shih, K. C. (2025). A phase Ib study evaluating the c-MET inhibitor INC280 (capmatinib) in combination with bevacizumab in patients with high-grade glioma. *Neuro-Oncology Advances*, *7*(1), vdae220. https://doi.org/10.1093/noajnl/vdae220

Fernando, D., Ahmed, A. U., & Williams, B. R. G. (2024). Therapeutically targeting the unique disease landscape of pediatric high-grade gliomas. *Frontiers in Oncology*, *14*. https://doi.org/10.3389/fonc.2024.1347694

Finesso, G., Willis, E., Tarrant, J. C., Lanza, M., Sprengers, J., Verrelle, J., Banerjee, E., Hermans, E., Assenmacher, C. A., & Radaelli, E. (2023). Spontaneous early-onset neurodegeneration in the brainstem and spinal cord of NSG, NOG, and NXG mice. *Vet Pathol*, *60*(3), 374-383. https://doi.org/10.1177/03009858231151403

Franken, N. A. P., Rodermond, H. M., Stap, J., Haveman, J., & van Bree, C. (2006). Clonogenic assay of cells in vitro. *Nature Protocols*, *1*(5), 2315-2319. https://doi.org/10.1038/nprot.2006.339

Friese-Hamim, M., Clark, A., Perrin, D., Crowley, L., Reusch, C., Bogatyrova, O., Zhang, H., Crandall, T., Lin, J., Ma, J., Bachner, D., Schmidt, J., Schaefer, M., & Stroh, C. (2022). Brain penetration and efficacy of tepotinib in orthotopic patient-derived xenograft models of *MET*-driven non-small cell lung cancer brain metastases. *Lung Cancer*, *163*, 77-86. https://doi.org/10.1016/j.lungcan.2021.11.020

Gainor, J., Dardaei, L., Yoda, S., Friboulet, L., Leischler, I., Katayama, R., Dagogo-Jack, I., Gadgeel, S., Schultz, K., Singh, M., Chin, E., Parks, M., Lee, D., DiCecca, R. H., Lockerman, E., Huynh, T., Logan, J., Benes, C. H., Engelman, J. A., & Shaw, A. (2016). 421 - Molecular mechanisms of resistance to first- and second-generation ALK inhibitors in ALK-rearranged lung cancer. *European Journal of Cancer*, *69*, S138. https://doi.org/10.1016/S0959-8049(16)33009-X

Gene-Olaciregui, N., Perez-Somarriba, M., Santa-María, V., Cruz, O., Gómez-González, S., Castañeda, A., Suñol, M., Rovira, C., Muchart, J., Hinojosa, J., La Madrid, A. M., & Lavarino, C. (2023). Clinical and Molecular Evolution of an ALK-Driven Infant-Type Hemispheric Glioma Treated Sequentially With Second- and Third-Generation Anaplastic Lymphoma Kinase Inhibitors. *JCO Precision Oncology*(7), e2200547. https://doi.org/10.1200/PO.22.00547

Geng, L., Cuneo, K. C., Fu, A., Tu, T., Atadja, P. W., & Hallahan, D. E. (2006). Histone Deacetylase (HDAC) Inhibitor LBH589 Increases Duration of γ-H2AX Foci and Confines HDAC4 to the Cytoplasm in Irradiated Non–Small Cell Lung Cancer. *Cancer Research*, *66*(23), 11298-11304. https://doi.org/10.1158/0008-5472.CAN-06-0049

Glaviano, A., Foo, A. S. C., Lam, H. Y., Yap, K. C. H., Jacot, W., Jones, R. H., Eng, H., Nair, M. G., Makvandi, P., Geoerger, B., Kulke, M. H., Baird, R. D., Prabhu, J. S., Carbone, D., Pecoraro, C., Teh, D. B. L., Sethi, G., Cavalieri, V., Lin, K. H., . . . Kumar, A. P. (2023). PI3K/AKT/mTOR signaling transduction pathway and targeted therapies in cancer. *Molecular Cancer*, *22*, 138. https://doi.org/10.1186/s12943-023-01827-6

Gong, L., Zhang, Y., Liu, C., Zhang, M., & Han, S. (2021). Application of Radiosensitizers in Cancer Radiotherapy. *International Journal of Nanomedicine*, *16*, 1083-1102. https://doi.org/10.2147/IJN.S290438

Gorick, C. M., Breza, V. R., Nowak, K. M., Cheng, V. W. T., Fisher, D. G., Debski, A. C., Hoch, M. R., Demir, Z. E. F., Tran, N. M., Schwartz, M. R., Sheybani, N. D., & Price, R. J. (2022). Applications of focused ultrasound-mediated blood-brain barrier opening. *Advanced Drug Delivery Reviews*, *191*, 114583. https://doi.org/10.1016/j.addr.2022.114583

Grabenbauer, F., Katzer, A., Sisario, D., Memmel, S., Flentje, M., Sukhorukov, V. L., & Djuzenova, C. S. (2018). MEK-inhibitor PD184352 enhances the radiosensitizing effect of the Hsp90 inhibitor NVP-AUY922: the role of cell type and drug-irradiation schedule. *Oncotarget*, *9*(100), 37379-37392. https://doi.org/10.18632/oncotarget.26436

Grassl, N., Poschke, I., Lindner, K., Bunse, L., Mildenberger, I., Boschert, T., Jähne, K., Green, E. W., Hülsmeyer, I., Jünger, S., Kessler, T., Suwala, A. K., Eisele, P., Breckwoldt, M. O., Vajkoczy, P., Grauer, O. M., Herrlinger, U., Tonn, J.-C., Denk, M., . . . Sahm, K. (2023). A H3K27M-targeted vaccine in adults with diffuse midline glioma. *Nature Medicine*, *29*(10), 2586-2592. https://doi.org/10.1038/s41591-023-02555-6

Grasso, C. S., Tang, Y., Truffaux, N., Berlow, N. E., Liu, L., Debily, M. A., Quist, M. J., Davis, L. E., Huang, E. C., Woo, P. J., Ponnuswami, A., Chen, S., Johung, T. B., Sun, W., Kogiso, M., Du, Y., Qi, L., Huang, Y., Hütt-Cabezas, M., . . . Monje, M. (2015). Functionally defined therapeutic targets in diffuse intrinsic pontine glioma. *Nat Med*, *21*(6), 555-559. https://doi.org/10.1038/nm.3855

Greenberg, E. F., Voorbach, M. J., Smith, A., Reuter, D. R., Zhuang, Y., Wang, J. Q., Wooten, D. W., Asque, E., Hu, M., Hoft, C., Duggan, R., Townsend, M., Orsi, K., Dalecki, K., Amberg, W., Duggan, L., Knight, H., Spina, J. S., He, Y., . . . Florian, H. (2024). Navitoclax safety, tolerability, and effect on biomarkers of senescence and neurodegeneration in aged nonhuman primates. *Heliyon*, *10*(16), e36483. https://doi.org/10.1016/j.heliyon.2024.e36483

Groselj, B., Kerr, M., & Kiltie, A. E. (2013). Radiosensitisation of bladder cancer cells by panobinostat is modulated by Ku80 expression. *Radiotherapy and Oncology*, *108*(3), 429-433. https://doi.org/10.1016/j.radonc.2013.06.021

Guerreiro Stucklin, A. S., Ryall, S., Fukuoka, K., Zapotocky, M., Lassaletta, A., Li, C., Bridge, T., Kim, B., Arnoldo, A., Kowalski, P. E., Zhong, Y., Johnson, M., Li, C., Ramani, A. K., Siddaway, R., Nobre, L. F., de Antonellis, P., Dunham, C., Cheng, S., . . . Hawkins, C. (2019). Alterations in ALK/ROS1/NTRK/MET drive a group of infantile hemispheric gliomas. *Nature Communications*, *10*, 4343. https://doi.org/10.1038/s41467-019-12187-5

Guo, Y., Li, Z., Parsels, L. A., Wang, Z., Parsels, J. D., Dalvi, A., The, S., Hu, N., Valvo, V. M., Doherty, R., Peterson, E., Wang, X., Venkataraman, S., Agnihotri, S., Venneti, S., Wahl, D. R., Green, M. D., Lawrence, T. S., Koschmann, C., . . . Zhang, Q. (2025). H3K27M diffuse midline glioma is homologous recombination defective and sensitized to radiotherapy and NK cell-mediated antitumor immunity by PARP inhibition. *Neuro-Oncology*, *27*(8), 2129-2146. https://doi.org/10.1093/neuonc/noaf097

Hallberg, B., & Palmer, R. H. (2016). The role of the ALK receptor in cancer biology. *Annals of Oncology*, *27*, iii4-iii15. https://doi.org/10.1093/annonc/mdw301

Han, L., Zhang, Q., Dail, M., Shi, C., Cavazos, A., Ruvolo, V. R., Zhao, Y., Kim, E., Rahmani, M., Mak, D. H., Jin, S. S., Chen, J., Phillips, D. C., Koller, P. B., Jacamo, R., Burks, J. K., DiNardo, C., Daver, N., Jabbour, E., . . . Konopleva, M. (2020). Concomitant targeting of BCL2 with venetoclax and MAPK signaling

with cobimetinib in acute myeloid leukemia models. *Haematologica*, *105*(3), 697-707. https://doi.org/10.3324/haematol.2018.205534

Hennika, T., Hu, G., Olaciregui, N. G., Barton, K. L., Ehteda, A., Chitranjan, A., Chang, C., Gifford, A. J., Tsoli, M., Ziegler, D. S., Carcaboso, A. M., & Becher, O. J. (2017). Pre-Clinical Study of Panobinostat in Xenograft and Genetically Engineered Murine Diffuse Intrinsic Pontine Glioma Models. *PLOS ONE*, *12*(1), e0169485. https://doi.org/10.1371/journal.pone.0169485

Hooker, J. M., Kim, S. W., Alexoff, D., Xu, Y., Shea, C., Reid, A., Volkow, N., & Fowler, J. S. (2010). Histone Deacetylase Inhibitor MS-275 Exhibits Poor Brain Penetration: Pharmacokinetic Studies of [11C]MS-275 using Positron Emission Tomography. *ACS Chemical Neuroscience*, *1*(1), 65-73. https://doi.org/10.1021/cn9000268

Hotchkiss, K. M., Cho, E. J., & Khasraw, M. (2024). A first-in-human peptide vaccine targeting H3K27M; encouraging early findings in 8 adults with diffuse midline glioma. *Neuro-Oncology*, *26*(1), 5-6. https://doi.org/10.1093/neuonc/noad203

Hou, X., Zaks, T., Langer, R., & Dong, Y. (2021). Lipid nanoparticles for mRNA delivery. *Nature Reviews Materials*, *6*(12), 1078-1094. https://doi.org/10.1038/s41578-021-00358-0

Houweling, M., Abdul, U. K., Brahm, C., Lagerweij, T., Heukelom, S., Koken, P. W., Honeywell, R., Wedekind, L. E., Peters, G. J., Verheul, H., Sminia, P., Noske, D., Wurdinger, T., & Westerman, B. A. (2023). Radio-sensitizing effect of MEK inhibition in glioblastoma in vitro and in vivo. *J Cancer Res Clin Oncol*, *149*(1), 297-305. https://doi.org/10.1007/s00432-022-04483-3

Hovestadt, V., Jones, D. T., Picelli, S., Wang, W., Kool, M., Northcott, P. A., Sultan, M., Stachurski, K., Ryzhova, M., Warnatz, H. J., Ralser, M., Brun, S., Bunt, J., Jäger, N., Kleinheinz, K., Erkek, S., Weber, U. D., Bartholomae, C. C., von Kalle, C., . . . Lichter, P. (2014). Decoding the regulatory landscape of medulloblastoma using DNA methylation sequencing. *Nature*, *510*(7506), 537-541. https://doi.org/10.1038/nature13268

Hrustanovic, G., Olivas, V., Pazarentzos, E., Tulpule, A., Asthana, S., Blakely, C. M., Okimoto, R. A., Lin, L., Neel, D. S., Sabnis, A., Flanagan, J., Chan, E., Varella-Garcia, M., Aisner, D. L., Vaishnavi, A., Ou, S.-H. I., Collisson, E. A., Ichihara, E., Mack, P. C., . . . Bivona, T. G. (2015). RAS-MAPK dependence underlies a rational polytherapy strategy in EML4-ALK–positive lung cancer. *Nature Medicine*, *21*(9), 1038-1047. https://doi.org/10.1038/nm.3930

Huehnchen, P., Springer, A., Kern, J., Kopp, U., Kohler, S., Alexander, T., Hiepe, F., Meisel, A., Boehmerle, W., & Endres, M. (2020). Bortezomib at therapeutic doses poorly passes the blood–brain barrier and does not impair cognition. *Brain Communications*, *2*(1), fcaa021. https://doi.org/10.1093/braincomms/fcaa021

Husband, H. R., Campagne, O., He, C., Zhu, X., Bianski, B. M., Baker, S. J., Shelat, A. A., Tinkle, C. L., & Stewart, C. F. (2021). Model-based evaluation of image-guided fractionated whole-brain radiation therapy in pediatric diffuse intrinsic pontine glioma xenografts. *CPT: Pharmacometrics & Systems Pharmacology*, *10*(6), 599-610. https://doi.org/10.1002/psp4.12627

Ioannou, M., Lalwani, K., Ayanlaja, A. A., Chinnasamy, V., Pratilas, C. A., & Schreck, K. C. (2024). MEK Inhibition Enhances the Antitumor Effect of Radiotherapy in NF1-Deficient Glioblastoma. *Mol Cancer Ther*, *23*(9), 1261-1272. https://doi.org/10.1158/1535-7163.Mct-23-0510

Iser, I. C., Lenz, G., & Wink, M. R. (2019). EMT-like process in glioblastomas and reactive astrocytes. *Neurochemistry International*, *122*, 139-143. https://doi.org/10.1016/j.neuint.2018.11.016

Ishida, J., Alli, S., Bondoc, A., Golbourn, B., Sabha, N., Mikloska, K., Krumholtz, S., Srikanthan, D., Fujita, N., Luck, A., Maslink, C., Smith, C., Hynynen, K., & Rutka, J. (2021). MRI-guided focused ultrasound enhances drug delivery in experimental diffuse intrinsic pontine glioma. *Journal of Controlled Release*, *330*, 1034-1045. https://doi.org/10.1016/j.jconrel.2020.11.010

Iwamoto, F. M., Lamborn, K. R., Kuhn, J. G., Wen, P. Y., Alfred Yung, W. K., Gilbert, M. R., Chang, S. M., Lieberman, F. S., Prados, M. D., & Fine, H. A. (2011). A phase I/II trial of the histone deacetylase inhibitor romidepsin for adults with recurrent malignant glioma: North American brain tumor consortium study 03-03. *Neuro-Oncology*, *13*(5), 509-516. https://doi.org/10.1093/neuonc/nor017

Izquierdo, E., Carvalho, D. M., Mackay, A., Temelso, S., Boult, J. K. R., Pericoli, G., Fernandez, E., Das, M., Molinari, V., Grabovska, Y., Rogers, R. F., Ajmone-Cat, M. A., Proszek, P. Z., Stubbs, M., Depani, S., O'Hare, P., Yu, L., Roumelioti, G., Choudhary, J. S., . . . Jones, C. (2022). DIPG Harbors Alterations Targetable by MEK Inhibitors, with Acquired Resistance Mechanisms Overcome by Combinatorial Inhibition. *Cancer Discovery*, *12*(3), 712-729. https://doi.org/10.1158/2159-8290.CD-20-0930

Jackson, E. R., Duchatel, R. J., Staudt, D. E., Persson, M. L., Mannan, A., Yadavilli, S., Parackal, S., Game, S., Chong, W. C., Jayasekara, W. S. N., Grand, M. L., Kearney, P. S., Douglas, A. M., Findlay, I. J., Germon, Z. P., McEwen, H. P., Beitaki, T. S., Patabendige, A., Skerrett-Byrne, D. A., . . . Dun, M. D. (2023). ONC201 in Combination with Paxalisib for the Treatment of H3K27-Altered Diffuse Midline Glioma. *Cancer Research*, *83*(14), 2421-2437. https://doi.org/10.1158/0008-5472.CAN-23-0186

Jakacki, R. I., Cohen, K. J., Buxton, A., Krailo, M. D., Burger, P. C., Rosenblum, M. K., Brat, D. J., Hamilton, R. L., Eckel, S. P., Zhou, T., Lavey, R. S., & Pollack, I. F. (2016). Phase 2 study of concurrent radiotherapy and temozolomide followed by temozolomide and lomustine in the treatment of children with high-grade glioma: a report of the Children's Oncology Group ACNS0423 study. *Neuro-Oncology*, *18*(10), 1442-1450. https://doi.org/10.1093/neuonc/now038

Jansen, M. H. A., van Vuurden, D. G., Vandertop, W. P., & Kaspers, G. J. L. (2012). Diffuse intrinsic pontine gliomas: A systematic update on clinical trials and biology. *Cancer Treatment Reviews*, *38*(1), 27-35. https://doi.org/10.1016/j.ctrv.2011.06.007

Jeggo, P. A. (1998). Identification of Genes Involved in Repair of DNA Double-Strand Breaks in Mammalian Cells. *Radiation Research*, *150*(5), S80-S91. https://doi.org/10.2307/3579810

Karajannis, M. A., Onar-Thomas, A., Lin, T., Baxter, P. A., Boué, D. R., Cole, B. L., Fuller, C., Haque, S., Jabado, N., Lucas, J. T., MacDonald, S. M., Matsushima, C., Patel, N., Pierson, C. R., Souweidane, M. M., Thomas, D. L., Walsh, M. F., Zaky, W., Leary, S. E. S., . . . Cohen, K. J. (2024). Phase 2 trial of veliparib, local irradiation, and temozolomide in patients with newly diagnosed high-grade glioma: a Children's Oncology Group study. *Neuro-Oncology*, *27*(4), 1092-1101. https://doi.org/10.1093/neuonc/noae247

Katayama, R., Shaw, A. T., Khan, T. M., Mino-Kenudson, M., Solomon, B. J., Halmos, B., Jessop, N. A., Wain, J. C., Yeo, A. T., Benes, C., Drew, L., Saeh, J. C., Crosby, K., Sequist, L. V., Iafrate, A. J., & Engelman, J. A. (2012). Mechanisms

of Acquired Crizotinib Resistance in ALK-Rearranged Lung Cancers. *Science Translational Medicine*, *4*(120), 120ra117-120ra117. https://doi.org/doi:10.1126/scitranslmed.3003316

Katayama, Y., Yamada, T., Tanimura, K., Tokuda, S., Morimoto, K., Hirai, S., Matsui, Y., Nakamura, R., Ishida, M., Kawachi, H., Yoneda, K., Hosoya, K., Tsuji, T., Ozasa, H., Yoshimura, A., Iwasaku, M., Kim, Y. H., Horinaka, M., Sakai, T., . . . Takayama, K. (2023). Adaptive resistance to lorlatinib via EGFR signaling in ALK-rearranged lung cancer. *NPJ Precis Oncol*, *7*(1), 12. https://doi.org/10.1038/s41698-023-00350-7

Kawakami, H., Huang, S., Pal, K., Dutta, S. K., Mukhopadhyay, D., & Sinicrope, F. A. (2016). Mutant BRAF Upregulates MCL-1 to Confer Apoptosis Resistance that Is Reversed by MCL-1 Antagonism and Cobimetinib in Colorectal Cancer. *Molecular Cancer Therapeutics*, *15*(12), 3015-3027. https://doi.org/10.1158/1535-7163.MCT-16-0017

Kemper, E. M., van Zandbergen, A. E., Cleypool, C., Mos, H. A., Boogerd, W., Beijnen, J. H., & van Tellingen, O. (2003). Increased penetration of paclitaxel into the brain by inhibition of P-Glycoprotein. *Clinical Cancer Research*, *9*(7), 2849-2855.

Khan, A., Gamble, L. D., Upton, D. H., Ung, C., Yu, D. M. T., Ehteda, A., Pandher, R., Mayoh, C., Hébert, S., Jabado, N., Kleinman, C. L., Burns, M. R., Norris, M. D., Haber, M., Tsoli, M., & Ziegler, D. S. (2021). Dual targeting of polyamine synthesis and uptake in diffuse intrinsic pontine gliomas. *Nature Communications*, *12*(1), 971. https://doi.org/10.1038/s41467-021-20896-z

Khare, P., Edgecomb, S. X., Hamadani, C. M., Tanner, E. E. L., & S Manickam, D. (2023). Lipid nanoparticle-mediated drug delivery to the brain. *Advanced Drug Delivery Reviews*, *197*, 114861. https://doi.org/10.1016/j.addr.2023.114861

Kim, S. Y., Jeong, E. H., Lee, T. G., Kim, H. R., & Kim, C. H. (2021). The Combination of Trametinib, a MEK Inhibitor, and Temsirolimus, an mTOR Inhibitor, Radiosensitizes Lung Cancer Cells. *Anticancer Res*, *41*(6), 2885-2894. https://doi.org/10.21873/anticanres.15070

Kline, C., Felton, E., Allen, I. E., Tahir, P., & Mueller, S. (2018). Survival outcomes in pediatric recurrent high-grade glioma: results of a 20-year systematic review and meta-analysis. *Journal of Neuro-Oncology*, *137*(1), 103-110. https://doi.org/10.1007/s11060-017-2701-8

Kline, C., Liu, S. J., Duriseti, S., Banerjee, A., Nicolaides, T., Raber, S., Gupta, N., Haas-Kogan, D., Braunstein, S., & Mueller, S. (2018). Reirradiation and PD-1 inhibition with nivolumab for the treatment of recurrent diffuse intrinsic pontine glioma: a single-institution experience. *Journal of Neuro-Oncology*, *140*(3), 629-638. https://doi.org/10.1007/s11060-018-2991-5

Krausert, S., Brabetz, S., Mack, N. L., Schmitt-Hoffner, F., Schwalm, B., Peterziel, H., Mangang, A., Holland-Letz, T., Sieber, L., Korshunov, A., Oehme, I., Jäger, N., Witt, O., Pfister, S. M., & Kool, M. (2022). Predictive modeling of resistance to SMO inhibition in a patient-derived orthotopic xenograft model of SHH medulloblastoma. *Neuro-Oncology Advances*, *4*(1), vdac026. https://doi.org/10.1093/noajnl/vdac026

Lakhani, N. J., Rasco, D., Wang, H., Men, L., Liang, E., Fu, T., Collins, M. C., Min, P., Yin, Y., Davids, M. S., Yang, D., & Zhai, Y. (2024). First-in-Human Study with Preclinical Data of BCL-2/BCL-xL Inhibitor Pelcitoclax in Locally Advanced or Metastatic Solid Tumors. *Clinical Cancer Research*, *30*(3), 506-521. https://doi.org/10.1158/1078-0432.CCR-23-1525

Lam, C. G., Howard, S. C., Bouffet, E., & Pritchard-Jones, K. (2019). Science and health for all children with cancer. *Science*, *363*(6432), 1182-1186. https://doi.org/10.1126/science.aaw4892

Lassaletta, Á., Morales, J. S., Valenzuela, P. L., Esteso, B., Kahalley, L. S., Mabbott, D. J., Unnikrishnan, S., Panizo, E., & Calvo, F. (2023). Neurocognitive outcomes in pediatric brain tumors after treatment with proton versus photon radiation: a systematic review and meta-analysis. *World Journal of Pediatrics*, *19*(8), 727-740. https://doi.org/10.1007/s12519-023-00726-6

Lassen, U. (2019). How I treat *NTRK* gene fusion-positive cancers. *ESMO Open*, *4*, e000612. https://doi.org/10.1136/esmoopen-2019-000612

Laurenge, A., Huillard, E., Bielle, F., & Idbaih, A. (2023). Cell of Origin of Brain and Spinal Cord Tumors. In N. Rezaei & S. Hanaei (Eds.), *Human Brain and Spinal Cord Tumors: From Bench to Bedside. Volume 1: Neuroimmunology and Neurogenetics* (pp. 85-101). Springer International Publishing. https://doi.org/10.1007/978-3-031-14732-6_6

Lawrie, A. M., Noble, M. E., Tunnah, P., Brown, N. R., Johnson, L. N., & Endicott, J. A. (1997). Protein kinase inhibition by staurosporine revealed in details of the molecular interaction with CDK2. *Nat Struct Biol*, *4*(10), 796-801. https://doi.org/10.1038/nsb1097-796

Lee, A., Chou, A. J., Williams, P. M., Roy-Chowdhuri, S., Patton, D. R., Coffey, B. D., Reid, J. M., Piao, J., Saguilig, L., Alonzo, T. A., Berg, S. L., Jaju, A., Fox, E., Hawkins, D. S., Mooney, M. M., Takebe, N., Tricoli, J. V., Janeway, K. A., Seibel, N., & Parsons, D. W. (2023). Erdafitinb in patients with FGFR-altered tumors: Results from the NCI-COG Pediatric MATCH trial arm B (APEC1621B). *Journal of Clinical Oncology*, *41*(16_suppl), 10007-10007. https://doi.org/10.1200/JCO.2023.41.16_suppl.10007

Lee, J. M., Kim, H. S., Kim, A., Chang, Y. S., Lee, J. G., Cho, J., & Kim, E. Y. (2022). ABT-737, a BH3 Mimetic, Enhances the Therapeutic Effects of Ionizing Radiation in K-ras Mutant Non-Small Cell Lung Cancer Preclinical Model. *Yonsei Med J*, *63*(1), 16-25. https://doi.org/10.3349/ymj.2022.63.1.16

Lemaire, M., Bruelisauer, A., Guntz, P., & Sato, H. (1996). Dose-dependent brain penetration of SDZ PSC 833, a novel multidrug resistance-reversing cyclosporin, in rats. *Cancer Chemotherapy and Pharmacology*, *38*(5), 481-486. https://doi.org/10.1007/s002800050515

Liang, S., Wang, Q., Qi, X., Liu, Y., Li, G., Lu, S., Mou, L., & Chen, X. (2021). Deciphering the Mechanism of Gilteritinib Overcoming Lorlatinib Resistance to the Double Mutant I1171N/F1174I in Anaplastic Lymphoma Kinase. *Frontiers in Cell and Developmental Biology*, *9*. https://doi.org/10.3389/fcell.2021.808864

Lin, F. Y., Stuckert, A., Tat, C., White, M., Ruggieri, L., Zhang, H., Mehta, B., Lapteva, N., Mei, Z., Major, A., Thakkar, S., Shum, T., Parikh, K., Wu, M.-F., Lindsay, H. B., Scherer, L., Shekar, M., Baxter, P., Wang, T., . . . Omer, B. (2024). Phase I Trial of GD2.CART Cells Augmented With Constitutive Interleukin-7 Receptor for Treatment of High-Grade Pediatric CNS Tumors. *Journal of Clinical Oncology*, *42*(23), 2769-2779. https://doi.org/10.1200/JCO.23.02019

Lin, G. L., & Monje, M. (2017). A Protocol for Rapid Post-mortem Cell Culture of Diffuse Intrinsic Pontine Glioma (DIPG). *Journal of Visualized Experiments (JoVE)*(121), e55360. https://doi.org/10.3791/55360

Lin, G. L., Wilson, K. M., Ceribelli, M., Stanton, B. Z., Woo, P. J., Kreimer, S., Qin, E. Y., Zhang, X., Lennon, J., Nagaraja, S., Morris, P. J., Quezada, M., Gillespie, S. M., Duveau, D. Y., Michalowski, A. M., Shinn, P., Guha, R., Ferrer, M.,

Klumpp-Thomas, C., . . . Monje, M. (2019). Therapeutic strategies for diffuse midline glioma from high-throughput combination drug screening. *Science Translational Medicine*, *11*(519), eaaw0064. https://doi.org/10.1126/scitranslmed.aaw0064

Löscher, W., Nau, H., & Siemes, H. (1988). Penetration of Valproate and its Active Metabolites into Cerebrospinal Fluid of Children with Epilepsy. *Epilepsia*, *29*(3), 311-316. https://doi.org/10.1111/j.1528-1157.1988.tb03725.x

Löser, D. A., Shibata, A., Shibata, A. K., Woodbine, L. J., Jeggo, P. A., & Chalmers, A. J. (2010). Sensitization to Radiation and Alkylating Agents by Inhibitors of Poly(ADP-ribose) Polymerase Is Enhanced in Cells Deficient in DNA Double-Strand Break Repair. *Molecular Cancer Therapeutics*, *9*(6), 1775-1787. https://doi.org/10.1158/1535-7163.MCT-09-1027

Louis, D. N., Perry, A., Reifenberger, G., von Deimling, A., Figarella-Branger, D., Cavenee, W. K., Ohgaki, H., Wiestler, O. D., Kleihues, P., & Ellison, D. W. (2016). The 2016 World Health Organization Classification of Tumors of the Central Nervous System: a summary. *Acta Neuropathol*, *131*(6), 803-820. https://doi.org/10.1007/s00401-016-1545-1

Louis, D. N., Perry, A., Wesseling, P., Brat, D. J., Cree, I. A., Figarella-Branger, D., Hawkins, C., Ng, H. K., Pfister, S. M., Reifenberger, G., Soffietti, R., von Deimling, A., & Ellison, D. W. (2021). The 2021 WHO Classification of Tumors of the Central Nervous System: a summary. *Neuro-Oncology*, *23*(8), 1231-1251. https://doi.org/10.1093/neuonc/noab106

Lupo, P. J., & Spector, L. G. (2020). Cancer Progress and Priorities: Childhood Cancer. *Cancer Epidemiol Biomarkers Prev*, *29*(6), 1081-1094. https://doi.org/10.1158/1055-9965.Epi-19-0941

Maeda, A., Chen, Y., Bu, J., Mujcic, H., Wouters, B. G., & DaCosta, R. S. (2017). In Vivo Imaging Reveals Significant Tumor Vascular Dysfunction and Increased Tumor Hypoxia-Inducible Factor-1α Expression Induced by High Single-Dose Irradiation in a Pancreatic Tumor Model. *International Journal of Radiation Oncology*Biology*Physics*, *97*(1), 184-194. https://doi.org/10.1016/j.ijrobp.2016.09.005

Mallick, S., Gandhi, A. K., Joshi, N. P., Kumar, A., Puri, T., Sharma, D. N., Haresh, K. P., Gupta, S., Julka, P. K., Rath, G. K., & Sarkar, C. (2015). Outcomes of pediatric glioblastoma treated with adjuvant chemoradiation with temozolomide and correlation with prognostic factors. *Indian Journal of Medical and Paediatric Oncology*, *36*(2), 99-104. https://doi.org/10.4103/0971-5851.158838

Malsy, M., Bitzinger, D., Graf, B., & Bundscherer, A. (2019). Staurosporine induces apoptosis in pancreatic carcinoma cells PaTu 8988t and Panc-1 via the intrinsic signaling pathway. *Eur J Med Res*, *24*(1), 5. https://doi.org/10.1186/s40001-019-0365-x

Manton, C. A., Johnson, B., Singh, M., Bailey, C. P., Bouchier-Hayes, L., & Chandra, J. (2016). Induction of cell death by the novel proteasome inhibitor marizomib in glioblastoma in vitro and in vivo. *Scientific Reports*, *6*(1), 18953. https://doi.org/10.1038/srep18953

Martín, F., Alcon, C., Marín, E., Morales-Sánchez, P., Manzano-Muñoz, A., Díaz, S., García, M., Samitier, J., Lu, A., Villanueva, A., Reguart, N., Teixido, C., & Montero, J. (2025). Novel selective strategies targeting the BCL-2 family to enhance clinical efficacy in ALK-rearranged non-small cell lung cancer. *Cell Death & Disease*, *16*(1), 194. https://doi.org/10.1038/s41419-025-07513-3

Mason, W. P., Kesari, S., Stupp, R., Aregawi, D. G., Piccioni, D. E., Roth, P., Desjardins, A., Reich, S. D., Casadebaig, M.-L., Elias, I., Winograd, B., Levin, N., & Bota, D. A. (2019). Full enrollment results from an extended phase I, multicenter, open label study of marizomib (MRZ) with temozolomide (TMZ) and radiotherapy (RT) in newly diagnosed glioblastoma (GBM). *Journal of Clinical Oncology*, *37*(15_suppl), 2021-2021. https://doi.org/10.1200/JCO.2019.37.15_suppl.2021

Mayr, L., Guntner, A. S., Madlener, S., Schmook, M. T., Peyrl, A., Azizi, A. A., Dieckmann, K., Reisinger, D., Stepien, N. M., Schramm, K., Laemmerer, A., Jones, D. T. W., Ecker, J., Sahm, F., Milde, T., Pajtler, K. W., Blattner-Johnson, M., Strbac, M., Dorfer, C., . . . Gojo, J. (2020). Cerebrospinal Fluid Penetration and Combination Therapy of Entrectinib for Disseminated ROS1/NTRK-Fusion Positive Pediatric High-Grade Glioma. *Journal of Personalized Medicine*, *10*(4). https://doi.org/10.3390/jpm10040290

Mayr, L., Neyazi, S., Schwark, K., Trissal, M., Beck, A., Labelle, J., Eder, S. K., Weiler-Wichtl, L., Marques, J. G., De Biagi-Junior, C. A. O., Lo Cascio, C., Chapman, O., Sridhar, S., Kenkre, R., Dutta, A., Wang, S., Wang, J., Hack, O., Nascimento, A., . . . Filbin, M. G. (2025). Effective targeting of PDGFRA-altered high-grade glioma with avapritinib. *Cancer Cell*, *43*(4), 740-756.e748. https://doi.org/10.1016/j.ccell.2025.02.018

Meacham, C. E., & Morrison, S. J. (2013). Tumour heterogeneity and cancer cell plasticity. *Nature*, *501*(7467), 328-337. https://doi.org/10.1038/nature12624

Melia, E., & Parsons, Jason L. (2023). DNA damage and repair dependencies of ionising radiation modalities. *Bioscience Reports*, *43*(10), BSR20222586. https://doi.org/10.1042/BSR20222586

Messiaen, J., Jacobs, S. A., & De Smet, F. (2023). The tumor micro-environment in pediatric glioma: friend or foe? *Front Immunol*, *14*, 1227126. https://doi.org/10.3389/fimmu.2023.1227126

Metselaar, D. S., du Chatinier, A., Stuiver, I., Kaspers, G. J. L., & Hulleman, E. (2021). Radiosensitization in Pediatric High-Grade Glioma: Targets, Resistance and Developments. *Frontiers in Oncology*, *11*. https://doi.org/10.3389/fonc.2021.662209

Monje, M., Cooney, T., Glod, J., Huang, J., Peer, C. J., Faury, D., Baxter, P., Kramer, K., Lenzen, A., Robison, N. J., Kilburn, L., Vinitsky, A., Figg, W. D., Jabado, N., Fouladi, M., Fangusaro, J., Onar-Thomas, A., Dunkel, I. J., & Warren, K. E. (2023). Phase I trial of panobinostat in children with diffuse intrinsic pontine glioma: A report from the Pediatric Brain Tumor Consortium (PBTC-047). *Neuro-Oncology*, *25*(12), 2262-2272. https://doi.org/10.1093/neuonc/noad141

Monje, M., Mahdi, J., Majzner, R., Yeom, K. W., Schultz, L. M., Richards, R. M., Barsan, V., Song, K.-W., Kamens, J., Baggott, C., Kunicki, M., Rietberg, S. P., Lim, A. S., Reschke, A., Mavroukakis, S., Egeler, E., Moon, J., Patel, S., Chinnasamy, H., . . . Mackall, C. (2025). Intravenous and intracranial GD2-CAR T cells for H3K27M+ diffuse midline gliomas. *Nature*, *637*(8046), 708-715. https://doi.org/10.1038/s41586-024-08171-9

Mueller, S., Cooney, T., Yang, X., Pal, S., Ermoian, R., Gajjar, A., Liu, X., Prem, K., Minard, C. G., Reid, J. M., Nelson, M., Haas-Kogan, D., Fox, E., & Weigel, B. J. (2022). Wee1 kinase inhibitor adavosertib with radiation in newly diagnosed diffuse intrinsic pontine glioma: A Children's Oncology Group phase I consortium study. *Neuro-Oncology Advances*, *4*(1), vdac073. https://doi.org/10.1093/noajnl/vdac073

Mueller, S., Kline, C., Lu, A. Y., Hoogendijk, R., Wembacher-Schroeder, E., Banerjee, A., Reddy, A. T., Raber, S., Hoffman, C., Stoller, S., Prados, M., Molinaro, A., & Gupta, N. (2025). PNOC009: Convection-enhanced delivery of liposomal irinotecan in patients with newly diagnosed diffuse intrinsic pontine glioma. *Neuro-Oncology Advances*, *7*(1), vdaf093. https://doi.org/10.1093/noajnl/vdaf093

Mueller, S., Kline, C., Stoller, S., Lundy, S., Christopher, L., Reddy, A. T., Banerjee, A., Cooney, T. M., Raber, S., Hoffman, C., Luks, T., Wembacher-Schroeder, E., Lummel, N., Zhang, Y., Bonner, E. R., Nazarian, J., Molinaro, A. M., Prados, M., Villanueva-Meyer, J. E., & Gupta, N. (2023). PNOC015: Repeated convection-enhanced delivery of MTX110 (aqueous panobinostat) in children with newly diagnosed diffuse intrinsic pontine glioma. *Neuro-Oncology*, *25*(11), 2074-2086. https://doi.org/10.1093/neuonc/noad105

Munshi, A., Hobbs, M., & Meyn, R. E. (2005). Clonogenic Cell Survival Assay. In R. D. Blumenthal (Ed.), *Chemosensitivity: Volume 1 In Vitro Assays* (pp. 21-28). Humana Press.

Muroi, A., Mizumoto, M., Ishikawa, E., Ihara, S., Fukushima, H., Tsurubuchi, T., Sakurai, H., & Matsumura, A. (2020). Proton therapy for newly diagnosed pediatric diffuse intrinsic pontine glioma. *Child's Nervous System*, *36*(3), 507-512. https://doi.org/10.1007/s00381-019-04420-9

Murty, S., Haile, S. T., Beinat, C., Aalipour, A., Alam, I. S., Murty, T., Shaffer, T. M., Patel, C. B., Graves, E. E., Mackall, C. L., & Gambhir, S. S. (2020). Intravital imaging reveals synergistic effect of CAR T-cells and radiation therapy in a preclinical immunocompetent glioblastoma model. *OncoImmunology*, *9*(1), 1757360. https://doi.org/10.1080/2162402X.2020.1757360

Narsinh, K. H., Kumar, K., Bankiewicz, K., Martin, A. J., Berger, M., Clarke, J., Taylor, J., Bush, N. A. O., Molinaro, A. M., Aghi, M., & Butowski, N. (2025). A phase I study of convection-enhanced delivery (CED) of liposomal-irinotecan using real-time magnetic resonance imaging in patients with recurrent high-grade glioma. *Journal of Neuro-Oncology*, *172*(1), 219-227. https://doi.org/10.1007/s11060-024-04904-y

Noll, A., Myers, C., Biery, M. C., Meechan, M., Tahiri, S., Rajendran, A., Berens, M. E., Paine, D., Byron, S., Zhang, J., Winter, C., Pakiam, F., Leary, S. E. S., Cole, B. L., Jackson, E. R., Dun, M. D., Foster, J. B., Evans, M. K., Pattwell, S. S., . . . Vitanza, N. A. (2023). Therapeutic HDAC inhibition in hypermutant diffuse intrinsic pontine glioma. *Neoplasia*, *43*, 100921. https://doi.org/10.1016/j.neo.2023.100921

Noon, A., & Galban, S. (2023). Therapeutic avenues for targeting treatment challenges of diffuse midline gliomas. *Neoplasia*, *40*, 100899. https://doi.org/10.1016/j.neo.2023.100899

O'Steen, S., Green, D. J., Gopal, A. K., Orozco, J. J., Kenoyer, A. L., Lin, Y., Wilbur, D. S., Hamlin, D. K., Fisher, D. R., Hylarides, M. D., Gooley, T. A., Waltman, A., Till, B. G., & Press, O. W. (2017). Venetoclax Synergizes with Radiotherapy for Treatment of B-cell Lymphomas. *Cancer Res*, *77*(14), 3885-3893. https://doi.org/10.1158/0008-5472.Can-17-0082

Obaidat, A., Weiss, J., Wahlgren, B., Manam, R. R., Macherla, V. R., McArthur, K., Chao, T.-H., Palladino, M. A., Lloyd, G. K., Potts, B. C., Enna, S. J., Neuteboom, S. T. C., & Hagenbuch, B. (2011). Proteasome Regulator Marizomib (NPI-0052) Exhibits Prolonged Inhibition, Attenuated Efflux, and Greater Cytotoxicity than

Its Reversible Analogs. *The Journal of Pharmacology and Experimental Therapeutics*, *337*(2), 479-486. https://doi.org/10.1124/jpet.110.177824

Ocasio, J. K., Budd, K. M., Roach, J. T., Andrews, J. M., & Baker, S. J. (2023). Oncohistones and disrupted development in pediatric-type diffuse high-grade glioma. *Cancer Metastasis Reviews*, *42*(2), 367-388. https://doi.org/10.1007/s10555-023-10105-2

Ochs, K., Ott, M., Bunse, T., Sahm, F., Bunse, L., Deumelandt, K., Sonner, J. K., Keil, M., von Deimling, A., Wick, W., & Platten, M. (2017). K27M-mutant histone-3 as a novel target for glioma immunotherapy. *OncoImmunology*, *6*(7), e1328340. https://doi.org/10.1080/2162402X.2017.1328340

Oldendorf, W. H. (1974). Lipid solubility and drug penetration of the blood brain barrier. *Proceedings of the Society for Experimental Biology and Medicine. Society for Experimental Biology and Medicine (New York, N.Y.)*, *147*(3), 813-815. https://doi.org/10.3181/00379727-147-38444

Palmer, A. C., & Sorger, P. K. (2017). Combination Cancer Therapy Can Confer Benefit via Patient-to-Patient Variability without Drug Additivity or Synergy. *Cell*, *171*(7), 1678-1691.e1613. https://doi.org/10.1016/j.cell.2017.11.009

Pan, W., & Kastin, A. J. (2001). Changing the chemokine gradient: CINC1 crosses the blood–brain barrier. *Journal of Neuroimmunology*, *115*(1), 64-70. https://doi.org/10.1016/S0165-5728(01)00256-9

Pant, S., Schuler, M., Iyer, G., Witt, O., Doi, T., Qin, S., Tabernero, J., Reardon, D. A., Massard, C., Minchom, A., Lugowska, I., Carranza, O., Arnold, D., Gutierrez, M., Winter, H., Stuyckens, K., Crow, L., Najmi, S., Hammond, C., . . . Investigators, R. (2023). Erdafitinib in patients with advanced solid tumours with FGFR alterations (RAGNAR): an international, single-arm, phase 2 study. *The Lancet. Oncology*, *24*(8), 925-935. https://doi.org/10.1016/S1470-2045(23)00275-9

Parasramka, S., Talari, G., Rosenfeld, M., Guo, J., & Villano, J. L. (2017). Procarbazine, lomustine and vincristine for recurrent high-grade glioma - Parasramka, S - 2017 | Cochrane Library.

Pardoll, D. M. (2012). The blockade of immune checkpoints in cancer immunotherapy. *Nature Reviews Cancer*, *12*(4), 252-264. https://doi.org/10.1038/nrc3239

Pardridge, W. M. (2005). The Blood-Brain Barrier: Bottleneck in Brain Drug Development. *NeuroRx*, *2*(1), 3-14. https://doi.org/10.1602/neurorx.2.1.3

Patel, Y. T., Davis, A., Baker, S. J., Campagne, O., & Stewart, C. F. (2019). CNS penetration of the CDK4/6 inhibitor ribociclib in non-tumor bearing mice and mice bearing pediatric brain tumors. *Cancer Chemotherapy and Pharmacology*, *84*(2), 447-452. https://doi.org/10.1007/s00280-019-03864-9

Pathania, M., De Jay, N., Maestro, N., Harutyunyan, A. S., Nitarska, J., Pahlavan, P., Henderson, S., Mikael, L. G., Richard-Londt, A., Zhang, Y., Costa, J. R., Hébert, S., Khazaei, S., Ibrahim, N. S., Herrero, J., Riccio, A., Albrecht, S., Ketteler, R., Brandner, S., . . . Salomoni, P. (2017). H3.3K27M cooperates with Trp53 loss and PDGFRA gain in mouse embryonic neural progenitor cells to induce invasive high-grade gliomas. *Cancer Cell*, *32*(5), 684-700.e689. https://doi.org/10.1016/j.ccell.2017.09.014

Paul, P. R., Mishra, M. K., Bora, S., Kukal, S., Singh, A., Kukreti, S., & Kukreti, R. (2025). The Impact of P-Glycoprotein on CNS Drug Efflux and Variability in Response. *Journal of Biochemical and Molecular Toxicology*, *39*(3), e70190. https://doi.org/10.1002/jbt.70190

Pearson, T., Shultz, L. D., Miller, D., King, M., Laning, J., Fodor, W., Cuthbert, A., Burzenski, L., Gott, B., Lyons, B., Foreman, O., Rossini, A. A., & Greiner, D. L. (2008). Non-obese diabetic–recombination activating gene-1 (NOD–Rag 1 null) interleukin (IL)-2 receptor common gamma chain (IL 2 rγnull) null mice: a radioresistant model for human lymphohaematopoietic engraftment. *Clinical and Experimental Immunology*, *154*(2), 270-284. https://doi.org/10.1111/j.1365-2249.2008.03753.x

Perreault, S., Larouche, V., Tabori, U., Hawkin, C., Lippé, S., Ellezam, B., Décarie, J.-C., Théoret, Y., Métras, M.-É., Sultan, S., Cantin, É., Routhier, M.-È., Caru, M., Legault, G., Bouffet, É., Lafay-Cousin, L., Hukin, J., Erker, C., & Jabado, N. (2019). A phase 2 study of trametinib for patients with pediatric glioma or plexiform neurofibroma with refractory tumor and activation of the MAPK/ERK pathway: TRAM-01. *BMC Cancer*, *19*(1), 1250. https://doi.org/10.1186/s12885-019-6442-2

Persson, M. L., Douglas, A. M., Alvaro, F., Faridi, P., Larsen, M. R., Alonso, M. M., Vitanza, N. A., & Dun, M. D. (2022). The intrinsic and microenvironmental features of diffuse midline glioma: Implications for the development of effective immunotherapeutic treatment strategies. *Neuro-Oncology*, *24*(9), 1408-1422. https://doi.org/10.1093/neuonc/noac117

Perwein, T., Giese, B., Nussbaumer, G., von Bueren, A. O., van Buiren, M., Benesch, M., & Kramm, C. M. (2023). How I treat recurrent pediatric high-grade glioma (pHGG): a Europe-wide survey study. *Journal of Neuro-Oncology*, *161*(3), 525-538. https://doi.org/10.1007/s11060-023-04241-6

Pesch, A. M., Chandler, B. C., Michmerhuizen, A. R., Carter, H. M., Hirsh, N. H., Wilder-Romans, K., Liu, M., Ward, T., Ritter, C. L., Nino, C. A., Jungles, K. M., Pierce, L. J., Rae, J. M., & Speers, C. W. (2022). Bcl-xL inhibition radiosensitizes PIK3CA/PTEN wild-type triple negative breast cancers with low Mcl-1 expression. *Cancer Res Commun*, *2*(7), 679-693. https://doi.org/10.1158/2767-9764.crc-22-0024

Peterziel, H., Jamaladdin, N., ElHarouni, D., Gerloff, X. F., Herter, S., Fiesel, P., Berker, Y., Blattner-Johnson, M., Schramm, K., Jones, B. C., Reuss, D., Turunen, L., Friedenauer, A., Holland-Letz, T., Sill, M., Weiser, L., Previti, C., Balasubramanian, G., Gerber, N. U., . . . Oehme, I. (2022). Drug sensitivity profiling of 3D tumor tissue cultures in the pediatric precision oncology program INFORM. *npj Precision Oncology*, *6*(1), 94. https://doi.org/10.1038/s41698-022-00335-y

Peyrl, A., Chocholous, M., Azizi, A. A., Czech, T., Dorfer, C., Mitteregger, D., Gojo, J., Minichmayr, E., & Slavc, I. (2014). Safety of Ommaya reservoirs in children with brain tumors: a 20-year experience with 5472 intraventricular drug administrations in 98 patients. *Journal of Neuro-Oncology*, *120*(1), 139-145. https://doi.org/10.1007/s11060-014-1531-1

Pfister, S. M., Reyes-Múgica, M., Chan, J. K. C., Hasle, H., Lazar, A. J., Rossi, S., Ferrari, A., Jarzembowski, J. A., Pritchard-Jones, K., Hill, D. A., Jacques, T. S., Wesseling, P., López Terrada, D. H., von Deimling, A., Kratz, C. P., Cree, I. A., & Alaggio, R. (2022). A Summary of the Inaugural WHO Classification of Pediatric Tumors: Transitioning from the Optical into the Molecular Era. *Cancer Discovery*, *12*(2), 331-355. https://doi.org/10.1158/2159-8290.CD-21-1094

Poei, D., Ali, S., Ye, S., & Hsu, R. (2024). ALK inhibitors in cancer: mechanisms of resistance and therapeutic management strategies. *Cancer Drug Resistance*, *7*(0), N/A-N/A. https://doi.org/10.20517/cdr.2024.25

Pollack, I. F., Jakacki, R. I., Blaney, S. M., Hancock, M. L., Kieran, M. W., Phillips, P., Kun, L. E., Friedman, H., Packer, R., Banerjee, A., Geyer, J. R., Goldman, S., Poussaint, T. Y., Krasin, M. J., Wang, Y., Hayes, M., Murgo, A., Weiner, S., & Boyett, J. M. (2007). Phase I trial of imatinib in children with newly diagnosed brainstem and recurrent malignant gliomas: A Pediatric Brain Tumor Consortium report. *Neuro-Oncology*, *9*(2), 145-160. https://doi.org/10.1215/15228517-2006-031

Pompos, A., Foote, R. L., Koong, A. C., Le, Q. T., Mohan, R., Paganetti, H., & Choy, H. (2022). National Effort to Re-Establish Heavy Ion Cancer Therapy in the United States. *Frontiers in Oncology*, *12*. https://doi.org/10.3389/fonc.2022.880712

Pont, L. M., Naipal, K., Kloezeman, J. J., Venkatesan, S., van den Bent, M., van Gent, D. C., Dirven, C. M., Kanaar, R., Lamfers, M. L., & Leenstra, S. (2015). DNA damage response and anti-apoptotic proteins predict radiosensitization efficacy of HDAC inhibitors SAHA and LBH589 in patient-derived glioblastoma cells. *Cancer Lett*, *356*(2 Pt B), 525-535. https://doi.org/10.1016/j.canlet.2014.09.049

Power, E. A., Rechberger, J. S., Gupta, S., Schwartz, J. D., Daniels, D. J., & Khatua, S. (2022). Drug delivery across the blood-brain barrier for the treatment of pediatric brain tumors – An update. *Advanced Drug Delivery Reviews*, *185*, 114303. https://doi.org/10.1016/j.addr.2022.114303

Prabhu, V. V., Morrow, S., Rahman Kawakibi, A., Zhou, L., Ralff, M., Ray, J., Jhaveri, A., Ferrarini, I., Lee, Y., Parker, C., Zhang, Y., Borsuk, R., Chang, W.-I., Honeyman, J. N., Tavora, F., Carneiro, B., Raufi, A., Huntington, K., Carlsen, L., . . . El-Deiry, W. S. (2020). ONC201 and imipridones: Anti-cancer compounds with clinical efficacy. *Neoplasia*, *22*(12), 725-744. https://doi.org/10.1016/j.neo.2020.09.005

Price, G., Bouras, A., Hambardzumyan, D., & Hadjipanayis, C. G. (2021). Current knowledge on the immune microenvironment and emerging immunotherapies in diffuse midline glioma. *EBioMedicine*, *69*, 103453. https://doi.org/10.1016/j.ebiom.2021.103453

Price, M., Ballard, C. A. P., Benedetti, J. R., Kruchko, C., Barnholtz-Sloan, J. S., & Ostrom, Q. T. (2025). CBTRUS Statistical Report: Pediatric Brain Tumor Foundation Childhood and Adolescent Primary Brain and Other Central Nervous System Tumors Diagnosed in the United States in 2017-2021. *Neuro-Oncology*, *27*(Supplement_1), i1-i42. https://doi.org/10.1093/neuonc/noaf168

Rajan, S. S., Amin, A. D., Li, L., Rolland, D. C., Li, H., Kwon, D., Kweh, M. F., Arumov, A., Roberts, E. R., Yan, A., Basrur, V., Elenitoba-Johnson, K. S. J., Chen, X. S., Puvvada, S. D., Lussier, Y. A., Bilbao, D., Lim, M. S., & Schatz, J. H. (2020). The mechanism of cancer drug addiction in ALK-positive T-Cell lymphoma. *Oncogene*, *39*(10), 2103-2117. https://doi.org/10.1038/s41388-019-1136-4

Ravikrishnan, J., Diaz-Rohena, D. Y., Muhowski, E., Mo, X., Lai, T.-H., Misra, S., Williams, C. D., Sanchez, J., Mitchell, A., Satpati, S., Perry, E., Kaufman, T., Liu, C., Lozanski, A., Lozanski, G., Rogers, K., Kittai, A. S., Bhat, S. A., Collins, M. C., . . . Sampath, D. (2025). LP-118 is a novel B-cell lymphoma 2 / extra-large inhibitor that demonstrates efficacy in models of venetoclaxresistant chronic lymphocytic leukemia. *Haematologica*, *110*(1), 78-91. https://doi.org/10.3324/haematol.2023.284353

Ribas, A., & Wolchok, J. D. (2018). Cancer immunotherapy using checkpoint blockade. *Science*, *359*(6382), 1350-1355. https://doi.org/10.1126/science.aar4060

Rieken, S., Habermehl, D., Haberer, T., Jaekel, O., Debus, J., & Combs, S. E. (2012). Proton and carbon ion radiotherapy for primary brain tumors delivered with active raster scanning at the Heidelberg Ion Therapy Center (HIT): early treatment results and study concepts. *Radiation Oncology*, *7*(1), 41. https://doi.org/10.1186/1748-717X-7-41

Riessland, M., Ximerakis, M., Jarjour, A. A., Zhang, B., & Orr, M. E. (2024). Therapeutic targeting of senescent cells in the CNS. *Nature Reviews Drug Discovery*, *23*(11), 817-837. https://doi.org/10.1038/s41573-024-01033-z

Rizzaro, M. D., Fanizzi, C., Fiore, G., Remore, L. G., Ampollini, A. M., Pluderi, M., Caroli, M., Locatelli, M., Rizzaro, M. D., Fanizzi, C., Fiore, G., Remore, L. G., Ampollini, A. M., Pluderi, M., Caroli, M., & Locatelli, M. (2025). TRK Inhibitors in Adult and Pediatric High-Grade Gliomas: A Systematic Review and Individual Participant Data Meta-Analysis. *Cancers*, *17*(13). https://doi.org/10.3390/cancers17132089

Rodriguez, A., Dixit, K., O'Hara, R. M., Jr, & Vojnic, M. (2025). Efficacy of tepotinib in patients with high-grade glioma with MET alterations: A case series. *Neuro-Oncology Practice*, npaf130. https://doi.org/10.1093/nop/npaf130

Roobol, S. J., Bent, I. v. d., Cappellen, W. A. v., Abraham, T. E., Paul, M. W., Kanaar, R., Houtsmuller, A. B., Gent, D. C. v., Essers, J., Roobol, S. J., Bent, I. v. d., Cappellen, W. A. v., Abraham, T. E., Paul, M. W., Kanaar, R., Houtsmuller, A. B., Gent, D. C. v., & Essers, J. (2020). Comparison of High- and Low-LET Radiation-Induced DNA Double-Strand Break Processing in Living Cells. *International Journal of Molecular Sciences*, *21*(18). https://doi.org/10.3390/ijms21186602

Rosen, L. S., LoRusso, P., Ma, W. W., Goldman, J. W., Weise, A., Colevas, A. D., Adjei, A., Yazji, S., Shen, A., Johnston, S., Hsieh, H.-J., Chan, I. T., & Sikic, B. I. (2016). A first-in-human phase I study to evaluate the MEK1/2 inhibitor, cobimetinib, administered daily in patients with advanced solid tumors. *Investigational new drugs*, *34*(5), 604-613. https://doi.org/10.1007/s10637-016-0374-3

Rosenblum, D., Gutkin, A., Kedmi, R., Ramishetti, S., Veiga, N., Jacobi, A. M., Schubert, M. S., Friedmann-Morvinski, D., Cohen, Z. R., Behlke, M. A., Lieberman, J., & Peer, D. (2020). CRISPR-Cas9 genome editing using targeted lipid nanoparticles for cancer therapy. *Science Advances*, *6*(47), eabc9450. https://doi.org/10.1126/sciadv.abc9450

Roth, P., Gorlia, T., Reijneveld, J. C., de Vos, F., Idbaih, A., Frenel, J.-S., Le Rhun, E., Sepulveda, J. M., Perry, J., Masucci, G. L., Freres, P., Hirte, H., Seidel, C., Walenkamp, A., Lukacova, S., Meijnders, P., Blais, A., Ducray, F., Verschaeve, V., . . . Group, f. t. E. B. T. G. a. t. C. C. T. (2024). Marizomib for patients with newly diagnosed glioblastoma: A randomized phase 3 trial. *Neuro-Oncology*, *26*(9), 1670-1682. https://doi.org/10.1093/neuonc/noae053

Saki, M., Bhat, K., Sodhi, S. S., Nguyen, N. T., Kornblum, H. I., & Pajonk, F. (2019). Effects of Brain Irradiation in Immune-Competent and Immune-Compromised Mouse Models. *Radiation Research*, *193*(2), 186-194. https://doi.org/10.1667/RR15373.1

Sale, M. J., Balmanno, K., Saxena, J., Ozono, E., Wojdyla, K., McIntyre, R. E., Gilley, R., Woroniuk, A., Howarth, K. D., Hughes, G., Dry, J. R., Arends, M. J., Caro, P., Oxley, D., Ashton, S., Adams, D. J., Saez-Rodriguez, J., Smith, P. D., & Cook, S. J. (2019). MEK1/2 inhibitor withdrawal reverses acquired resistance driven by BRAFV600E amplification whereas KRASG13D amplification

promotes EMT-chemoresistance. *Nature Communications*, *10*(1), 2030. https://doi.org/10.1038/s41467-019-09438-w

Sasaki, T., Watanabe, J., He, X., Katagi, H., Suri, A., Ishi, Y., Abe, K., Natsumeda, M., Frey, W. H., Zhang, P., & Hashizume, R. (2022). Intranasal delivery of nanoliposomal SN-38 for treatment of diffuse midline glioma. *Journal of Neurosurgery*, *138*(6), 1570-1579. https://doi.org/10.3171/2022.9.JNS22715

Schick, U., Kyula, J., Barker, H., Patel, R., Zaidi, S., Gregory, C., Hafsi, H., Roulstone, V., Deutsch, E., McLaughlin, M., & Harrington, K. (2015). Trametinib radiosensitises RAS- and BRAF-mutated melanoma by perturbing cell cycle and inducing senescence. *Radiother Oncol*, *117*(2), 364-375. https://doi.org/10.1016/j.radonc.2015.06.026

Schoof, M., Zheng, T., Sill, M., Imle, R., Cais, A., Altendorf, L., Fürst, A., Hofmann, N., Ernst, K., Vonficht, D., Chan, K. C.-H., Holland-Letz, T., Postlmayr, A., Shiraishi, R., Wang, W., Morcavallo, A., Spohn, M., Göbel, C., Niesen, J., . . . Zuckermann, M. (2026). Investigation of a global mouse methylome atlas reveals subtype-specific copy number alterations in pediatric cancer models. *Nature Genetics*, *58*(1), 143-156. https://doi.org/10.1038/s41588-025-02419-4

Shaffer, S. M., Dunagin, M. C., Torborg, S. R., Torre, E. A., Emert, B., Krepler, C., Beqiri, M., Sproesser, K., Brafford, P. A., Xiao, M., Eggan, E., Anastopoulos, I. N., Vargas-Garcia, C. A., Singh, A., Nathanson, K. L., Herlyn, M., & Raj, A. (2017). Rare cell variability and drug-induced reprogramming as a mode of cancer drug resistance. *Nature*, *546*(7658), 431-435. https://doi.org/10.1038/nature22794

Shahab, S. W., Schniederjan, M., Vega, J. V., Little, S., Reisner, A., MacDonald, T., & Aguilera, D. (2023). Case report: ATIC-ALK fusion in infant-type hemispheric glioma and response to lorlatinib. *Frontiers in Oncology*, *13*. https://doi.org/10.3389/fonc.2023.1123378

Sharie, S. A., Laban, D. A., Al-Hussaini, M., Sharie, S. A., Laban, D. A., & Al-Hussaini, M. (2023). Decoding Diffuse Midline Gliomas: A Comprehensive Review of Pathogenesis, Diagnosis and Treatment. *Cancers*, *15*(19). https://doi.org/10.3390/cancers15194869

Sharma, S. V., Lee, D. Y., Li, B., Quinlan, M. P., Takahashi, F., Maheswaran, S., McDermott, U., Azizian, N., Zou, L., Fischbach, M. A., Wong, K. K., Brandstetter, K., Wittner, B., Ramaswamy, S., Classon, M., & Settleman, J. (2010). A chromatin-mediated reversible drug-tolerant state in cancer cell subpopulations. *Cell*, *141*(1), 69-80. https://doi.org/10.1016/j.cell.2010.02.027

Shi, C., Wang, X., Diao, C., Zhu, H., Yuan, Q., Liu, J., Li, S., Gu, M., & Zhang, Y. (2021). Toxicities and Associated Factors in Patients Receiving Temozolomide-Containing Regimens: A 12-Year Analysis of Hospital Data. *Drug Design, Development and Therapy*, *15*, 2151-2159. https://doi.org/10.2147/DDDT.S305792

Siegel, B. I., Patil, P., Prakash, A., Klawinski, D. M., & Hwang, E. I. (2025). Targeted therapy in pediatric central nervous system tumors: a review from the National Pediatric Cancer Foundation. *Frontiers in Oncology*, *15*. https://doi.org/10.3389/fonc.2025.1504803

Smith, D. A., Di, L., & Kerns, E. H. (2010). The effect of plasma protein binding on in vivo efficacy: misconceptions in drug discovery. *Nature Reviews Drug Discovery*, *9*(12), 929-939. https://doi.org/10.1038/nrd3287

Sokol, O., & Durante, M. (2023). Carbon Ions for Hypoxic Tumors: Are We Making the Most of Them? *Cancers*, *15*(18), 4494. https://doi.org/10.3390/cancers15184494

Spanggaard, I., Matrana, M., Rocha Lima, C., Mahipal, A., Vieito, M., Hervieu, A., Goyal, L., Rodón, J., Veronese, M. L., Oliveira, N., Li, X., Schaffer, M., & Kesari, S. (2025). Pemigatinib for previously treated metastatic or unresectable central nervous system tumors with fibroblast growth factor receptor mutations or rearrangements: FIGHT-207 results. *The Oncologist*, *30*(11), oyaf272. https://doi.org/10.1093/oncolo/oyaf272

Sperring, C. P., Argenziano, M. G., Savage, W. M., Teasley, D. E., Upadhyayula, P. S., Winans, N. J., Canoll, P., & Bruce, J. N. (2023). Convection-enhanced delivery of immunomodulatory therapy for high-grade glioma. *Neuro-Oncology Advances*, *5*(1), vdad044. https://doi.org/10.1093/noajnl/vdad044

Sriramulu, S., Thoidingjam, S., Brown, S. L., Siddiqui, F., Movsas, B., & Nyati, S. (2023). Molecular targets that sensitize cancer to radiation killing: From the bench to the bedside. *Biomedicine & Pharmacotherapy*, *158*, 114126. https://doi.org/10.1016/j.biopha.2022.114126

Stapleton, S. L., Thompson, P. A., Ou, C.-N., Berg, S. L., McGuffey, L., Gibson, B., & Blaney, S. M. (2008). Plasma and cerebrospinal fluid pharmacokinetics of valproic acid after oral administration in non-human primates. *Cancer Chemotherapy and Pharmacology*, *61*(4), 647-652. https://doi.org/10.1007/s00280-007-0519-3

Sterner, R. C., & Sterner, R. M. (2021). CAR-T cell therapy: current limitations and potential strategies. *Blood Cancer Journal*, *11*(4), 69. https://doi.org/10.1038/s41408-021-00459-7

Stupp, R., Mason, W. P., Bent, M. J. v. d., Weller, M., Fisher, B., Taphoorn, M. J. B., Belanger, K., Brandes, A. A., Marosi, C., Bogdahn, U., Curschmann, J., Janzer, R. C., Ludwin, S. K., Gorlia, T., Allgeier, A., Lacombe, D., Cairncross, J. G., Eisenhauer, E., & Mirimanoff, R. O. (2005). Radiotherapy plus Concomitant and Adjuvant Temozolomide for Glioblastoma. *New England Journal of Medicine*, *352*(10), 987-996. https://doi.org/10.1056/NEJMoa043330

Sturm, D., Capper, D., Andreiuolo, F., Gessi, M., Kölsche, C., Reinhardt, A., Sievers, P., Wefers, A. K., Ebrahimi, A., Suwala, A. K., Gielen, G. H., Sill, M., Schrimpf, D., Stichel, D., Hovestadt, V., Daenekas, B., Rode, A., Hamelmann, S., Previti, C., . . . Jones, D. T. W. (2023). Multiomic neuropathology improves diagnostic accuracy in pediatric neuro-oncology. *Nature Medicine*, *29*(4), 917-926. https://doi.org/10.1038/s41591-023-02255-1

Su, J. M., Murray, J. C., McNall-Knapp, R. Y., Bowers, D. C., Shah, S., Adesina, A. M., Paulino, A. C., Jo, E., Mo, Q., Baxter, P. A., & Blaney, S. M. (2020). A phase 2 study of valproic acid and radiation, followed by maintenance valproic acid and bevacizumab in children with newly diagnosed diffuse intrinsic pontine glioma or high-grade glioma. *Pediatr Blood Cancer*, *67*(6), e28283. https://doi.org/10.1002/pbc.28283

Suda, K., Tomizawa, K., Osada, H., Maehara, Y., Yatabe, Y., Sekido, Y., & Mitsudomi, T. (2012). Conversion from the "oncogene addiction" to "drug addiction" by intensive inhibition of the EGFR and MET in lung cancer with activating EGFR mutation. *Lung Cancer*, *76*(3), 292-299. https://doi.org/10.1016/j.lungcan.2011.11.007

Sullivan, J. K., Fahey, P. P., Agho, K. E., Hurley, S. P., Feng, Z., Day, R. O., & Lim, D. (2023). Valproic acid as a radio-sensitizer in glioma: A systematic review and

meta-analysis. *Neurooncol Pract*, *10*(1), 13-23. https://doi.org/10.1093/nop/npac078

Szychot, E., Giraud, G., Hargrave, D., van Vuurden, D., Grill, J., Biassoni, V., Massimino, M., von Bueren, A. O., Kebudi, R., Gil-da-Costa, M. J., van Zanten, S. V., Bailey, S., Karremann, M., Bolle, S., Ajithkumar, T., Krause, M., Lassen-Ramshad, Y., Janssens, G., Morana, G., . . . Kramm, C. M. (2025). European standard clinical practice recommendations for paediatric high-grade gliomas. *EJC Paediatric Oncology*, *5*, 100210. https://doi.org/10.1016/j.ejcped.2024.100210

Talwelkar, S. S., Mäyränpää, M. I., Schüler, J., Linnavirta, N., Hemmes, A., Adinolfi, S., Kankainen, M., Sommergruber, W., Levonen, A.-L., Räsänen, J., Knuuttila, A., Verschuren, E. W., & Wennerberg, K. (2023). PI3Kβ inhibition enhances ALK-inhibitor sensitivity in ALK-rearranged lung cancer. *Molecular Oncology*, *17*(5), 747-764. https://doi.org/10.1002/1878-0261.13342

Taube, J. H., Herschkowitz, J. I., Komurov, K., Zhou, A. Y., Gupta, S., Yang, J., Hartwell, K., Onder, T. T., Gupta, P. B., Evans, K. W., Hollier, B. G., Ram, P. T., Lander, E. S., Rosen, J. M., Weinberg, R. A., & Mani, S. A. (2010). Core epithelial-to-mesenchymal transition interactome gene-expression signature is associated with claudin-low and metaplastic breast cancer subtypes. *Proceedings of the National Academy of Sciences*, *107*(35), 15449-15454. https://doi.org/10.1073/pnas.1004900107

Tinkle, C. L., Broniscer, A., Chiang, J., Campagne, O., Huang, J., Orr, B. A., Li, X., Patay, Z., Zhang, J., Baker, S. J., Merchant, T. E., Jain, V., Onar-Thomas, A., Stewart, C. F., Wetmore, C., & Gajjar, A. (2021). Phase I study using crenolanib to target PDGFR kinase in children and young adults with newly diagnosed DIPG or recurrent high-grade glioma, including DIPG. *Neuro-Oncology Advances*, *3*(1), vdab179. https://doi.org/10.1093/noajnl/vdab179

Tong, H., Ma, Z., Yu, J., Li, D., Zhu, Q., Shi, H., Wu, Y., Yang, H., Zheng, Y., Sun, D., Shi, P., Chu, J., Lv, P., Li, B., & Tian, C. (2025). Optimizing Peptide-Conjugated Lipid Nanoparticles for Efficient siRNA Delivery across the Blood–Brain Barrier and Treatment of Glioblastoma Multiforme. *ACS Chemical Biology*, *20*(4), 942-952. https://doi.org/10.1021/acschembio.5c00039

Trippett, T., Toledano, H., Campbell Hewson, Q., Verschuur, A., Langevin, A.-M., Aerts, I., Howell, L., Gallego, S., Rossig, C., Smith, A., Patel, D., Pereira, L. R., Cheeti, S., Musib, L., Hutchinson, K. E., Devlin, C., Bernardi, R., & Geoerger, B. (2022). Cobimetinib in Pediatric and Young Adult Patients with Relapsed or Refractory Solid Tumors (iMATRIX-cobi): A Multicenter, Phase I/II Study. *Targeted Oncology*, *17*(3), 283-293. https://doi.org/10.1007/s11523-022-00888-9

Tsai, C. C., Huang, M.-H., Fang, C.-L., Hsieh, K. L.-C., Hsieh, T.-H., Ho, W.-L., Chang, H., Tsai, M.-L., Kao, Y.-C., Miser, J. S., Wong, T.-T., Su, M.-Y., & Liu, Y.-L. (2024). An Infant-Type Hemispheric Glioma With SOX5::ALK: A Novel Fusion. *Journal of the National Comprehensive Cancer Network*, *22*(1). https://doi.org/10.6004/jnccn.2023.7102

Tsuji, T., Ozasa, H., Aoki, W., Aburaya, S., Yamamoto Funazo, T., Furugaki, K., Yoshimura, Y., Yamazoe, M., Ajimizu, H., Yasuda, Y., Nomizo, T., Yoshida, H., Sakamori, Y., Wake, H., Ueda, M., Kim, Y. H., & Hirai, T. (2020). YAP1 mediates survival of ALK-rearranged lung cancer cells treated with alectinib via pro-apoptotic protein regulation. *Nat Commun*, *11*(1), 74. https://doi.org/10.1038/s41467-019-13771-5

Vaidhyanathan, S., Mittapalli, R. K., Sarkaria, J. N., & Elmquist, W. F. (2014). Factors Influencing the CNS Distribution of a Novel MEK-1/2 Inhibitor: Implications for Combination Therapy for Melanoma Brain Metastases. *Drug Metabolism and Disposition*, *42*(8), 1292-1300. https://doi.org/10.1124/dmd.114.058339

Vanan, M. I., & Eisenstat, D. D. (2014). Management of high-grade gliomas in the pediatric patient: Past, present, and future. *Neuro-Oncology Practice*, *1*(4), 145-157. https://doi.org/10.1093/nop/npu022

Vardon, A., Haston, S., Hamdi, H., Cooksley, G., Guiho, R., Carvalho, D., Carter, R., Boult, J. K. R., Gharai, D., Cloete, I., Grey, J., Apps, J., Zhou, D., Zheng, G., Martínez-Máñez, R., Lythgoe, M. F., Donovan, L. K., Carcaboso, A. M., Williams, O., . . . Martinez-Barbera, J.-P. (2025). Navitoclax acts synergistically with irradiation to induce apoptosis in preclinical models of H3K27M-altered diffuse midline glioma. *Scientific Reports*, *15*, 45094. https://doi.org/10.1038/s41598-025-32676-6

Venneti, S., Kawakibi, A. R., Ji, S., Waszak, S. M., Sweha, S. R., Mota, M., Pun, M., Deogharkar, A., Chung, C., Tarapore, R. S., Ramage, S., Chi, A., Wen, P. Y., Arrillaga-Romany, I., Batchelor, T. T., Butowski, N. A., Sumrall, A., Shonka, N., Harrison, R. A., . . . Koschmann, C. (2023). Clinical Efficacy of ONC201 in H3K27M-Mutant Diffuse Midline Gliomas Is Driven by Disruption of Integrated Metabolic and Epigenetic Pathways. *Cancer Discovery*, *13*(11), 2370-2393. https://doi.org/10.1158/2159-8290.CD-23-0131

Verdura, S., Encinar, J. A., Teixidor, E., Segura-Carretero, A., Micol, V., Cuyàs, E., Bosch-Barrera, J., Menendez, J. A., Verdura, S., Encinar, J. A., Teixidor, E., Segura-Carretero, A., Micol, V., Cuyàs, E., Bosch-Barrera, J., & Menendez, J. A. (2022). Silibinin Overcomes EMT-Driven Lung Cancer Resistance to New-Generation ALK Inhibitors. *Cancers*, *14*(24). https://doi.org/10.3390/cancers14246101

Vitanza, N. A., Ronsley, R., Choe, M., Seidel, K., Huang, W., Rawlings-Rhea, S. D., Beam, M., Steinmetzer, L., Wilson, A. L., Brown, C., Beebe, A., Lindgren, C., Gustafson, J. A., Wein, A., Holtzclaw, S., Hoeppner, C., Goldstein, H. E., Browd, S. R., Hauptman, J. S., . . . Jensen, M. C. (2025). Intracerebroventricular B7-H3-targeting CAR T cells for diffuse intrinsic pontine glioma: a phase 1 trial. *Nature Medicine*, *31*(3), 861-868. https://doi.org/10.1038/s41591-024-03451-3

Vlashi, E., Mattes, M., Lagadec, C., Donna, L. D., Phillips, T. M., Nikolay, P., McBride, W. H., & Pajonk, F. (2010). Differential Effects of the Proteasome Inhibitor NPI-0052 against Glioma Cells. *Translational Oncology*, *3*(1), 50-55. https://doi.org/10.1593/tlo.09244

Vogler, M., Dickens, D., Dyer, M. J., Owen, A., Pirmohamed, M., & Cohen, G. M. (2011). The B-cell lymphoma 2 (BCL2)-inhibitors, ABT-737 and ABT-263, are substrates for P-glycoprotein. *Biochem Biophys Res Commun*, *408*(2), 344-349. https://doi.org/10.1016/j.bbrc.2011.04.043

Vuurden, D. G. V., Hulleman, E., Meijer, O. L. M., Wedekind, L. E., Kool, M., Witt, H., Vandertop, W. P., Würdinger, T., Noske, D. P., Kaspers, G. J. L., & Cloos, J. (2011). PARP inhibition sensitizes childhood high grade glioma, medulloblastoma and ependymoma to radiation. *Oncotarget*, *2*(12), 984-996. https://doi.org/10.18632/oncotarget.362

Wagner, C. C., Bauer, M., Karch, R., Feurstein, T., Kopp, S., Chiba, P., Kletter, K., Löscher, W., Müller, M., Zeitlinger, M., & Langer, O. (2009). A Pilot Study to Assess the Efficacy of Tariquidar to Inhibit P-glycoprotein at the Human Blood–

Brain Barrier with (R)-11C-Verapamil and PET. *Journal of Nuclear Medicine*, *50*(12), 1954-1961. https://doi.org/10.2967/jnumed.109.063289

Wagner, S., Peters, O., Fels, C., Janssen, G., Liebeskind, A.-K., Sauerbrey, A., Suttorp, M., Hau, P., & Wolff, J. E. A. (2008). Pegylated-liposomal doxorubicin and oral topotecan in eight children with relapsed high-grade malignant brain tumors. *Journal of Neuro-Oncology*, *86*(2), 175-181. https://doi.org/10.1007/s11060-007-9444-x

Wang, C., Xue, Y., Markovic, T., Li, H., Wang, S., Zhong, Y., Du, S., Zhang, Y., Hou, X., Yu, Y., Liu, Z., Tian, M., Kang, D. D., Wang, L., Guo, K., Cao, D., Yan, J., Deng, B., McComb, D. W., . . . Dong, Y. (2025). Blood–brain-barrier-crossing lipid nanoparticles for mRNA delivery to the central nervous system. *Nature Materials*, *24*(10), 1653-1663. https://doi.org/10.1038/s41563-024-02114-5

Wang, C., Zhu, N., Wang, L., & An, Z. (2015). Radiotherapy with temozolomide provides better survival in the newly diagnosed glioblastoma multiforme: A meta-analysis. *Journal of Cancer Research and Therapeutics*, *11*(Suppl 2), S196. https://doi.org/10.4103/0973-1482.168184

Wang, L., Doherty, G. A., Judd, A. S., Tao, Z.-F., Hansen, T. M., Frey, R. R., Song, X., Bruncko, M., Kunzer, A. R., Wang, X., Wendt, M. D., Flygare, J. A., Catron, N. D., Judge, R. A., Park, C. H., Shekhar, S., Phillips, D. C., Nimmer, P., Smith, M. L., . . . Souers, A. J. (2020). Discovery of A-1331852, a First-in-Class, Potent, and Orally-Bioavailable BCL-XL Inhibitor. *ACS Medicinal Chemistry Letters*, *11*(10), 1829-1836. https://doi.org/10.1021/acsmedchemlett.9b00568

Wang, Z. J., Ge, Y., Altinok, D., Poulik, J., Sood, S., Taub, J. W., Edwards, H., Kieran, M. W., & Steven, M. (2017). Concomitant Use of Panobinostat and Reirradiation in Progressive DIPG: Report of 2 Cases. *Journal of Pediatric Hematology/Oncology*, *39*(6), e332. https://doi.org/10.1097/MPH.0000000000000806

Wei, F., Yan, J., Tang, D., Lin, X., He, L., Xie, Y., Tao, L., & Wang, S. (2013). Inhibition of ERK activation enhances the repair of double-stranded breaks via non-homologous end joining by increasing DNA-PKcs activation. *Biochimica et Biophysica Acta (BBA) - Molecular Cell Research*, *1833*(1), 90-100. https://doi.org/10.1016/j.bbamcr.2012.10.016

Weiss, T., Weller, M., Guckenberger, M., Sentman, C. L., & Roth, P. (2018). NKG2D-Based CAR T Cells and Radiotherapy Exert Synergistic Efficacy in Glioblastoma. *Cancer Research*, *78*(4), 1031-1043. https://doi.org/10.1158/0008-5472.CAN-17-1788

Wilson, D., Jayappa, S., Parker, L., Ocal, E., Tanaka, T., Gokden, M., Bielamowicz, K., Wilson, D., Jayappa, S., Parker, L., Ocal, E., Tanaka, T., Gokden, M., & Bielamowicz, K. (2025). Targeted Inhibition in Pediatric MET and ALK-Altered Hemispheric Gliomas: Objective Responses Followed by Treatment Resistance. *International Journal of Molecular Sciences*, *26*(20). https://doi.org/10.3390/ijms26209864

Wilson, F. H., Johannessen, C. M., Piccioni, F., Tamayo, P., Kim, J. W., Van Allen, E. M., Corsello, S. M., Capelletti, M., Calles, A., Butaney, M., Sharifnia, T., Gabriel, S. B., Mesirov, J. P., Hahn, W. C., Engelman, J. A., Meyerson, M., Root, D. E., Jänne, P. A., & Garraway, L. A. (2015). A Functional Landscape of Resistance to ALK Inhibition in Lung Cancer. *Cancer Cell*, *27*(3), 397-408. https://doi.org/10.1016/j.ccell.2015.02.005

Wilson, W. H., O'Connor, O. A., Czuczman, M. S., LaCasce, A. S., Gerecitano, J. F., Leonard, J. P., Tulpule, A., Dunleavy, K., Xiong, H., Chiu, Y.-L., Cui, Y.,

Busman, T., Elmore, S. W., Rosenberg, S. H., Krivoshik, A. P., Enschede, S. H., & Humerickhouse, R. A. (2010). Navitoclax, a targeted high-affinity inhibitor of BCL-2, in lymphoid malignancies: a phase 1 dose-escalation study of safety, pharmacokinetics, pharmacodynamics, and antitumour activity. *The Lancet Oncology*, *11*(12), 1149-1159. https://doi.org/10.1016/S1470-2045(10)70261-8

Wu, C.-C., Szalontay, L., Pouliopoulos, A. N., Bae, S., Berg, X., Wei, H.-J., Webster Carrion, A., Kokossis, D., Sethi, C., Fino, J., Shatravka, H., Lipina, J., Ji, R., Liu, K., Yousefian, O., Gallitto, M., Yoh, N., Englander, Z., McQuillan, N., . . . Zacharoulis, S. (2025). Blood-brain barrier opening with neuronavigation-guided focused ultrasound in pediatric patients with diffuse midline glioma. *Science Translational Medicine*, *17*(824), eadq6645. https://doi.org/10.1126/scitranslmed.adq6645

Wu, D., Chen, Q., Chen, X., Han, F., Chen, Z., & Wang, Y. (2023). The blood–brain barrier: Structure, regulation and drug delivery. *Signal Transduction and Targeted Therapy*, *8*(1), 217. https://doi.org/10.1038/s41392-023-01481-w

Xiang, W., Zhang, X., Dong, M., Wan, L., Zhang, B., & Wan, F. (2025). Differentiation therapy targeting the stalled epigenetic developmental programs in pediatric high-grade gliomas. *Pharmacological Research*, *212*, 107599. https://doi.org/10.1016/j.phrs.2025.107599

Xiao, J. J., Foraker, A. B., Swaan, P. W., Liu, S., Huang, Y., Dai, Z., Chen, J., Sadée, W., Byrd, J., Marcucci, G., & Chan, K. K. (2005). Efflux of Depsipeptide FK228 (FR901228, NSC-630176) Is Mediated by P-Glycoprotein and Multidrug Resistance-Associated Protein 1. *The Journal of Pharmacology and Experimental Therapeutics*, *313*(1), 268-276. https://doi.org/10.1124/jpet.104.072033

Xiao, W., Graham, P. H., Hao, J., Chang, L., Ni, J., Power, C. A., Dong, Q., Kearsley, J. H., & Li, Y. (2013). Combination Therapy with the Histone Deacetylase Inhibitor LBH589 and Radiation Is an Effective Regimen for Prostate Cancer Cells. *PLOS ONE*, *8*(8), e74253. https://doi.org/10.1371/journal.pone.0074253

Xie, J., Kuriakose, T., Bianski, B., Twarog, N., Savage, E., Xu, K., Zhu, X., He, C., Hansen, B., Wang, H., High, A., Li, Y., Rehg, J. E., Tillman, H. S., Freeman, B. B., Rankovic, Z., Onar-Thomas, A., Fan, Y., Wu, G., . . . Tinkle, C. L. (2023). ATM inhibition enhances the efficacy of radiation across distinct molecular subgroups of pediatric high-grade glioma. *Neuro-Oncology*, *25*(10), 1828-1841. https://doi.org/10.1093/neuonc/noad064

Xu, C., Liu, H., Pirozzi, C. J., Chen, L. H., Greer, P. K., Diplas, B. H., Zhang, L., Waitkus, M. S., He, Y., & Yan, H. (2021). TP53 wild-type/PPM1D mutant diffuse intrinsic pontine gliomas are sensitive to a MDM2 antagonist. *Acta Neuropathologica Communications*, *9*(1), 178. https://doi.org/10.1186/s40478-021-01270-y

Xu, S.-p., Sun, G.-p., Shen, Y.-x., Peng, W.-r., Wang, H., & Wei, W. (2007). Synergistic effect of combining paeonol and cisplatin on apoptotic induction of human hepatoma cell lines. *Acta Pharmacologica Sinica*, *28*(6), 869-878. https://doi.org/10.1111/j.1745-7254.2007.00564.x

Xue, L. Y., Chiu, S. M., & Oleinick, N. L. (2003). Staurosporine-induced death of MCF-7 human breast cancer cells: a distinction between caspase-3-dependent steps of apoptosis and the critical lethal lesions. *Exp Cell Res*, *283*(2), 135-145. https://doi.org/10.1016/s0014-4827(02)00032-0

Yang, J., Antin, P., Berx, G., Blanpain, C., Brabletz, T., Bronner, M., Campbell, K., Cano, A., Casanova, J., Christofori, G., Dedhar, S., Derynck, R., Ford, H. L.,

Fuxe, J., García de Herreros, A., Goodall, G. J., Hadjantonakis, A.-K., Huang, R. Y. J., Kalcheim, C., . . . Sheng, G. (2020). Guidelines and definitions for research on epithelial–mesenchymal transition. *Nature Reviews Molecular Cell Biology*, *21*(6), 341-352. https://doi.org/10.1038/s41580-020-0237-9

Yang, L., Li, G., Zhao, L., Pan, F., Qiang, J., & Han, S. (2014). Blocking the PI3K pathway enhances the efficacy of ALK-targeted therapy in EML4-ALK-positive nonsmall-cell lung cancer. *Tumor Biology*, *35*(10), 9759-9767. https://doi.org/10.1007/s13277-014-2252-y

Yang, T., Temkin, N., Barber, J., Geyer, J. R., Leary, S., Browd, S., Ojemann, J. G., & Ellenbogen, R. G. (2013). Gross Total Resection Correlates with Long-Term Survival in Pediatric Patients with Glioblastoma. *World Neurosurgery*, *79*(3-4), 537-544. https://doi.org/10.1016/j.wneu.2012.09.015

Yesilkanal, A. E., Johnson, G. L., Ramos, A. F., & Rosner, M. R. (2021). New strategies for targeting kinase networks in cancer. *J Biol Chem*, *297*(4), 101128. https://doi.org/10.1016/j.jbc.2021.101128

Zafar, S., Furqan, M., Binte Rahim, S., & Haider, M. U. (2025). Dordaviprone in H3K27M-mutant diffuse midline glioma: an editorial on emerging targeted therapy. *Annals of Medicine and Surgery*, *87*(12), 7886-7888. https://doi.org/10.1097/MS9.0000000000004079

Zając-Grabiec, A., Biesaga, B., Krzyżowska, M., Drosik-Rutowicz, K., & Miszczyk, J. (2025). Non-cancer effects after proton beam therapy for pediatric tumors- a narrative review. *Frontiers in Oncology*, *15*. https://doi.org/10.3389/fonc.2025.1554765

Zeng, J., See, A. P., Phallen, J., Jackson, C. M., Belcaid, Z., Ruzevick, J., Durham, N., Meyer, C., Harris, T. J., Albesiano, E., Pradilla, G., Ford, E., Wong, J., Hammers, H.-J., Mathios, D., Tyler, B., Brem, H., Tran, P. T., Pardoll, D., . . . Lim, M. (2013). Anti-PD-1 Blockade and Stereotactic Radiation Produce Long-Term Survival in Mice With Intracranial Gliomas. *International Journal of Radiation Oncology*Biology*Physics*, *86*(2), 343-349. https://doi.org/10.1016/j.ijrobp.2012.12.025

Zhang, Y., Rabinovsky, R., Deforzh, E., Kobayashi, A., Kuzkina, A., Varghese, J. F., Rai, D., Korecka, J. A., Khurana, V., Murugaiyan, G., Morrissey, D., Uhlmann, E. J., & Krichevsky, A. M. (2025). Lipid nanoparticle formulation for gene editing and RNA-based therapies for glioblastoma. *Neuro-Oncology*, noaf162. https://doi.org/10.1093/neuonc/noaf162

Zhao, Y., Qin, J., Yu, D., Liu, Y., Song, D., Tian, K., Chen, H., Ye, Q., Wang, X., Xu, T., Xuan, H., Sun, N., Ma, W., Zhong, J., Sun, P., Song, Y., Hu, J., Zhao, Y., Hou, X., . . . Cai, J. (2024). Polymer-locking fusogenic liposomes for glioblastoma-targeted siRNA delivery and CRISPR–Cas gene editing. *Nature Nanotechnology*, *19*(12), 1869-1879. https://doi.org/10.1038/s41565-024-01769-0

Zhou, L., Zhang, L., Zhang, J., Wu, L. J., Zhang, S., George, A., Hahn, M., Safran, H. P., Chen, C. C., Seyhan, A. A., Wong, E. T., & El-Deiry, W. S. (2025). Imipridones ONC201/ONC206 + RT/TMZ triple (IRT) therapy reduces intracranial tumor burden, prolongs survival in orthotopic IDH-WT GBM mouse model, and suppresses MGMT. *Oncotarget*, *16*, 230-248. https://doi.org/10.18632/oncotarget.28707

Zhu, H., Allwin, C., Bassous, M. G., & Pouliopoulos, A. N. (2024). Focused ultrasound-mediated enhancement of blood-brain barrier permeability for brain tumor

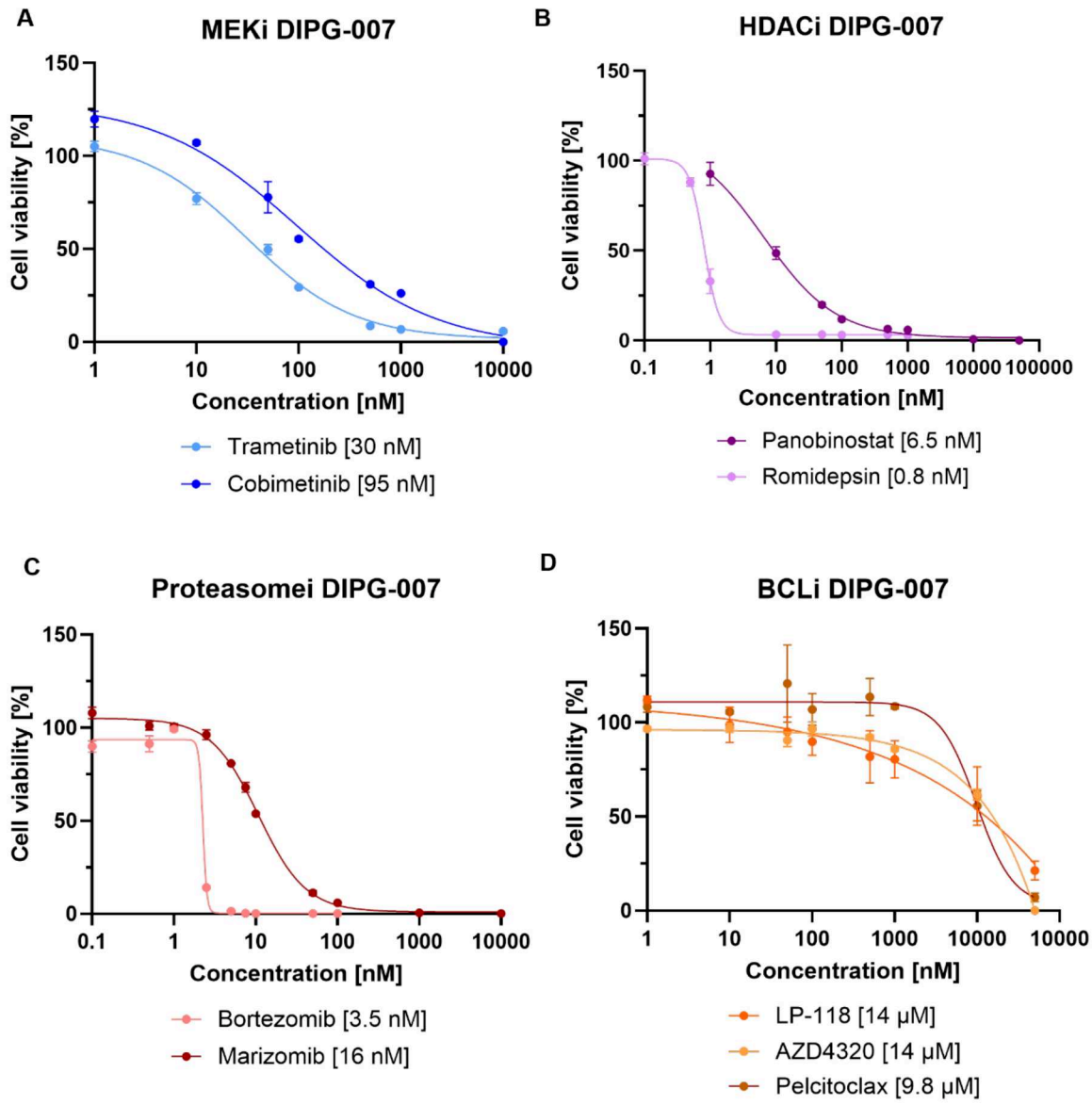
treatment: a systematic review of clinical trials. *J Neurooncol*, *170*(2), 235-252. https://doi.org/10.1007/s11060-024-04795-z

Zou, H. Y., Friboulet, L., Kodack, D. P., Engstrom, L. D., Li, Q., West, M., Tang, R. W., Wang, H., Tsaparikos, K., Wang, J., Timofeevski, S., Katayama, R., Dinh, D. M., Lam, H., Lam, J. L., Yamazaki, S., Hu, W., Patel, B., Bezwada, D., . . . Smeal, T. (2015). PF-06463922, an ALK/ROS1 Inhibitor, Overcomes Resistance to First and Second Generation ALK Inhibitors in Preclinical Models. *Cancer Cell*, *28*(1), 70-81. https://doi.org/10.1016/j.ccell.2015.05.010

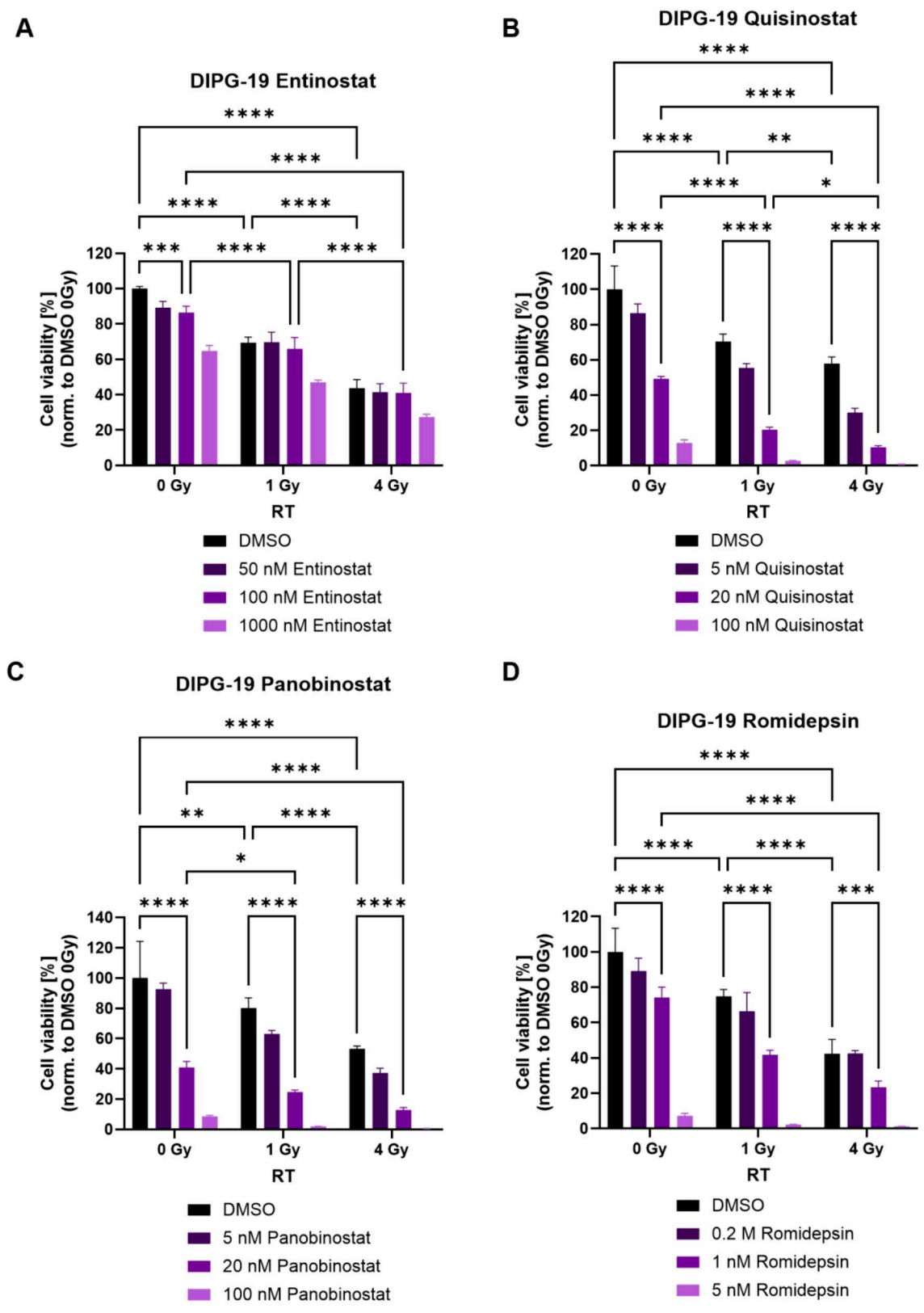
Zuberi, A., Rehman, U., Gupta, G., Ghazwani, M., Hani, U., & Kesharwani, P. (2025). Smart liposomal systems for brain cancer: Technological innovations in drug delivery. *Colloids and Surfaces B: Biointerfaces*, *255*, 114904. https://doi.org/10.1016/j.colsurfb.2025.114904

Zuckermann, M., He, C., Andrews, J., Bagchi, A., Sloan-Henry, R., Bianski, B., Xie, J., Wang, Y., Twarog, N., Onar-Thomas, A., Ernst, K. J., Yang, L., Li, Y., Zhu, X., Ocasio, J. K., Budd, K. M., Dalton, J., Li, X., Chepyala, D., . . . Baker, S. J. (2024). Capmatinib is an effective treatment for MET-fusion driven pediatric high-grade glioma and synergizes with radiotherapy. *Molecular Cancer*, *23*(1), 123. https://doi.org/10.1186/s12943-024-02027-6

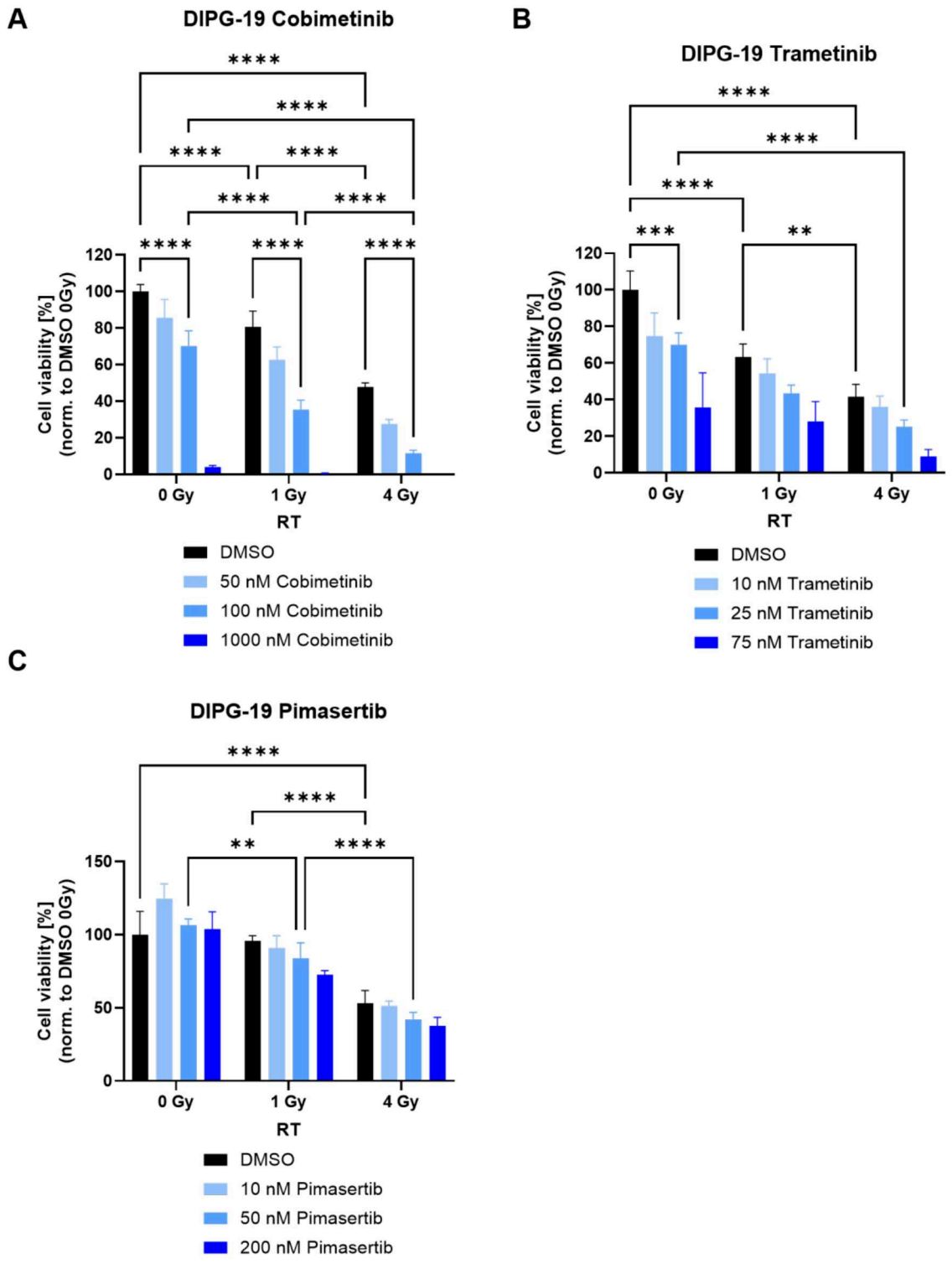
7. Supplementary data



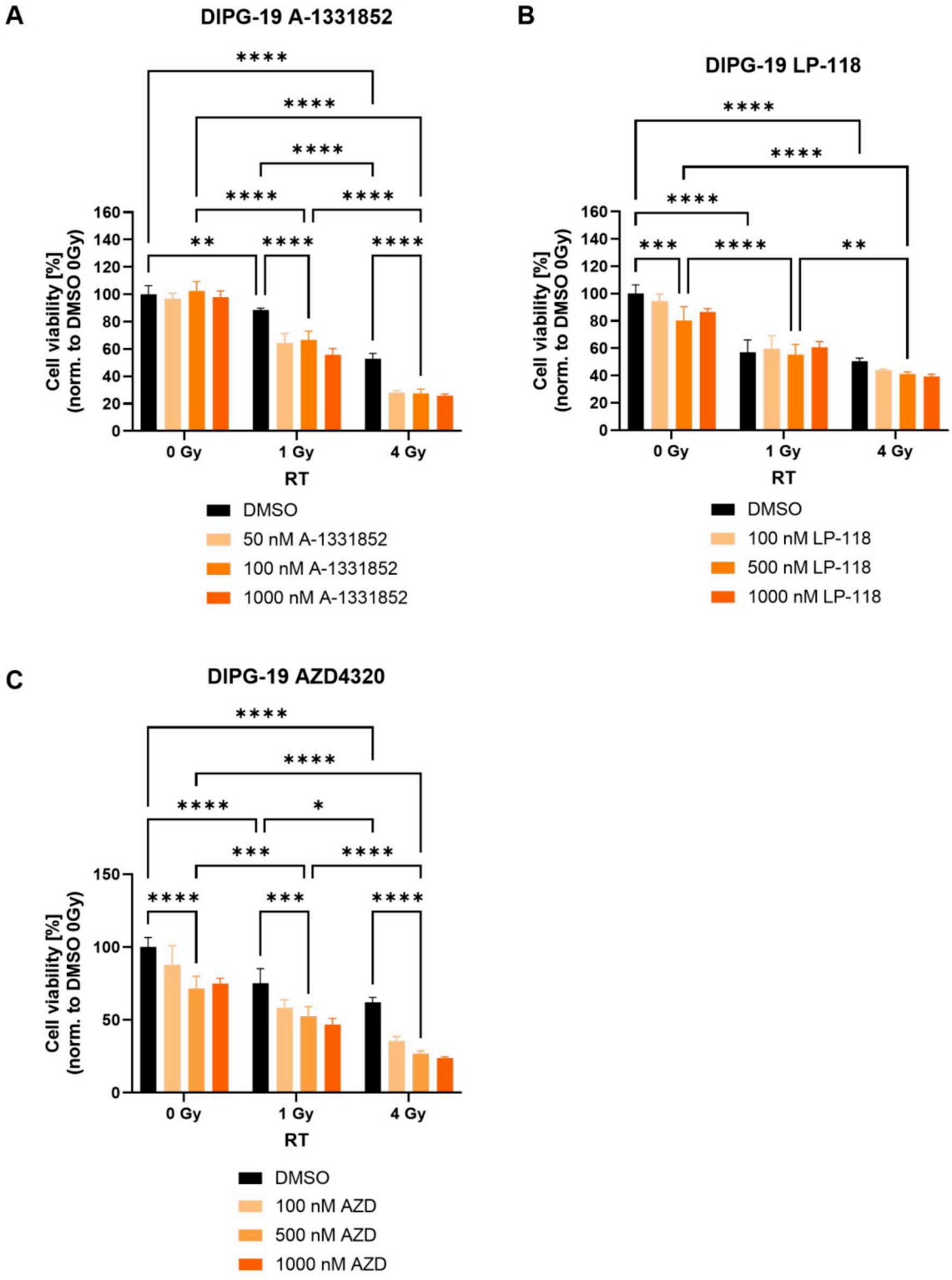
Supplementary figure 1: Drug response curves of selected drug candidates in DIPG-007 (H3K27M).
The cell viability of the pHGG cells was assessed 3 days after incubation with increasing drug concentrations and a non-linear regression curved was fitted to the data to determine the IC50. The respective IC50 are displayed in brackets after drug name. A) MEK inhibitors (MEKi), B) HDAC inhibitors (HDACi), C) Proteasome inhibitors (Proteaseomei), and D) BCL inhibitors (BCLi). Mean ± SD, n=3.



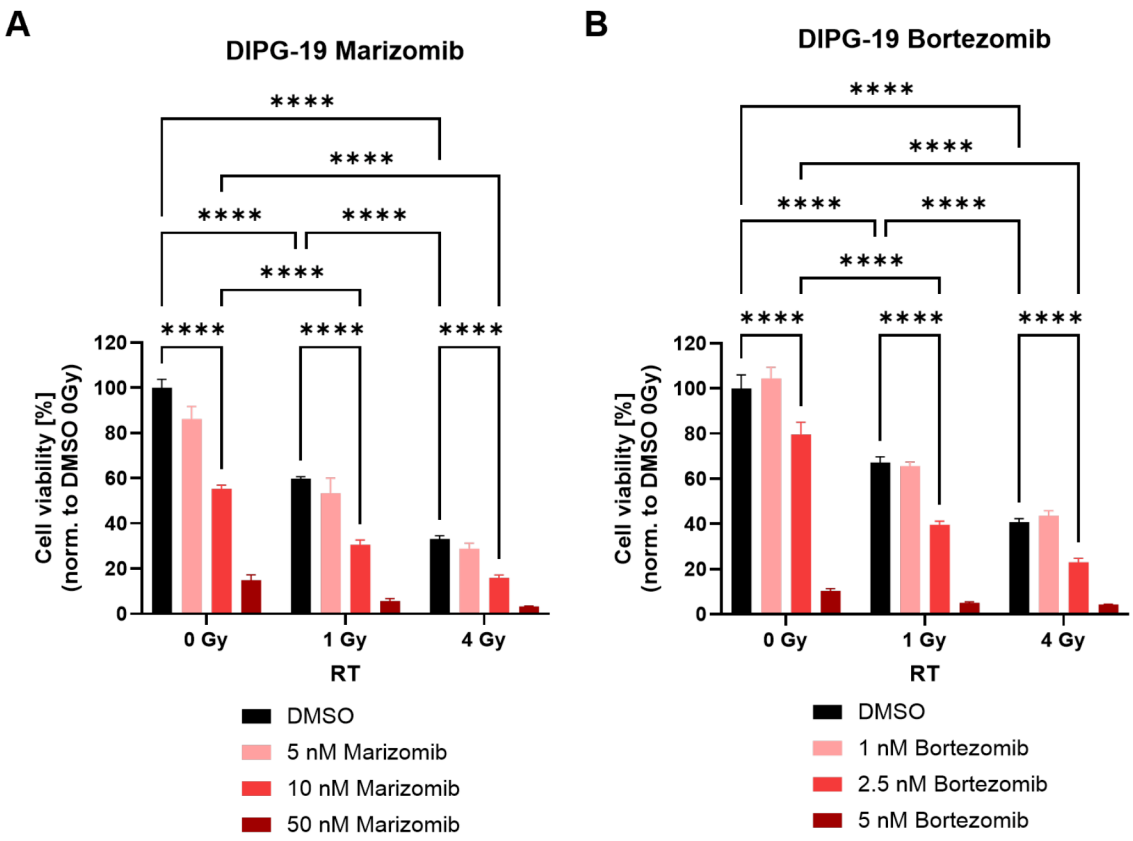
Supplementary figure 2: Cell viability assays after HDACi and RT combination treatment in DIPG-19 cells. Cells were irradiated 2 h after being in contact with the drugs and their cell viability was assessed after 3 days of incubation. Cells were tested at 0 Gy and at two RT doses (~ 60 % viability and ~ 40 % viability after RT), as well as in three drug concentrations (< IC50, ~ IC50, > IC50). Statistics of only selected comparisons at IC50 are shown. Mean ± SD, n=3.



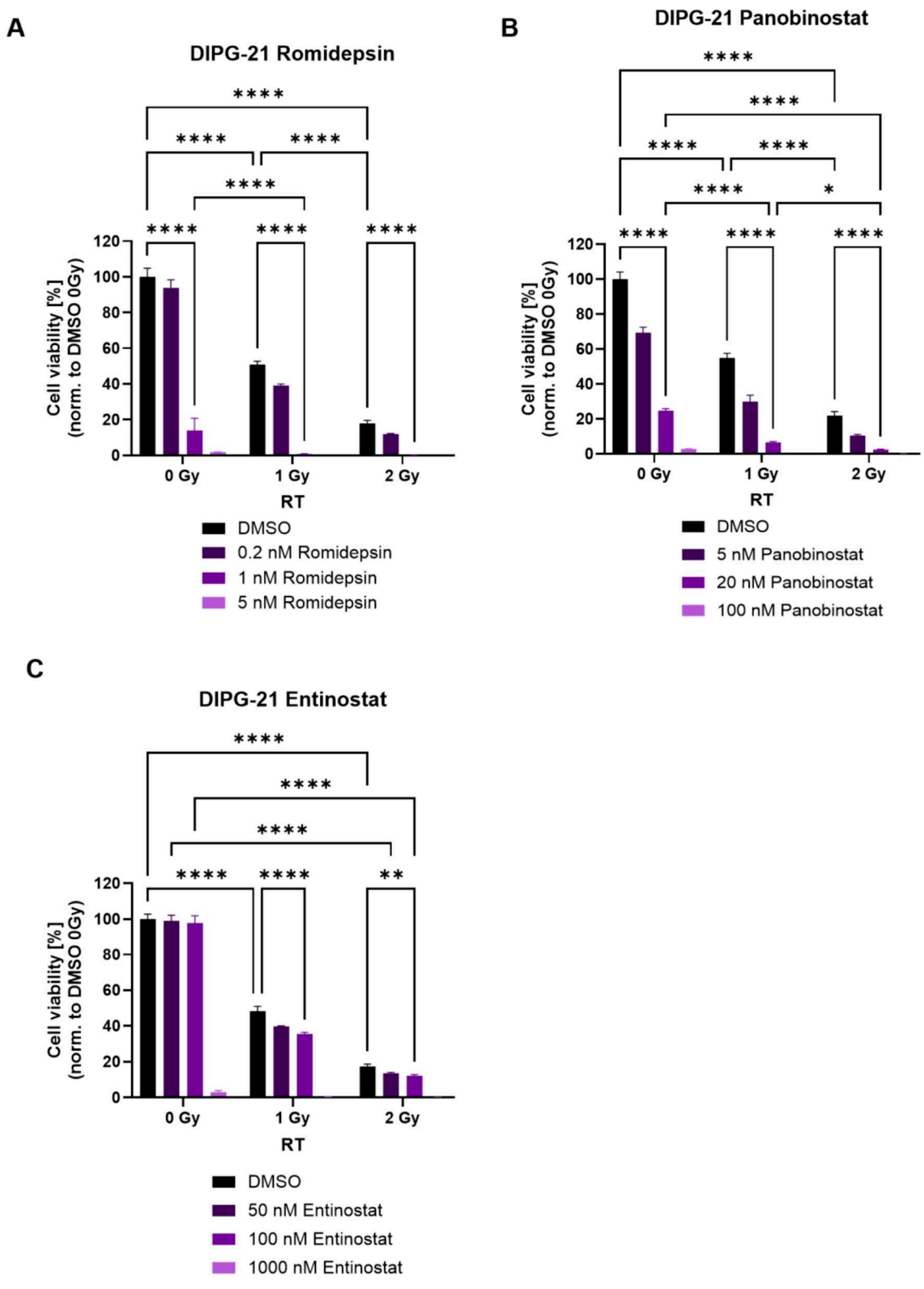
Supplementary figure 3: Cell viability assays after MEKi and RT combination treatment in DIPG-19 cells. Cells were irradiated 2 h after being in contact with the drugs and their cell viability was assessed after 3 days of incubation. Cells were tested at 0 Gy and at two RT doses (~ 60 % viability and ~ 40 % viability after RT), as well as in three drug concentrations (< IC50, ~ IC50, > IC50). Statistics of only selected comparisons at IC50 are shown. Mean ± SD, n=3.



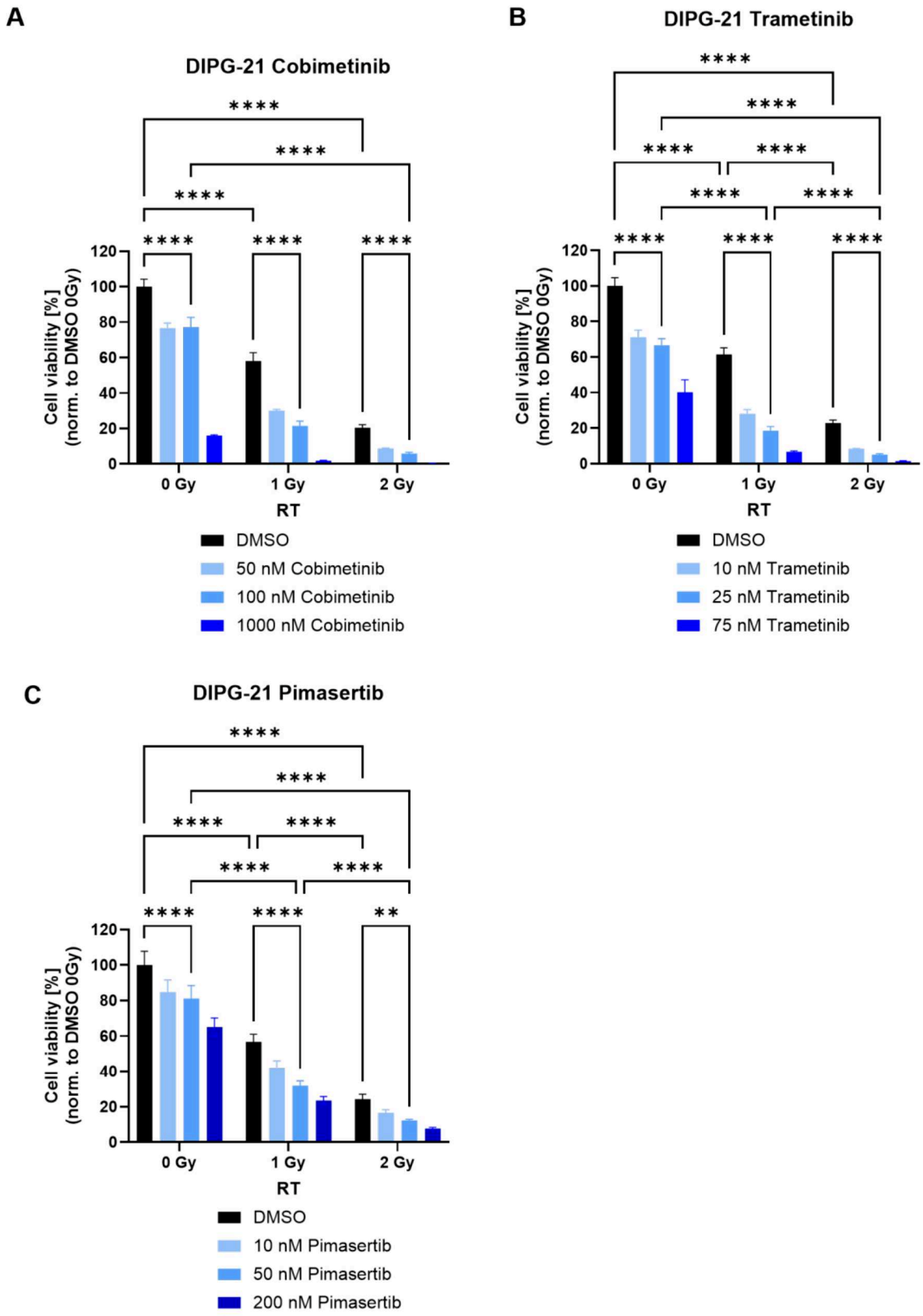
Supplementary figure 4: Cell viability assays after BCLi and RT combination treatment in DIPG-19 cells. Cells were irradiated 2 h after being in contact with the drugs and their cell viability was assessed after 3 days of incubation. Cells were tested at 0 Gy and at two RT doses (~60 % viability and ~40 % viability after RT), as well as in three drug concentrations (< IC50, ~ IC50, > IC50). Statistics of only selected comparisons at IC50 are shown. Mean ± SD, n=3.



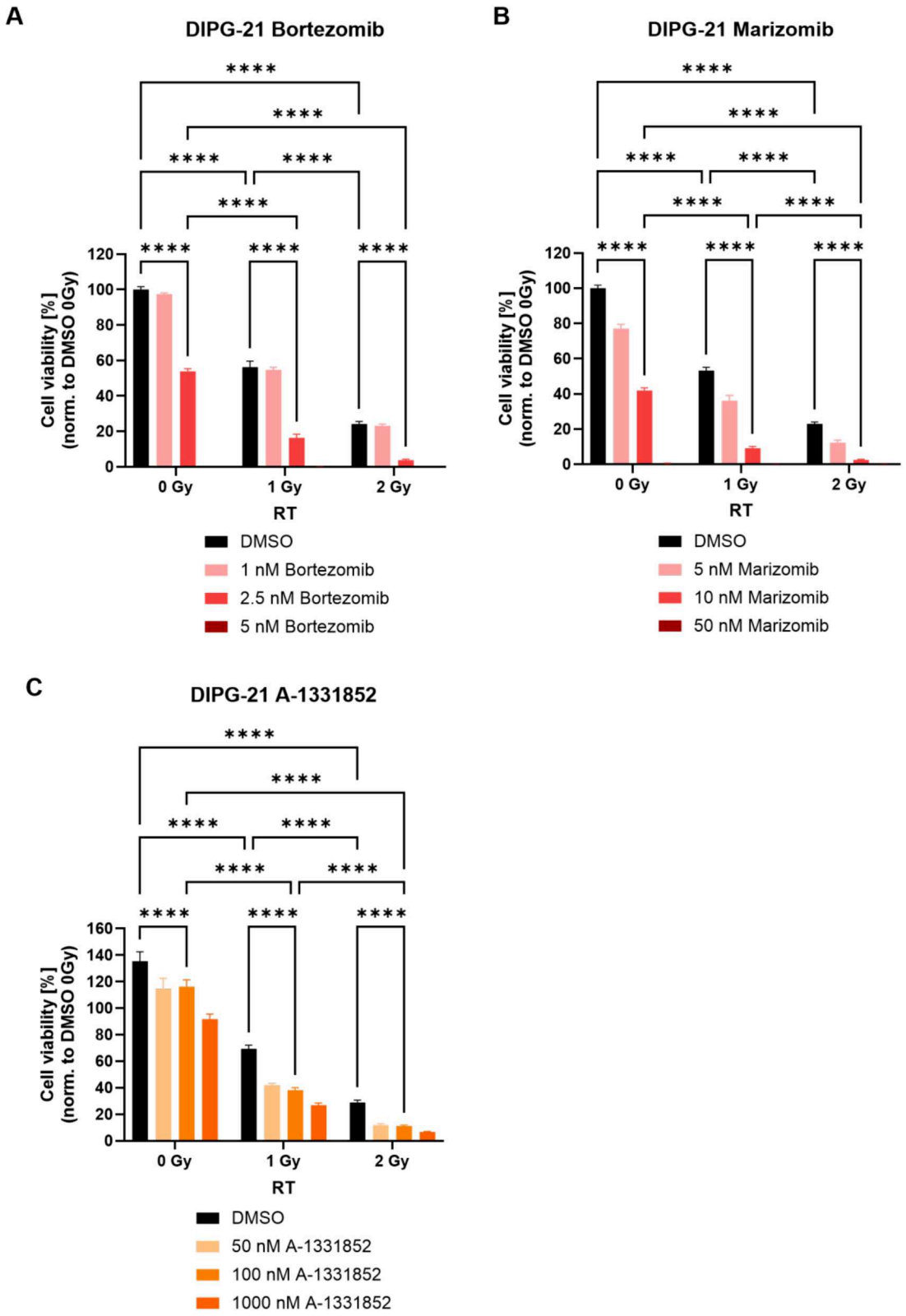
Supplementary figure 5: Cell viability assays after Proteasomei and RT combination treatment in DIPG-19 cells. Cells were irradiated 2 h after being in contact with the drugs and their cell viability was assessed after 3 days of incubation. Cells were tested at 0 Gy and at two RT doses (~ 60 % viability and ~ 40 % viability after RT), as well as in three drug concentrations (< IC50, ~ IC50, > IC50). Statistics of only selected comparisons at IC50 are shown. Mean ± SD, n=3.



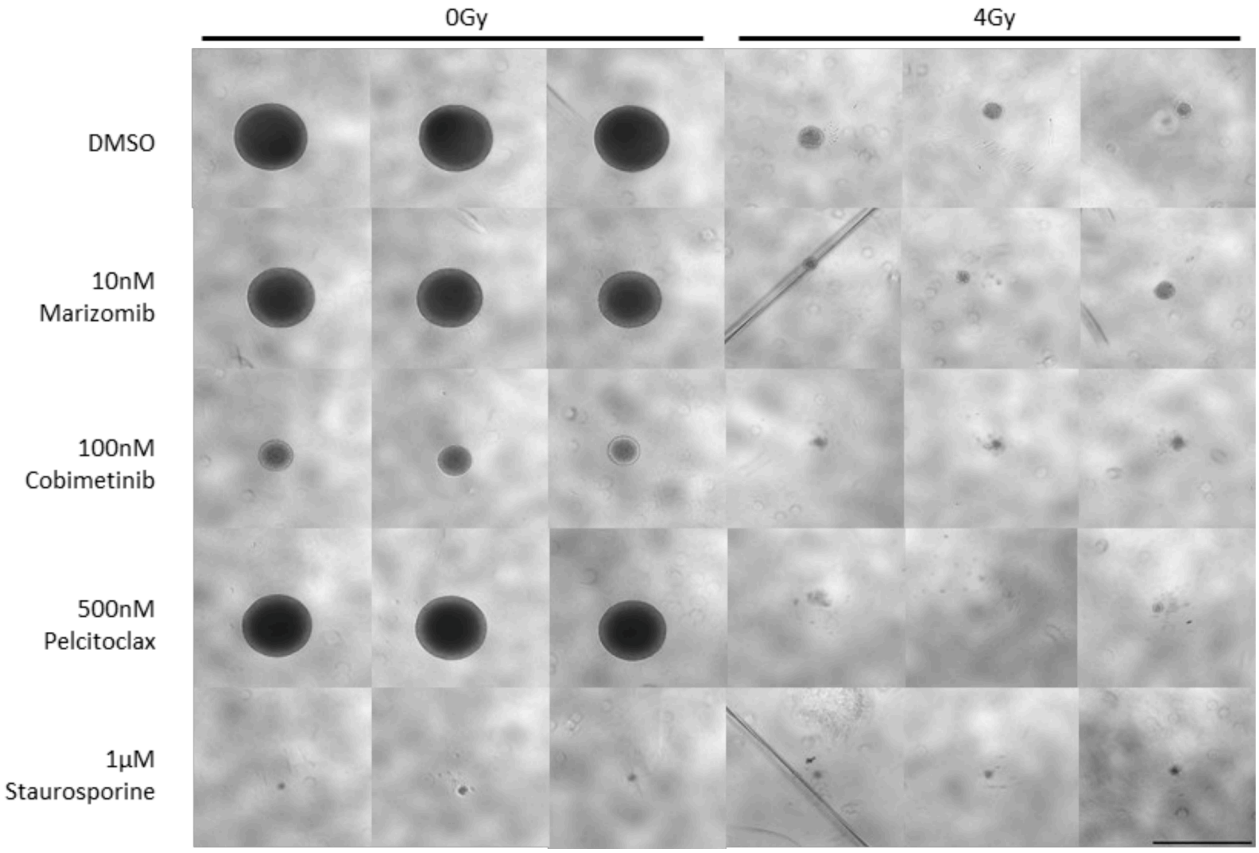
Supplementary figure 6: Cell viability assays after HDACi and RT combination treatment in DIPG-21 cells. Cells were irradiated 2 h after being in contact with the drugs and their cell viability was assessed after 3 days of incubation. Cells were tested at 0 Gy and at two RT doses (~ 60 % viability and ~ 40 % viability after RT), as well as in three drug concentrations (< IC50, ~ IC50, > IC50). Statistics of only selected comparisons at IC50 are shown. Mean ± SD, n=3.



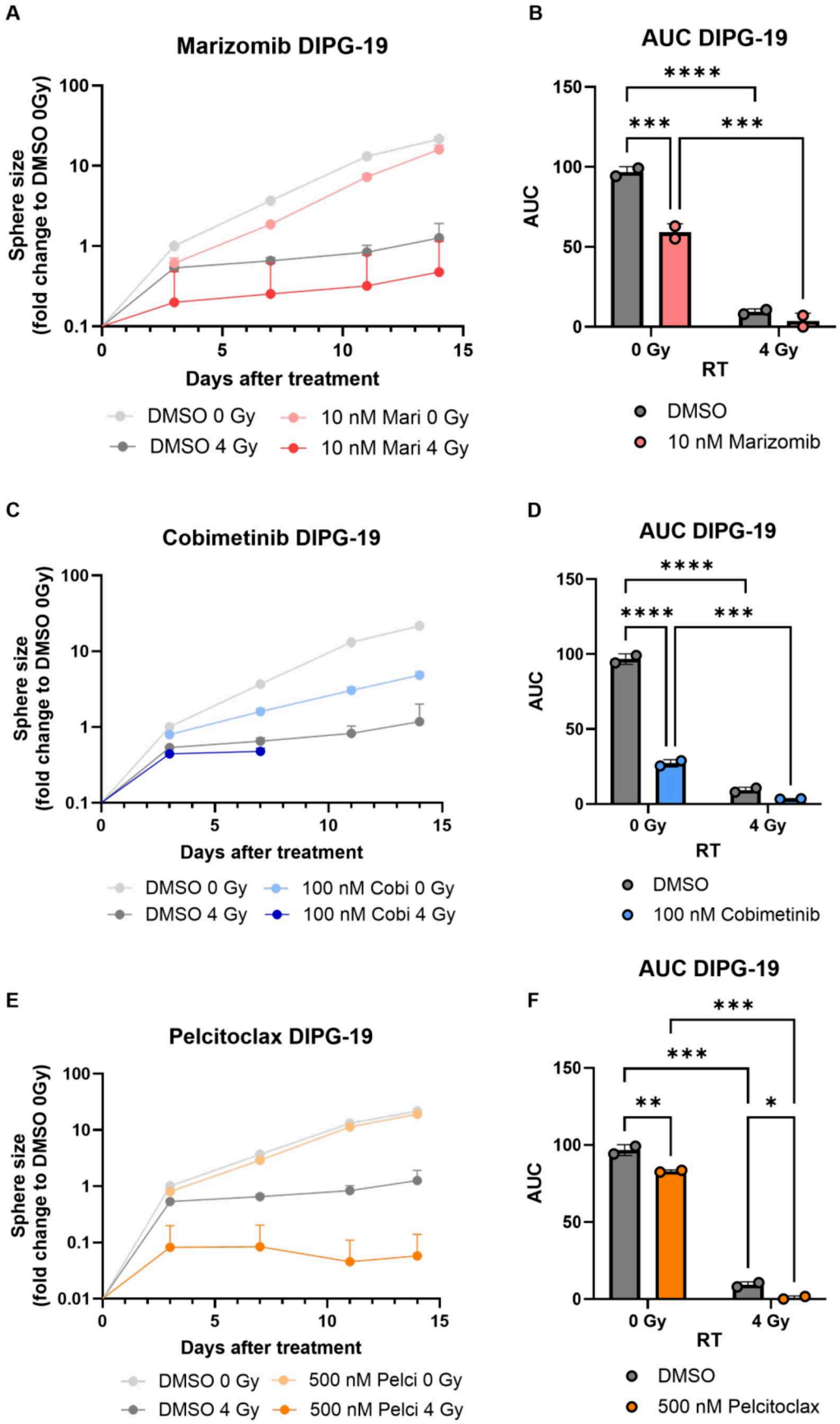
Supplementary figure 7: Cell viability assays after MEKi and RT combination treatment in DIPG-21 cells. Cells were irradiated 2 h after being in contact with the drugs and their cell viability was assessed after 3 days of incubation. Cells were tested at 0 Gy and at two RT doses (~ 60 % viability and ~ 40 % viability after RT), as well as in three drug concentrations (< IC50, ~ IC50, > IC50). Statistics of only selected comparisons at IC50 are shown. Mean ± SD, n=3.



Supplementary figure 8: Cell viability assays after A-B) Proteasomei and C) BCLi and RT combination treatment in DIPG-21 cells.
Cells were irradiated 2 h after being in contact with the drugs and their cell viability was assessed after 3 days of incubation. Cells were tested at 0 Gy and at two RT doses (~ 60 % viability and ~ 40 % viability after RT), as well as in three drug concentrations (< IC50, ~ IC50, > IC50). Statistics of only selected comparisons at IC50 are shown. Mean ± SD, n=3.

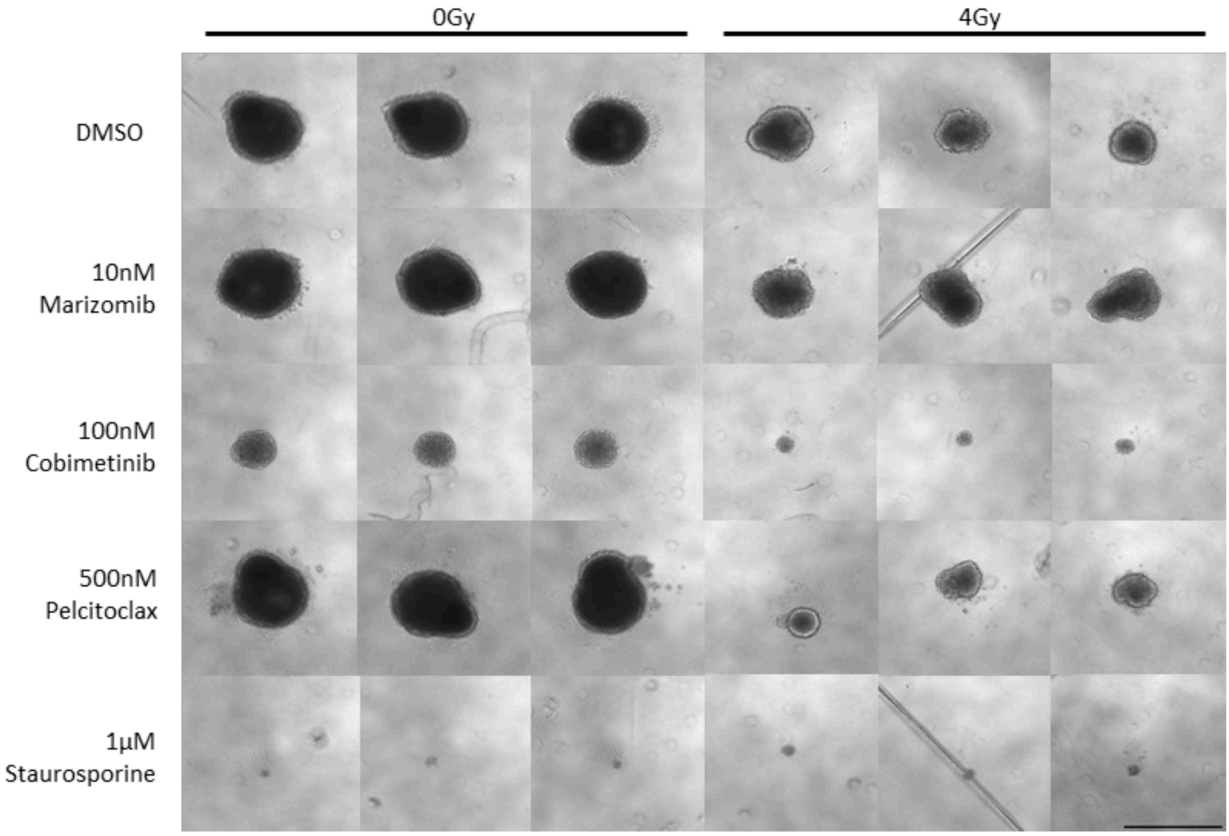


Supplementary figure 9: Representative pictures of the long-term growth inhibition assay in DIPG-19 spheres at day 14.
Pictures were taken at brightfield 10x magnification using the Nikon EclipseTi2 microscope. The scale bar represents 1mm. Three independent technical replicates are shown. DMSO served as negative control and Staurosporine as positive control.

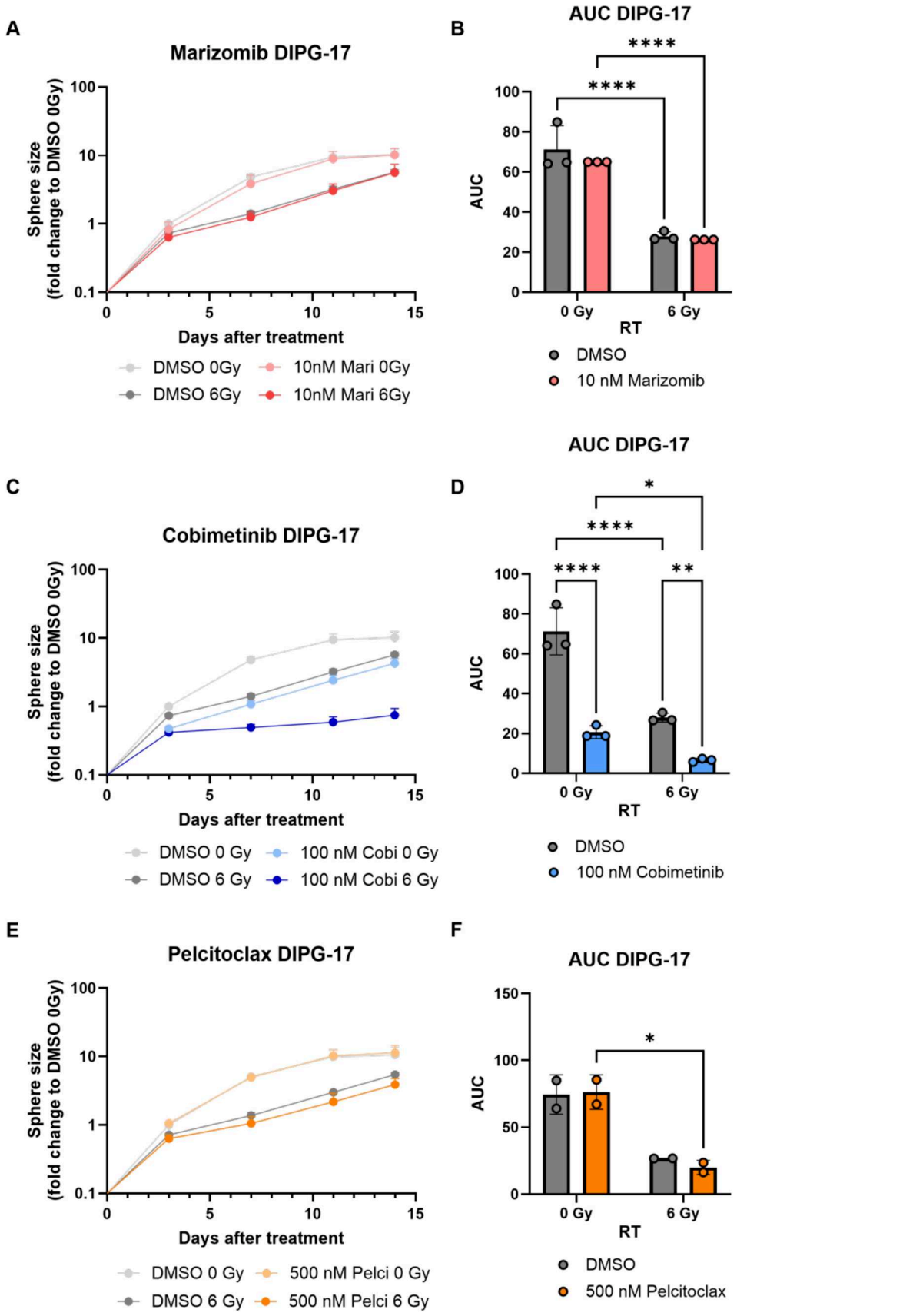


Supplementary figure 10: Quantification of the sphere size of the long-term growth inhibition assays in DIPG-19 cells.

The area of each sphere was assessed on day 3, 7, 11 and 14 after drug+RT treatment. The area under the curve (AUC) was then calculated for each biological replicate. Sphere size over time (left) and respective AUC (right) after A) Marizomib+RT treatment, B) Cobimetinib+RT treatment, and C) Pelcitoclax+RT treatment. Mean ± SD, n=2.

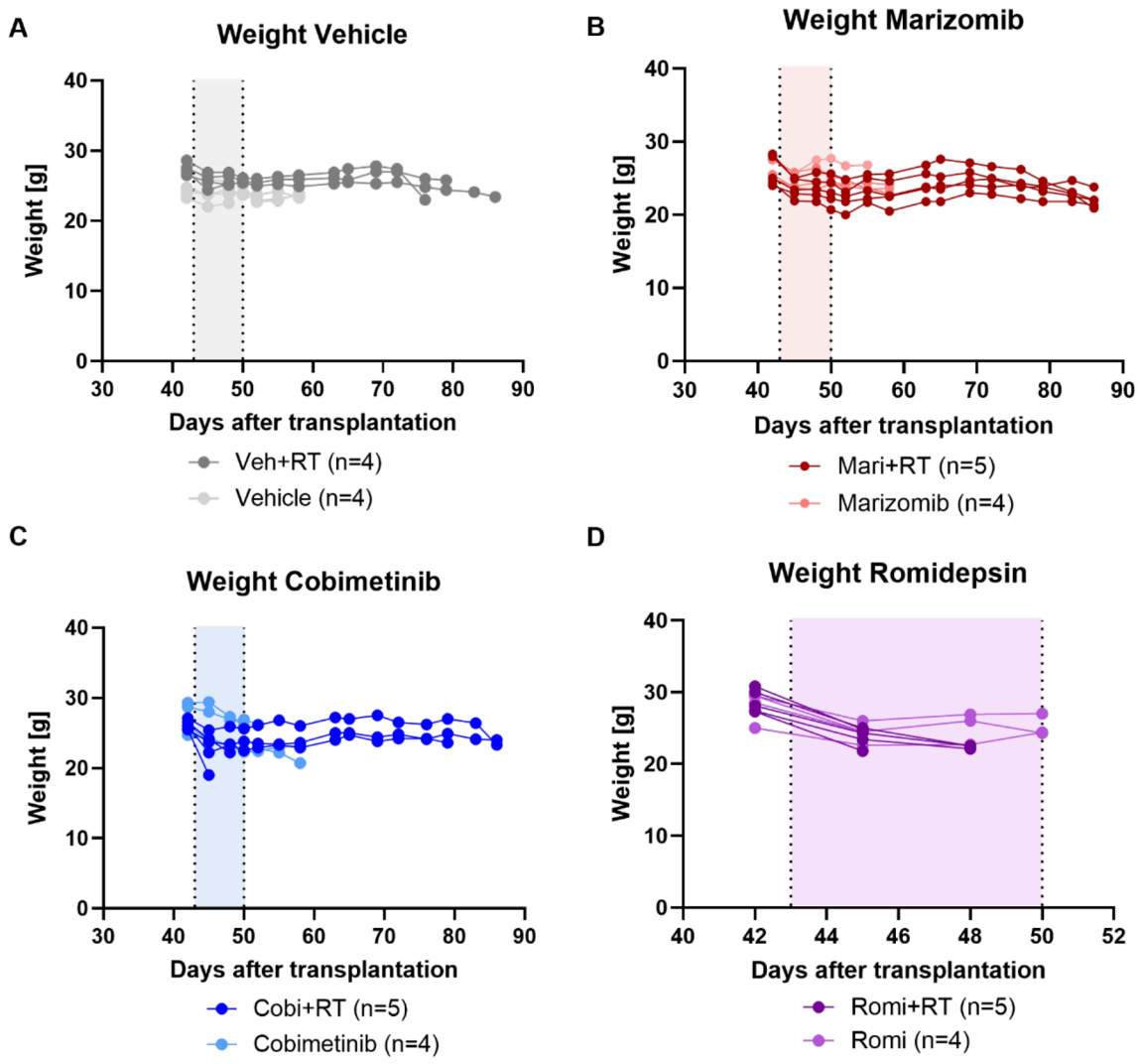


Supplementary figure 11: Representative pictures of the long-term growth inhibition assay in DIPG-17 spheres at day 14.
Pictures were taken at brightfield 10x magnification using the Nikon EclipseTi2 microscope. The scale bar represents 1mm. Three independent technical replicates are shown. DMSO served as negative control and Staurosporine as positive control.

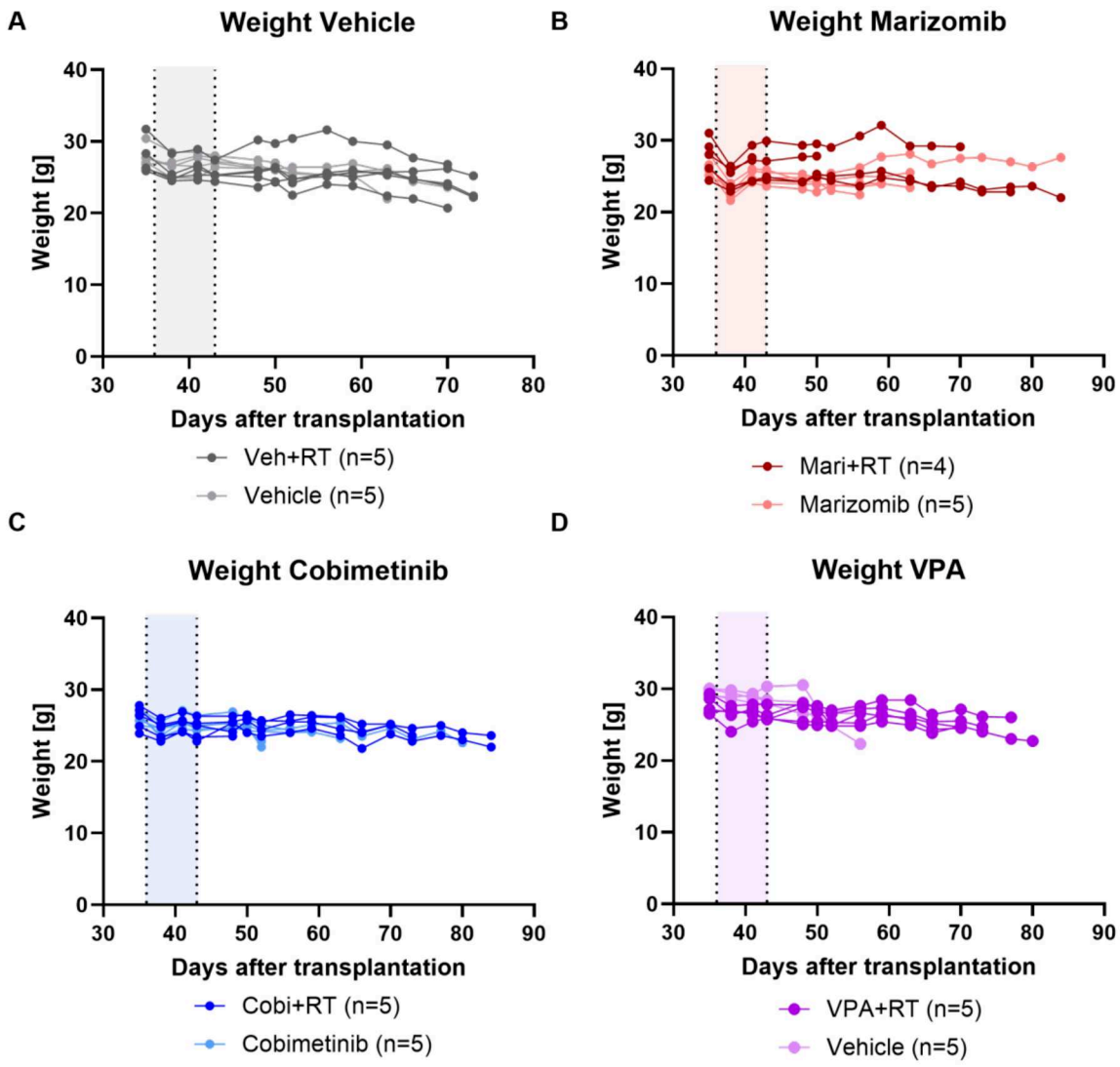


Supplementary figure 12: Quantification of the sphere size of the long-term growth inhibition assays in DIPG-17 cells.

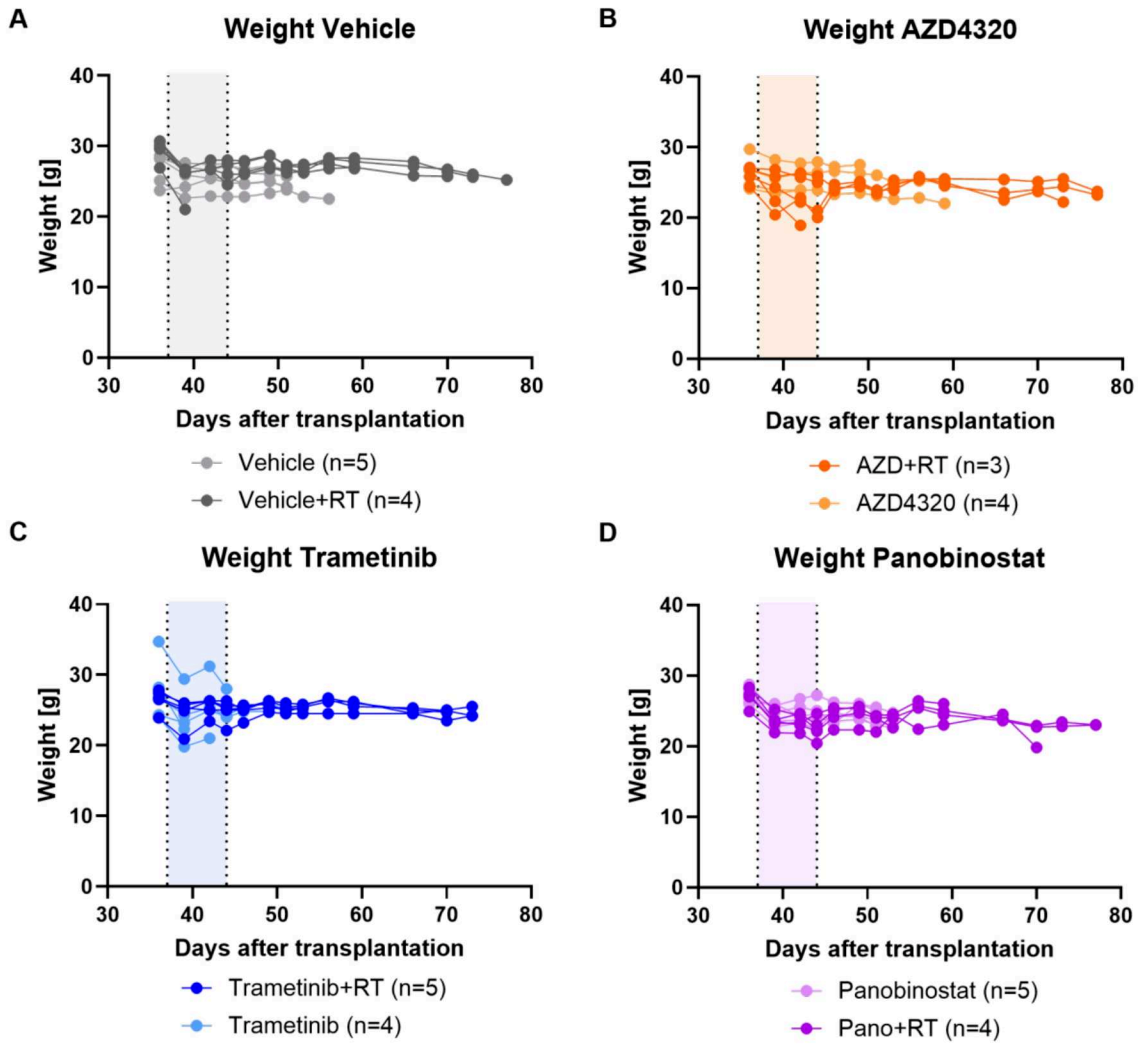
The area of each sphere was assessed on day 3, 7, 11 and 14 after drug+RT treatment. The area under the curve (AUC) was then calculated for each biological replicate. Sphere size over time (left) and respective AUC (right) after A) Marizomib+RT treatment (n=3), B) Cobimetinib+RT treatment (n=3), and C) Pelcitoclax+RT treatment (n=2). Mean ± SD.



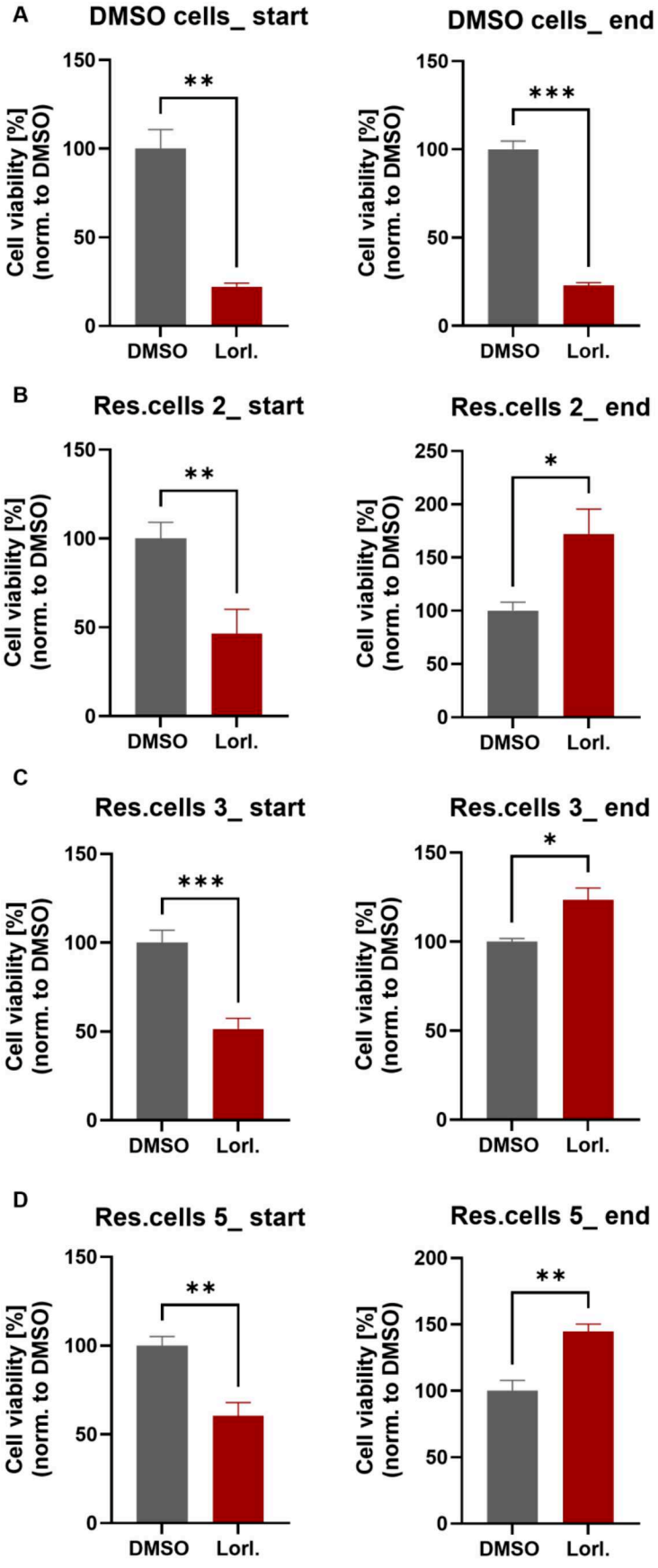
Supplementary figure 13: Body weight of the animals from the first preclinical trial (Figure 22).
Mice treated with A) Vehicle (Veh), B) Marizomib (Mari), C) Cobimetinib (Cobi), and D) Romidepsin (Romi) alone and in combination with 12 Gy RT during the preclinical study in the DIPG-007 mouse model.



Supplementary figure 14: Body weight of the animals from the second preclinical trial (Figure 23). Mice treated with A) Vehicle (Veh), B) Marizomib (Mari), C) Cobimetinib (Cobi), and D) Valproic acid (VPA) alone and in combination with 12 Gy RT during the preclinical study in the DIPG-007 mouse model.

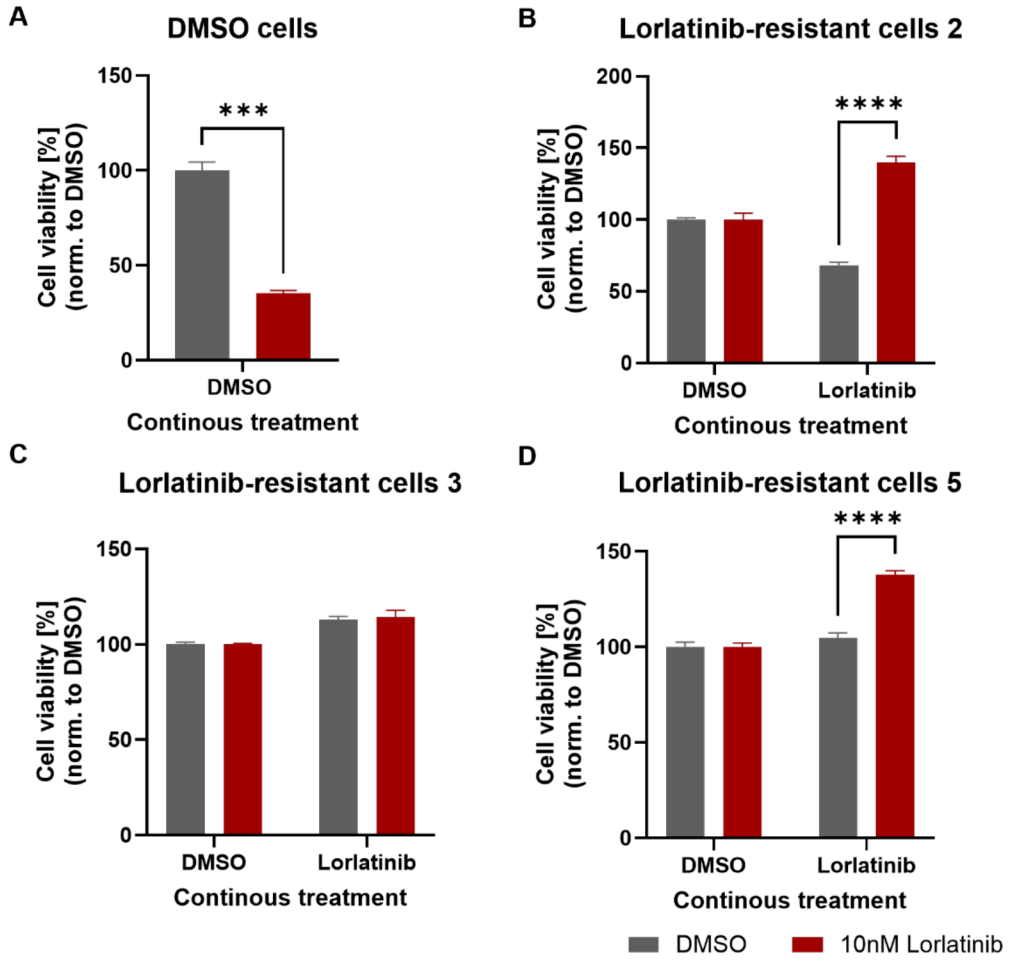


Supplementary figure 15: Body weight of the animals from the third preclinical trial (Figure 25). Mice treated with A) Vehicle (Veh), B) AZD4320 (AZD), C) Trametinib, and D) Panobinostat (Pano) alone and in combination with 12 Gy RT during the preclinical study in the DIPG-007 mouse model.

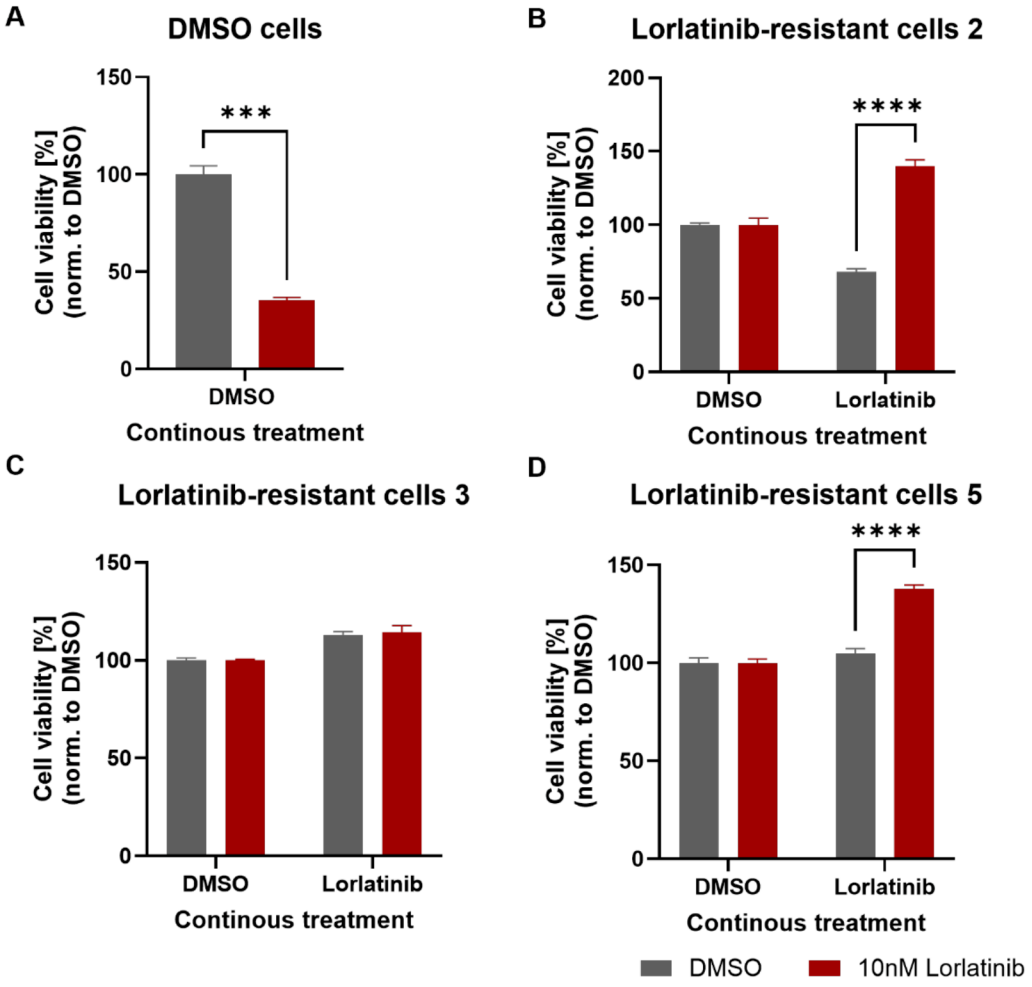


Supplementary figure 16: Generation of Lorlatinib-resistant cell replicates in vitro.

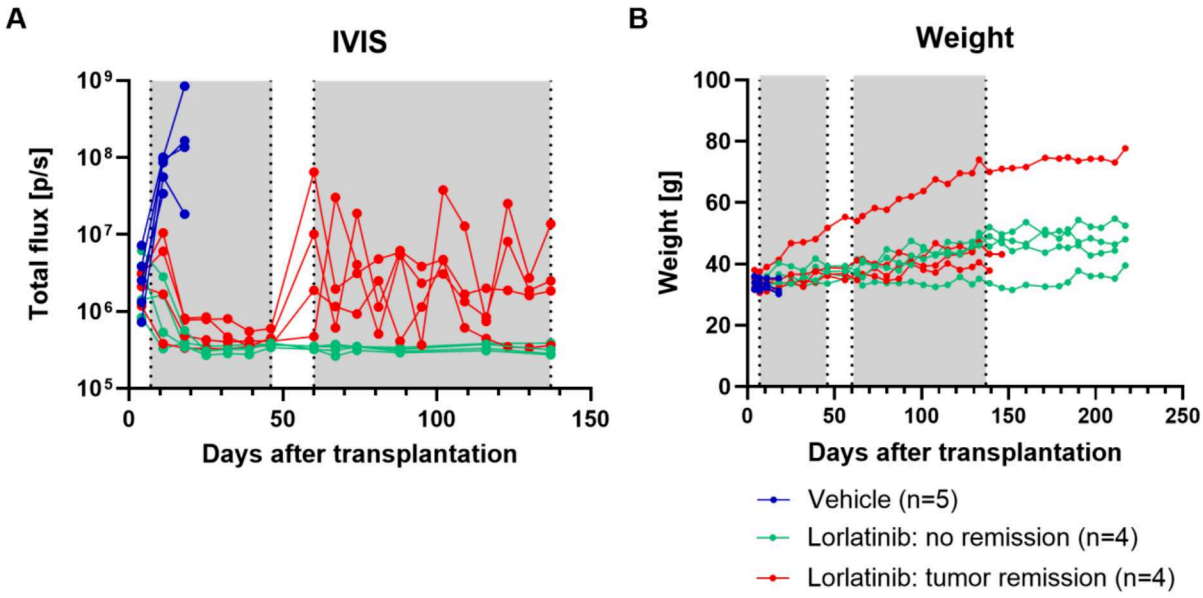
BI#190 cells were seeded into four wells and continuously cultured with either DMSO (DMSO cells) or 10 nM Lorlatinib (Lorlatinib-resistant cells). After 10 weeks, all cell cultures were seeded into 96-well plates and treated with either DMSO or 10 nM Lorlatinib (Lorl.). After 3 days, the cell viability of all cell cultures was assessed by CellTiterGlo (CTG). Cell viability of A) DMSO cells, B) Res.cells 2, C) Res.cells 3, and D) Res.cells 5 in response to DMSO and 10 nM Lorlatinib (Lorl.) treatment at the start (left panel) versus at the end (right panel) of the experiment. Mean ± SD, n=3.



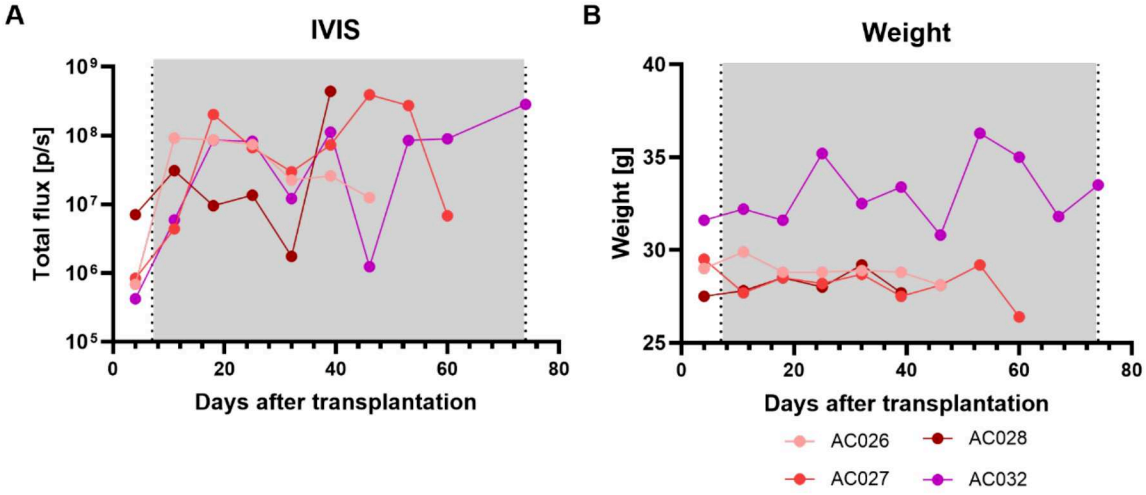
Supplementary figure 17: Lorlatinib resistance is stable even after Lorlatinib withdrawal for 3 weeks.
Lorlatinib-resistant cells were seeded into two wells and continuously cultured with either DMSO or 10nM Lorlatinib. After 3 weeks, both cell cultures were seeded into 96-well plates and treated with either DMSO or 10 nM Lorlatinib. After 3 days, the cell viability of both cell cultures was assessed by CellTiterGlo (CTG). A) Cell viability of DMSO cells in response to DMSO and 10 nM Lorlatinib treatment. B-D) Cell viability of Lorlatinib-resistant cells 2, 3 and 5 continuously cultured with DMSO or Lorlatinib for 3 weeks (X-axis), in response to DMSO and 10 nM Lorlatinib treatment after 3 days (grey and red respectively). Mean ± SD, n=3.



Supplementary figure 18: Lorlatinib resistance is stable even after Lorlatinib withdrawal for 8 weeks. Lorlatinib-resistant cells were seeded into two wells and continuously cultured with either DMSO or 10nM Lorlatinib. After 8 weeks, both cell cultures were seeded into 96-well plates and treated with either DMSO or 10 nM Lorlatinib. After 3 days, the cell viability of both cell cultures was assessed by CellTiterGlo (CTG). A) Cell viability of DMSO cells in response to DMSO and 10 nM Lorlatinib treatment. B-D) Cell viability of Lorlatinib-resistant cells 2, 3 and 5 continuously cultured with DMSO or Lorlatinib for 8 weeks (X-axis), in response to DMSO and 10 nM Lorlatinib treatment after 3 days (grey and red respectively). Mean ± SD, n=3.



Supplementary figure 19: A) IVIS signal and B) body weight of the animals treated with vehicle and Lorlatinib during the first transplantation experiment (Figure 30).
Lorlatinib-treated animals were subdivided into two groups: Lorlatinib-treated animals that stayed tumor-free after the initial continuous treatment (green) and Lorlatinib-treated animals with tumor remission (red). In these mice Lorlatinib-treatment was resumed in treatment cycles. Grey areas demonstrate the Lorlatinib treatment frame.



Supplementary figure 20: A) IVIS signal and B) body weight of the animals treated with Lorlatinib during the second transplantation experiment (Figure 31).
Grey areas demonstrate the Lorlatinib treatment frame.

8. Acknowledgments

It’s incredible how fast four years can pass. It feels like only yesterday that I was putting together the first outline of this project, unsure of where it would eventually lead. At that time, finishing it within a couple of years seemed almost impossible to imagine. Looking back now, I can see how much this journey has shaped me through persistence, challenges and constant learning. Reaching this point feels both humbling and deeply rewarding.
Because doing a PhD (and science in general) is rarely an immediately rewarding path, but instead involves a great deal of frustration, I would like to express my sincere gratitude to all the people who supported, encouraged, and guided me through this challenging chapter of my life.

First and foremost, I would like to thank my direct supervisor, Marc Zuckermann, for all the help, support, and guidance over the past years. I truly appreciated (and still appreciate) your ‘strong opinions’ and honest feedback, which helped me grow not only as a scientist, but also on a personal level. Thank you for trusting me with leading these two remarkable projects, which I genuinely enjoyed working on.

I would also like to thank Stefan Pfister for warmly welcoming me into the ‘Division of Pediatric Neurooncology’ and for serving as my formal supervisor, TAC member, and defense examiner. I have always valued your scientific input and deeply appreciated the inspiring scientific environment you created within your division and the KiTZ.

Furthermore, I would like to thank Peter Angel for being my faculty supervisor, TAC member, and defense examiner. I truly appreciated your genuine interest in my projects and your valuable scientific feedback and advice. I am also grateful to Gert Fricker and Ana Banito for taking the time and effort to be part of my defense committee.

Both of my projects were supported by outstanding collaborations that I would like to sincerely acknowledge.
A big thank you to Ina Kurth, Mareike Rocher, and Rosemarie Euler-Lange for all the help, support and time spent on animal irradiation. None of this was taken for granted, and I always genuinely enjoyed working with you.
Further I wish to acknowledge Jürgen Burhenne and Kevin Steimel for their help with the mass spectrometry analysis.
Many thanks to Olaf Witt for his constant help with drug selection and for always supporting whenever possible. In addition, I would like to thank Ina Oehme, Heike Peterziel, and Aileen

Friedenauer for their help with the drug screens and for providing the drug plates. A big thank you also goes to Florian Selt and Simon Zeuner for their willingness to help and for sharing reagents.

I would especially like to express my deepest gratitude to those who supported me on a daily basis - scientifically, technically, and emotionally - and without whom my PhD experience would not have been the same.

I honestly don't know if I can fully express how grateful I am to Nina Hofmann for ALWAYS being by my side during these four years. Thank you for everything one could possibly think of: teaching, organizing, helping, motivating, troubleshooting, and, of course, for all the fun we had together. There is a reason you are called the 'lab mom', and you truly deserve it. I always admired your professional, reliable, and ambitious way of working while also being one of the funniest people I have ever met. Long live the 'Hofmann'sche Randomisierung'!

I would also like to thank Chun Ho Chan and Laura von Soosten, who contributed substantially to getting both of my projects started. Without their expertise, time, effort, and genuine motivation to help whenever possible, I would not have been able to master many scientific and personal challenges as well as I did.

One of my deepest thanks go to my 'lab buddies' Lena Parzer and Michelle Arnet - simply for existing. I cannot imagine my PhD time without you. Thank you for all the support, discussions, feedback, help, and for all the fun we had both inside and outside the lab. Thank you for broadening my horizons regarding Swiss German and South Franconian dialects. Honestly, my life would have been much more boring without you two!

I would also like to genuinely thank the two students I supervised during my PhD, Szymon Lipiec and Sofia Kasapidou. Thank you for all your efforts, contributions, and help with the projects - I truly appreciated the time we spent working together.

At this point, I would like to thank all current and former members of 'AG Zuckermann', 'AG Kutscher', and 'AG Jones' for their support, discussions, and feedback. I highly appreciate all the time we shared in the lab, during retreats and conferences, and at Christmas and summer parties. In particular, I would like to acknowledge Frederik Arnskötter, Jan Vaillant, Franziska Schelb, Jana Nolle, Diego Yair Grinman, Nathalie Wilke, Tuyu Zheng, Chiara Lukasch, Lena Kutscher, and David Jones for their contributions to these projects.

A special thank you also goes to Clara Gade, who started her project at the same time as I did and has stayed in contact ever since.

I would further like to thank the Mouse Open Lab - Norman Mack, Benjamin Schwalm, Calvin Hug, and Eric Konrath - for their help and expertise with animal experiments, drug formulations, and health monitoring.

I am also very grateful to Michael Hain and Torben Wagner for supporting me with all my (sometimes silly) IT problems over the years.

Many thanks as well to all the wonderful BioContact members of the 2023/2024 and 2024/2025 seasons for the amazing time we spent planning the CONTACT job fairs together.

An extraordinary thank you goes to Klopsi for always brightening my days - and those of many others!

Last but by no means least, my most special thanks go to my parents, who have supported me unconditionally throughout my entire life. Without you, none of this would have been possible. Thank you for always being there for me in both good and difficult times. I cannot put into words how grateful I am to you!

Infine, ma non certo per importanza, il mio ringraziamento più speciale va ai miei genitori, che mi hanno sostenuta incondizionatamente per tutta la vita. Senza di voi, nulla di tutto questo sarebbe stato possibile. Grazie per esserci stati sempre, nei momenti belli come in quelli difficili. Non riesco a esprimere a parole quanto vi sono grata!